Formulations of Lazaroid-U74389G for Organ Targeting and Potential Chemotherapy

A dissertation Presented to the

Faculty of the Department of Pharmacological and Pharmaceutical Sciences

College of Pharmacy, University of Houston

In Partial Fulfillment of

the Requirements for the Degree of

Doctor of Philosophy

By

Fady Ibrahim

December, 2010

ACKNOWLEDGEMENT

"Delight yourself in the Lord and he will give you the desires of your heart", **Psalm 37:4**. I would like to thank GOD for the blessings that I had during my work in Dr. Chow's lab. Dr. Chow is a great supervisor on the scientific and the human level. She leads with a smile and advice with wisdom. I would like to express my appreciation for all her unconditional support for me and my family.

I sincerely thank my wife who supported me and made everything she could to give me the chance to focus on my work. Also, I would love to thank my parents, brother and sister who prayed a lot for me and supported me during my study. I would love to thank Dr. Bates in my committee who departed on Jan 13th, 2011 for all his input and support. I hope he is in a better place now and looking down at all the wonderful things people have come together and done, and sees that everyone cares for him. I would like to thank Dr Pamela New who proposed the project to our laboratory. Also, I would like to thank Dr Chun Li and Dr Vincent Tam for their input and support of the work.

I am very grateful to everyone who taught or helped me do something either in my work or in my personal life.

ABSTRACT

Radiotherapy is an important tool in the treatment of brain tumors. However, radiotherapy‘s success is limited by its toxic lipid peroxidation effects on the surrounding tissues. Lazaroid U74389G (LAZ) is a 21-aminosteroid that has a potent inhibitory effect on iron-dependent lipid peroxidation. It acts as an antioxidant and a membrane stabilizer. It prevents the damage in the brain after radiation by a selective distribution to vascular endothelium and its anti-oxidant activity. LAZ suffers from high liver uptake and short half life after an IV administration. We propose to circumvent this problem by using intravenous administration of nanosuspension or liposomal formulations or intracranial implantation of sustained release formulation. The nanosuspensions can provide a dramatic change in the biodistribution of the drug especially targeting RES organs. The nanosuspensions were prepared by wet milling techniques to produce nanosuspensions of 250 and 125 nm. The surface potential of the particles were modified in a later stage by adding ionic surfactants to produce neutral, anionic and cationic nanosuspensions. The anionic nanosuspension accumulated in the lungs 3-8 folds of that from the solution demonstrating a promising formulation for targeting lung cancers. The microspheres were formulated using the biodegradable polymer PLGA with various molecular weights and densities. The microspheres sustained the release of 90% of LAZ over 21 days using the lowest molecular weight PLGA 0.43 g/dL and only 40% of LAZ load was released from the highest density PLGA 0.65 g/dL over the same period of time. By using a

mixture of microspheres formulated from various PLGA polymers, the release profile can be potentially tailored to match the therapy protocol of different patients.

LAZ was formulated in conventional (Lipo B) and PEGylated (Lipo G) liposomes. The formulations were characterized for the size, zeta potential and release in PBS and plasma. Healthy nude mice received 1 mg/kg IV doses of the solution or liposomes to characterize the plasma pharmacokinetics and organ biodistribution. Lipo G increased the brain exposure of LAZ 13 folds of that from the solution, and was further used in a brain Glioblastoma bearing model expressing luciferase enzyme as a reporter gene. The animals received no treatment or were treated with radiation together with Lipo G or Lipo G alone at a dose of 5mg/kg IP. The tumor size was monitored by bioluminescence imaging and malondialdehyde level was used as a surrogate for lipid peroxidation in the brain tissue.

Lipo G showed higher stability in plasma compared Lipo B. In healthy mice, Lipo G yielded a higher AUC in plasma and prolonged $t_{1/2}$ compared to those from the solution and Lipo B. Brain exposure from Lipo G was 4 and13 times those from LipoB and solution, respectively. Both tumor size and lipid peroxidation were significantly reduced in Lipo G treated group compared to the no-treatment control. PEGylated LAZ liposomes demonstrated cytotoxic effects against Glioblastoma and protection against radiation induced necrosis.

TABLE OF CONTENTS

LIST OF TABLES

LIST OF FIGURES

LIST OF ABBREVIATIONS

AUC	Area Under the Curve
BA	The relative bioavailability
BBB	Blood Brain Barrier
BLI	Bio Luminescence Imaging
BMI	Bioluminescence Imaging
CSF	Cerebro Spinal Fluid
CTAB	Cetyl Trimethyl Ammonium Bromide
EE	Encapsulation Efficiency
EPR	Enhanced Permeability and Retention
GBM	Glioblastoma
HSPC	Hydrogenated Soy Phosphatidylcholine
Ig	Immunoglobulin
K_{el}	elimination rate constant
K_{el}	Elimination Rate Constant
LAZ	Lazaroid U-74389G
LLOQ	Lower Limit of Quantification
MDA	Malondialdehyde
MPS	Mononuclear Phagocytic System
MTS	17 α– Methyl Testosterone
NS	Nanosuspension
PBS	Phosphate Buffered Saline
PEG	poly ethylene glycol
PK	Pharmacokinetics
PLGA	Poly Lactic Glycolic Acid
QC	Quality Control
RES	Reticulo-Endothelial System

SDS	Sodium Dodecyl Sulfate
SEM	Scanning Electron Microscope
$t_{1/2}$	Half Life
TMZ	Tirilazad Mesylate
UPLC-MS/MS	Ultra performance liquid Chromatography Mass Spectrometry
V_d	Volume of Distribution

CHAPTER 1 INTRODUCTION

Glioblastoma (GBM) is the most common and malignant type of primary brain tumors in adults [1]. The standard therapy of the early diagnosed tumor is surgical resection followed by radiotherapy and or chemotherapy with Temozolimide. The median survival of the patients is between 12-14 months with no further improvement in the last decade [2]. Delivery of drugs to the brain is a challenging mission due to the presence of the blood brain barrier (BBB) which restricts entry to the lipophilic compounds with molecular weight less than 400 Dalton[3]. Even the small number of drugs that have suitable physicochemical properties to cross the BBB may be forced out by the efflux transporters in the BBB[4].

Radiotherapy is a standard therapy for GBM patients but it suffers from developing necrotic lesions which restricts the dose and duration of radiotherapy. Radiotherapy-induced necrosis was demonstrated to depend on the radiation dose, frequency, size of the irradiated area and duration. Necrosis appears either at early stage, less than 2 months, or at late stage several months afterwards the radiation [5]. Vascular damage, inflammation, altered cell membrane permeability, and increased collagen production are significant in the pathophysiology of radiation injury. The underlying mechanism of radiation-induced injury is lipid peroxidation in the presence of oxygen free radicals and iron [5, 6]. The problem of lipid peroxidation is more serious in the brain than other tissues due to the high content of unsaturated fatty acids in the brain tissues. The

neuronal membrane and the myelin sheath are the two brain structures that have the highest lipid content in their cell components (50 and 70 %, respectively)[7].

1.1 Lazaroid U-74389G

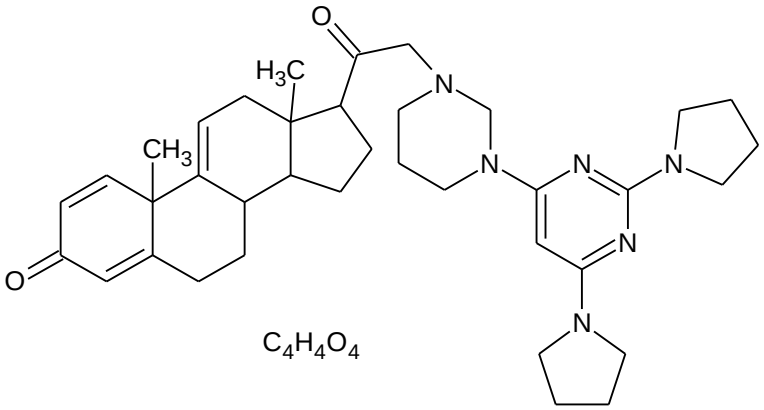

Figure 1.1 Chemical Structure of Lazaroid U-74389G

Lazaroid U-74389G (LAZ) is [21-(4-(2,6-di-1-Pyrrolidinyl-4-pyrimidinyl)-1-piperazinyl)-pregna-1,4,9(11)-triene-3,20-dione(Z)-2-butenedioate] (Figure 1.1). LAZ belongs to 21- aminosteroids family. This family is derived from glucocorticoids but lacks glucocorticoid and mineralocorticoid activities, due to the replacement of carbon 21 of the steroid nucleus by an amine group and removal of C11 and C17 hydroxyl groups [8]. The members of Lazaroids family exert an antioxidant activity by capturing lipid peroxyl radicals and iron leading to inhibition of the iron–dependent lipid peroxidation [9]. Also, Lazaroids exert cytoprotective effects by inhibiting arachidonic acid release, stabilizing cell membranes, suppressing Kupffer cell activation, suppressing the cytokine

production by inhibiting nuclear factor kappa B activation, and improving intestinal microcirculation in endotoxin-shock rat model [10].

In addition to the general features of the family, LAZ attenuates liver damage in ischemia-reperfusion injury in a swine model [11]. In *in-vitro* cell cultures, LAZ reduces neuronal death associated with lipid peroxidation involved in acute chemical hypoxia[12]. LAZ administered during cardiac arrest mitigates post-resuscitation myocardial dysfunction and improves survival in rats[13]. LAZ exerts protection on the BBB, attenuates brain edema and neuronal necrosis caused by radiotherapy in rats[14]. In 1996 John *et al*., reported that LAZ provided protection against radiosurgery-induced injury [15]. In 1997 Kondziolka *et al*., reported that LAZ protected the brain vasculature after a single intravenously administered dose of 15 mg/kg against radiation-induced vasculopathy and edema [16].

Lazaroids family is a good candidate for protection against radiation-induced injuries for the following reasons. First, Lazaroids provided protection against radiation–induced injuries in rat brain and intestine. Second, these compounds have chemotherapeutic activities *in-vitro*. Third, Lazaroids selectively distribute at the level of the vascular endothelium, to protect the normal tissues without protecting tumor tissue. Fourth, there was no post-administration complication noticed in a dose range of 5-15 mg/kg [15-17].

In-vitro antiproliferative effect against C6 glioblastoma cell line was demonstrated using LAZ and other family members [18, 19] .The inhibitory effects of 21-aminosteroids on

the proliferation of cancer cells *in-vitro*, was attributed to the structural similarities with corticosteroids. This similarity allows Lazaroids to interact with the same glucocorticoid receptors [18, 19]. Macuinas *et al*. reported that dexamethasone caused cell death in a dose dependent manner, but the IC_{50} of dexamethasone was found to be higher than the human tolerable doses by systemic delivery [20]. Kim *et al.* have shown that the inhibitory activity of the Lazaroid U-74500A varied depending on time and dose, suggesting that it has cytotoxic effect [18, 19].

In C6 cell line, U-83836E caused a reduction of cell survival in a dose-dependent manner for does over 1 mM, but the same effect was not obtained with LAZ. But LAZ was more effective on primary cell lines than U-83836E using the same dose. Both compounds were found to be less effective on cell lines established from patients compared to the primary cell cultures [19].

LAZ can be used as a radioprotective against the radiation-induced lipid peroxidation to slow down or prevent the process of necrosis. LAZ delivery to the brain is a crucial determinant of the success of the treatment to ensure high LAZ level for a prolonged exposure period. One obstacle against achieving high brain concentrations of LAZ is its difficulty in crossing the BBB. No research to date has investigated how to increase LAZ concentration in the brain or how to target other organs in order to provide higher level of radioprotection. Given the potential benefits to radiation therapy of increased concentrations of LAZ in the brain or other organs after systemic administration, studies

to improve the delivery of LAZ across the BBB or to target other organs appear warranted.

Many strategies can be followed either to overcome the BBB or to change the drug pharmacokinetics (PK) and organ distribution pattern to passively target other organs. Nanocarrier formulations such as nanosuspension (NS)[21] and liposomes[22] are examples of these promising strategies. Another strategy to circumvent the BBB is to implant sustained release formulation (such as microspheres) in the brain tissue after brain surgery [23].

1.2 Nanosuspension

Nanosuspension (NS) formulations are carrier-free colloidal drug delivery systems for water-insoluble drugs. It contains a pure drug nanoparticles and a minimum amount of surface active agents required for stabilization of the suspended drug particles in the aqueous medium [24]. Nanosuspensions have revealed their success to solve the problems associated with the delivery of poor water-soluble drugs. As NS is stabilized by the minimum amount of surfactants and the drugs remain in a solid state, the formulation has low toxicity, higher mass per volume loading, and higher physiochemical stability compared to the drug solution [25]. The IV administration of nanosuspensions results in various pharmacokinetic profiles depending on its physical characteristics. For example, the pharmacokinetic profile and tissue distribution of a fast dissolving nanosuspension will be similar to that of the solution upon injection [21]. On the other hand, if the NS

particles had a slow dissolution profile, there will be a high possibility to be captured by the macrophages of the mononuclear phagocytic system (MPS), primarily by Kupffer cells in the liver, spleen and lungs in a process known as phagocytosis [21, 26]. Phagocytosis is triggered by the adsorption of certain plasma proteins (opsonins) on the surface of the foreign particles. The opsonization of hydrophobic, charged nanoparticles, as compared to hydrophilic, neutral nanoparticles, occurs more quickly due to the enhanced opsonin adsorption on their surfaces[27]. Some studies showed that nanoparticles coated with Tween 80 on the surface could anchor apolipoprotein E, which plays an important role in the transport of low density lipoprotein into brain. The same role can be played to facilitate Tween 80-coated particles entry into the brain [28].

Advantages of nanosuspensions[29]:

1- Increase in the dissolution velocity and saturation solubility of the drugs

2- Improved biological performance

3- Ease of manufacture and scale-up

4- Long-term physical stability

Nanosuspensions can be formed by breaking larger micron-sized particles down by milling. A new surface area is formed which leads to an increase in free-energy in the system. The system becomes unstable due to the increased energy due to the creation of new surface area of the milled particles. To correct this energy imbalance, the small particles tend to agglomerate to decrease the surface area and re-stabilize the system. To overcome the self-correction step, a surface active agent is added during the milling step.

The addition of surface-active agents will reduce the free energy of the system by two main actions:

1- To impart a charge on the suspended particle to affect electrostatic repulsion among the particles (ionic surfactants).
2- To impart a steric repulsion; that is, they resist compression (nonionic polymers). Non-ionic polymeric surfactant is used to coat the surface with a hydrophobic chain, and permits a hydrophilic tail to project into water. This provides the necessary repulsive barrier between two neighboring particles.

Both electrostatic and steric hindrance mechanisms can be used by combining polymers and ionic surfactants in the nanosuspension formulation using wet milling technique. *Wet milling* is a manufacturing technique for preparing nanosuspensions, in which the drug powder is milled in the presence of surface stabilizers using grinding beads[30].

1.3 Microspheres

The drug release can be sustained by encapsulating the drug in a controlling device such as polymeric microspheres, hydrogels or reservoir devices. The release rate can be tailored to suite the purpose for which the system was developed. For example, an initial burst effect may be needed followed by sustained release. Also, the controlled release device may provide a protection for the drug against the degradation by the surrounding environment.

The idea of controlled release was enforced in the 1960s[31] but the problem of non-degradation restricted the use of these systems at that time. In 1970s the idea of using the

biodegradable polymers floated on the surface to circumvent the removal procedures of the implanted devices. Polymeric microspheres delivery system is one of the sustained-release systems that can accommodate a variety of drugs including small molecules proteins and nucleic acids. It can be easily injected in the site of action, for example brain tissue, if they have a proper size. Biocompatibility can be achieved by the use of natural polymers such as cellulose, chitin, and chitosan or by the employment of polymers made from naturally occurring monomers such as lactic and glycolic acids (Figure 1.2).

BBB is a major obstacle to develop effective pharmacological treatments for CNS using IV administration route. The unique structure of the cerebral endothelial cells in the BBB inhibits the diffusion of most pharmaceutical agents. The implantation of the controlled release formulations in the brain tissues either post-surgery or using a burr-hole and a catheter, will overcome the difficulty of crossing the BBB. GLIADEL® implant was approved by the FDA for use in postsurgical local chemotherapy against recurrent malignant glioma [32]. Despite its potential, Gliadel has a drawback of being limited to the area where it was implanted. The formulation of the drug in microspheres improves the penetration into the surrounding tissues by multiple site injections of the spherical particles [33]. Many researchers implemented the microsphere formulation to overcome the difficulties in crossing the BBB by intracranial implantation of microspheres [34-37]. The most widely used biodegradable polymer for microspheres formulation is poly lactic glycolic acid (PLGA). PLGA degrades by hydrolysis in the body to produce the original monomers, lactic acid and glycolic acids. These two monomers are by-products of

various metabolic pathways in the body. Since the body effectively deals with the two monomers, there is a very minimal systemic toxicity associated with using PLGA for drug delivery or biomaterial applications [38].

PLGA's are known for undergoing bulk degradation in an aqueous medium, which means that rate of medium penetration is faster than polymer solubilization [39]. The biodegradation of PLGA is believed to occur through four consecutive steps: hydration, initial degradation, further degradation, and solubilization. Many factors influence the biodegradation of PLGA which may include polymers composition (or the ratio of lactic to glycolic acid moieties), molecular weight, surface area, nature of hydrolyzing media such as pH and ionic strength of a medium. It has been shown that the time required for degradation of PLGA is related to the monomers' ratio used; the higher the content of glycolide units, the shorter the time required for degradation.

1.3.1 Microspheres Preparation

Three main methods are widely used to prepare microspheres:

1- Polymerization of Monomers.

2- Emulsion-Solvent Evaporation.

3- Extrusion.

The method of solvent evaporation is less sophisticated than the other methods and widely used in small scale preparation. In this method, a solution of the polymer and the drug is emulsified in a non solvent phase. The emulsion is stabilized by the addition of a stabilizer. For example, to produce microspheres of PLGA, solvents such as methylene

chloride and ethyl acetate are used in conjunction with an aqueous phase containing polyvinyl alcohol as the stabilizer to produce the emulsion. After emulsification, the emulsion is poured into a larger volume of the continuous phase allowing the organic phase to migrate leaving the polymer and the drug to enrich the organic phase. The polymer is precipitated along with the drug forming the microspheres which can be separated, washed and dried [40].

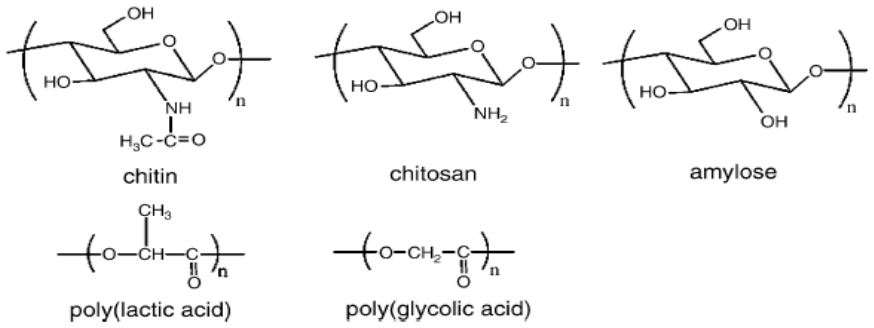

Figure 1.2 Chemical Structures of Biodegradable Polymers

1.4 Liposomes

The use of liposomes as a drug delivery system can improve the pharmacological properties of the traditional chemotherapeutics by altering drug pharmacokinetics and biodistribution [41, 42]. Liposomes are spherical vesicles consisting of one or more phospholipid bilayer surrounding an aqueous core. The diameter of the liposomes varies from 0.02-10 μm[43]. The vesicles are built by the amphiphilic phospholipids. The polar head groups of the phospholipids form the interface to the aqueous media. The lipophilic

agents are incorporated into the bilayer of the membrane while the hydrophilic agents are located within the water phase inside the vesicles[44].

The physicochemical properties of liposomes can be modified by changing [45]:

1- The composition and proportion of lipids
2- The size of the liposomes
3- The charge on the liposomal surface
4- The fluidity of the liposomal membrane.

1.4.1 Advantages of liposomes:

1- Improved pharmacokinetics and biodistribution of drug candidates:

   The advantage of liposomes is the possibility of gradual and sustained release of the drugs in the circulation. This allows maintaining high drug concentration for long time [46]. Conventional liposomes are recognized by mononuclear phagocytic system (MPS) which leads to fast clearance from the circulation. Conventional liposomes will accumulate in the reticulo-endothelial system (RES). This phenomenon is desirable to target RES but with short plasma circulation time [47]. The MPS uptake depends on several factors such as size, charge and hydrophobicity of the particle surface[47]. The plasma circulation time can be improved by reducing the liposomes' size to less than 100 nm and by anchoring poly ethylene glycol (PEG) on the surface of the liposomes [43] .

2- Decreased Toxicity:

Doxorubicin solution has a serious toxicity of bone marrow suppression and cumulative cardiac toxicity. PEGylated liposomal doxorubicin (PLD) has 80-90 nm vesicle size and a half life of 2-3 days. The most striking advantage of PLD is the reduced toxicity that limited its use. [48].

3- Increased stability of encapsulated drugs [49, 50].

4- Target selectivity:

Tissue targeting may be a passive or active targeting. In passive targeting, the liposomes distribute selectively to a specific tissue due to the physical properties of the liposomes such as the size and surface potential. Liposomes can be modified to actively target a specific tissue or organ by the following:

a- Addition of specific immunoglobulins [51].

b- Addition of cell penetrating peptides and proteins[52].

c- Addition of saccharides chains[53]

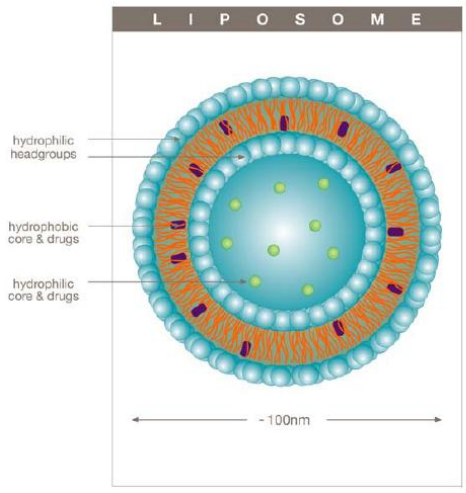

Figure 1.3 Liposome Structure and Drug Positioning in the Liposomes

1.4.2 Formulation of Lipophilic Drugs in Liposomes:

Highly lipophilic drugs, with log P_{oct}>5, are entrapped almost completely in the lipid bilayer of the liposomes. Since they are very poorly soluble in water, problems like loss of entrapped drug on storage are minimal with this class of drugs. Drugs with intermediate partition coefficients, i.e. 1.7< log P_{oct}<4, pose a major problem because they partition easily between the lipid and aqueous phases and are very easily lost from the liposomes. However, the most problematic candidates for liposomal entrapment are the drug molecules which have poor biphasic solubility. Being insoluble in either aqueous or lipid phase, they show only a low uptake by the liposomes. Typical examples include 6-mercaptopurine, azathioprine and allopurinol [54].

1.5 Concepts of Passive Targeting

Tumor blood vessels are generally characterized by abnormalities such as high proportion of proliferating endothelial cells, pericyte deficiency and aberrant basement membrane formation leading to an enhanced vascular permeability. Particles, such as nanocarriers (in the size range of 20–200 nm), can extravasate and accumulate inside the interstitial space [55]. Endothelial pores have sizes varying from 10 to 1000 nm [56]. Moreover, lymphatic vessels are absent or non-functional in tumor which contributes to inefficient drainage from the tumor tissue. Nanocarriers entered into the tumor are not removed efficiently and are thus retained in the tumor. This passive phenomenon has been called the “Enhanced Permeability and Retention (EPR) effect,” discovered by Matsumura and Maeda [57]. The abnormal vascular architecture plays a major role for the EPR effect in

tumor for selective macromolecular drug targeting at tissue level that can be summarized as follows and illustrated in Figure1.4:

(1) Extensive angiogenesis and hyper-vasculature

(2) Lack of smooth-muscle layer, pericytes

(3) Defective vascular architecture: fenestrations

(4) No constant blood flow and direction

(5) Inefficient lymphatic drainage that leads to enhanced retention in the interstitium of tumors

(6) Slow venous return that leads to accumulation from the interstitium of tumor

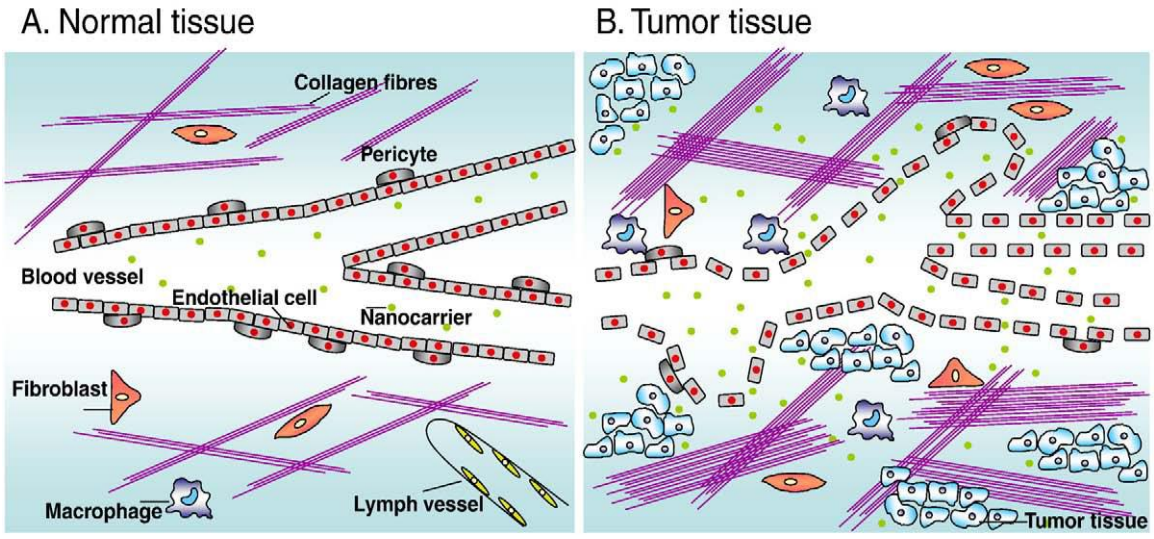

Figure 1.4 Differences between normal and tumor tissues that explain the passive targeting of nanocarriers by the Enhanced Permeability and Retention effect. A. Normal tissues contain linear blood vessels maintained by pericytes. Collagen fibers, fibroblasts and macrophages are in the extracellular matrix. Lymph vessels are present. B. Tumor tissues contain defective blood vessels with many sac-like formations and fenestrations. The extracellular matrix contains more collagen fibers, fibroblasts and macrophages than in normal tissue. Lymph vessels are lacking. Adapted from [58]

Table 1.1 Some of the Published Methods to Encapsulate Lipophilic Drugs in Liposomes

Drug	Lipids	Preparation	Method of Loading	Size (nm)	Route
Flavopiridol [59]	HSPC, CH, and DSPE-PEG200	Rehydration of dry lipid	Remote loading	120.7	IV
Prednisolone [60]	ePC/CH and/ or 1% (DSPE)-PEG 2000	~		45± 25	IV
Nystatin[61]	(DPPC):CH (2:1, mol:mol), with 6 mol% DSPE–PEG 2000	~	Temp at 60		
Paclitaxel[62]	(DOPC/CH/cardiolipin molar ratio: 90:5:5	~	Temp 30-40	150	IV
Aryl-imidazole[63]	(ePC) and DSPE-PEG 2000	~	Temp 60	89	IV
Minoxidil[64]	81.7μmol DPPC, 0–103.44 μmol CH	~	Temp 55	140-230	
Prodrug of 5-fluorouracil [65]	soy lecithin, Chol (8:1, w/w)	~	Temp 40	400	P.O
Ethinylestradiol [66]	Soy PC, surfactant in different ratios (95–75:5–25% w/w PC:surfactant)	~	Temp 55	160	IP
Benzocaine[67]	50% w/w PC and 50% w/w CH	~	Temp 55	372	
Fenofibrate[68]	Soy PC: CH (4:1)	~	Temp 30	200	P.O
Albendazole[69]	Egg PC:CH:PEG-(5:4:1)	Thin film hydration	Hydration at 55^{o}C	50-150	In-vitro
Peptide[70]	Peptide (2.35 μmol), sucrose (278μmol) and ePC (23.1 μmol) were dissolved completely in *tert*-butanol and water (1:1, v/v, 5 mL).	Freeze drying			

CHAPTER 2 OBJECTIVES AND SPECIFIC AIMS

2.1 Main Hypothesis

The incorporation of LAZ in nano-formulations (liposomes and nanosuspensions) will change its pharmacokinetics and organ distribution in athymic nude mice. The nano-formulations have the potential to passively target the brain and other organs. An alternative approach of local implantation of sustained release microspheres in the brain post-surgery will be followed if the nano-formulation could not target the brain.

2.2 Objectives

1- To investigate the effect of the nano-formulations on the pharmacokinetics and biodistribution of LAZ in athymic nude mice. The *working hypothesis* is that the nano-formulations will increase the brain uptake by enhancing the particles uptake by brain endocytosis mechanism. The inclusion of PEGylated lipids in liposomes will help reduce liver uptake which clears most of the circulating LAZ.

2- To formulate LAZ in sustained release microspheres as an alternative approach. The *working hypothesis* is that the microspheres will release LAZ for more than three weeks when implanted post-surgery in the brain.

3- To investigate a proof-of-concept efficacy of LAZ nano-formulation for glioblastoma tumor growth suppression *in-vivo*. The *working hypothesis* is that the formulation that will target the brain will be able to deliver LAZ in a

therapeutic concentration to protect the brain tissues from the harmful radiation. At the same time, this will be the first research to investigate the antineoplastic effect of LAZ *in-vivo*.

2.3 Specific Aims

1- Development and characterization of LAZ nanosuspension (NS) formulations of two sizes (250 and 125 nm) with various potentials on the particles' surfaces (neutral, cationic and anionic): We hypothesize that we will be able to develop NS using the wet milling technique with various sizes and charges. The use of a mixture of glass beads and surfactants will impart a change in the size and surface charge, respectively. The NS will be characterized by their size, charge and dissolution in PBS and plasma.

2- Establishment of plasma pharmacokinetics and organ distribution of NS with various sizes and charges in athymic nude mice: We hypothesize that the size and charge of the NS will have impacts on the pharmacokinetics and biodistribution of LAZ *in-vivo*. There will be a favorable uptake of certain size and charge of the NS by different organs compared to that of the solution.

3- Development and characterization of LAZ liposomes: the working hypothesis is that we will be able to develop two liposomes formulations (conventional and PEGylated). The two liposomes will be similar in size, encapsulation efficiency (EE) but differ in the lipid composition. The liposomes will be characterized by

their size, charge, EE, release in plasma and PBS, and thermal analysis using differential scanning calorimetry (DSC).

4- Establishment of the pharmacokinetics and organ distribution of LAZ from conventional and PEGylated liposomes in athymic nude mice: The working hypothesis is that PEGylated liposomes will have a higher systemic exposure (AUC) than those of conventional liposomes and solution. This higher AUC increases the chances of brain uptake by passive diffusion and endocytosis.

5- Development and characterization of LAZ microspheres: The incorporation of LAZ in a polymer matrix such as poly lactic-glycolic acid (PLGA) will control the release of the free LAZ out of the matrix according to the matrix biodegradation. By modifying the PLGA composition, various release behaviors can be achieved. The microspheres will be characterized by their size, scanning electron microscope (SEM) and the release profile in cerebrospinal fluid (CSF).

6- Perform a proof-of-concept study of efficacy in brain tumor bearing mouse model of LAZ formulation that targets the brain for Glioblastom tumor growth suppression: The nano-formulation that targets to the brain will be used for the efficacy study. The working hypothesis is that LAZ will reduce the lipid peroxidation in the brains of irradiated animals and at the same time suppress the tumor growth in treated animals compared to the control groups. The radioprotection will be evaluated by measuring Malondialdehyde (MDA) level in the harvested brain tissue at the end of the experiment.

CHAPTER 3 MATERIALS AND METHODS

3.1 Materials

3.1.1 Chemicals and Materials

- 1,2-distearoyl-*sn*-glycero-3-phosphoethanolamine-N-[methoxy(polyethylene glycol)-2000] (ammonium salt)
- 17-α-methyl testosterone (Sigma Chemical Co., St. Louis, MO, USA) was used as internal standard for HPLC analysis of LAZ.
- 18:0 PEG2000 PE [1,2-distearoyl-*sn*-glycero-3-phosphoethanolamine-N-[methoxy(polyethylene glycol)-2000] (ammonium salt)]-DSPE-PEG2000 (Avanti Polar Lipids INC., Alabster,AL.).
- Acetic acid (EMD, Gibbstown, NJ, USA) was used to adjust the pH of the mobile phase.
- Acetonitrile (ACN) HPLC grade (EMD, Gibbstown, NJ, USA) was used for the preparation of the mobile phase for HPLC assays.
- Acetopromazine, ketamine and xylazine (Sigma Chemical Co., St. Louis, MO, USA) were used for the preparation of the anesthetic cocktail in the pharmacokinetic studies.
- Cholesterol (Avanti Polar Lipids INC., Alabster,AL.)
- Daidzein was purchased from LC Laboratories (Woburn, MA) as internal standard for UPLC/MS/MS.

- Dichloromethane (DCM) (EMD, Gibbstown, NJ, USA) was used in the preparation of microspheres.
- Dimethylsulfoxide (DMSO) (J. T. Baker Chemical Co., Phillipsburg, NJ, USA) was used in preparing stock solutions of LAZ and in the release medium of the protein binding and release studies.
- Glass beads (0.5-0.75 ,0.75-1 , 1-1.3 μm) (Glenmills , Clifton, NJ, USA)
- Heparin sodium salt (Sigma Chemical Co., St. Louis, MO, USA) used to prepare heparinized eppendorf tubes for blood collection in the pharmacokinetic studies.
- Hexadecyl Trimethyl Ammonium Bromide (Sigma Chemicals Co., St. Louis, MO, USA)
- Hydrogenated Soy Phophatidylcholine – HSPC (Avanti Polar Lipids INC.,Alabster,AL.).
- Lazaroid U-74389G (Biomol International LP , Plymouth Meeting, PA, USA).
- Methanol HPLC grade (EMD, Gibbstown, NJ, USA) was used to prepare wash solution for HPLC and stock solution of hydrocortisone.
- Phosphate-buffered saline (PBS) containing 140 mM NaCl (Sigma Chemical Co., St. Louis, MO, USA), 0.4 mM KH_2PO_4 (Sigma Chemicals Co., St. Louis, MO, USA) and 2 mM K_2HPO_4 (Fisher Scientific Co., Fair Lawn, NJ, USA), was used as release media for *in vitro* release studies of .
- Pluronic F108 (BASF Corporation, Mount Olive,N.J) was used to prepare the nanosuspension.

- Poly Lactic-Glycolic Acid Co-Polymer (PLGA) [Three polymers were used PLGA 85/15 (0.65 g/dL), PLGA 50/50 (0.5 g/dL) and PLGA 50/50 (0.45 g/dL)] Birmingham Polymers Inc., Birmingham, AL, USA
- Polyvinyl alcohol was used in the microsphere preparation (Sigma Chemicals Co., St. Louis, MO, USA) .
- Sodium Dodecyl Sulfate (Sigma Chemicals Co., St. Louis, MO, USA)
- Swiss nude mice (male, 25 – 30 gm) were provided by the Stehlin Foundation for Cancer Research (Houston, TX, USA) and were used for all *in vivo* pharmacokinetic and biodistribution experiments.
- Tetraethylammonim acetate tetrahydrate (Sigma Chemicals Co., St. Louis, MO, USA) was used to prepare the mobile phase of HPLC assay.
- Tween 80 (PCCA, Houston, TX, USA) were used for preparing LAZ nanosuspension formulations.

3.1.2 Supplies

- 250 ml rounded bottom flask for liposomes preparation.
- Alcohol wipes (Webcol® Alcohol Preps, Kendall Healthcare Products Co., Mansfield, MA, USA) were used to disinfect animal skin prior to administering the anesthesia in animal surgery.

- Cotton swabs (Q-tips, 6 inch) (Sherwood Medical, St. Louis, MO, USA) were used in animal surgery procedures in PK studies.
- Dialysis membrane (Spectra/Por Membrane, MW cutoff: 12-14,000, width: 23mm, diameter: 14.6 mm, Spectrum Labs. Inc., Rancho Dominguez, CA, USA) was used for in vitro release study of LAZ from nanosuspensions.
- Gloves (lightly powdered, Latex) were used during all experiments
- high-pressure extruder (Northern Lipids, Inc., Canada).
- Inserts (small volume) for samples in vials for HPLC analysis:
- Insulin syringes (1/2 cc, sterile) (Becton Dickinson & Co., Rutherford, NJ, USA) were used to administer the anesthesia intraperitoneally.
- Membrane filters (47mm, 0.45 µm, hydrophilic polypropylene; Pall Corp., Ann Arbor, MI, USA) were used to filter the mobile phase for the HPLC assays of CZ48 and MA.
- Paraffin laboratory film (Parafilm M, Pechiney Plastic Packaging, Chicago, IL, USA) was used whenever a temporary seal was required.
- Pipette tips (disposable, 1-10 µl, 10-100 µl and 100-1000 µl, VWR, West Chester,PA, USA) were used with appropriate pipettes (VWR, West Chester,PA, USA) to measure solutions for all experiments.
- Polycarbonate filters 50,80,100 and 200 nm (Whatman, Inc., Clifton, NJ, USA) for liposomes extrusion.

- Polyethylene microcentrifuge tubes (1.5 ml, Axygen Scientific Inc., Union City, CA, USA) were used for collecting and storing samples from the pharmacokinetic and efficacy studies.
- Surgical absorbent pads (Medline, Mundelein, IL, USA) were used during PK studies.

3.1.3 Equipments, Apparatus and Software

- ADAPT II (Biomedical Simulations Resource, University of Southern California, Los Angeles, CA, USA) was used to develop pharmacokinetic models for LAZ formulations.
- Balance (digital, 0.0001-g sensitivity, Mettler AE100, Mettler Instrument Corp., Hightstown, NJ, USA).
- Brookhaven Zetasizer with Zeta Plus Particle Sizing software Ver.3.85 (Brookhaven Instrument Corporation, NY, USA).
- BÜCHI R200 rotary evaporator (Flawil, Switzerland) and water bath (Buchi B-490) for liposomes preparation
- Centrifuge (Marathon 13K/M, B Hermle AG, Germany) .
- Computer software package NONMEM (Non Linear Mixed Effect Model) for population pharmacokinetics, version VI (Icon Development Solutions, Ellicott City, MD, USA).
- HPLC system consisted of :

    1- A XTerra® C18 column (5 μm, 150 x 4.6 mm i.d., Waters).

2- Empower 2 chromatography software applied for peak area integration with this system (Waters Corp., Milford, MA, USA).

3- Waters 515 pump as the solvent delivery system with a photodiode array detector (Waters 2996) and an auto-sampler (Waters 717).

- LC/MS/MS 3200 Q trap mass spectrometer (Applied Biosystem/MDS SCIEX, Foster City, CA, USA)
- Minitab student version 15 (Minitab Inc., PA, USA) was applied for statistical data analysis including ANOVA, ANOVA post-hoc tests and survival analysis.
- pH-meter (Corning Scholar 425, Corning, NY, USA).
- Pipettes (Eppendorf®, three sizes: 1-10 µl, 10-100 µl and 100-1000 µl).
- Reverse-phase C18 (XTerra®: 4.6 mm x 150 mm, particle size of 5 µm; Waters Corp., Milford, MA, USA).
- Shaking water bath (model YB-521, American Scientific Products, Japan).
- Tissue tearor (BioSpec Products, Inc).
- UPLC System:

  1- Waters AcquityTM with diode array detector (DAD)

  2- column, Acquity UPLC BEH C18 column (50×2.1mm I.D., 1.7_m, Waters, Milford, MA, USA);

- Vortex mixer (Vortex-2 Genie, Scientific Industries, Bohemia, NY, USA).
- WinNonlin Professional version 3.3 (Pharsight Corp., Mountainview, CA, USA.
- SEM (JEOL JSM 6400 Scanning Electron Microscope, Tokyo, Japan).

3.2 Methods

3.2.1 HPLC Assay

3.2.1.1 Chromatographic Conditions

The HPLC apparatus consisted of Waters Model 515 pump, Waters Model 717 plus autosampler and Waters Model 2996 photodiode array detector. The baseline resolution was achieved on an XTerra® C18 column (5 μm, 150 x 4.6 mm i.d.) at room temperature. The mobile phase consisted of acetonitrile: 22mM tetraethyl ammonium acetate 70:30 (v/v) at pH 6.8. The flow rate was 1.0 ml/min and LAZ detected at 254 nm.

3.2.1.2. Calibration Curves

3.2.1.2.1 Aqueous Standard Curves

Stock solutions of LAZ and MTS (1 mg/ml and 100 μg/ml, respectively) were prepared in methanol/acetonitrile (1:1). Various volumes of LAZ solution were diluted with methanol to make up 1 ml to obtain standard solutions with concentrations of 0.4, 2.5, 5, 10, 50 and 100 μg/ml. MTS (10μl of 100 μg/ml) was added to the LAZ standard solutions to yield a concentration of 1 μg/ml. For precision, accuracy and recovery studies, aliquots of the above stock solution were spiked to blank plasma and tissue homogenates to prepare calibration standards of 0.4 -100 μg/ml and quality control (QC) samples of 4, 40 and 80 μg/ml. The standard curves were constructed by plotting the peak area ratio of LAZ to MTS versus LAZ concentrations.

3.2.1.2.2 Plasma and Tissue Calibration Curves

Mouse organ homogenates were prepared by placing 1.5 gm of individual organs into 20 ml glass vials. Each organ was homogenized in 5 ml of acetonitrile by a tissue tearor

(Biospec Products Inc., USA). The same set of standard solutions and internal standard were spiked to either 100 µl of plasma or 200 µl of tissue homogenate. The samples were extracted as described below. The calibration curves were constructed by plotting the peak area ratio of LAZ to MTS versus LAZ concentrations.

3.2.1.3 Preparation of Quality Control (QC) Samples

Quality control samples with concentrations of 4.0, 40.0 and 80.0 µg/ml in various matrices were prepared to represent low, medium and high QC samples, respectively, and stored at −20 ^{o}C. The QC samples were thawed before analysis to determine intra- and inter-day precision and accuracy.

3.2.1.4 Precision and Accuracy

For the calculation of the intra-day precision and accuracy, three replicates of QC samples (4.0, 40.0 and 80.0 µg/ml) were prepared for aqueous, plasma and tissue homogenate samples as previously described. The concentrations were calculated from the calibration curves prepared on the same day of the assay. For the calculations of inter-day precision and accuracy, six replicates of the same QC samples were analyzed on three consecutive days along with the freshly prepared calibration curves.

3.2.1.5 Extraction Recovery

3.2.1.5.1 Extraction Procedure

Hundred 100 µL of plasma and organ homogenate samples were extracted by adding equal volume of acetonitrile. The mixture was vortexed for 30 sec and centrifuged at 10,000 rpm for 10 min. Ten µL of the supernatant was injected onto the HPLC system.

3.2.1.5.2 Extraction Recovery from Plasma and Organs

The recovery of LAZ from plasma and organ homogenate samples was calculated by preparing two sets of calibration curves. In the first set, LAZ standard solutions were added to the biomatrices followed by adding ACN to precipitate the proteins. The MTS solution was added to the extracted samples (supernatant after the centrifugation). In the second set, both LAZ and MTS solutions were added to the supernatant after the centrifugation of the biomatrices, taking the matrix effect into consideration. The assay recovery was calculated by dividing the mean slopes of the calibration curves from the first procedure (Extracted) by that from the second procedure (NON-Extracted) (Equation1).

$$\%Recovery = \frac{Slope\ of\ \ Extracted\ \ calibration\ Curve}{Slope\ of\ \ NON\text{-}Extracted\ \ Standard\ \ curve} \times 100 \qquad \text{Equation 1}$$

3.2.1.6 Stability Study

3.2.1.6.1 Stability Study of LAZ Stored Samples

The short-term stability of the extracted QC samples was determined as the percentage of remaining LAZ at room temperature for 6 hr. The long-term storage stability was determined after 10 day storage of the three extracted QC samples at -20 ^{o}C.

3.2.1.6.2 Stability Study of LAZ Samples in PBS, Plasma and CSF at 37^{o}C

A standard solution of LAZ was used to prepare a solution of 2 µg/ml in human plasma, CSF and PBS. Tween 80 was added to the solutions to yield a concentration of 0.2%v/v

to mimic the release media in release studies. At predetermined time points, a sample was withdrawn from the solution and analyzed by HPLC for LAZ content.

3.2.2 UPLC/MS/MS Assay

3.2.2.1 Instruments and Conditions

Linear ion trap quadrupole LC/MS/MS 3200Q trap mass spectrometer (Applied Biosystem/MDS SCIEX, Foster City, CA, USA) was used to determine LAZ in aqueous and biological matrices. The positive ion mode for MS/MS analyses was selected. The main working parameters of the mass spectrometer were: Curtain gas, 20 psi; gas 1 (nebulizer gas) 40 psi; gas 2 (heater gas) 50 psi; TurboIonSpray voltage 2500V; entrance potential (EP) 10V; collision energy (CE) 65V; collision cell exit potential (CXP) 3V; source temperature 600 ^{o}C; and declustering potential (DP) 99V. The quantification was performed using MRM method with the transitions of m/z 612→m/z 260 for LAZ, m/z 255→m/z 199 for Daidzein (IS) (Figure 3.1).

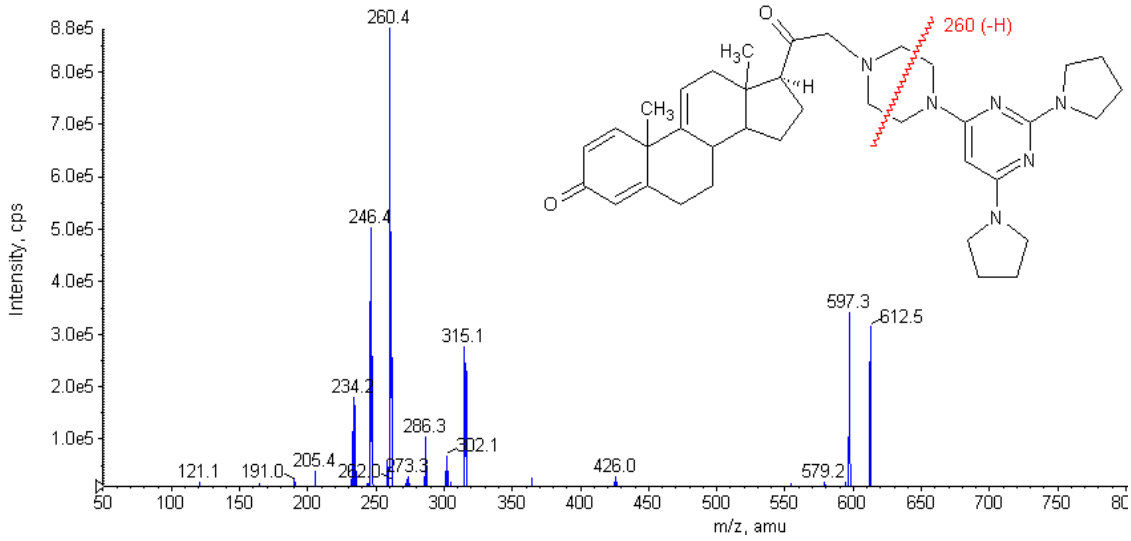

Figure 3.1 Chemical Structure and the MS^2 Full Scan for LAZ

3.2.2.2 UPLC Conditions

UPLC for analyzing LAZ in aqueous and biological samples consisted of Waters AcquityTM with diode array detector (DAD). The separation was performed on by injecting 10 µL of the sample on Acquity UPLC BEH C18 column (50×2.1 mm I.D., 1.7µm, Waters, Milford, MA, USA). Gradient elution with a mobile phase consisted of A, 0.1% formic acid and mobile phase B, 100% acetonitrile in the following sequence 0–0.5 min, 0–5% B, 0.5–2.4 min, 5–90% B, 2.4–3.1 min, 90–5% B was used to separate LAZ and IS from the matrices. The flow rate was 0.45 ml/min and the column temperature was kept at 45 ◦C.

3.2.2.3 Standard Stock and Working Solutions

Standard stock solutions of LAZ and IS were prepared in Acetonitrile at concentrations of 1.0 mg/ml and 100 µg/ml, respectively. Stock solutions were stored at -20^{o}C until they

were used for working solutions by adding appropriate volume of mobile phase (acetonitrile and 0.1% formic acid solution, 10:90, v/v).

3.2.2.4 Calibration Curves

3.2.2.4.1 Aqueous Standard Curves

Various volumes of LAZ solution were diluted with mobile phase to make up 1 ml to obtain standard solutions with concentrations of 15.6, 62.5, 250, 1000 and 4000 ng/ml of LAZ. Daidzein (10µl of 100 µg/ml) was added to the LAZ standard solutions to yield a concentration of 1 µg/ml..

3.2.2.4.2 Plasma and Tissue Calibration Curves

Mouse organ homogenates were prepared by placing 1.5 gm of individual organs into 20 ml glass vials. Each organ was homogenized in 5 ml of acetonitrile by a tissue tearor (Biospec Products Inc., USA). The same set of standard solutions and internal standard were spiked to 100 µl of plasma or tissue homogenate. The samples were extracted as described in section **3.2.1.5**. The calibration curves were constructed by plotting the peak area ratio of LAZ to Daidzein versus LAZ concentrations.

3.2.2.5 Preparation of Quality Control (QC) Samples

Quality control samples with concentrations of 125.0, 500.0 and 4000.0 ng/ml in various matrices were prepared to represent low, medium and high QC samples, respectively, and stored at −20 ^{o}C. The QC samples were thawed before analysis to determine intra- and inter-day precision and accuracy.

For precision, accuracy and recovery studies, aliquots of the above stock solution were spiked to blank plasma and tissue homogenates to prepare calibration standards of 15.6 - 4,000 ng/ml and quality control (QC) samples of 125, 500 and 4,000 ng/ml. The standard curves were constructed by plotting the peak area ratio of LAZ to IS versus LAZ concentrations

3.2.2.6 Method Validation

3.2.2.6.1 Linearity and Sensitivity

Calibration curves were constructed by plotting the ratios of the peak areas of LAZ to that of the IS versus LAZ concentration. The curves were fitted to the straight line by 1/y weighted least-squares linearity regression. The lower limit of quantification (LLOQ) was determined based on the signal-to noise ratio of 10:1.

3.2.2.6.2 Extraction Recovery and Matrix Effect

Blank plasma and tissue homogenates samples spiked with known LAZ concentration were used for testing specificity of the method. The extraction recovery of LAZ was evaluated by comparing the LAZ peak areas from blank plasma spiked with LAZ before the extraction with those from samples to which LAZ was added after the extraction. The potential matrix effect on the ionization was evaluated by comparing the peak areas of blank samples spiked with LAZ to those of the corresponding standard solution samples.

3.2.2.6.3 Accuracy and Precision

The intra-day and inter-day precision and accuracy were determined by analyzing three replicates of QC samples (125, 500 and 4,000 ng/ml) were prepared for aqueous, plasma

and tissue homogenate samples as previously described in one and three consecutive days. The concentration of each sample was calculated using a freshly prepared calibration curve.

3.2.3 LAZ Nanosuspension

3.2.3.1 Preparation of LAZ Nanosuspensions

LAZ nanosuspensions (NS) were prepared by wet milling technique. An appropriate amount of LAZ powder (40 mg), 0.5-0.75μm glass beads (1gm), 10% (w/w) pluronic F108 solution (0.1ml), 10% of Tween 80 solution (0.1ml) and water (0.2 ml) were added to a 10 ml scintillation vial. The mixture was stirred at 1,600 rpm for 8hr to produce LAZ nanosuspensions (NS-A). In another procedure, a mixture of glass beads (0.5-0.75: 0.75-1: 1-1.3 μm 1:1:1) instead of the single-sized beads was used. The same aforementioned procedure was followed to prepare the nanosuspension (NS-B) but with longer milling time (12hr). After preparing the nanosuspensions, the potential on the particles' surfaces was modified by adding 13 mM of CTAB to impart positive charge ($NS\text{-}A^{(+)}$) or by adding 1mM SDS to impart negative charge ($NS\text{-}A^{(-)}$ & $NS\text{-}B^{(-)}$).

3.2.3.2 Nanosuspension Characterization

3.2.3.2.1 Particle Size and Zeta Potential Measurements

The nanosuspensions were diluted (1:200) using double distilled water in a 4ml cuvette. The size and the surface potential of different NS formulations were determined using the Brookhaven Zetasizer with Zeta Plus Particle Sizing software Ver.3.85 (Brookhaven Instrument Corporation, NY, USA).

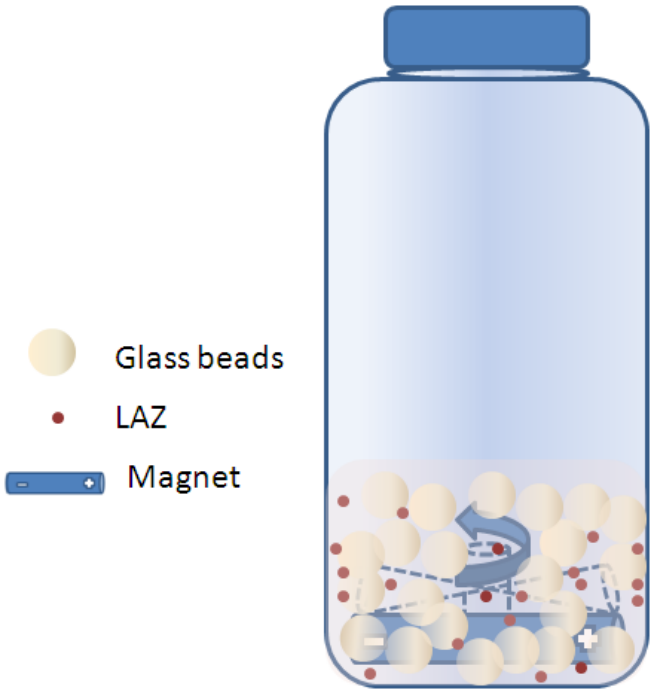

Figure 3.2 Wet Milling Technique for Nanosuspension Preparation

3.2.3.2.2 *In-vitro* Release of LAZ from Solution and Nanosuspensions of Two Sizes NS-A 250nm (NS-A, NS-A $^{(+)}$ and NS-A$^{(-)}$) and NS-B$^{(-)}$ 125 nm in PBS

In-vitro release experiments were performed by placing LAZ solution (control) or the four nanosuspensions (NS-A, NS-A $^{(+)}$, NS-A$^{(-)}$ and NS-B$^{(-)}$) in dialysis bags (Spectrum Labs. Inc., Rancho Dominguez, CA, USA) containing 0.5 ml of PBS. The length of the bags was approximately 4 cm. The dialysis bags were immersed in plastic tubes containing 20 ml of PBS with 0.2% Tween 80. The tubes were placed in a temperature controlled water bath at 37^{o}C and were shaken at 30 rpm. At 0.25, 0.5, 1, 2, 4, 6 and 8 hr a half ml of the solution outside the dialysis bag was drawn and immediately replenished with fresh medium. At 10, 24, 34 and 48 hr the whole medium outside the bag was replaced with a fresh medium. The samples taken at each time point were analyzed by HPLC to determine the amount of LAZ released.

3.2.3.2.3 *In-vitro* Release of LAZ from Solution and Nanosuspensions of Two Sizes NS-A 250nm (NS-A, NS-A $^{(+)}$ and NS-A$^{(-)}$) and NS-B$^{(-)}$ 125 nm in Human Plasma

In-vitro release profiles of the solution and the four NS formulations in human plasma were developed using the same procedure described in section 3.2.3.2.2., except that 0.5 ml of human plasma instead of PBS with was mixed with LAZ and placed in the dialysis bag.

3.2.3.2.3.1 Release Kinetics of LAZ from Nanosuspensions

To characterize the release profiles, zero order, first order, Higuchi's and Hixson-Crowell's equations were fitted to the release profiles. The goodness of fit was evaluated by comparing the **coefficient of determination**, $\boldsymbol{R^2}$, of the models fit.

The kinetic models are zero order (Equation 1) as percent drug remaining vs. time, first order (Equation 2) as log percent drug remaining vs. time, Higuchi's model (Equation 3) as cumulative percentage of drug released vs. square root of time and Hixson-Crowell model (Equation 4) as the cube root of the percentage of drug remaining in the matrix vs. time .

$$C = C_o - K_o t \qquad \text{Equation -2}$$

Where K_0 is the zero-order rate constant (hr^{-1}) and t is the time (hr). The zero-order rate describes the systems where the drug release rate is independent of its concentration.

$$lnC = lnC_o - Kt \qquad \text{Equation -3}$$

Where C_0 is the initial concentration of LAZ, k is the first order constant (% hr^{-1}), and t is the time. The first order describes the release from systems where the release rate is concentration dependent.

$$Q = Kt^{1/2} \qquad \text{Equation -4}$$

Where Q the Cumulative release and K is is the constant and t is the time in hours. Higuchi's model describes the release of drugs from an insoluble matrix as a square root of a time-dependent process based on Fickian diffusion.

To evaluate the drug release with changes in the surface area and the diameter of the particles, the data were also plotted using the Hixson-Crowell cube root law:

$$\sqrt[3]{Q_o} - \sqrt[3]{Q_t} = k_{HC} \times t \qquad \text{Equation -5}$$

where Q_t *is the amount of drug released in time t,* Q_o *is the initial amount of the drug , and* K_{HC} *is the rate constant for the Hixson-Crowell rate equation.*

3.2.3.3 Plasma Pharmacokinetics and Organ Distribution of LAZ Nanosuspensions with Various Sizes and Surface Potentials

3.2.3.3.1 Preparation of Dosing Formulations

LAZ solution (1.50 mg/ml) was prepared by dissolving LAZ into an acidic buffer (4.50 mg/ml NaCl, 0.94 mg/ml sodium citrate anhydrous, and 2.84 mg/ml citric acid in water, pH 3.0). LAZ NS were diluted using the milling medium to the same concentration as that of solution.

3.2.3.3.2 Mouse Study Protocol

All experiments were conducted in accordance with NIH Guidelines for the Care and Use of Animals and with approved animal protocol from the University of Houston Institutional Animal Care and Use Committee (IACUC). Male Swiss athymic nude mice (20-25 g) were a gift from Stehlin Foundation for Cancer Research (Houston, TX, USA). Mice were maintained in individual ventilated cages under standard laboratory conditions (12-hour light/dark cycle) with free access to food and water. Before pharmacokinetic

and biodistribution studies, the mice were randomized among 5 groups and anesthetized by anesthesia cocktail (ketamin 50 mg/ml, Xylazine 3.3 mg/ml and Acetopromazine 3.3 mg/ml) prior to dosing. LAZ solution (1.5 mg/ml) was prepared by dissolving LAZ with an acidic buffer. LAZ concentration in the NS formulations was adjusted to 1.5 mg/ml as well. The formulations of solution, NS-A, cationic NS-$A^{(+)}$, anionic NS-$A^{(-)}$ or anionic NS-$B^{(-)}$ were administered to the animal groups at a dose of 10 mg/kg by injection through the retro-orbital venous sinus. Three mice were sacrificed at 10, 15, 30, 45, 60 and 180 min post dose, and blood was collected in heparinized tubes by syringe cardiac puncture from the heart. The plasma was obtained by centrifuging the blood samples at 10,000 rpm for 10 min and stored at -20 ^{o}C until HPLC assay. The organs of liver, kidneys, spleen, heart, lungs and brain were harvested after cardiac perfusion with 10 ml of saline to remove the residual blood. The harvested organs were stored at -20^{o}C until HPLC assay. The frozen samples were thawed at room temperature prior to the assay.

3.2.3.3.3 Pharmacokinetics Analysis

PK and statistical data analyses were performed using WinNonlin and MINITAB 14. WinNonlin was used to model LAZ profiles using a non- compartment model for mouse samples. The non-compartment model uses Linear Trapezoidal Method, Equation (6), applied to each pair of consecutive points in the data set and sums up these areas to estimate the area under the curve (AUC).

$$AUC_{t2}^{t1} = \Delta t \times \frac{C_1 + C_2}{2} \qquad Equation - 6$$

To estimate the elimination rate constant (K_e or lambda *z*), regressions of the concentration time profile are repeated using the last three points with non-zero concentration, then the last four points etc.. For each regression, an adjusted R^2 is computed:

$$Adjusted\ R^2 = 1 - \frac{(1-R^2)\times(n-1)}{(n-2)} \qquad Equation-7$$

Where n is the number of data points in the regression and R^2 is the square of the correlation coefficient. The regression with the largest adjusted R^2 is selected to estimate lambda *z*. Once the time points have been determined, lambda *z* is estimated by performing a regression of the natural logarithm of the concentrations on sampling time, for those times in the specified time range.

$$Lamdda\ z = -1\times slope\ of\ \ regression\ line \qquad Equation-8$$

3.2.3.3.4 Statistical Analysis

Sparse sampling was used in the collection of *in-vivo* data; that is, each animal contributed with a single observation and the area under the concentration-time curve was constructed from the mean plasma concentration from multiple mice at each time point. Therefore, the variance of AUC_{0-t} was estimated using the method described by Bailer (1988)[71]. This method allows for the determination of the variability in AUC estimate from the variability about the mean concentration at each time point, assuming that the mean at each time point is independent and the terminal rate constant is the same for each

animal. The statistical significance of the differences ($P<0.05$) between the other parameters were evaluated by one-way ANOVA followed by post hoc Tukey's test.

3.2.4 Microspheres

3.2.4.1 Microsphere preparation

To prepare LAZ microspheres, three PLGA polymers were used; PLGA-A 85/15 (0.65 g/dL), PLGA-B 50/50 (0.5 g/dL) and PLGA-C 50/50 (0.43 g/dL). Various amounts of the polymer were dissolved in Dichloromethane (DCM) to give different polymer concentrations in the organic solvent. Various amounts of LAZ were dissolved in the polymer solution in DCM with the aid of a magnetic stirrer for 1 min. This organic phase was then poured into 20 ml of 1-5 % (w/v) aqueous polyvinyl alcohol (PVA) solution and was homogenized (at a speed of 3000 rpm) for 5 min. The organic and the aqueous phases formed an O/W emulsion which was poured into 200 ml of a 0.1% (w/v) aqueous PVA solution and stirred for 3 hr. During the period of 3 hr, the organic phase started to migrate into the large stabilizer solution to evaporate and the resulting microspheres precipitated. The microspheres were collected by filtration and were lyophilized after being washed three times with distilled water.

3.2.4.1.1 An Alternative Approach

The formulation composition that yielded the highest EE from the aforementioned method was selected to test another method for microspheres preparation. After formation of the primary emulsion as in the previous method, the preparation was kept in

-20^{o}C freezer for 10 min to increase the emulsion viscosity. The cold preparation was centrifuged to separate the viscous emulsified drug from the continuous phase. Different temperatures and speeds of the centrifugation process were tested to enhance the EE. The microspheres were separated as a cake in the bottom of the centrifuge tubes and were separated by removing the top decantant leaving the cake. The cake was collected, washed and lyophilized. Tables 3.1and 3.2 show the formulations variables that were tried in order to obtain the highest EE. Each formulation was prepared in triplicate.

3.2.4.2 Microspheres Characterization

3.2.4.2.1 Determination of Lazaroid Content in the Microspheres

Lazaroid content in the microspheres was quantified using the extraction method. Accurately 10 mg of the microspheres was incubated with 1 ml of acetonitrile to dissolve the polymer. After 30 min sonication, the mixture was poured into water: acetonitrile (1:2) to constitute a volume of 20 ml, whereupon the polymer was precipitated and the drug dissolved in the solvent mixture. The suspension was centrifuged at 4000 rpm for 20 min and the supernatant was collected for HPLC assay. The actual drug loading and encapsulation efficiency (EE) was calculated using the following equations:

$$Theoretical\ Drug\ Loading = \frac{Drug\ Weight}{Weight\ of\ (Drug + Polymer)} \quad Equation - 9$$

$$Actual\ Drug\ Loading = \frac{Encapsulated\ Drug\ Weight}{Weight\ of\ (Drug + Polymer)} \quad Equation - 10$$

$$Enacapsulation\ efficiency = \frac{Actual\ Drug\ Loading}{Theoretical\ Drug\ Loading}\ Equation\text{-}11$$

$$Loading\ Capacity = \frac{Encapsulated\ drug\ weight}{Actual\ Microsphere\ weight} \times 100\ Equation\text{-}12$$

3.2.4.2.2 Scanning Electron Microscope (SEM)

The shape, size and surface morphology of the microspheres were observed by SEM (JEOL JSM 6400 Scanning Electron Microscope, Tokyo, Japan). The microspheres were fixed on a carbon specimen stub and examined under the microscope.

3.2.4.2.3 *In-vitro* LAZ Release from Microspheres Consisted of Three PLGA Polymers (0.43, 0.50 and 0.65 g/dL) in CSF

In vitro release experiments were performed by placing microspheres equivalent to 5 mg of LAZ in dialysis bags (Spectrum Labs. Inc., Rancho Dominguez, CA, USA) containing 1 ml CSF with 0.1% sodium azide. The dialysis bags were placed in plastic tubes with 20 ml of PBS with 0.2% Tween 80. The tubes were placed in a temperature controlled water bath at 37 ^{o}C and were shaken at 30 rpm. At 0.25, 0.5, 1, 2, 4 and 6 hr and 1 day a half ml of the solution outside the dialysis bag was drawn and immediately replenished with fresh medium. On the following 2, 4, 6, 9, 12, 17 and 21 days the PBS medium was completely replaced with a fresh one. The samples taken at each time point were analyzed by HPLC to determine the amount of LAZ released. For control group, LAZ solution was used instead of the microspheres in the dialysis bag.

3.2.4.2.3.1 Release Kinetics of LAZ from Microspheres

To characterize the release profiles, the procedures in section **3.2.3.2.3.1** were followed.

Table 3.1 Various Microspheres Formulations Composition Using O/W Emulsion Solvent Evaporation Method

Formulation #	Drug (mg)	PLGA		PVA
		type	conc	
1	40	85/15 0.65 g/dL	250 mg/5ml DCM	1%
2	40			5%
3	40		500 mg/5ml DCM	1%
4	40			5%
5	40		1 g/5ml DCM	1%
6	40			5%
7	20	50/50 0.5g/dL	250 mg/5ml DCM	1%
8	40			
9	80			
10	20			5%
11	40			
12	80			
13	40		500 mg/5ml DCM	1%
14	40			5%
15	40		1 g/5ml DCM	1%
16	40			5%
17	20	50/50 0.43g/dL	250 mg/ 5ml DCM	5%
18	40			
19	80			
20 cold	40			

Table 3.2 Various Microspheres Formulation Conditions for Formulation #20 Cold

	Centrifugation speed	Temperature (^{o}C)
20-A	rpm 3000	15
20-B	rpm 7000	15
20-C	rpm 7000	5
20-D	rpm 7000	-10
20-E	rpm 10 000	15
20-F	rpm 10 000	25
20-G	rpm 10000	5
20-H	rpm 15 000	15

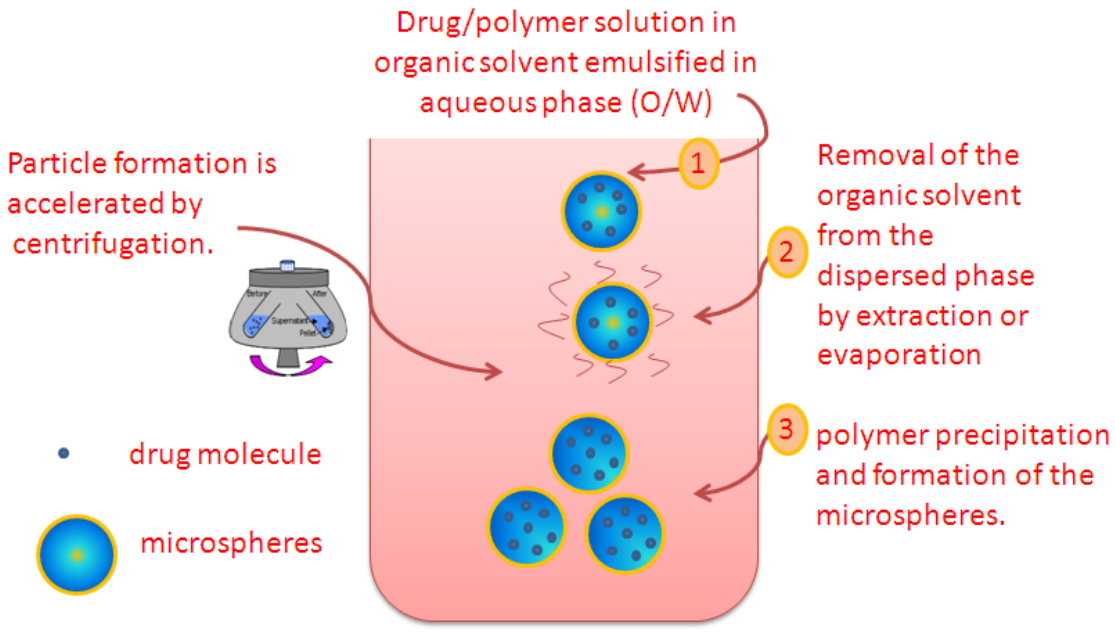

Figure 3.3 Microspheres Preparation Using O/W Emulsion Solvent Evaporation Method

3.2.5 Liposomes

3.2.5.1 Liposomes Preparation

LAZ liposomes were prepared by the modified thin-film hydration method. The lipid components of the liposomes were dissolved in (chloroform: methanol - 1:1) to give a stock solution of 20mg/ml of each lipid component. The hydrophobic components, such as lipids (HSPC, cholesterol and/or DSPE-PEG 2000) and LAZ (1mg solution in methanol) were transferred into a suitable rounded-bottom flask according the volume ratios for each preparation (Table 3.3). The flask was then connected to a BÜCHI R200 rotary evaporator (Flawil, Switzerland) and immersed in a water bath (Buchi B-490) with temperature maintained at 60^{o}C. The organic solvent was evaporated by immersing the flask in the water bath and was kept rotating at 40 rpm speed for 2hr with the aid of vacuum applied into the flask. The dry lipid film was maintained overnight under vacuum after removing the flask from the water bath to remove traces of the organic solvents. The lipid film was then hydrated with 3 ml normal saline by rotating the flask at 40rpm for 1 hr at 60^{o}C until the lipid film was completely hydrated and a homogeneous dispersion was formed. The liposomal dispersion was then extruded by the pressure of nitrogen gas through polycarbonate filters (Whatman, Inc., Clifton, NJ, USA) using a high-pressure extruder (Northern Lipids, Inc., Canada) at 60^{o}C. The extrusion was done through a single membrane filter in the following order 200 nm, 100 nm, 80 nm and 50 nm, three cycles each. The free un-entrapped LAZ was removed by equilibrium dialysis using dialysis membrane (cut-off 12-14 KD, Spectrum Labs. Inc., Rancho Dominguez , CA,

USA) against saline at 4°C. The liposomes dispersions were then stored in the refrigerator at 4°C.

Table 3.3 LAZ Liposomes Composition

Formulation	Lipid		
	HSPC	Cholesterol	DSPE-PEG2000
Lipo A	9	1	0
Lipo B	8	2	0
Lipo C	7	3	0
Lipo G	6	2	2
LAZ : Lipid 1:10 wt/wt (2.5/25 mg)			

3.2.5.2 Liposomes Characterization

3.2.5.2.1 Vesicle Size and Zeta Potential

The liposomes size and surface zeta potential for each preparation was determined using the Brookhaven Zetasizer with Zeta Plus Particle Sizing software Ver.3.85 (Brookhaven Instrument Corporation, NY, USA).

3.2.5.2.2 Entrapment Efficiency of LAZ

Entrapment efficiency of LAZ in liposomes was determined after removal of free un-entrapped LAZ. Briefly, 100 µL of liposomes dispersion was dissolved in 500uL methanol. LAZ concentration was determined using HPLC after spiking the solution with MTS as IS. The entrapment efficiency was determined by comparing the LAZ actually entrapped in the liposomes to the theoretical amount added to the preparation.

$$Entrapment\ Efficiency\ (EE\%) = \frac{Entrapped\ Drug\ in\ liposomes}{Theoretical\ Drug\ in\ liposomes} \times 100 \qquad Equation\ 13$$

3.2.5.2.3 Differential Scanning Calorimetry (DSC)

Transition phase temperatures (T_c) of Lipo G membranes were studied by differential scanning calorimetry (DSC) using Q2000 Model Differential Scanning Calorimeter (DSC-TA Instruments, New Castle, DE, USA). The liposomal dispersions were lyophilized before DSC analysis. Two hermitically sealed pans were used, the first as a reference (empty pan) and the second one contained a known weight of lipids, LAZ or liposomes powder. The pans were heated at 10^{o}C/min from 35 - 100 ^{o}C or 200^{o}C. Phase transition (T_c) temperatures and melting points (T_m) were computed using the TA Universal Analysis program V.4.7A.

3.2.5.2.4 *In-vitro* LAZ Release from Liposomes of Four Lipid Composition (Conventional Lipo A, B, C and PEGylated Lipo G) in PBS and Plasma

In vitro release experiments were performed by placing an equivalent amount of liposomes to 30 µg of LAZ in dialysis bags (Spectrum Labs. Inc., Rancho Dominguez, CA, USA) containing 0.5 ml of PBS or plasma. The dialysis bags were placed in plastic tubes with 20 ml of PBS containing 0.2% Tween 80. The tubes were placed in a temperature controlled water bath at 37 ^{o}C and were shaken at 30 rpm. At 15 min, 30 min, 45 min, 2 hr, 4 hr, 6 hr, 8 hr, 10 hr and 24 hr, a half ml of the solution outside the dialysis bags was withdrawn and immediately replenished with fresh medium. The samples taken at each time point were analyzed using UPLC-MS/MS to determine the amount of LAZ released. For control group, LAZ solution was used instead of the liposomes in the dialysis bag.

3.2.5.2.4.1 Release Kinetics of LAZ from Liposomes

To characterize the release profiles, the procedures in section **3.2.3.2.3.1.** were followed.

3.2.5.2.5 Physical Stability of Liposomes

The physical stability of liposomes was assessed by measuring the size, polydispersity index and encapsulation efficiency of the refrigerated preparations over time.

3.2.5.3 Pharmacokinetic and Biodistribution Studies of Lipo B and Lipo G in Athymic Swiss Nude Mice

The aim of this study was to establish the PK of LAZ from the solution, Lipo B and Lipo G upon 1 mg/kg IV administration to athymic Swiss nude mice. Also, we wanted to estimate the possible brain passive targeting using the liposomes to pursue the efficacy study in brain tumor bearing model.

3.2.5.3.1 Mouse Study Protocol

Male athymic Swiss nude mice (20-25 g, three month old of age) were obtained from Stehlin Foundation for Cancer Research (Houston, TX, USA). Mice were maintained in individual ventilated cages under standard laboratory conditions (12-hour light/dark cycle) with free access to food and water. Before pharmacokinetic and biodistribution studies, the mice were randomized among 3 groups and anesthetized by anesthesia cocktail (ketamin 50 mg/ml, Xylazine 3.3 mg/ml and Acetopromazine 3.3 mg/ml) prior to dosing. LAZ solution (0.75 mg/ml) was prepared by dissolving LAZ into an acidic buffer (4.5 mg/ml NaCl, 0.936 mg/ml sodium citrate anhydrous, and 2.84 mg/ml citric acid in water, pH 3.0). LAZ concentration in Lipo B and Lipo G formulations was

adjusted to 0.75 mg/ml. The formulations of the solution, Lipo B or Lipo G were administered to the animal groups at a dose of 1 mg/kg by injection through the retro-orbital venous sinus. Three mice were sacrificed at 0.25, 0.5, 0.75, 1, 2, 4, 6 and 8 hr post dose, and blood was collected in heparinized tubes by syringe cardiac puncture. The plasma was obtained by centrifuging the blood samples at 10,000 rpm for 10 min and stored at -20 ^{o}C until the UPLC/MS/MS assay. The organs of liver, kidneys, spleen, heart, lungs and brain were harvested after cardiac perfusion with 10 ml of saline to remove the residual blood. The harvested organs were stored at -20^{o}C until the UPLC-MS/MS assay. The frozen samples were thawed at room temperature prior to the assay.

3.2.5.3.2 Pharmacokinetics Analyses

PK and statistical data analyses were performed using WinNonlin, ADAPT II, and MINITAB 14. WinNonlin was used to model LAZ profiles using a non- compartment model for mouse samples to estimate the area under the curve (AUC), clearance (CL), elimination rate constant (K_e), volume of distribution (V_d) and elimination half life ($t_{1/2}$) for the formulations. Moreover, an ADAPT II model was constructed to provide the capability of co-modeling LAZ plasma concentrations with those of the brain to estimate the inter-compartmental distribution constants to and from the brain. Three-compartment model with zero-order input and 1st-order elimination from both the central compartment and the brain was best fit to data.

Two models were constructed using ADAPT II for co-modeling. Appropriate model selection was based on: (a) Minimum value for the diagnostic statistic of Akaike's information criterion (AIC) (b) Correlation coefficient, R^2, between the observed datum points and the calculated ones based on the selected model; (c) Visual inspection of the observed datum points and the corresponding model-generated plasma concentration-time profiles. The equation used for AIC was:

$$AIC = n \times ln\, W_{SS} + 2p \qquad \text{Equation 14}$$

Where n is the number of datum points, p is the number of parameters to be estimated and W_{SS} is the weighted sum of squares calculated according to Equation 13:

$$W_{SS} = \sum (Y_{obs,\,i} - Y_{cal,\,i})^2 \times W_i \qquad \text{Equation 15}$$

Where W_i is a weighting factor for fitting the model to the experimental data (drug concentration) and can be $1/Y$ or $1/Y^2$, $Y_{obs,i}$ is the measured drug concentration and $Y_{cal,i}$ is the estimated value for that drug concentration.

3.2.5.3.3 Statistical Data Analysis

Statistical significance was evaluated by ANOVA and Tukey's post-hoc for more than two groups with a $P<0.05$ for significance. MINITAB student 15 was used for the statistical analysis. In case of mouse pharmacokinetics and distribution study, Sparse sampling was used in the collection of in-vivo data; that is, each animal contributed with

a single observation and the area under the concentration-time curve was constructed from the mean plasma concentration from multiple mice at each time point. Therefore, the variance of AUC_{0-t} was estimated using the method described by Bailer (1988)[71]. This method allows for the determination of the variability in the AUC estimate from the variability about the mean concentration at each time point, assuming that the mean at each time point is independent and the terminal rate constant is the same for each animal.

3.2.5.4 Pharmacokinetics and Proof of Concept Efficacy of Lipo G of Suppressing Glioblastoma Tumor Growth in Mice

3.2.5.4.1 Cell Lines

Glioblastoma cell line U87-luc (U87 glioblastoma cells expressing firefly luciferase reporter gene) was obtained from Santosh Kesari in Dana-Farber Cancer Institute at Harvard Medical University. U87-luc cells were grown in DMEM containing 10% fetal bovine serum (FBS), 1% penicillin/ streptomycin, 1% L-glutamine, and 0.5mg/ml G418 (Geneticin sulfate).

3.2.5.4.2 Animals

Male SCID (severe combined immune deficiency) hairless outbred mice (4 weeks old, 15–25gm body weight) were purchased from Charles River Laboratories (Wilmington, MA) and were bred and kept with controlled temperature and humidity with 12 h light: dark cycles in Methodist Hospital Research Institute laboratory. All experiments were

performed according to guidelines of the Methodist Hospital Research Institute (TMHRI).

3.2.5.4.3 Intracerebral Xenograft

Mice were anesthetized (fails to respond to a foot-pinch test) by intraperitoneal injection of a cocktail of Ketamine and Xylazine and immobilized in a stereotaxic instrument (David Kopf Instruments, Tujunga, CA). A burr hole was drilled 0.5mm posterior and 2.5mm lateral to the bregma. U87-Luc cell suspension (100,000 cells in 2 μL of phosphate-buffered saline) was injected over a period of 5 minutes using a 5 μL Hamilton syringe (Reno, NV) with a 1-in, 26-gauge needle at a depth of 3.5 mm from the brain surface. Upon withdrawal of the needle, the wound was immediately sealed with Wound Clips. Tumor cells were allowed to form solid tumor mass during the following seven days and confirmed by *bioluminescence* imaging (BLI).

3.2.5.4.4 Study Design

The mice were randomized among the following groups: control (M), control received radiation (M+R), control received radiation with Lipo G (M+R+L) or control received Lipo G (M+L). The liposomal formulation was given at a dose of 5mg/kg by intraperitoneal injection (IP) twice a week to M+L and M+R+L groups. For the radiation treated groups, the Lipo G dose was given 5 min prior to radiation to ensure the highest concentration in the brain prior to radiation. The animals had a whole body irradiation at

a dose of 2 Gy once a week. Blood samples were drawn from the tail veins one and two hours after injection in heparinized tubes. Plasma was separated by centrifuging the heparinized samples at 14,600 rpm for 20 min. The plasma samples were kept at -20^{o}C until UPLC-MS/MS assay.

3.2.5.4.5 Bioluminescence Imaging (BLI)

Mice were imaged every week to monitor the growth of the engrafted tumors with the Xenogen IVIS 200 system. A freshly prepared solution of D-Luciferin (Caliper Life Sciences, Hopkinton, MA) at 15 mg/ml in DPBS was given to the animals at a dose of 150 mg D-Luciferin/kg intraperitoneally 10 minutes before imaging. A bioluminescent acquisition sequence of 4 images was performed between 10 and 25 minutes after D-luciferin injections to determine peak signals. The Living Image®2.50.1 software (Xenogen Corp.) was used for data analysis based on total photon flux emission (photons/sec) in the region of interest over the intracranial space.

3.2.5.4.6 Harvest and Immunohistochemistry of Brain Tissues

At the end of the experiments, brains were harvested for immunohistochemistry. Briefly, mice were deeply anesthetized by intraperitoneal injection of cocktail of Ketamine and Xylazine, and then were perfused transcardially with PBS followed by 4% paraformaldehyde. The brain tissue were harvested and fixed in 4% formaldehyde for immunohistochemistry. Brain sections (10μm thick) were serially cut and stained with

hematoxylin and eosin (H & E), CD34 and Ki67 according to manufacturer's suggested procedures.

3.2.5.4.7 Malondialdehyde (MDA) Detection in Brain Tissues

Prior to analysis of MDA, brain samples from the three treatment groups were placed in 0.5 ml PBS buffer with 50 µl of 5 mM butylated hydroxytoluene (BHT; Oxis Research, Portland, OR) to prevent further lipid peroxidation. MDA levels were assessed using the commercially available colorimetric MDA-586 assay kit from OXIS Research with the absorbance read at a wavelength of 586 nm. MDA concentrations were normalized to tissue weight (mg).

3.2.5.4.8 Statistical Data Analysis

Statistical significance was evaluated by ANOVA and Tukey's post-hoc for more than two groups with a $P < 0.05$ for significance. MINITAB student 15 was used for the statistical analysis and Kaplan Meir survival analysis in the efficacy studies.

3.2.5.4.9 Population Pharmacokinetics Modeling

LAZ plasma concentration–time data were modeled using the computer software package NONMEM (Non Linear Mixed Effect Model), version VI (Icon Development Solutions, Ellicott City, MD, USA). Compilation and linking was achieved using Compaq Visual Fortran version 6.6 compiler. The subroutines of ADVAN1 TRANS1 (1-Compartment IV), ADVAN3 TRANS1 (2-Compartment IV), ADVAN11 TRANS1 (3-Compartment

IV), ADVAN2 TRANS1 (1-Compartment EXIV), ADVAN4 TRANS1 (2-Compartment EXIV) and ADVAN12 TRANS1 (3-Compartment EXIV) were fitted to the data. Models were selected based upon: (a) a 3.84 reduction in the objective function value (OFV) (P value 0.05 in approximate Chi^2 distribution), (b) improvement in individual plots and (c) Akaike's Criteria (AIC).

3.2.5.4.9.1 Fixed Effects Modeling

The population analysis was performed in the absence of potential covariates (i.e., base model), then each candidate covariate was screened in turn by adding it to the base model and noting the value of the OFV. Changes in the OFV approximate the $[chi]^2$ distribution with a degree of freedom equal to the number of covariates introduced. A drop of more than 3.84 in the OFV after the addition of a single covariate indicates a statistically significant ($p < 0.05$) improvement in the fit of the data. Significant covariates were added stepwise to the base model in descending order of their contribution to the reduction in the OFV during the initial screening until the decrease in OFV was <3.84 units.

3.2.5.4.9.2 Random Effects Modeling

The difference between the apparent LAZ clearance in the j*th* individual (k_j) and the typical value (TVK) in the study population was estimated using the following error models:

$K_j = TVK + [\eta]_{jK}$ Additive interpatient variability, or

$K_j = TVK \times (1 + [\eta]_{jK})$ Proportional interpatient variability

in which $[\eta]_{jK}$ is a random variable distributed with a mean of 0, and variance (estimated by NONMEM) of Ω_k^2, the latter term representing interpatient variability in K_j about TVK.

Intra-patient variability representing deviations among pairs of observed responses (i.e., plasma LAZ concentrations) and those predicted by the population model was also modeled:

$$C_{ij} = C_{pred,ij} + [\varepsilon]_{1,ij} \qquad \text{Additive intrapatient}$$

in which C_{ij} is the *i*th observed LAZ concentration for the *j*th patient, $C_{pred,ij}$ is the LAZ concentration predicted by the pharmacokinetic model, and $\varepsilon_{1,ij}$ is randomly distributed term in which each ε has zero mean and variances of σ_k^2. Such ε errors are caused by influences such as assay variability, choice of an inappropriate pharmacokinetic model, and timing errors in drug administration and blood sampling. The same random errors were generated for the volume of distribution.

CHAPTER 4 RESULTS

4.1 HPLC Assays for Quantification of LAZ in Aqueous Solution and Biological Samples

The reported HPLC assay is a rapid and convenient method for the quantification of LAZ in mouse plasma and organs of liver, lungs, kidneys, spleen, heart and brain. This is the first reported assay to quantify LAZ in aqueous and biological samples. The developed method was simple using solvent extraction with acetonitrile. MTS was chosen as the internal standard for its chemical structure similarity to LAZ. The chromatograms of aqueous, blank plasma and organs had no interfering peaks to LAZ and MTS (Figures 4.1- 4.8). The retention times of LAZ and MTS were 6.8 and 2.7 min, respectively. The calibration curves were linear in the range of 0.4 –100 µg/ml for all matrices with an average correlation (R^2) > 0.99. The LLOQ was 0.4 µg/ml. The mean recovery of LAZ was 94-105% except that from the liver, 68% (Figure 4.3). The intra-day precision (%C.V.) was less than 8% (n = 3) and accuracy ranged from 96 to 106% (Table 4.1). The inter-day precision (%C.V.) was less than 8% and accuracy ranged from 96 to 107% (Table 4.1). LAZ QC samples (4, 40 and 80 µg/ml) were stable when left at room temperature for 6 hr (short term stability) or stored at -20^{o}C for 10 days. The percentage variation observed for the short term stability was within the range of 93-104 % (Table 4.2). The long term storage stability was performed over a period of 10 days at -20^{o}C and the percentage variation observed was within the range of 98-101 % (Table 4.2).

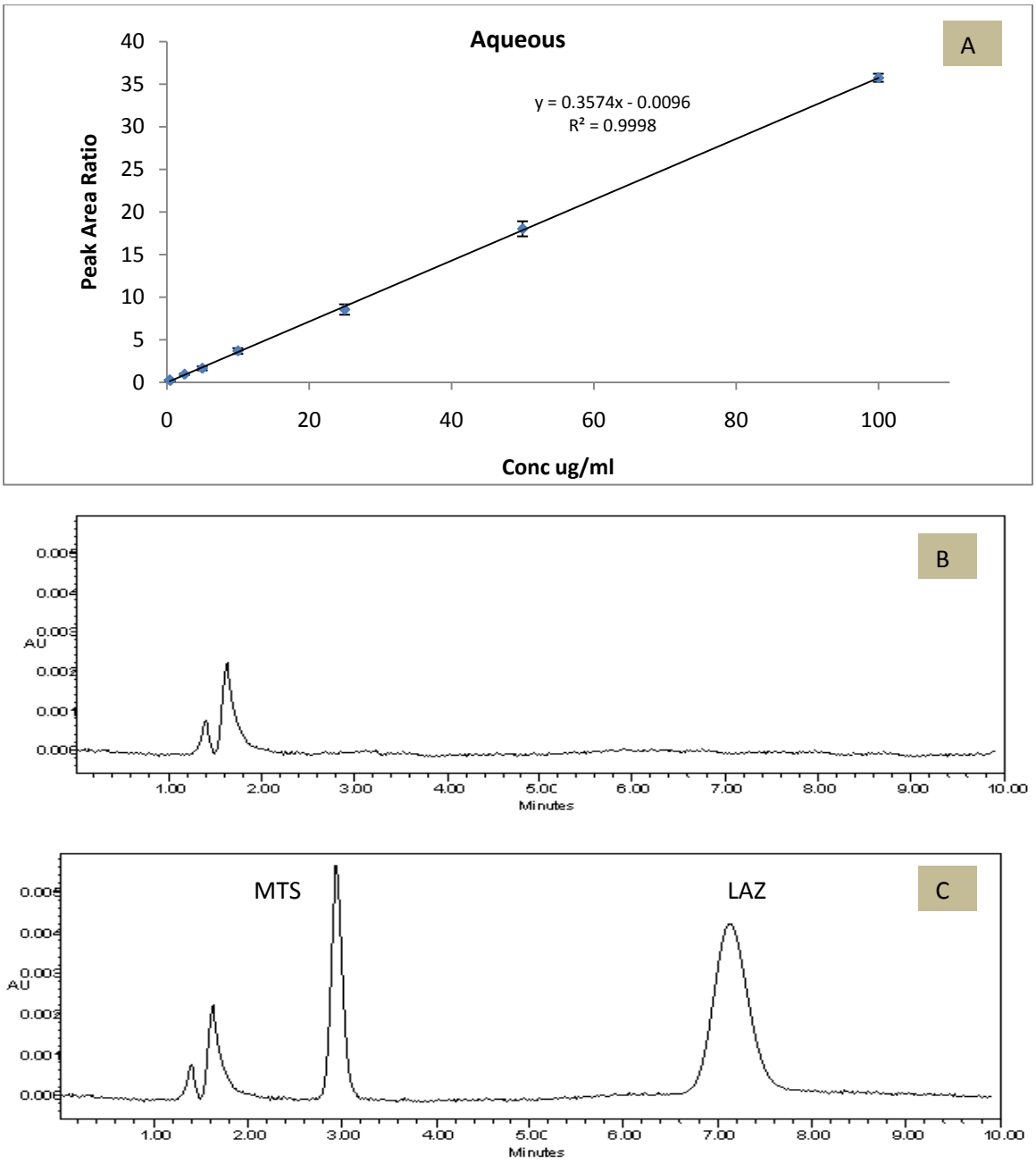

Figure 4.1 (A) Standard Curve of LAZ in PBS and HPLC Chromatograms of LAZ in (B) Blank PBS Sample and (C) Spiked PBS Sample at 10 µg/ml

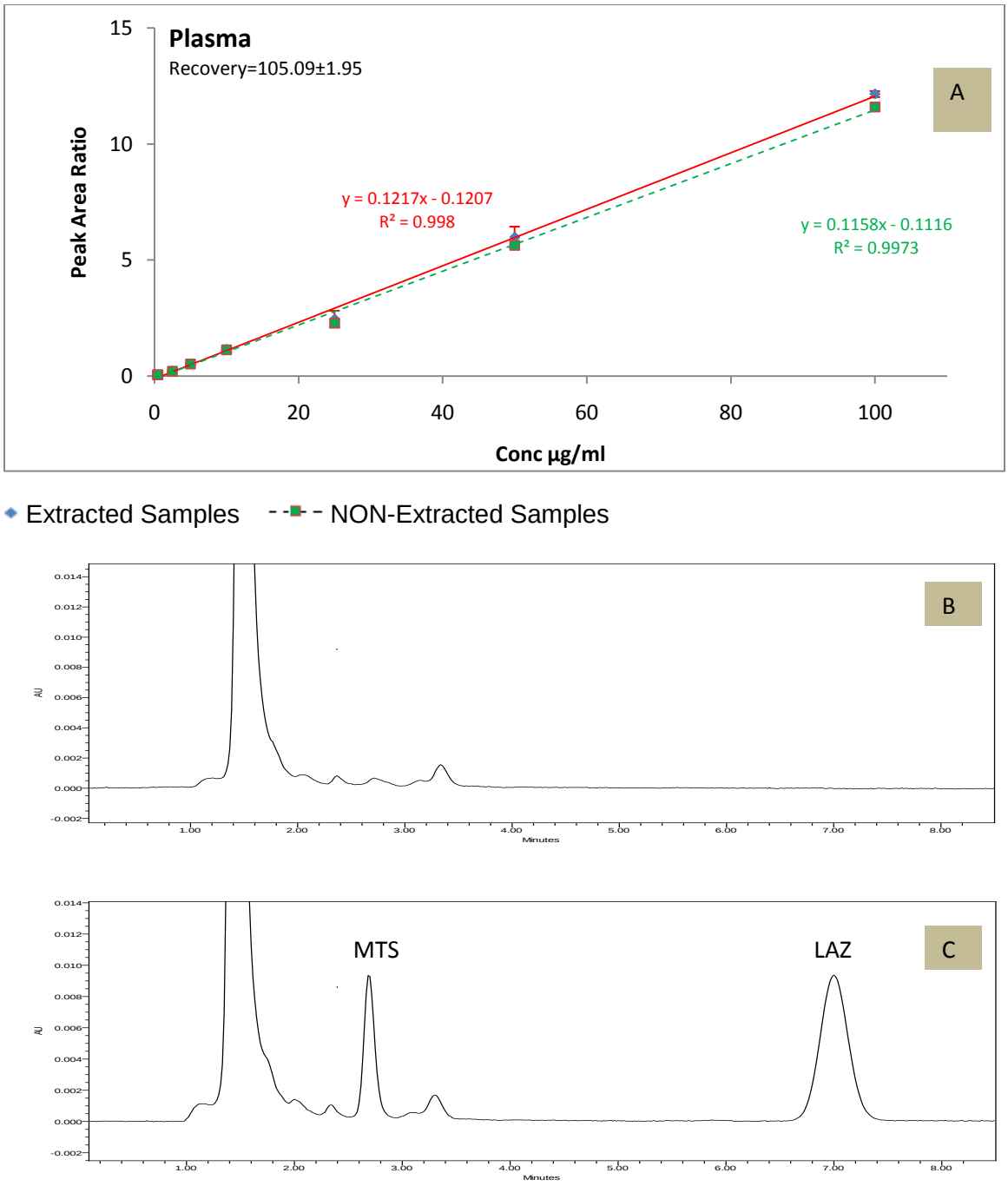

Figure 4.2 (A) Calibration Curves of LAZ in Plasma Samples and HPLC Chromatograms of LAZ in (B) Blank Plasma Sample and (C) Spiked Plasma Sample at 10 µg/ml

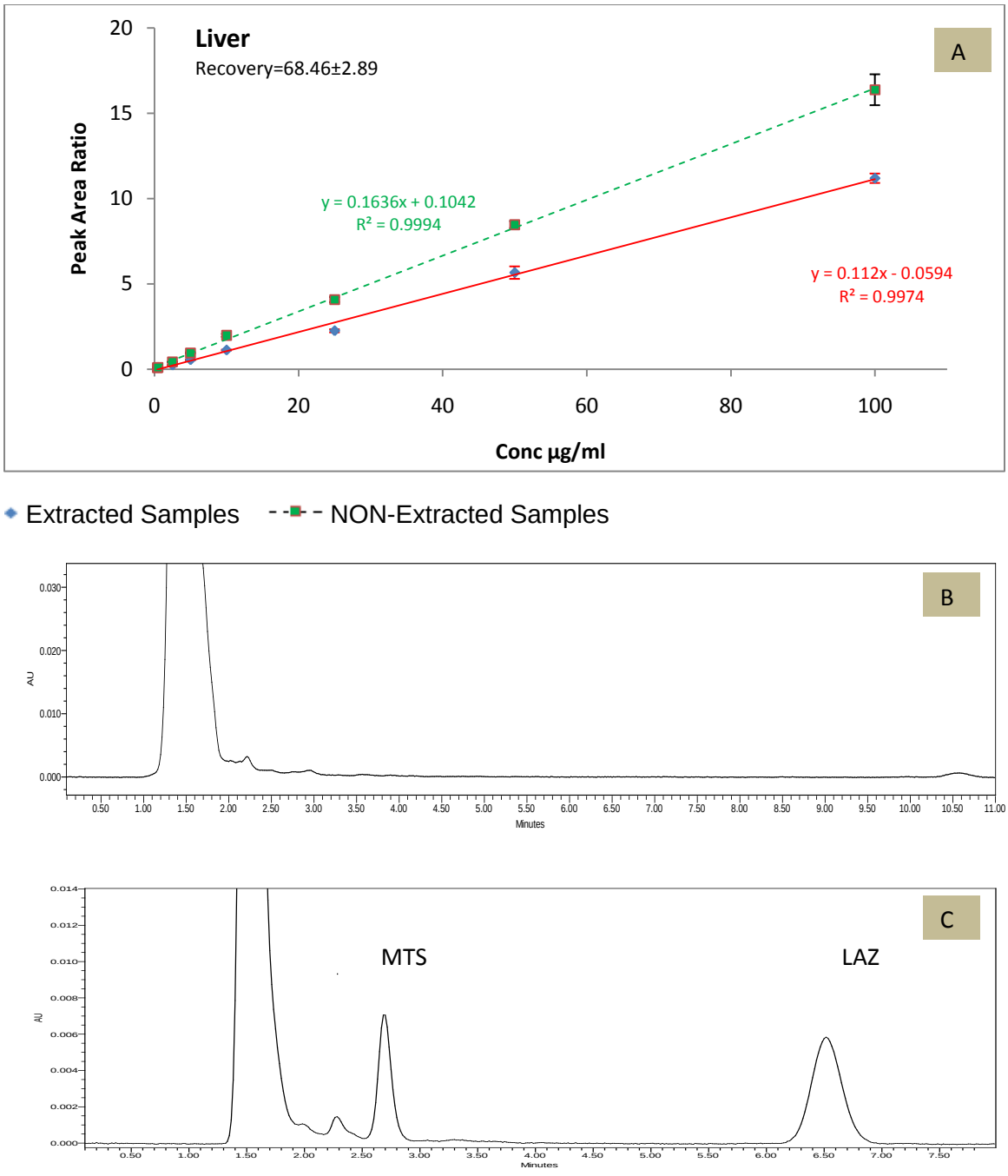

Figure 4.3 (A) Calibration Curves of LAZ in Liver Samples and HPLC Chromatograms of LAZ in (B) Blank Liver Sample and (C) Spiked Liver Sample at 10 µg/ml

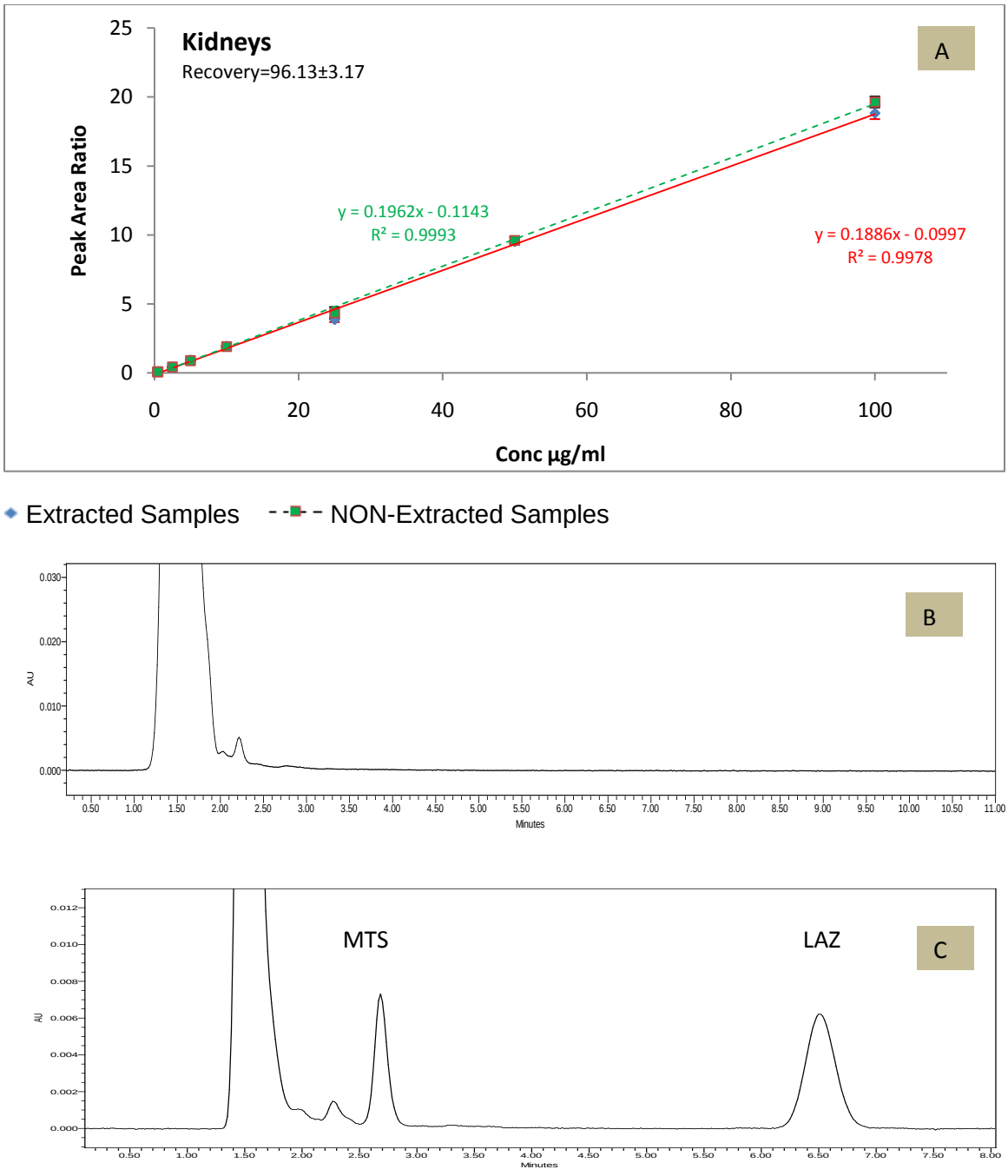

Figure 4.4 (A) Calibration Curves of LAZ in Kidney Samples and HPLC Chromatograms of LAZ in (B) Blank Kidney Sample and (C) Spiked Kidney Sample at 10 µg/ml

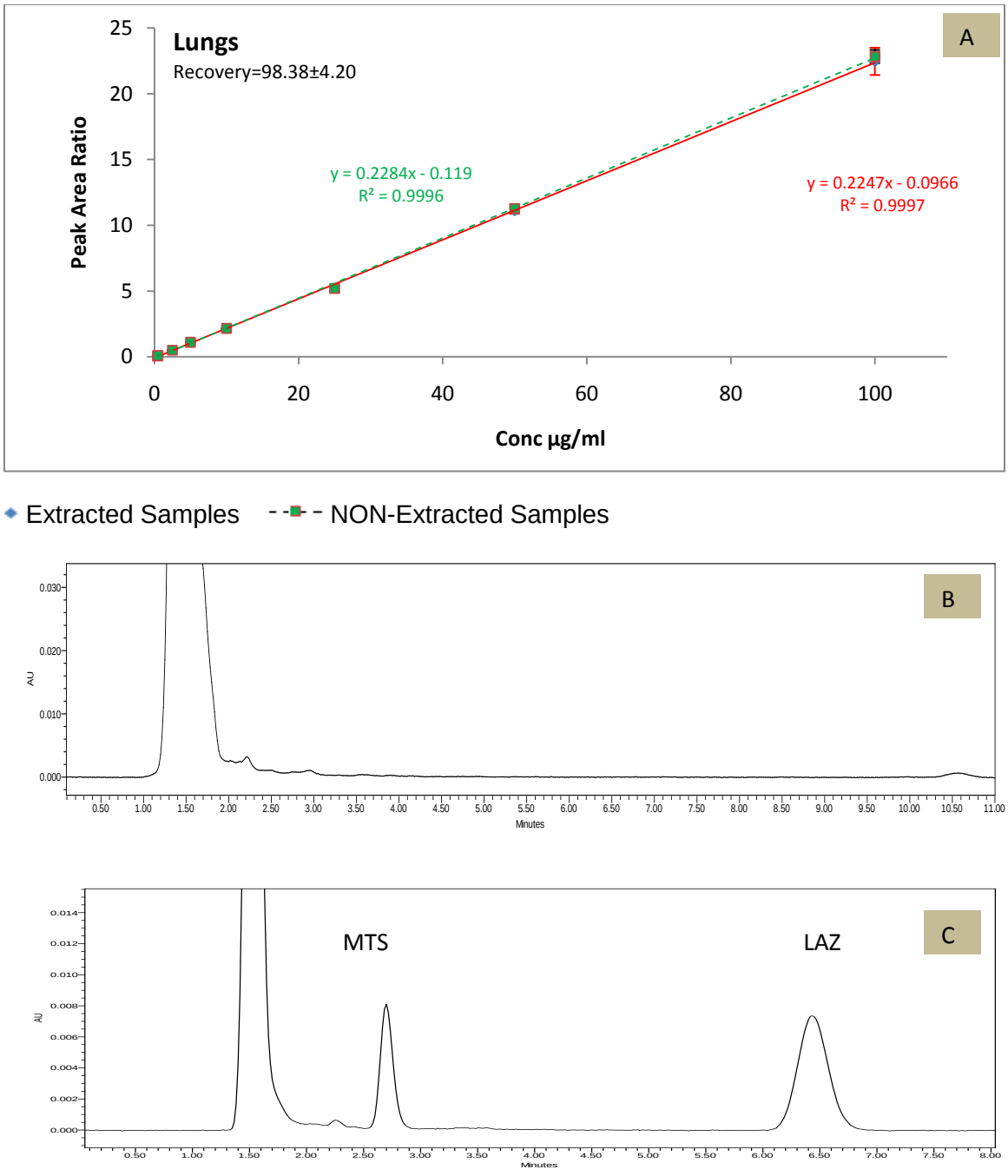

Figure 4.5 (A) Calibration Curves of LAZ in Lung Samples and HPLC Chromatograms of LAZ in (B) Blank Lung Sample and (C) Spiked Lung Samples at 10 µg/ml

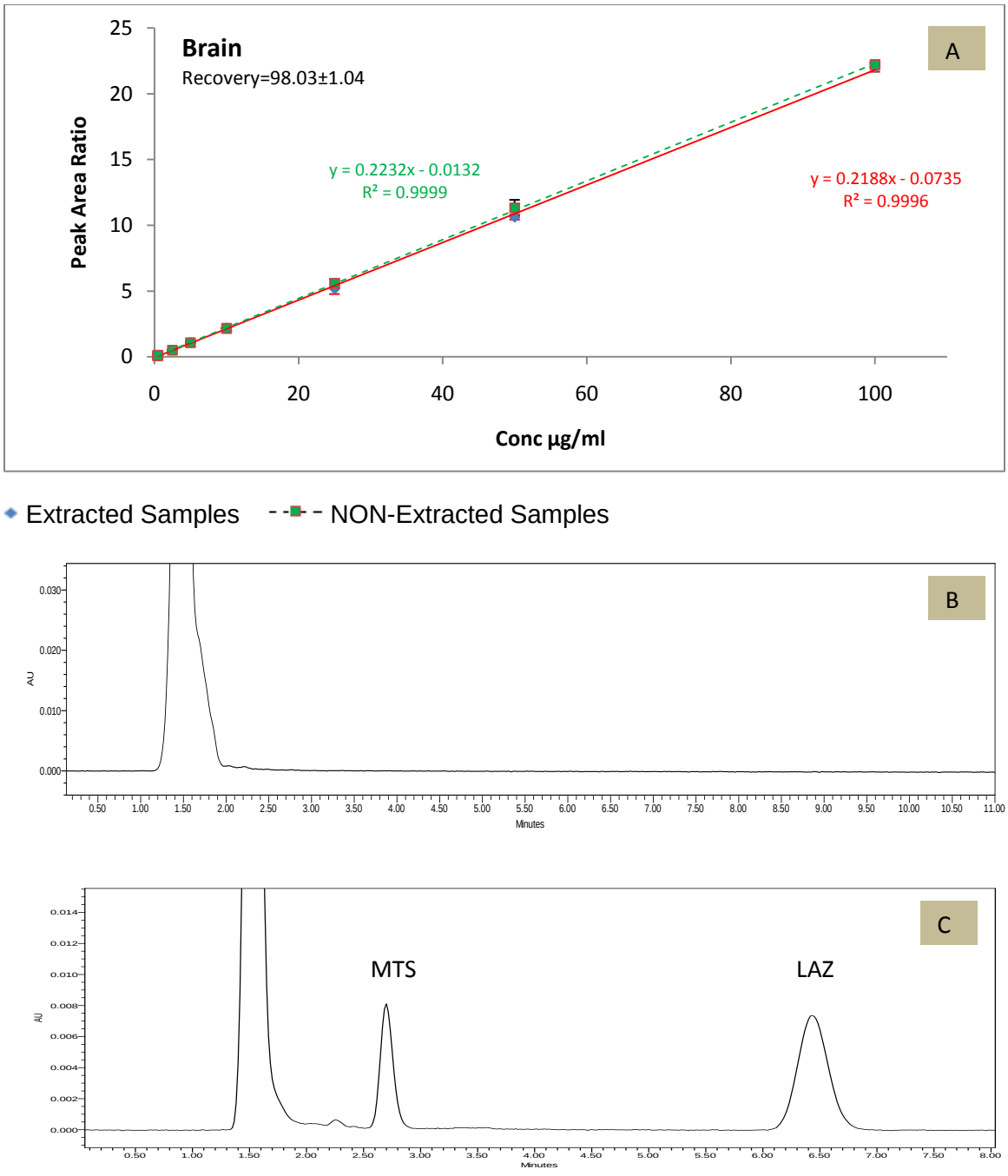

Figure 4.6 (A) Calibration Curves of LAZ in Brain Samples and HPLC Chromatograms of LAZ in (B) Blank Brain Sample and (C) Spiked Brain Sample at 10 µg/ml

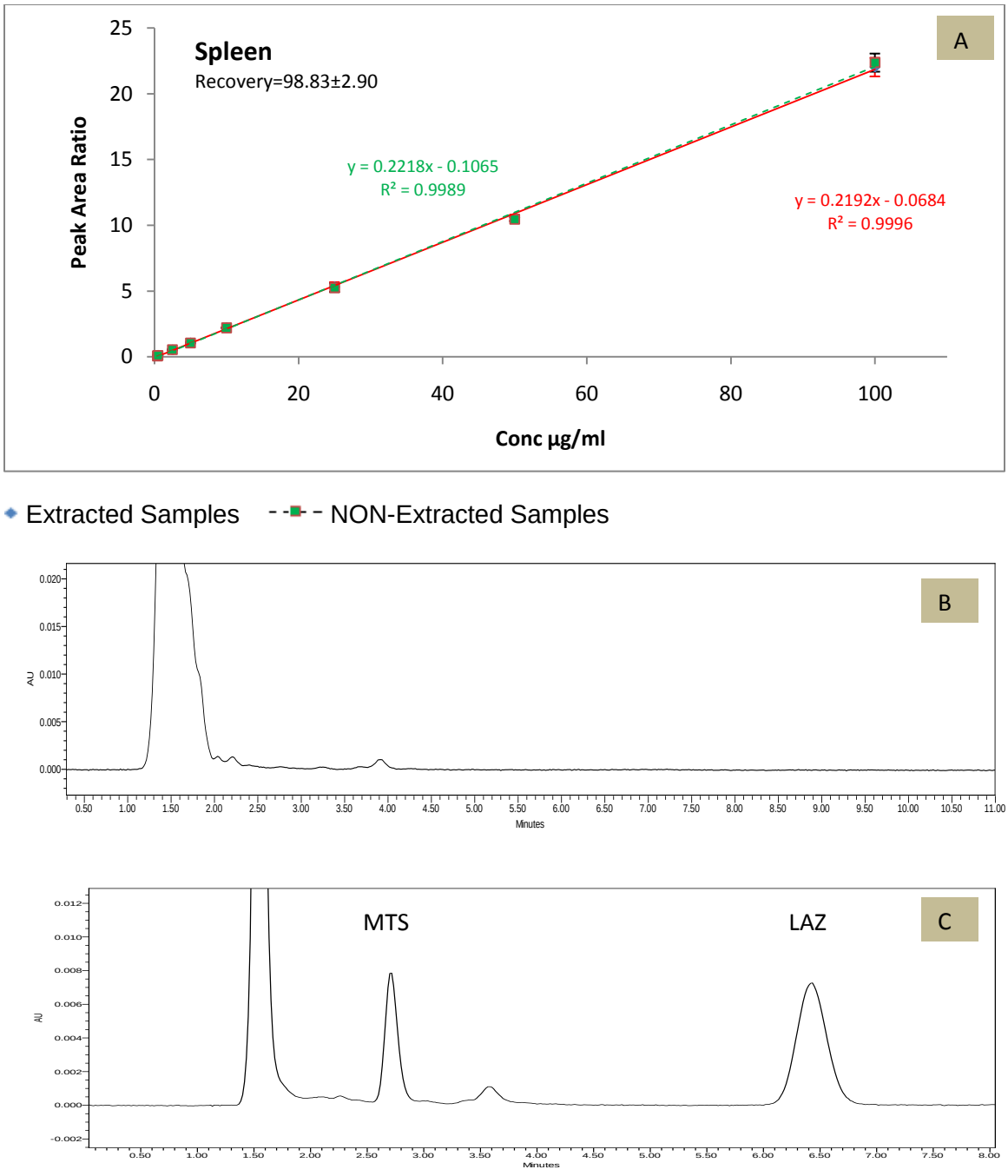

Figure 4.7 (A) Calibration Curve of LAZ in Spleen Samples and HPLC Chromatograms of LAZ in (B) Blank Spleen Sample and (C) Spiked Spleen Sample at 10 µg/ml

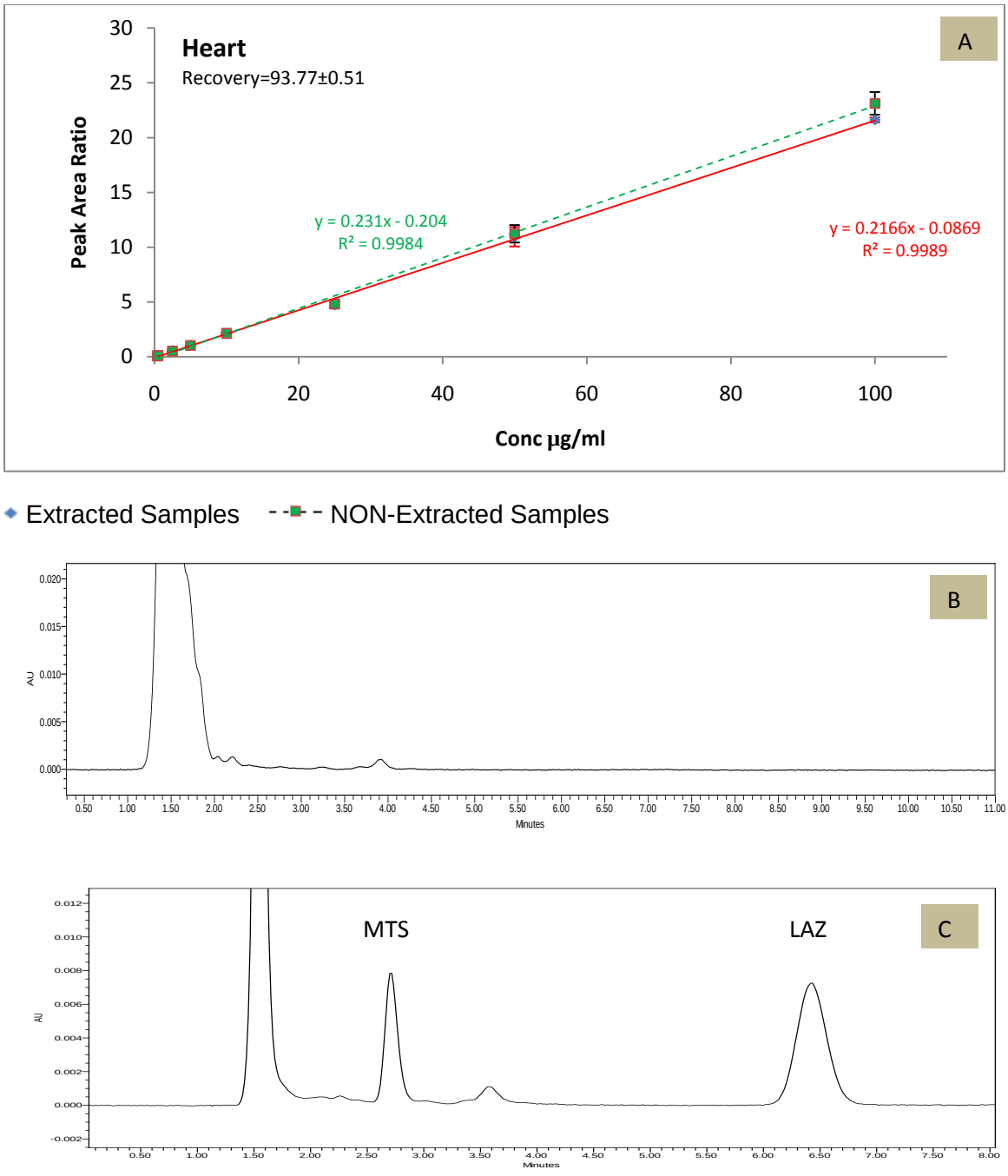

Figure 4.8 (A) Calibration Curves of LAZ in Heart Samples and HPLC Chromatograms of LAZ in (B) Blank Heart Sample and (C) Spiked Heart Sample at 10 µg/ml

Table 4.1 Intra-day (n=3) and Inter-day (n=6) Precision and Accuracy of Quantification of LAZ QC Samples

Matrix	Conc. µg/ml	Intra-day variation(n=3)				Inter-day variation(n=6)			
		Mean	SD	Precision%	Accuracy%	Mean	SD	Precision%	Accuracy%
Aqueous	4.00	4.04	0.32	7.96	101.01	3.93	0.31	7.98	98.37
	40.00	39.18	1.06	2.69	97.95	38.94	1.45	3.73	97.36
	80.00	84.25	0.99	1.17	105.31	83.02	2.84	3.42	103.77
Plasma	4.00	3.96	0.16	4.07	99.06	4.03	0.17	4.24	100.63
	40.00	38.88	0.76	1.95	97.20	38.43	0.95	2.46	96.07
	80.00	82.54	5.22	6.32	103.17	85.29	4.52	5.30	106.62
Liver	4.00	4.09	0.19	4.56	102.13	3.86	0.29	7.57	96.49
	40.00	40.13	2.46	6.13	100.33	39.98	1.62	4.04	99.95
	80.00	83.26	4.42	5.31	104.08	81.31	3.57	4.39	101.63
Kidneys	4.00	4.13	0.12	2.84	103.24	4.15	0.11	2.59	103.68
	40.00	40.95	1.11	2.70	102.38	40.96	1.87	4.57	102.41
	80.00	80.92	0.45	0.55	101.15	79.26	3.11	3.93	99.07
Lungs	4.00	4.07	0.19	4.65	101.86	4.15	0.15	3.62	103.80
	40.00	38.39	1.51	3.93	95.98	39.19	1.29	3.30	97.97
	80.00	81.41	3.98	4.89	101.76	80.62	3.02	3.74	100.77
Brain	4.00	4.13	0.22	5.33	103.29	4.06	0.26	6.40	101.46
	40.00	39.39	1.27	3.22	98.48	39.90	1.00	2.51	99.75
	80.00	81.78	4.70	5.75	102.23	79.91	3.63	4.54	99.89
Spleen	4.00	4.26	0.15	3.49	106.42	4.11	0.26	6.28	102.65
	40.00	40.42	0.54	1.33	101.05	39.60	1.42	3.58	98.99
	80.00	80.07	1.69	2.11	100.09	79.92	1.74	2.18	99.90
Heart	4.00	4.06	0.09	2.21	101.60	4.11	0.08	2.04	102.76
	40.00	39.46	0.65	1.64	98.65	39.26	0.78	2.00	98.15
	80.00	79.03	0.96	1.22	98.79	79.46	0.80	1.01	99.33

Table 4.2 Stability of LAZ QC Samples (n=3)

Matrix	% Remaining of LAZ					
	6 hr at Room Temperature			10 Days at -20^{o}C		
	4.00µg/ml	**40.00µg/ml**	**80.00 µg/ml**	**4.00µg/ml**	**40.00µg/ml**	**80.00 µg/ml**
Aqueous	94.82±4.83	98.89±6.88	97.06±3.82	98.95±2.42	98.44±0.46	98.42±2.55
plasma	103.17±2.30	100.30±3.55	102.01±1.87	99.13±2.49	98.18±4.18	98.13±1.25
Liver	98.57±3.67	99.53±7.44	95.50±5.67	97.20±1.59	98.32±2.37	100.42±3.55
Kidneys	100.86±1.86	100.07±6.25	95.92±2.42	97.74±3.85	99.31±1.81	100.60±1.58
Lungs	103.99±5.87	104.23±3.86	98.11±2.02	99.36±2.24	98.96±1.08	98.44±0.58
Brain	96.44±5.22	102.63±3.05	95.64±5.22	99.50±1.85	100.37±1.40	100.64±2.48
Spleen	93.00±7.38	95.89±2.82	99.63±1.99	99.34±1.05	99.51±0.89	99.08±0.53
Heart	102.31±2.76	98.99±1.28	101.10±1.52	99.91±1.67	94.88±4.65	99.87±0.90

4.2 UPLC-MS/MS Assays

Rapid and selective ultra performance liquid chromatography- mass spectrometry method (UPLC-MS/MS) was developed and validated for the quantification of LAZ in plasma and various mouse organs. LAZ and Daidzein (IS) were extracted from various matrices using acetonitrile. LAZ and IS were eluted using a gradient flow of 0.1% formic (A) acid and acetonitrile (B) (0–0.5 min, 0–5% B, 0.5–2.4 min, 5–90% B, 2.4–3.1 min, 90–5% B). Daidzein was chosen as internal standard for being detected at the same positive mode as LAZ with a high sensitivity. The chromatograms of blank plasma and organs had no interfering peaks to LAZ or IS, and the retention times were 1.58 and 1.54 min, respectively (Figure 4.9). The Calibration curves for LAZ in all the matrices were linear in the concentration range of 15.6–4,000 ng/ml with correlation coefficient values >0.99 (Figures 4.10- 4-13). The LLOQ was 15.6 ng/ml. The Intra-day and Inter-day precision and accuracy were determined by quantifying QC samples triplicates at three concentration levels (125, 500 and 4,000 ng/ml) in the various matrices. The intra-day precision (%C.V.) was less than 7% (n = 3) and accuracy ranged from 95 to 108% (Table 4.3). The inter-day precision (%C.V.) was less than 9% and accuracy ranged from 96 to 114% (Table 4.3). The mean extraction recoveries determined using three replicates of QC samples at three concentration levels in the various matrices were found to vary according to the tissue matrix. The recovery was 59 -65% from heart samples, 73-84% from brain samples, 79-87% from liver samples and 82-99% from kidney, spleen and lung samples (Table 4.4). For matrix effect, the peak areas of LAZ from spiked tissue

samples were compared to those from the aqueous standard solution. LAZ ionization was suppressed in the presence of the biological matrices. The suppression was about 70% in liver samples, 50% in heart samples and to a lower extent in case of samples from kidneys (35%), spleen (32%), plasma and brain (15%), and lungs (5%) (Table 4.6).

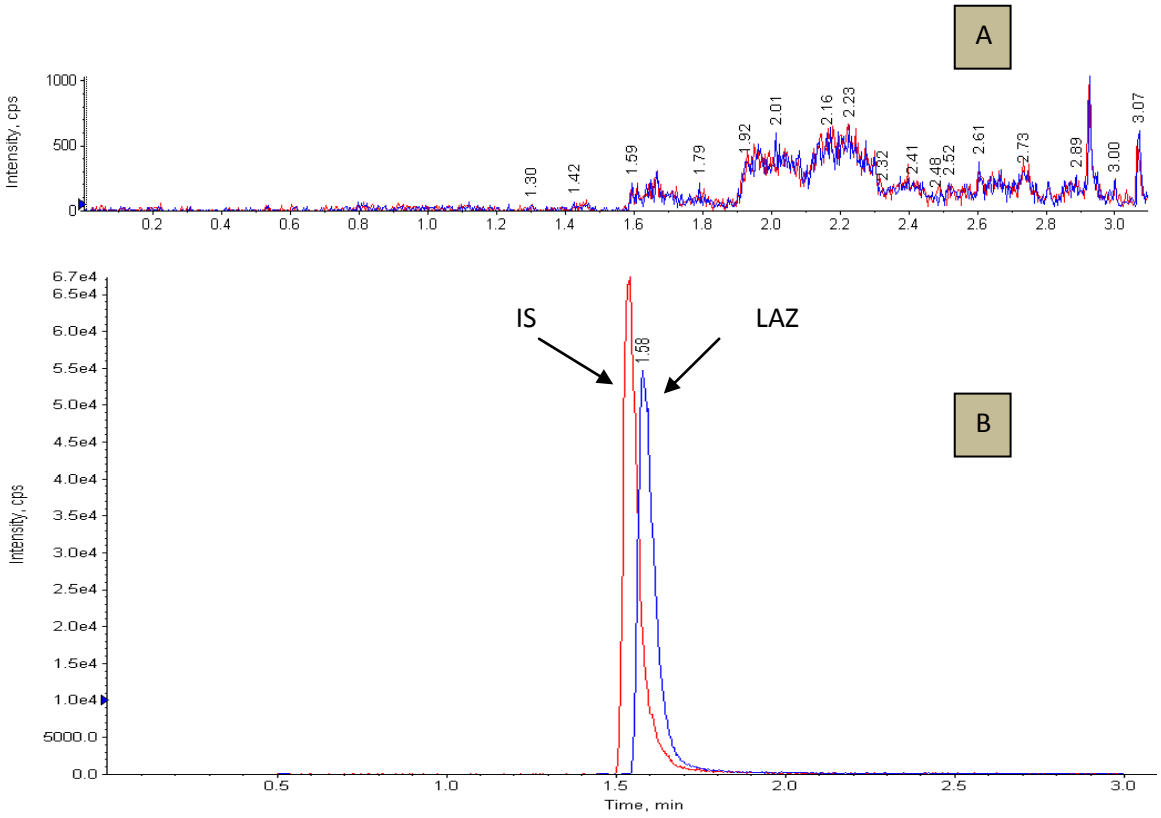

Figure 4.9 Authentic UPLC Chromatograms with MS/MS detection of (A) Blank Plasma Sample and (B) Plasma Sample Spiked with 1000 ng/ml LAZ.

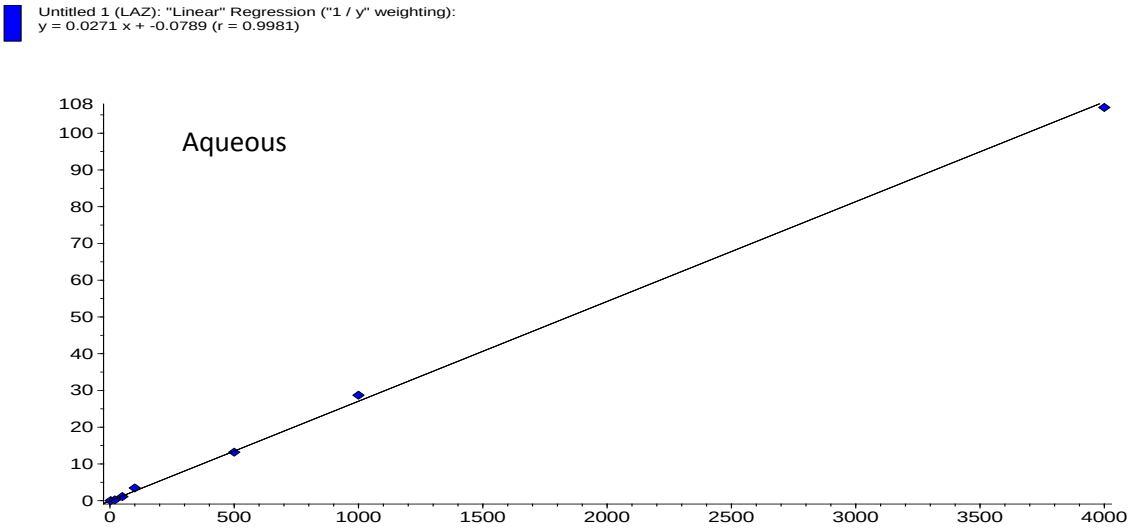

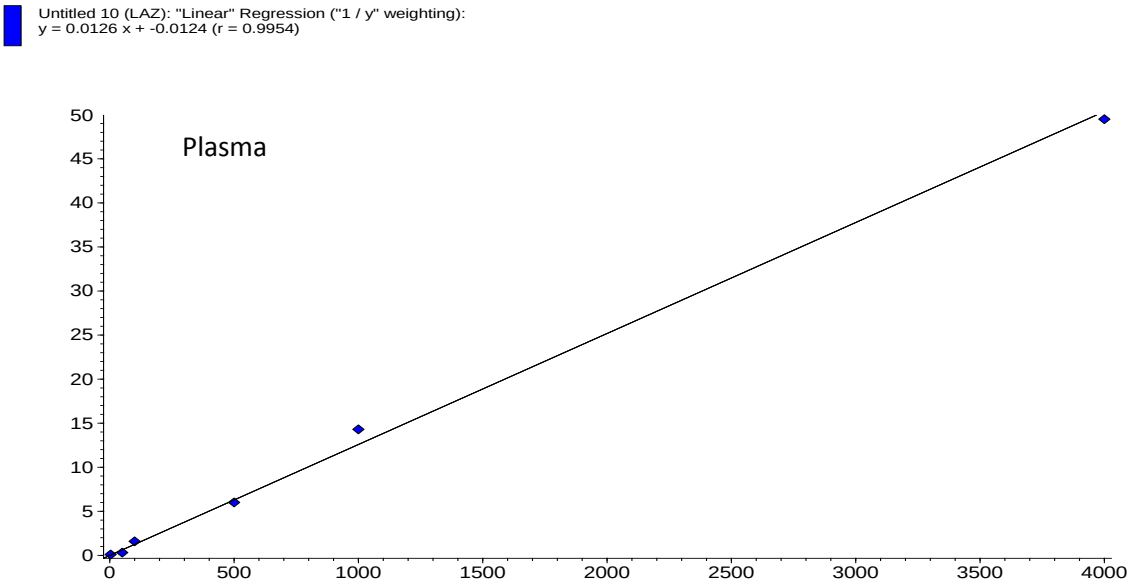

Figure 4.10 Individual Calibration Curves of LAZ in Aqueous and Plasma Samples as Reported by Analyst Software

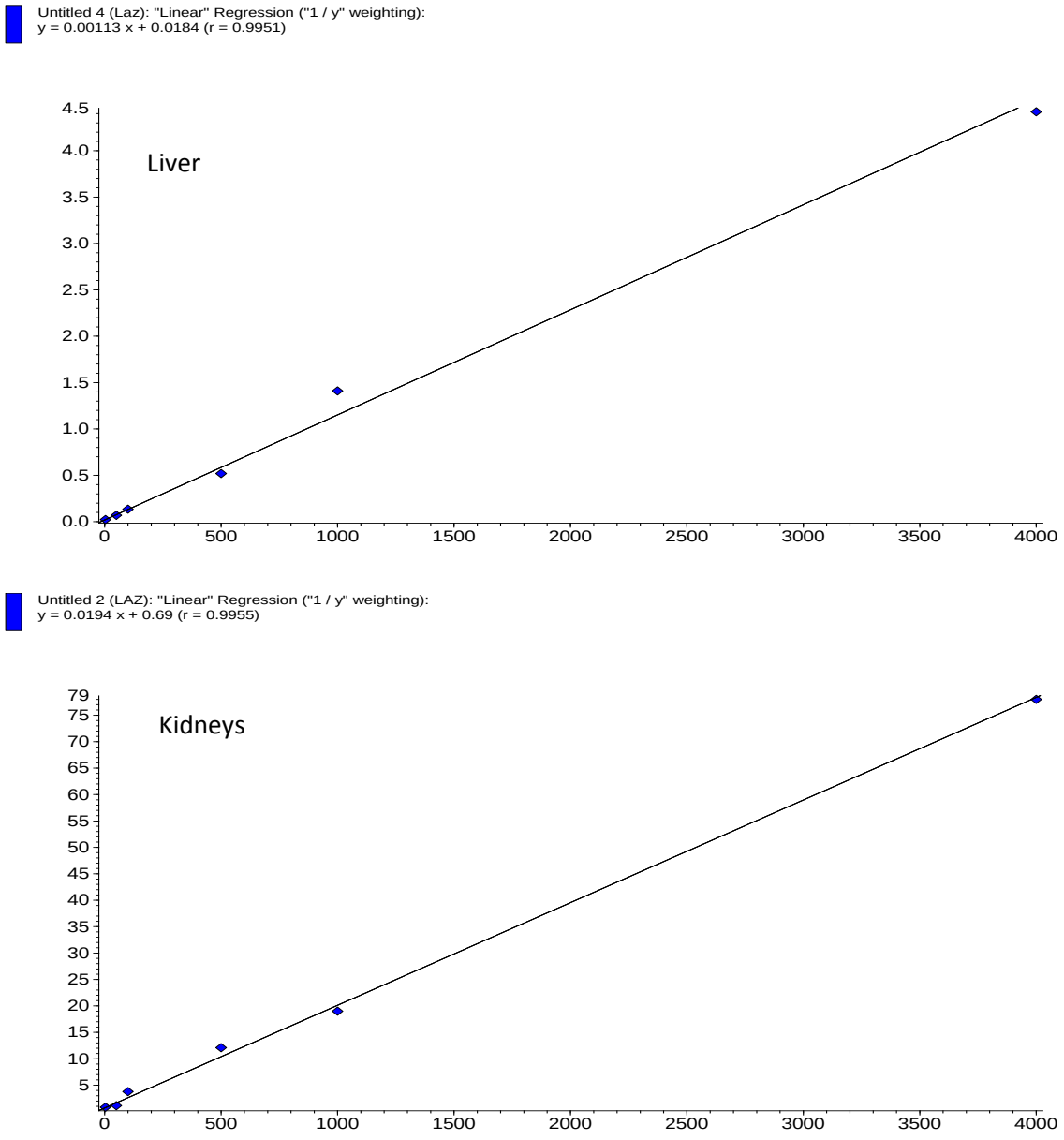

Figure 4.11 Individual Calibration Curves of LAZ in Liver and Kidneys Samples as Reported by the Analyst Software

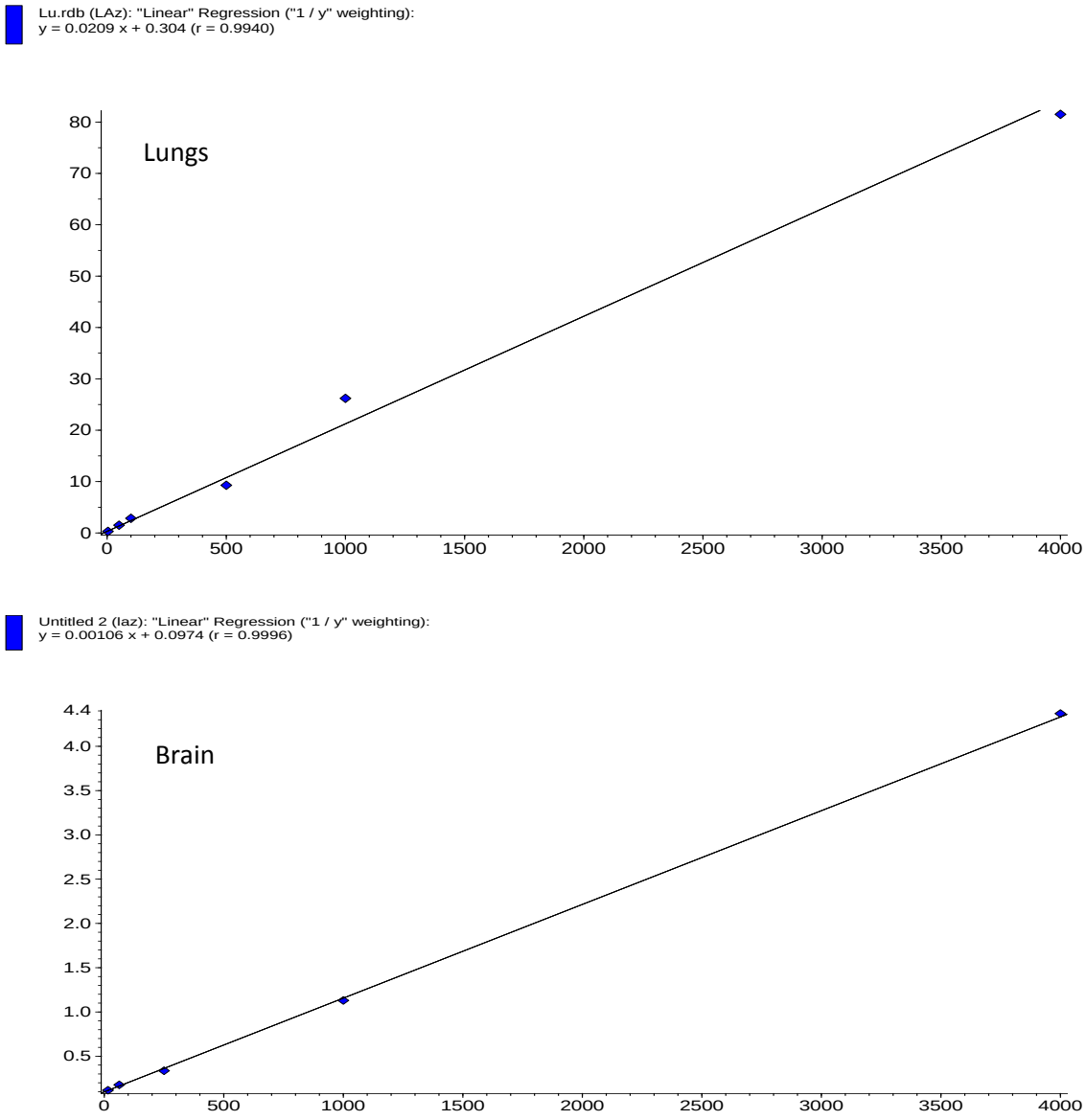

Figure 4.12 Individual Calibration Curves of LAZ in Lung and Brain Samples as Reported by the Analyst Software

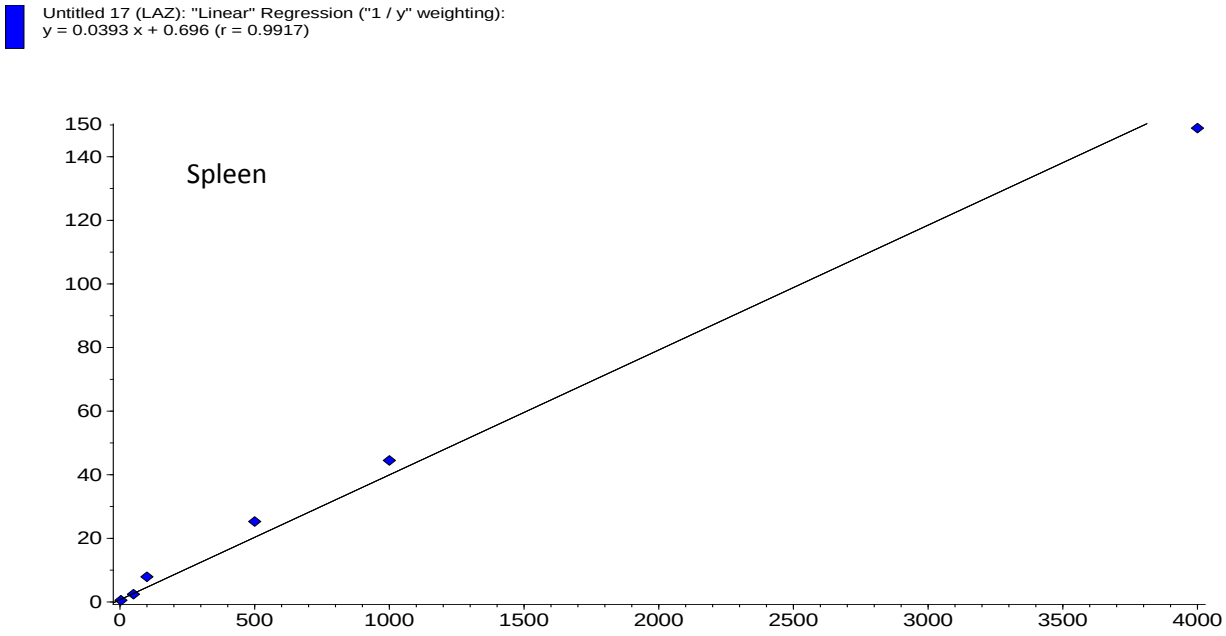

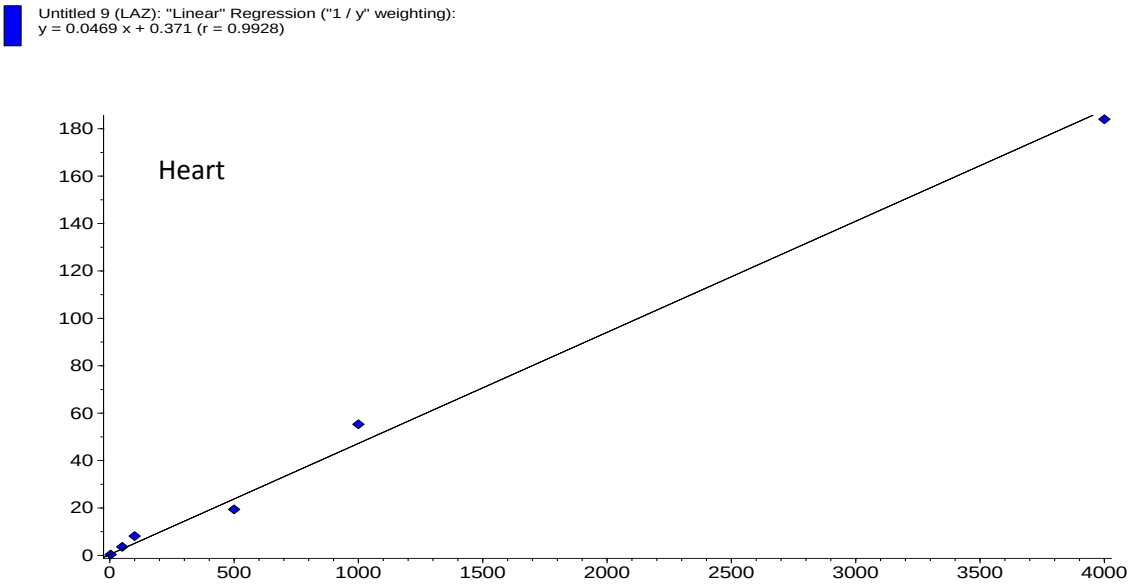

Figure 4.13 Calibration Curves of LAZ in Spleen and Heart Samples as Reported by the Analyst Software

Table 4.3 Inter-day and Intra-day Precision and Accuracy of LAZ QC Standards in Various Mouse Tissues (n=3, each)

		Intra-day			Inter-day		
Aqueous	Conc.(ng/ml)	125.00	500.00	4,000.00	125.00	500.00	4,000.00
	Mean	124.18	475.37	4,101.36	134.76	487.52	4,270.24
	SD	1.93	20.29	159.89	8.33	5.61	203.44
	CV%	1.56	4.27	3.90	6.18	1.15	4.76
	Accuracy	99.35	95.07	102.53	107.81	97.50	106.76
Plasma	Conc.(ng/ml)	125.00	500.00	4,000.00	125.00	500.00	4,000.00
	Mean	124.28	491.85	3,950.76	131.23	488.30	3,843.82
	SD	2.98	17.67	148.86	6.17	20.19	208.98
	CV%	2.40	3.59	3.77	4.70	4.14	5.44
	Accuracy	99.42	98.37	98.77	104.98	97.66	96.10
Liver	Conc.(ng/ml)	125.00	500.00	4,000.00	125.00	500.00	4,000.00
	Mean	127.33	495.33	3,950.00	124.02	515.95	3,887.67
	SD	3.79	35.57	95.39	5.92	44.32	185.22
	CV%	2.97	7.18	2.42	4.77	8.59	4.76
	Accuracy	101.87	99.07	98.75	99.22	103.19	97.19
Kidneys	Conc.(ng/ml)	125.00	500.00	4,000.00	125.00	500.00	4,000.00
	Mean	123.67	500.00	3,998.00	130.00	497.67	3,953.67
	SD	4.73	15.87	43.00	5.20	20.26	65.24
	CV%	3.82	3.17	1.08	4.00	4.07	1.65
	Accuracy	98.93	100.00	99.95	104.00	99.53	98.84
Lungs	Conc.(ng/ml)	125.00	500.00	4,000.00	125.00	500.00	4,000.00
	Mean	126.28	538.13	3,954.33	129.36	517.77	3,844.81
	SD	5.21	16.63	95.95	8.38	21.41	148.19
	CV%	4.13	3.09	2.43	6.48	4.14	3.85
	Accuracy	101.02	107.63	98.86	103.49	103.55	96.12
Brain	Conc.(ng/ml)	125.00	500.00	4,000.00	125.00	500.00	4,000.00
	Mean	129.33	481.67	3,990.00	143.10	536.18	4,037.58
	SD	1.15	11.24	70.00	7.00	16.57	192.36
	CV%	0.89	2.33	1.75	4.89	3.09	4.76
	Accuracy	103.47	96.33	99.75	114.48	107.24	100.94
Spleen	Conc.(ng/ml)	125.00	500.00	4,000.00	125.00	500.00	4,000.00
	Mean	127.33	511.00	3,990.00	125.04	488.65	3,898.60
	SD	4.51	21.52	115.33	7.68	20.21	150.26
	CV%	3.54	4.21	2.89	6.14	4.14	3.85
	Accuracy	101.87	102.20	99.75	100.03	97.73	97.46
Heart	Conc.(ng/ml)	125.00	500.00	4,000.00	125.00	500.00	4,000.00
	Mean	125.87	506.33	3,981.00	124.00	488.00	3,978.00
	SD	4.59	24.79	59.92	5.29	24.76	68.15
	CV%	3.65	4.90	1.51	4.27	5.07	1.71
	Accuracy	100.69	101.27	99.53	99.20	97.60	99.45

Table 4.4 Recovery Percentage of LAZ from Various Biomatrices (n=3, each)

Tissue	% Recovery			CV%
	Conc. (ng/ml)	Mean	SD	
Brain	125.00	72.74	5.60	7.70
	500.00	77.84	1.03	1.32
	4,000.00	83.61	0.96	1.15
	Conc. (ng/ml)	Mean	SD	CV%
Plasma	125.00	76.95	1.61	2.10
	500.00	82.59	6.28	7.60
	4,000.00	89.72	1.73	1.93
	Conc. (ng/ml)	Mean	SD	CV%
Liver	125.00	87.17	2.69	2.39
	500.00	79.20	4.12	4.91
	4,000.00	85.83	8.82	5.09
	Conc. (ng/ml)	Mean	SD	CV%
Kidneys	125.00	98.39	11.20	3.09
	500.00	86.27	1.78	5.20
	4,000.00	92.22	6.74	10.27
	Conc. (ng/ml)	Mean	SD	CV%
Lungs	125.00	96.32	2.30	6.91
	500.00	81.58	4.01	13.07
	4,000.00	86.67	4.41	2.88
	Conc. (ng/ml)	Mean	SD	CV%
Spleen	125.00	94.17	7.09	11.39
	500.00	98.81	0.91	2.07
	4,000.00	95.28	4.81	7.30
	Conc. (ng/ml)	Mean	SD	CV%
Heart	125.00	58.92	4.07	6.91
	500.00	64.88	8.48	13.01
	4,000.00	60.28	8.73	14.48

Table 4.5 Effect of Tissue Homogenate Matrix on LAZ Ionization (n=3, each)

Tissue		% Relative Peak Area		CV%
	Conc. ng/ml	Mean	SD	
Plasma	125	80.70	7.82	9.69
	500	89.05	3.60	4.04
	4,000	88.00	7.90	8.98
	Conc. ng/ml	Mean	SD	CV%
Liver	125	27.98	1.61	5.75
	500	22.36	0.27	1.21
	4,000	32.72	4.11	12.56
	Conc. ng/ml	Mean	SD	CV%
Kidneys	125	64.55	9.96	15.43
	500	71.74	1.31	1.83
	4,000	65.36	9.01	13.79
	Conc. ng/ml	Mean	SD	CV%
Lungs	125	97.46	1.81	1.86
	500	96.70	4.36	4.51
	4,000	95.11	4.24	4.46
	Conc. ng/ml	Mean	SD	CV%
Brain	125	87.07	8.71	10.00
	500	83.50	10.99	13.16
	4,000	90.38	10.76	11.91
	Conc. ng/ml	Mean	SD	CV%
Spleen	125	70.53	14.56	20.64
	500	72.96	3.17	4.34
	4,000	64.81	5.27	8.13
	Conc. ng/ml	Mean	SD	CV%
Heart	125	46.45	6.39	13.76
	500	49.99	2.50	5.00
	4,000	54.39	3.47	6.38

4.3 Stability of LAZ in PBS, Plasma and CSF Containing Tween 80 (n=3, each)

The stability of LAZ was studied in PBS, Plasma and CSF, respectively, which are used as the release media for the dissolution and release studies. The percentage of the remaining amount of LAZ that was spiked in the release media was measured over a period of 15 days. LAZ concentration in the media started to decline on the second day of the study. The rate of LAZ decomposition (K_{De} % day^{-1}) was faster in PBS compared to those from plasma and CSF (2.74 % day^{-1}vs. 1.43 and 1.42 % day^{-1}, respectively). The time required for 50% decomposition in PBS was 19 days compared to 35 days in both plasma and CSF (Figure 4.14 & Table 4.6).

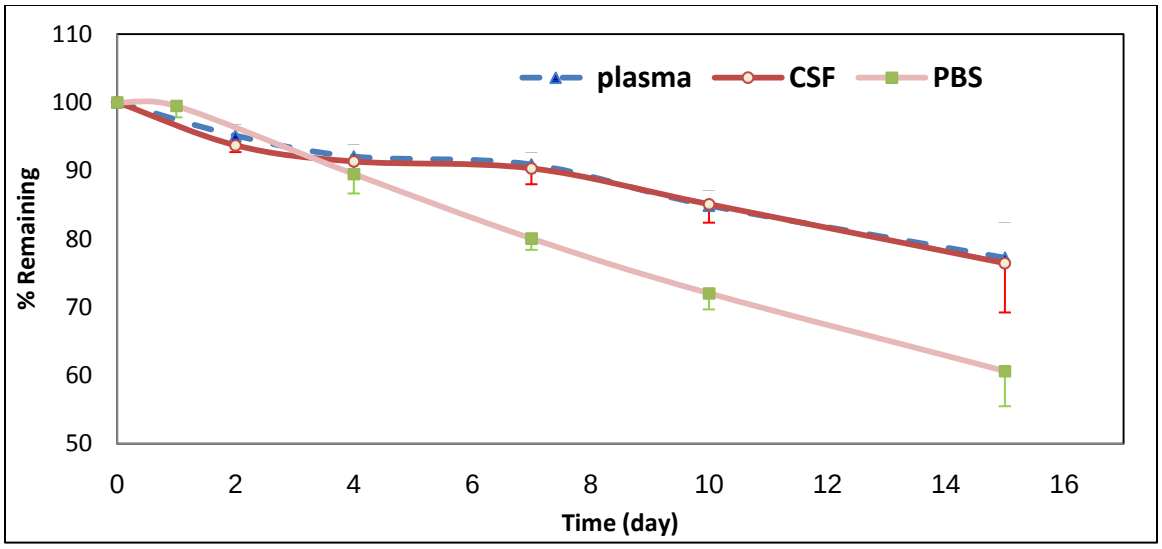

Figure 4.14 Stability of LAZ in Plasma, CSF and PBS at 37^{o}C (n=3, each)

Table 4.6 Stability Kinetics of LAZ in Plasma, CSF and PBS at 37^{o}C (n=3, each)

Time (day)	Plasma		CSF		PBS	
	% remaining	S.D	% remaining	S.D	% remaining	S.D
0	100.00	0.00	100.00	0.00	100	0.00
2	95.13	1.62	93.70	0.98	99.47	1.66
4	92.06	1.80	91.33	1.79	89.50	2.85
7	90.89	1.70	90.32	2.31	80.05	1.66
10	84.87	2.25	85.08	2.70	72.01	2.34
15	77.23	5.20	76.43	7.21	60.61	5.13
Zero order Eq.	y = -1.4297x + 99.086 R^2 = 0.98		y = -1.4215x + 100.68 R^2 = 0.96		y = -2.7412x + 101.2 R^2 = 0.99	
K_{De} (% day^{-1}) (2-7 days)	1.06		0.85		2.74	
K_{De} (% day^{-1}) (overall)	1.43*		1.42*		2.74	
Time (day) for 50% loss	34.33		35.39		18.68	

4.4 Nanosuspension

4.4.1 Nanosuspension Formulations

LAZ nanosuspensions were prepared using wet milling technique where the drug was mixed with surfactants and ground in-between the sliding glass beads. The size of the nanosuspensions was in the range of 123-253 nm. The use of a single-size glass beads produced a nanosuspension of average size of 250 nm (NS-A) which had bimodal distribution, while the use of a mixture of multiple size glass beads narrowed the polydispersity index (PI of 0.2 to 0.1) and contributed to a greater extent of size reduction (125 nm, NS-B) (Table 4.7& Figure 4.15). The zeta potential on NS-A and NS-B particle surfaces was +2 *mv* and +5 *mv*, respectively, and they are considered neutral. The addition of the ionic surfactants modified the charge on the surface of the NS, and 13 mM of CTAB imparting a positive potential on NS-$A^{(+)}$ of +41*mv*, and 1 mM SDS yielding a negative potential of -22 *mv* and -13 *mv* on NS-$A^{(-)}$ and NS-$B^{(-)}$, respectively (Table 4.7 & Figure 4.15).

4.4.2 *In-vitro* Release of LAZ from Solution and Four Nanosuspensions (Neutral, Cationic and Anionic 250 nm and Anionic 125 nm) in PBS (n=3)

LAZ release from the nanosuspensions (NS-A 250nm, NS-$A^{(+)}$ 250 nm, NS-$A^{(-)}$ 250 nm and NS-$B^{(-)}$ 125 nm) was studied in PBS at 37^{o}C. The release profiles had a biphasic pattern with a rapid initial release up to 1 hr followed by a slow release phase afterwards (Table 4.8 & Figure 4.16). LAZ release from nanosuspensions was slower compared to

that of the solution which was complete after 4 hr. The initial release rates of all nanosuspension formulations (< 6% hr^{-1}) were slower than that of the solution (32% hr^{-1}). Among the nanosuspension formulations, the initial release rates of all the NS-A group (250 nm) were slower than that of the NS-$B^{(-)}$ (2.61, 1.99 and 1.37 % hr^{-1} for NS-A, NS-$A^{(+)}$ and NS-$A^{(-)}$, respectively,vs. 5.56 %hr^{-1} for NS-$B^{(-)}$) (Table 4.9).

The extent of LAZ release from the solution out the dialysis bag was complete after 4 hr, while it was 94 % for NS-B 125 nm and < 72% for NS-A 250 nm groups after 48 hr. Among the nanosuspensions, LAZ release was almost complete from NS-B 125 nm (94 %) after 48 hr, but it was comparable among the NS-A 250nm formulations with release extent of 72, 70 and 71 % for NS-A, NS-$A^{(+)}$ and NS-$A^{(-)}$, respectively (Table 4.10).

Table 4.7 Characterization Parameters of Nanosuspensions (n=3, each)

Sample	Size (nm)	Polydispersity Index (PI)	Zeta Potential ζ (*mv*)
NS-A	250.00 (±9.60)	0.29 (±0.03)	+ 2.20 (± 1.44)
NS-$A^{(-)}$	253.00 (±9.60)	0.18 (±0.01)	-22.02 (± 0.93)
NS-$A^{(+)}$	241.00 (±9.70)	0.13 (±0.15)	+40.78 (±1.48)
NS-B	123.90 (±1.20)*	0.11 (±0.02)	+5 .00 (±1.21)
NS-$B^{(-)}$	125.00 (±2.20)*	0.10 (±0.03)	-13.10 (±3.50)

***indicates significant difference compared to NS-A (P< 0.05) , $^{(-)}$ After Addition of 1 mM sodium dodecyl sulfate (SDS) $^{(+)}$ After Addition of 0.5% (13 mM) of cetyl trimethyl ammonium Br (CTAB).**

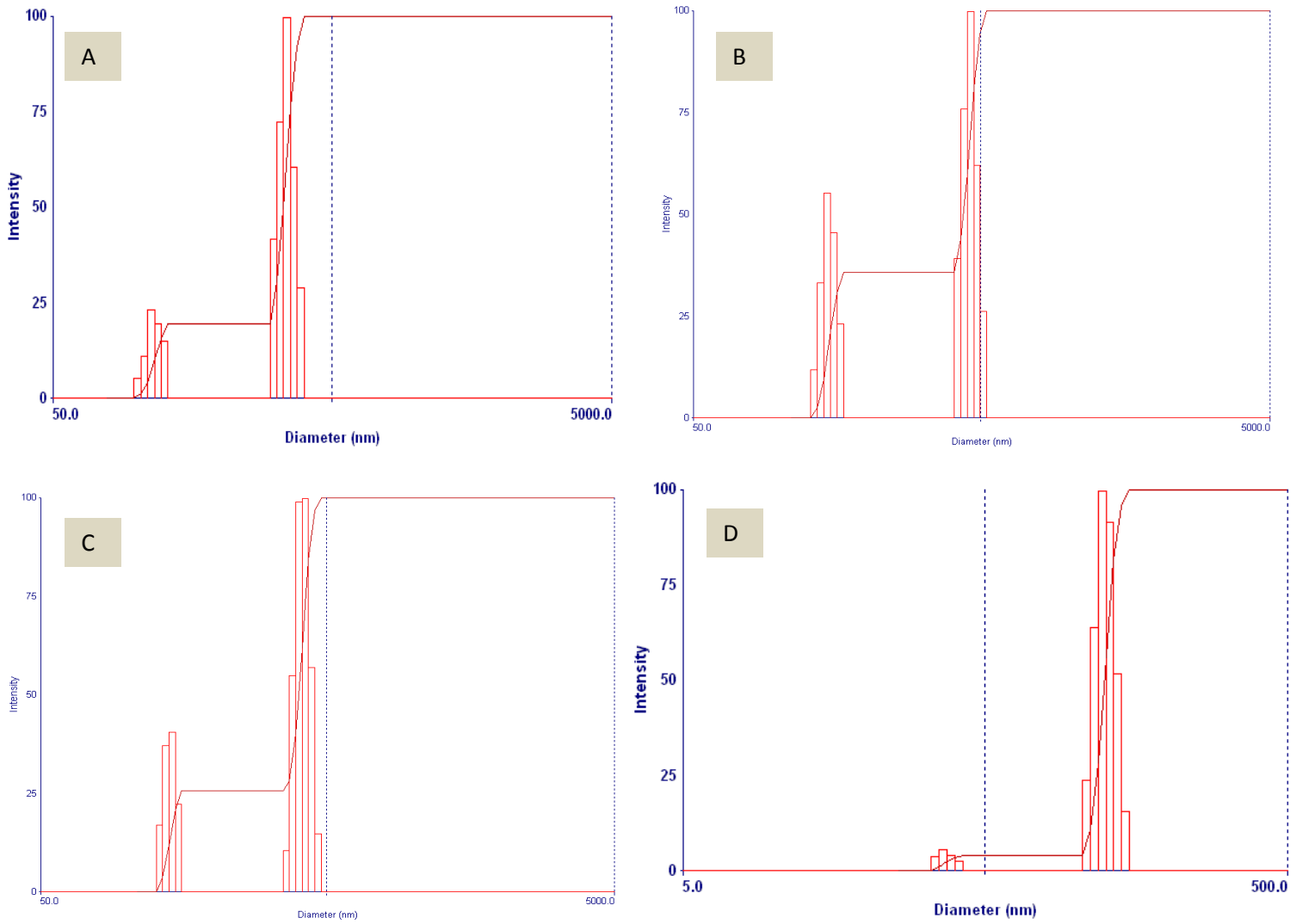

Figure 4.15 Particle Size Distributions of (A) NS-A, (B) NS-A$^{(+)}$, (C) NS-A$^{(-)}$ and (D) NS-B$^{(-)}$.

Table 4.8 Cumulative LAZ Release from LAZ Solution and Nanosuspensions of Different Sizes and Surface Potentials in PBS at 37°C (n=3, each).

Time(hr)	Cumulative % Released in PBS									
	Solution		125 nm NS		250 nm NS		250 nm/+ NS		250 nm/- NS	
	Mean	SD	Mean	SD	Mean	SD	Mean	SD	Mean	SD
0.25	11.92	0.78	-	-	-	-	-	-	-	-
0.5	17.89	1.43	4.71	1.95	1.91	0.29	1.84	0.05	1.04	0.47
0.75	32.01	4.28	-	-	-	-	-	-	-	-
1	40.72	2.87	7.49	1.24	2.72	0.79	4.00	0.17	1.72	0.84
1.5	52.81	3.08	-	-	-	-	-	-	-	-
2	75.23	12.77	10.65	1.86	4.30	0.56	5.81	0.78	4.40	3.34
3	96.26	3.44	-	-	-	-	-	-	-	-
4	98.22	3.69	18.07	4.17	6.48	1.49	9.08	1.87	6.55	0.75
6			25.34	2.41	8.44	1.97	10.40	2.73	7.21	0.65
8			35.85	1.87	11.25	1.14	11.41	3.68	9.40	1.42
10			62.50	3.80	28.88	2.64	26.98	3.99	24.55	3.08
24			87.86	3.45	56.92	2.17	51.88	3.56	47.06	4.76
36			92.28	2.78	67.31	3.49	63.05	1.78	60.73	5.96
48			93.71	1.00	71.43	2.71	69.92	1.57	70.95	6.71

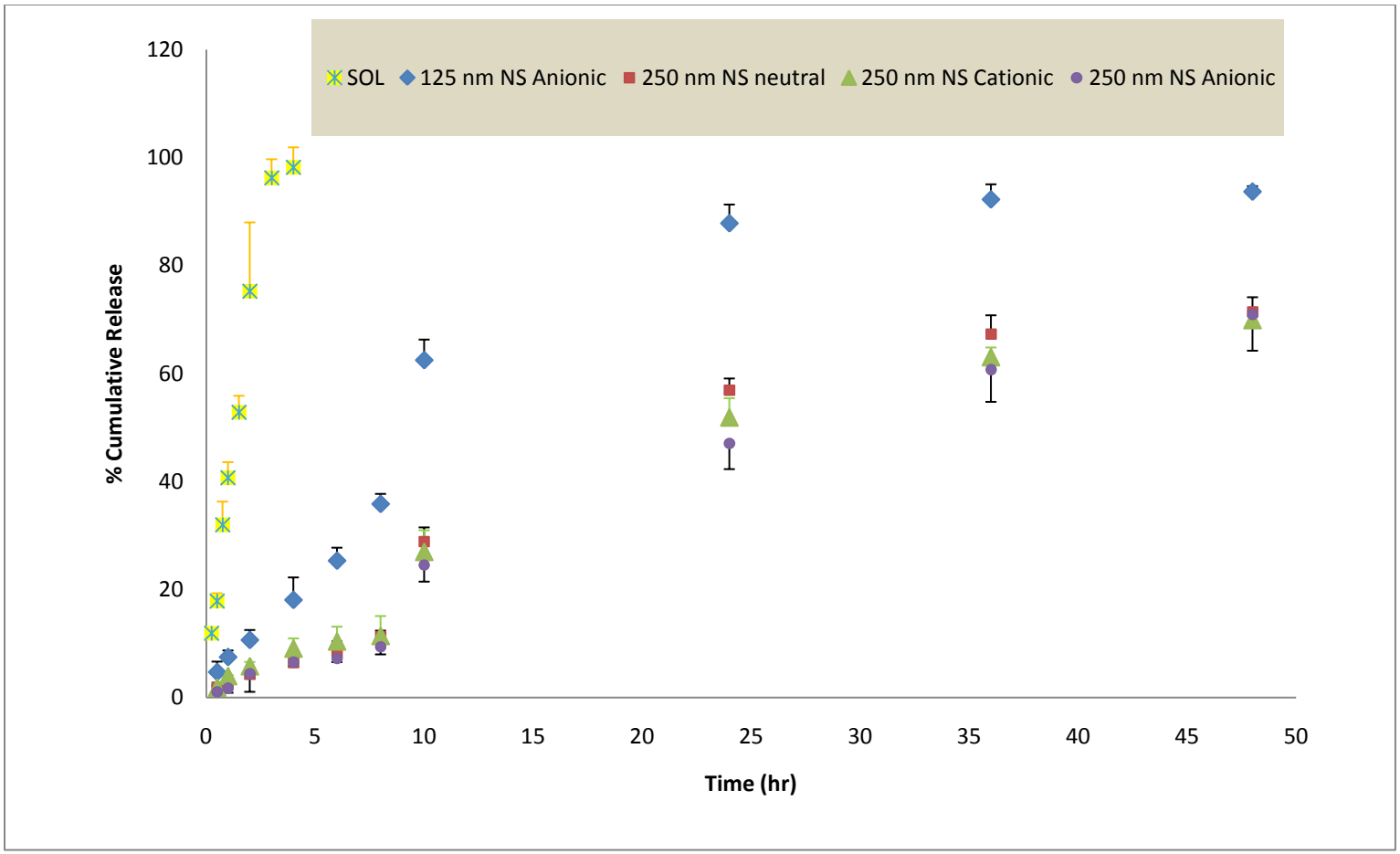

Figure 4.16 Release Profiles of LAZ Solution and Nanosuspensions of Different Sizes and Surface Potentials in PBS at 37°C (n=3).

Table 4.9 Initial Release Rates (%hr^{-1}) of LAZ Solution and Nanosuspensions of Different Sizes and Surface Potentials in PBS at 37^{o}C (n=3).

The Initial Release Rate in PBS up to 1 hr (%/hr)					
	1	2	3	Mean	SD
Solution	40.27	23.05	32.35	31.89	8.62
125 nm NS-B Anionic	5.66	7.01	4.01	5.56*	1.50
250 nm NS-A neutral	1.81	3.56	2.468	2.61**	0.88
250 nm NS-A Cationic	2.04	1.4	2.52	1.99**	0.56
250 nm NS-A Anionic	1.43	2.37	0.31	1.37**	1.03

Table 4.10 Extent of Release (%) of LAZ Solution and Nanosuspensions of Different Sizes and Surface Potentials in PBS at 37^{o}C (n=3).

The Extent of % Cumulative Release after 48 hr in PBS					
	1	3	3	Mean	SD
Solution	99.47	101.22	94.07	98.25	3.73
125 nm NS Anionic	94.67	93.80	92.68	93.71	1.00
250 nm NS neutral	73.88	72.91	68.30	71.70*	2.98
250 nm NS Cationic	70.30	71.26	68.19	69.92*	1.57
250 nm NS Anionic	63.42	73.15	76.29	70.95*	6.71

* Significant difference compared to solution ($P<0.05$)

4.4.3 *In-vitro* Release of LAZ from Solution and Four Nanosuspensions (Neutral, Cationic and Anionic 250 nm and Anionic 125 nm) in Human Plasma (n=3)

LAZ release from the nanosuspensions was also studied in human plasma at 37^{o}C. The release profiles were biphasic with an initial rapid release up to 1 hr followed by a slow phase afterwards (Table 4.11& Figure 4.17), the same trend like those from the PBS. LAZ release from nanosuspensions was slower compared to that from the solution. The Initial release rate of LAZ from solution (12% hr^{-1}) was higher than those of nanosuspensions. The initial release rates of LAZ from 125 nm NS-B and 250 nm NS-A group was <3.3 % hr^{-1} and 0.9 hr^{-1}, respectively, and significantly lower than that from the solution. Among the 250 nm NS-A group, there was no significant difference in LAZ initial release rates (Table 4.12).

The release extents from all nanosuspensions were less than that of the solution. While LAZ release extent from the solution was 82% after 4 hrs, it reached the same extent from NS-B 125 nm after 48 hr. The release extent was < 47% from other 250nm NS-A formulations after 48 hr. LAZ release extent was comparable among NS-A, NS-A$^{(+)}$ and NS-A$^{(-)}$(47, 45 and 47%, respectively) (Table 4.13) .

By comparing the initial release rate of LAZ from solution in PBS and plasma, the release extent in human plasma was less than that in PBS by 16 %. The same trend was observed for nanosuspensions where the release extents of NS-B, NS-A, NS-A$^{(+)}$ and NS-A$^{(-)}$ were less than those of the same formulations in PBS by 13, 36, 35 and 34%, respectively. This lower extent can be explained by LAZ binding to plasma protein inside

Table 4.11 Cumulative LAZ Release from LAZ Solution and Nanosuspensions of Different Sizes and Surface Potentials in Human Plasma at 37°C (n=3).

Time(hr)	Cumulative % Released in Human Plasma									
	Solution		125 nm NS		250 nm NS		250 nm/+ NS		250 nm/- NS	
	Mean	SD	Mean	SD	Mean	SD	Mean	SD	Mean	SD
0.25	10.87	0.57	-	-	-	-	-	-	-	-
0.5	12.81	0.48	5.02	7.13	3.42	1.78	1.33	0.80	0.84	0.06
0.75	20.12	3.47	-	-	-	-	-	-	-	-
1	26.81	3.92	10.01	10.03	2.98	1.67	1.41	0.25	1.26	0.22
1.5	38.80	5.16	-	-	-	-	-	-	-	-
2	50.98	3.74	12.43	8.77	4.44	2.49	2.56	0.19	2.15	0.26
3	76.21	1.78	-	-	-	-	-	-	-	-
4	82.49	2.00	22.48	3.03	6.34	3.33	3.79	0.58	4.24	1.90
6			22.64	4.20	6.33	3.02	6.94	1.84	5.31	0.50
8			32.32	7.43	8.28	3.71	9.69	2.69	6.05	0.55
10			45.91	3.58	17.25	3.43	18.13	3.98	17.56	2.18
24			65.66	4.28	26.10	4.24	26.99	6.16	29.91	2.46
36			69.07	3.70	44.05	7.77	42.49	10.22	45.62	3.07
48			81.82	1.80	47.26	6.99	46.65	11.85	47.15	1.76

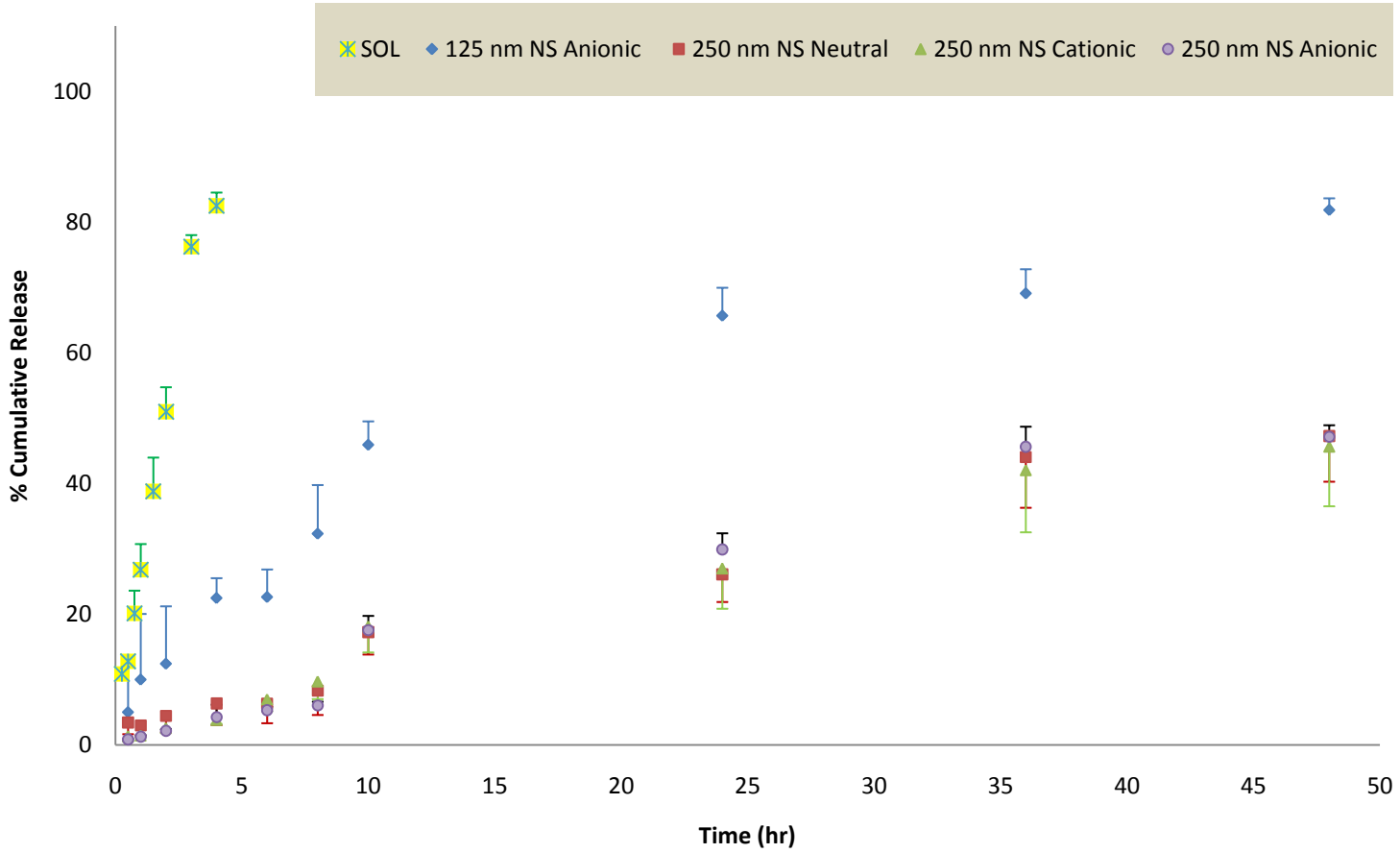

Figure 4.17 Release Profiles of LAZ Solution and Nanosuspensions of Different Sizes and Surface Potentials in Human Plasma at 37°C (n=3).

Table 4.12 Initial Release Rates (%hr^{-1}) of LAZ Solution and Nanosuspensions of Different Sizes and Surface Potentials in Human Plasma at 37^{o}C (n=3).

The Initial Release Rate in Human Plasma up to 1 hr					
	1	3	3	Mean	SD
Solution	9.41	15.29	11.08	11.93	3.03
125 nm NS Anionic	2.22	3.96	1.71	3.30*	1.46
250 nm NS neutral	1.95	0.294	0.423	0.89*	0.92
250 nm NS Cationic	1.32	1.08	0.29	0.90*	0.54
250 nm NS Anionic	0.49	1.45	0.62	0.85*	0.52

Table 4.13 Extent of Release (%hr^{-1}) of LAZ Solution and Nanosuspensions of Different Sizes and Surface Potentials in Human Plasma at 37^{o}C (n=3).

The Extent of % Cumulative Release after 48 hr in Human Plasma					
	1	3	3	Mean	SD
Solution	80.58	82.32	84.58	82.49#	2.00
125 nm NS	79.85	82.19	83.40	81.81#	1.81
250 nm NS neutral	39.89	53.80	48.08	47.26*#	6.99
250 nm NS Cationic	53.00	47.57	35.00	45.19*#	9.23
250 nm NS Anionic	46.15	46.11	49.17	47.15*#	1.76

***Significant difference compared to solution , # significant difference compared to PBS (P<0.05)**

the bag that yielded less available free LAZ. It was reported by Laizure et al., 1993, that LAZ family has a high plasma protein binding of ~ 90% [17].

From the previous study there was no difference in the release rate or extent among the group of the same size with different surface potentials (250 nm NS-A). But, the small size 125nm NS had a faster release rate and a higher extent compared to those of the larger size 250nm NS. The release in plasma was of slower rate and less extent compared to those from PBS due to the LAZ binding to plasma proteins.

4.4.4 *In-vitro* Release Kinetics of LAZ from Solution and Four Nanosuspensions (Neutral, Cationic and Anionic 250 nm and Anionic 125 nm) in PBS and Human Plasma (n=3)

The kinetics of LAZ release were characterized by fitting the equations of zero order, first order, Higuchi and Hixson-Crowell models to LAZ cumulative release. The coefficient of determination was the criterion for the goodness of fit of the model to the data. Table 4.14 and Figure 4.18 show the fit criteria and the plots of the kinetic equations to the cumulative release of LAZ solution, NS-A, NS-$A^{(+)}$, NS-$A^{(-)}$ and NS-$B^{(-)}$ in PBS. There was no single equation that had best fit to the profile compared to the others. There was no significant difference among the fit to the nanosuspension profiles to the kinetic equations except for the anionic 250 nm NS which had a poor fit to Higuchi's equation. The release from the four nanosuspensions was best described by the first order kinetics equation whichThis means that the release from the nanosuspensions was dependent upon how much was available for release after dissolution of LAZ

particles in PBS inside the bag. At the same time, the release from 250 nm NS group showed good fit to Hixson-Crowell‘s equation. The Hixson-Crowell equation explains that the release was dependent on the size of NS particles. Higuchi’s equation indicates that the drug release is controlled by the diffusion distance of the dissolved molecules. As the diffusion distance increases, the release from the bag becomes slower.

LAZ release in human plasma was best explained by First Order release kinetics for solution and the nanosuspension formulations. This could be due to the effect of plasma protein binding of LAZ which slowed down the release especially from the solution. The release from 125 nm NS was poorly fitted to zero order equation but the fit was good for the other three equations. Higuchi’s equation had poor fit to the cationic and anionic 250 nm NS. The release profiles of the 250nm NS group were fitted well to the Hixson-Crowell equation. This indicates that the release in plasma depended upon diameter of the large particles which imparted a slow dissolution of 250 nm particles compared to the fast dissolution of 125nm NS (Table 4.15 and Figure 4.19).

Table 4.14 Release Kinetics Criteria for LAZ Solution, NS-A, NS-A$^{(+)}$, NS-A$^{(-)}$ and NS-B$^{(-)}$ in PBS (n=3).

Kinetics in PBS	Zero Order		First		Higuchi		Hixson	
	K_o	r^2	K	r^2	K_H	r^2	K_{HC}	r^2
Solution	24.80 ±(1.29)	0.92 ±(0.04)	1.19 ±(0.35)	0.95 ±(0.02)	64.56 ±(3.09)	**0.96** ±(0.02)	1.10 ±(0.32)	0.95 ±(0.02)
125 nm NS-B$^{(-)}$	2.03 ±(0.08)	0.83 ±(0.03)	0.07 ±(0.01)	**0.94** ±(0.02)	16.60 ±(0.73)	0.93 ±(0.02)	0.06 ±(0.01)	0.91 ±(0.02)
250 nm NS (A)	1.65 ±(0.06)	0.93 ±(0.01)	0.03 ±(0.00)	**0.97** ±(0.02)	12.92 ±(0.47)	0.94 ±(0.02)	0.04 ±(0.00)	**0.96** ±(0.02)
250 nm NS (A)$^{(+)}$	1.55 ±(0.05)	0.95 ±(0.01)	0.03 ±(0.00)	**0.97** ±(0.02)	12.04 ±(0.46)	0.95 ±(0.02)	0.03 ±(0.01)	**0.97** ±(0.01)
250 nm NS(A)$^{(-)}$	1.58 ±(0.19)	0.97 ±(0.01)	0.03 ±(0.01)	**0.99** ±(0.01)	7.95 ±(0.94)	0.83 ±(0.01)	0.04 ±(0.01)	**0.99** ±(0.01)

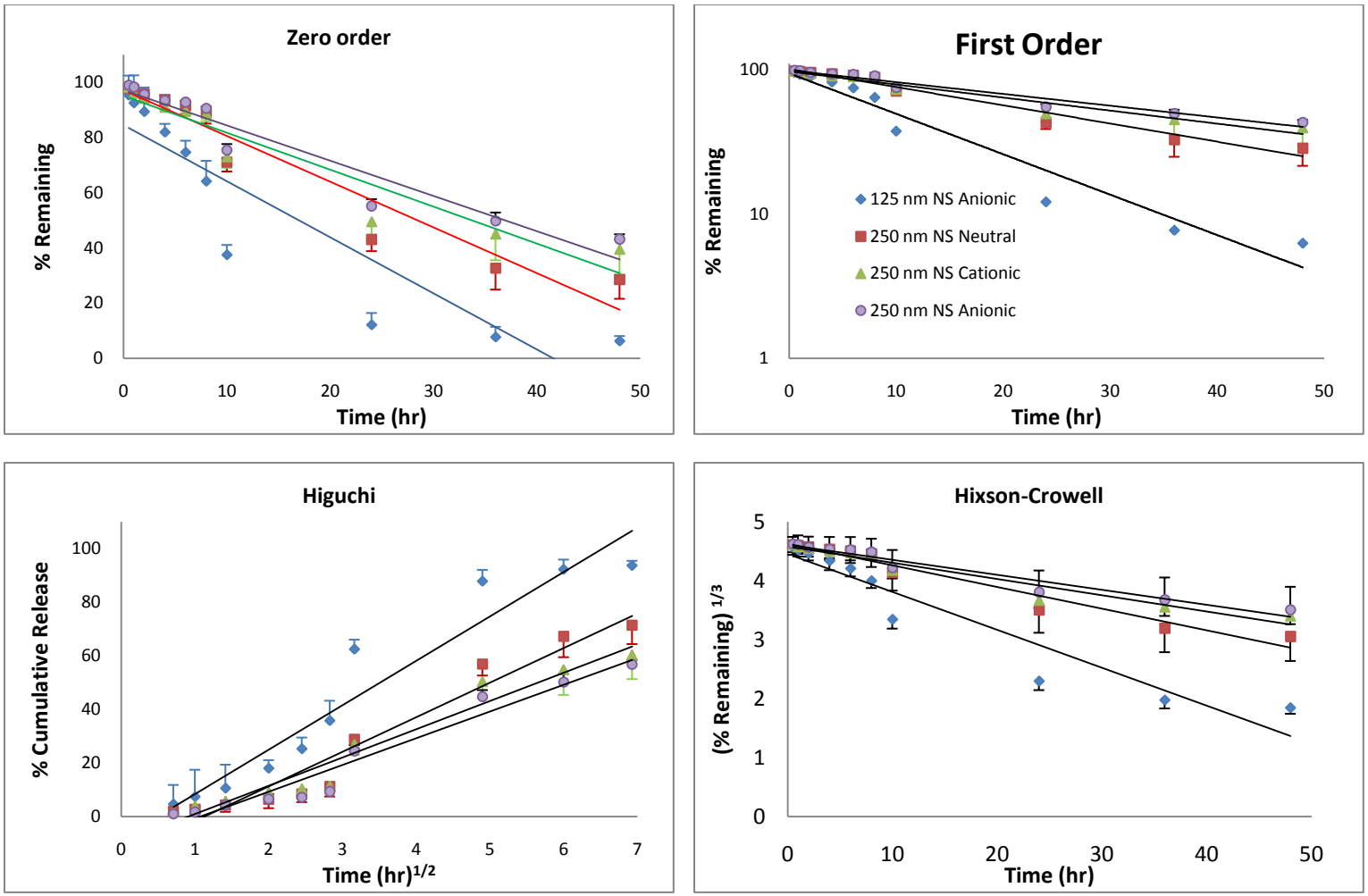

Figure 4.18 Release Kinetics from LAZ Solution, NS-A, NS-A$^{(+)}$, NS-A$^{(-)}$ and NS-B$^{(-)}$ in PBS.

Table 4.15 Release Kinetics Criteria for LAZ Solution, NS-A, NS-A$^{(+)}$, NS-A$^{(-)}$ and NS-B$^{(-)}$ in Human Plasma.

Kinetics in Plasma	Zero Order		First Order		Higuchi		Hixson	
	K_o	r^2	K	r^2	K_H	r^2	K_{HC}	r^2
Solution	20.94 ± (0.80)	0.96 ±(0.003)	0.47 (±0.03)	**0.97** ±(0.02)	7.68 ±(0.85)	0.94 ±(0.02)	0.54 ±(0.03)	0.95 ±(0.02)
125 nm NS-B$^{(-)}$	1.57 ±(0.18)	0.89 ±(0.01)	0.03 ±(0.01)	**0.97** ±(0.01)	12.64 ±(1.46)	**0.97** ±(0.01)	0.04 ±(0.01)	0.95 ±(0.01)
250 nm NS (A)	1.01 ±(0.12)	**0.97** ±(0.01)	0.01 ±(0.01)	**0.97** ±(0.01)	7.68 ±(0.85)	0.94 ±(0.02)	0.02 ±(0.003)	**0.97** ±(0.01)
250 nm NS (A)$^{(+)}$	1.00 ±(0.22)	0.97 ±(0.01)	0.01 ±(0.01)	**0.98** ±(0.01)	5.16 ±(1.16)	0.86 ±(0.01)	0.02 ±(0.01)	**0.98** ±(0.01)
250 nm NS(A)$^{(-)}$	1.09 ±(0.05)	0.95 ±(0.01)	0.01 ±(0.01)	**0.97** ±(0.01)	5.50 ±(0.29)	0.82 ±(0.01)	0.02 ±(0.001)	**0.97** ±(0.01)

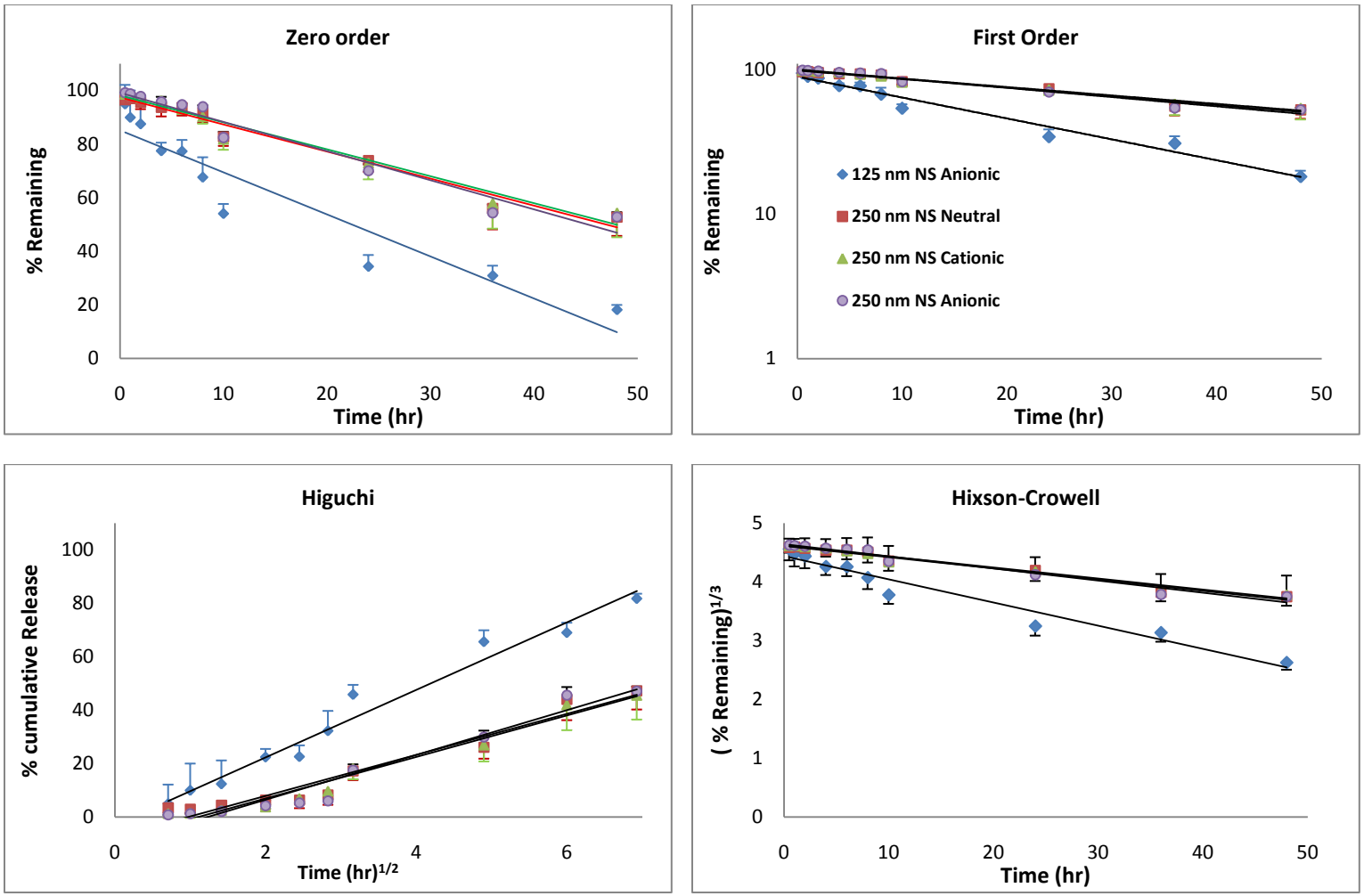

Figure 4.19 Release Kinetics from LAZ Solution, NS-A, NS-A$^{(+)}$, NS-A$^{(-)}$ and NS-B$^{(-)}$ in Human Plasma.

4.4.5 Plasma Pharmacokinetics of LAZ Solution and Four Nanosuspensions (NS-A 250 nm, NS-A $^{(+)}$ 250nm, NS-A$^{(-)}$ 250nm and NS-B$^{(-)}$125nm) in Nude Mice

Plasma pharmacokinetics of LAZ solution and four nanosuspensions (NS-A 250 nm, NS-A $^{(+)}$ 250nm, NS-A$^{(-)}$ 250nm and NS-B$^{(-)}$125nm) were studied in nude mice. Sparse sampling design was followed to collect *in-vivo* samples; that is, each animal contributed with a single observation and the area under the concentration-time curve (AUC) was constructed from the mean plasma concentration from multiple mice at individual time points. The sparse sampling approach produced only one mean plasma profile for the study. There was no statistics performed for the pharmacokinetics parameters as it was derived from one profile. However, the variance of AUC_{0-t} was estimated using the method described by Bailer (1988) [71].

For all the five formulations, the plasma concentrations rapidly declined after administering the formulation and then slowly removed from the central compartment (Figure 4.20). The NS-A$^{(+)}$ 250 nm and NS-B$^{(-)}$125nm profiles showed higher plasma concentration over the whole profile range compared to the other formulations. The mean plasma concentrations of the five formulations were fitted to non-compartmental model to derive the pharmacokinetics parameters (Table 4.16.). The C_o of the solution (10.87 µg/ml) was comparable to that of NS-B$^{(-)}$ (7.8 µg/ml), higher than those of NS-A (3.67 µg/ml) and NS-A$^{(-)}$(1.42 µg/ml) but lower than that of NS-A$^{(+)}$(15.56 µg/ml). Within the same 250 nm group, NS-A$^{(+)}$ had higher C_o than those of NS-A and NS-A$^{(-)}$.

Table 4.17 Plasma Concentration of LAZ Solution and Nanosuspensions at Different Time Points in Nude Mice.

	Concentration of LAZ in Plasma Samples µg/ml									
Time(hr)	Solution		NS-A 250 nm		NS-A$^{(+)}$ 250 nm		NS-A$^{(-)}$ 250 nm		NS-B$^{(-)}$ 125 nm	
	Mean	SD	Mean	SD	Mean	SD	Mean	SD	Mean	SD
0.16	3.73	0.19	2.52	0.94	7.34	0.27	1.33	0.17	4.15	0.56
0.25	2.01	0.38	2.04	0.38	4.81	0.30	1.28	0.24	2.91	0.75
0.5	0.96	0.17	0.70	0.23	2.66	0.39	0.86	0.07	2.67	0.22
0.75	0.83	0.27	0.69	0.11	1.86	0.49	0.64	0.12	1.69	0.64
1	0.82	0.16	0.55	0.18	1.73	0.67	0.62	0.12	1.42	0.08
3	0.51	0.16	0.41	0.02	0.69	0.41	0.43	0.03	0.77	0.30

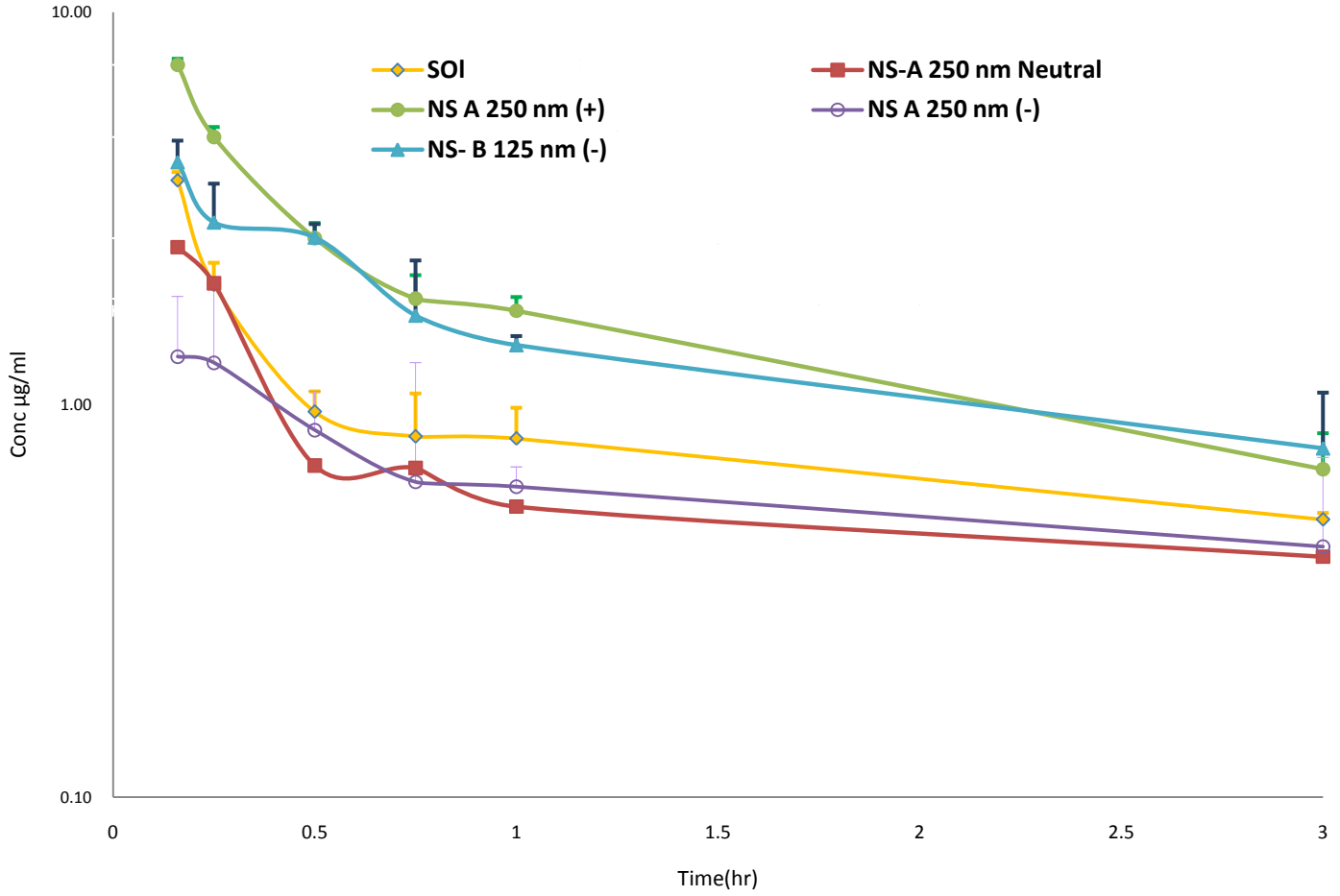

Figure 4.20 Plasma Concentration-Time Profile of LAZ Solution and Nanosuspension Formulations of 250nm (Neutral, cationic and Anionic) and 125 nm (Anionic) in Nude Mice

Table 4.16 Non –Compartmental PK Parameters of LAZ Formulations in Mice Plasma (from naïve pool data, 3 mice per each datum point)

PK parameters	Solution	NS-A (250 nm)	NS-A$^{(+)}$ (250 nm)	NS-A$^{(-)}$ (250 nm)	NS-B$^{(-)}$ (125 nm)
C_o (µg/ml)	10.87	3.67	15.56	1.42	7.80
AUC_{0-t} (hr.µg/ml)	3.61 ± 0.20	2.33 ± 0.10**	6.75 ± 0.50$^{\#\#}$	2.00 ± 0.05*	5.10 ± 0.37$^{\#}$
Cl (ml/hr)	38.28	69.85	36.85	68.17	40.50
V_{ss} (ml)	119.86	284.48	54.89	354.00	102.00
K_{el} (hr^{-1})	0.25	0.21	0.50	0.18	0.33
$t_{1/2}$(hr)	2.85	3.31	1.40	3.87	2.08
Systemic Exposure	1	0.73	2.10	0.62	1.59

*indicates significantly Lower compared to the solution, $^{\#}$ indicates significantly higher compared to the solution using ANOVA followed by Post-hoc Tukey's comparison P<0.05.

Number of * and $^{\#}$ indicates different ranking among the groups

Note: Systemic Exposure = the ratio of AUC of the formulation by that of the solution.

By comparing the negatively charged NS-$A^{(-)}$ 250 nm and NS-$B^{(-)}$125nm, NS-$B^{(-)}$ had a higher C_o as compared to that of the larger 250 nm NS-$A^{(-)}$.

The AUC of the solution (3.61 hr.µg/ml) was larger than those of NS-A and NS-$A^{(-)}$ (2.33 and 2.00 hr.µg/ml, respectively) but smaller than those of NS-$A^{(+)}$and NS-$B^{(-)}$ (6.75 and 5.10 hr.µg/ml, respectively). The AUC of the positively charged NS-$A^{(+)}$ was three times of those of NS-A and NS-$A^{(-)}$. Also, NS-$B^{(-)}$ had an AUC 2.5 folds of that of NS-$A^{(-)}$. The clearance of the solution was comparable to those of NS-$A^{(+)}$ and NS-$B^{(-)}$ but slower than those of NS-A and NS-$A^{(-)}$ (38.28, 36.85 and 40.5 ml/hr vs. 69.85 and 68.17 ml/hr, respectively). Among the NS-A 250 nm group, the clearance of the positively charged NS-$A^{(+)}$ was almost half of those of neutral (NS-A) and the negatively charged NS-$A^{(-)}$. The K_{el} of NS-$A^{(+)}$ was 2-2.5 folds of those of solution NS-A and NS-$A^{(-)}$ and 1.5 fold of that of NS-$B^{(-)}$ (0.5 hr^{-1} vs. 0.25, 0.21, 0.18 hr^{-1} and 0.33 hr^{-1}, respectively). The relative systemic exposure was calculated by dividing the AUC of each formulation by that of the solution. The highest relative BA was from NS-$A^{(+)}$ (2.10) and it was almost three folds of those of NS-A and NS-A $^{(-)}$ (0.73 and 0.62, respectively) and 1.3 fold that of NS-$B^{(-)}$ (1.59).

4.4.6 Organ Distribution of LAZ Solution and Four Nanosuspensions (NS-A 250 nm, NS-A $^{(+)}$ 250nm, NS-A$^{(-)}$ 250nm and NS-B$^{(-)}$125nm) in Nude Mice

The distribution of LAZ among mouse organs varied with the charge and particle size of the nanosuspensions (Figure 4.21). The general pattern of distribution among the mouse organs was the same from all the formulations except that a higher distribution to the lungs was noticed from anionic nanosuspensions. The liver uptake and exposure of the nanosuspensions was higher from all the nanosuspensions as compared to that of the solution (Table 4.18 & Figure 4.21). The C_{max} values calculated for NS-A, NS-A$^{(+)}$, NS-A$^{(-)}$ and NS-B$^{(-)}$ were twice that of the solution (75.82, 93.54, 98.88 and 89.29 µg/gm, respectively, vs. 43.97 µg/gm). The liver exposure was in the ascending order of: solution < NS-A and NS-A$^{(+)}$ < NS-A$^{(-)}$ and NS-B$^{(-)}$ (28.35, 33.99 / 40.07 and 58.61 / 63.57 hr.µg/gm, respectively). The liver uptake of the negatively charged nanosuspension was about 1.5 folds those of the neutral and cationic NS. The $t_{1/2}$ of LAZ in the liver tissue was comparable for the solution NS-A and NS-A$^{(-)}$ (0.85, 1.01 and 0.94 hr, respectively). The half life of LAZ from NS-A$^{(+)}$ and NS-B$^{(-)}$ was less than those from the solution and NS-A and NS-A$^{(-)}$. (0.69 and 0.59 hr, respectively) (Figure 4.22 & Table 4.19) (Table 4.18).

LAZ uptake by the lungs from NS-A$^{(-)}$ and NS-B$^{(-)}$ yielded a significantly higher C_{max} (63.85 and 50.14 µg/gm)than those from the solution, NS-A and NS-A$^{(+)}$ (14.55, 13.73 and 18.60 µg/gm). The lung exposure AUC was comparable among the solution, NS-A and NS-A$^{(+)}$ (11.94, 12.31 and 13.53 hr.µg/gm, respectively) but a higher exposure was

obtained from NS-$B^{(-)}$ and NS-$A^{(-)}$ (33.57 and 99.64 hr.µg/gm). LAZ $t_{1/2}$ of the solution in the lung tissues (1.38 hr) was comparable to that of NS-$A^{(-)}$ (1.34 hr) but those of NS-A , NS-$A^{(+)}$ and NS-$B^{(-)}$ appeared to be shorter, 0.80 , 0.68 and 0.82 hr (Figure 4.23 & Table 4.20).

The C_{max} values in the kidneys from solution, NS-A and NS-$A^{(-)}$ was comparable (19.19 , 11.30 and14.90 µg/gm, respectively), but smaller than those of NS-$A^{(+)}$ and NS-$B^{(-)}$ (45.92 and 30.01µg/gm). The C_{max} of NS-$B^{(-)}$ was 2 fold of that of NS-$A^{(-)}$ (30.01 µg/gm vs. 14.90 µg/gm). The kidneys exposure of LAZ from the solution was comparable to that of NS-$A^{(-)}$ and 3 folds of that of NS-A (17.65 and 14.27 hr.µg/gm vs. 6.26 hr.µg/gm) but was less than those of NS-$A^{(+)}$ and NS-$B^{(-)}$ (17.65 hr.µg/gm vs. 27.94 and 28.04 hr.µg/gm, respectively). The exposure of NS-$A^{(+)}$ was comparable to that of NS-$B^{(-)}$, and 2 and 4 folds of those of NS-$A^{(-)}$ and NS-A, respectively. LAZ $t_{1/2}$ in kidney tissue was comparable from the solution, NS-A, NS-$A^{(+)}$ and NS-$B^{(-)}$ (1.32 ,1.04, 0.92 and 0.85 hr, respectively) but it was longer from of NS-$A^{(-)}$ (2.23 hr) (Figure 4.24 & Table 4.21).

The C_{max} values of LAZ in the heart from solution was comparable to those of the NS-A and NS-$B^{(-)}$ (15.09, 14.76 and 16.01, respectively). The C_{max} was the lowest from NS-$A^{(-)}$ and the highest from NS-$A^{(+)}$ (7.73 µg/gm vs. 24.66 µg/gm). The heart exposure from the solution was comparable to those of NS-A and NS-$B^{(-)}$(14.34, 12.14 and 15.02 hr.µg/gm, respectively). The exposure from NS-$A^{(+)}$ and NS-$A^{(-)}$ (7.00 and 8.65 hr.µg/gm)was

comparable and half of those from the solution, NS-A and NS-$B^{(-)}$ (Figure 4.25 & Table 4.22).

The C_{max} of LAZ in the spleen from solution, NS-A and NS-$A^{(+)}$ were comparable (7.76, 5.87 and 9.50 µg/gm, respectively). LAZ uptake by the spleen from NS-$A^{(-)}$ and NS-$B^{(-)}$ (28.7 and 13.74 µg/gm) was higher than those from the solution, NS-A and NS-$A^{(+)}$.The spleen exposure was in the following ascending order: the solution< NS-A and NS-$A^{(+)}$ < NS-$B^{(-)}$ < NS-$A^{(-)}$ (4.30 hr.µg/gm ,8.38 / 9.80, 16.04 and 32.06 hr.µg/gm, respectively) (Figure 4.26 & Table 4.23).

The highest uptake in the brain was from solution (1.04 µg/gm) followed by NS-A (0.58 µg/gm), however the brain uptake from NS-$A^{(+)}$, NS-$A^{(-)}$ and NS-$B^{(-)}$ was comparable (0.32, 0.36 and 0.38 µg/gm, respectively). The brain exposure AUC of LAZ from different formulation was limited. The AUC of the solution was the highest among the formulations which was in the following rank NS-A > NS-$B^{(-)}$ > NS-$A^{(+)}$ and NS-$A^{(-)}$ (0.42 hr.µg/gm vs. 0.17, 0.11and 0.05 / 0.05 hr.µg/gm, respectively) (Figure 4.27 & Table 4.24).

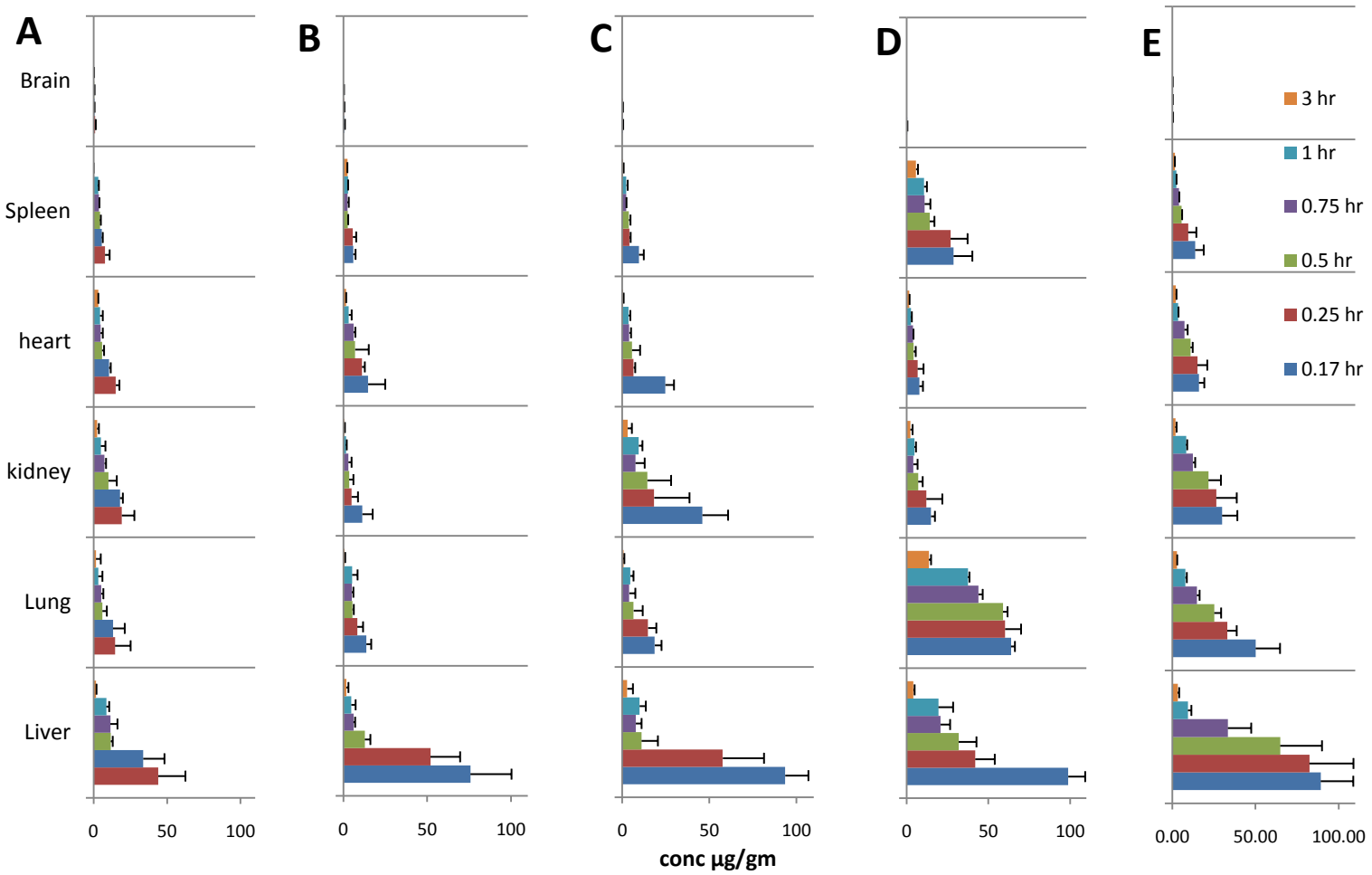

Figure 4.21 Organ Distribution of LAZ in Swiss Nude Mice from (A) Solution, (B) NS-A , (C) NS-A$^{(+)}$, (D) NS-A$^{(-)}$ and (E) NS-B$^{(-)}$.

Table 4.18 Non-Compartmental Parameters of LAZ Formulations in Mouse Organs

Solution						
	Liver	Lungs	Kidneys	Heart	Spleen	Brain
C_{max} (µg/gm)	43.97	14.55	19.19	15.09	7.76	1.04
AUC_{0-t}	28.35	11.94	17.65	14.34	4.30	0.42
(hr.µg/gm)	(± 2.06)	(± 4.00)	(± 1.90)	(± 0.47)	(± 0.11)	(± 0.05)
$t_{1/2}$(hr)	0.85	1.38	1.32	3.54	1.03	0.26
NS-A (250 nm) Neutral						
	Liver	Lungs	Kidneys	Heart	Spleen	Brain
C_{max} (µg/gm)	75.82	13.73	11.30	14.76	5.87	0.58
AUC_{0-t}	33.99*	12.31	6.26*	12.14	8.38*	0.17*
(hr.µg/gm)	(±2.94)	(± 0.71)	(± 0.82)	(± 1.74)	(± 0.21)	(± 0.04)
$t_{1/2}$(hr)	1.01	0.80	1.04	1.24	1.55	0.25
NS-A$^{(+)}$ (250 nm) Cationic						
	Liver	Lungs	Kidneys	Heart	Spleen	Brain
C_{max} (µg/gm)	93.54	18.60	45.92	24.66	9.50	0.32
AUC_{0-t}	40.07*	13.53	27.94***	7.00*	9.80**	0.05**
(hr.µg/gm)	(±4.40)	(± 1.10)	(± 3.89)	(± 0.84)	(± 0.13)	(± 0.01)
$t_{1/2}$(hr)	0.69	0.68	0.92	0.39	0.47	0.17
NS-A$^{(-)}$ (250 nm) Anionic						
	Liver	Lungs	Kidneys	Heart	Spleen	Brain
C_{max} (µg/gm)	98.88	63.85	14.90	7.73	28.70	0.36
AUC_{0-t} (hr.µg/gm)	58.61** (±2.62)	99.64** (± 1.78)	14.27** (±1.78)	8.65* (± 0.99)	32.06**** (± 1.14)	0.05** (± 0.01)
$t_{1/2}$(hr)	0.94	1.34	2.23	1.97	2.47	0.14
NS-B$^{(-)}$ (125 nm) Anionic						
	Liver	Lungs	Kidneys	Heart	Spleen	Brain
C_{max} (µg/gm)	89.29	50.14	30.01	16.01	13.74	0.38
AUC_{0-t}	63.57**	33.57*	28.04***	15.02	16.04***	0.11*
(hr.µg/gm)	(±4.88)	(± 1.55)	(± 1.79)	(± 0.82)	(± 0.48)	(± 0.02)
$t_{1/2}$(hr)	0.59	0.82	0.85	0.98	0.39	0.40

*indicates significant difference compared to the solution using ANOVA followed by Post-hoc Tukey's comparison $P<0.05$. Number of asterisks indicates different ranking among the groups

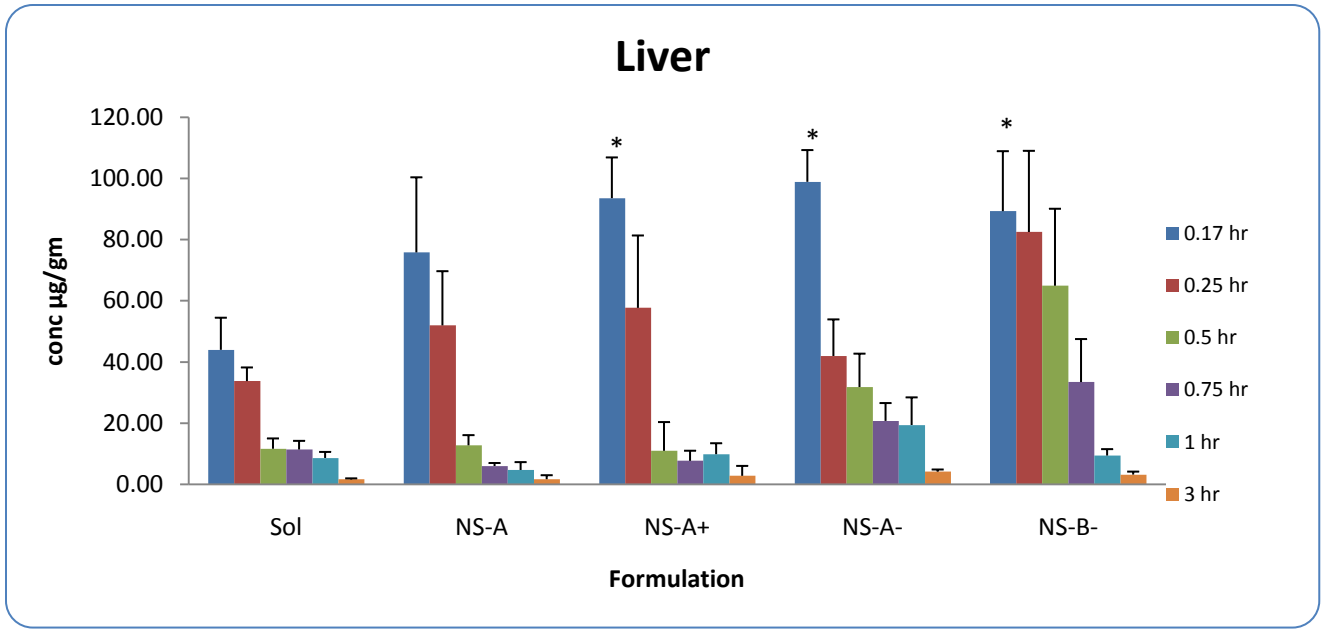

Figure 4.22 LAZ Distribution to the Liver of Nude Mice from Solution and Nanosuspension Formulations

Table 4.19 LAZ concentrations in Liver Samples from Solution and Nanosuspensions in Nude Mice

	Concentration of LAZ in Liver Samples µg/gm									
Time(hr)	Solution		NS-A		NS-A+		NS-A-		NS-B-	
	Mean	SD	Mean	SD	Mean	SD	Mean	SD	Mean	SD
0.17	43.97	8.5	75.82	24.54	93.54	13.31	98.88	10.38	89.29	19.61
0.25	33.75	4.47	51.96	17.72	57.69	23.66	41.96	11.96	82.48	26.53
0.50	11.64	3.38	12.77	3.33	10.98	9.39	31.81	10.91	64.93	25.15
0.75	11.40	2.83	6.00	0.99	7.70	3.30	20.74	5.84	33.44	14.06
1.00	8.63	1.97	4.71	2.57	9.87	3.58	19.41	9.03	9.42	2.10
3.00	1.65	0.32	1.69	1.31	2.80	3.24	4.14	0.72	3.20	0.98

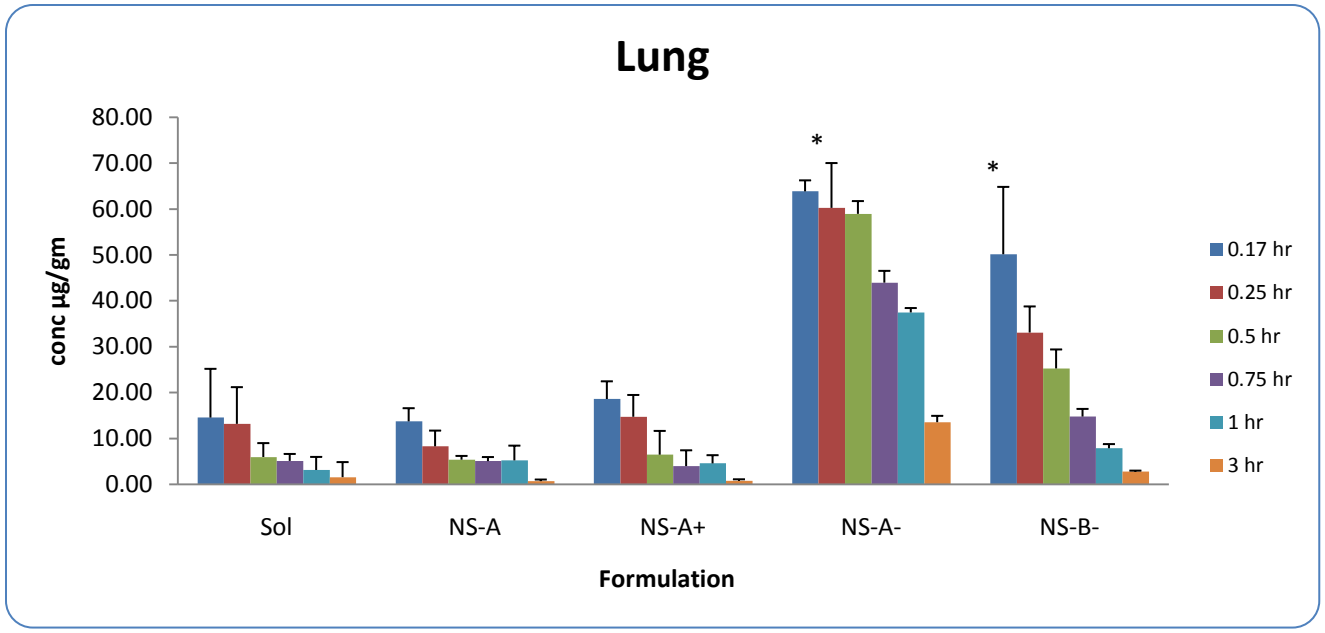

Figure 4.23 LAZ Distribution to the Lungs of Nude Mice from Solution and Nanosuspension Formulations

Table 4.20 LAZ concentrations in Lung Samples from Solution and Nanosuspensions in Nude Mice

	Concentration of LAZ in Lung Samples µg/gm									
Time(hr)	Solution		NS-A		NS-A+		NS-A-		NS-B-	
	Mean	SD	Mean	SD	Mean	SD	Mean	SD	Mean	SD
0.17	14.55	10.62	13.73	2.87	18.60	3.85	63.84	2.4	50.14	14.68
0.25	13.19	8.00	8.29	3.43	14.73	4.75	60.24	9.77	33.08	5.69
0.50	5.97	3.03	5.38	0.82	6.47	5.18	58.94	2.78	25.26	4.14
0.75	5.12	1.51	5.06	0.89	3.98	3.45	43.95	2.57	14.77	1.67
1.00	3.14	2.85	5.23	3.21	4.57	1.79	37.46	0.96	7.87	0.91
3.00	1.57	0.62	0.70	0.35	0.77	0.34	13.55	1.38	2.82	0.18

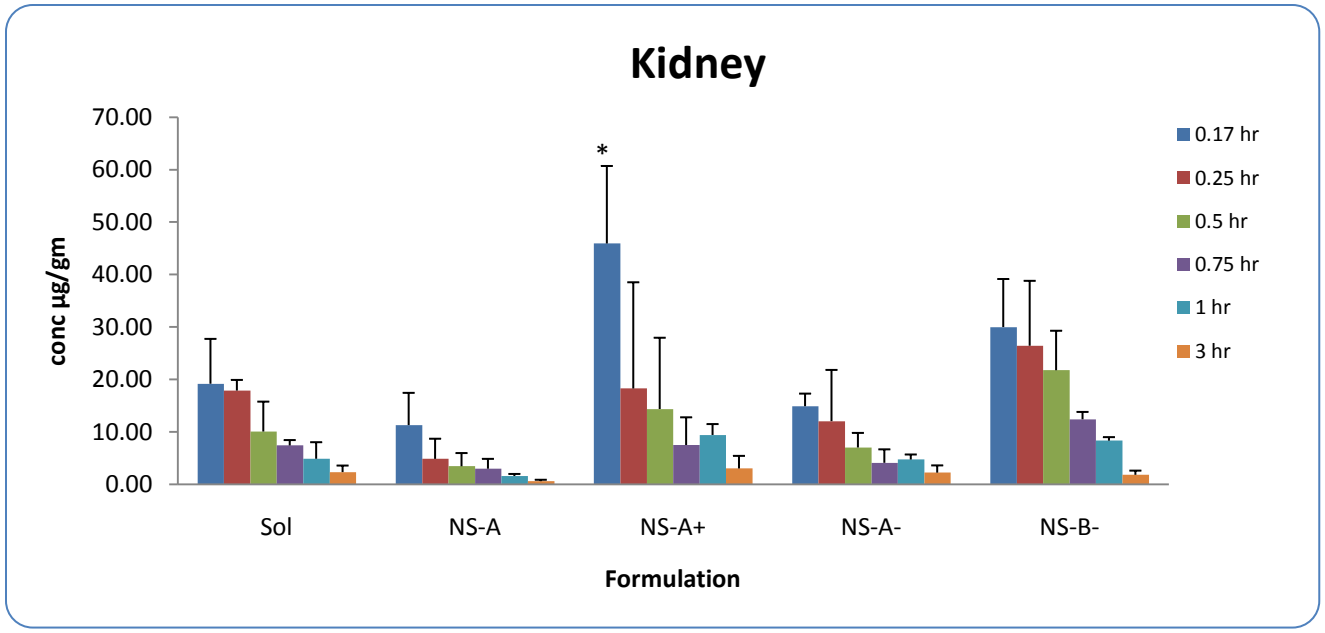

Figure 4.24 LAZ Distribution to the Kidneys of Nude Mice from Solution and Nanosuspension Formulations

Table 4.21 LAZ concentrations in Kidney Samples from Solution and Nanosuspensions in Nude Mice

Time(hr)	Concentration of LAZ in Kidney Samples µg/gm									
	Solution		NS-A		NS-A+		NS-A-		NS-B-	
	Mean	SD	Mean	SD	Mean	SD	Mean	SD	Mean	SD
0.17	19.19	8.55	11.30	6.15	45.92	14.78	14.90	2.40	29.99	9.17
0.25	17.88	2.03	4.86	3.84	18.28	20.25	12.05	9.77	26.43	12.37
0.50	10.08	5.70	3.45	2.52	14.37	13.59	7.03	2.78	21.76	7.53
0.75	7.42	1.03	2.99	1.88	7.50	5.28	4.11	2.57	12.41	1.40
1.00	4.89	3.16	1.60	0.39	9.42	2.08	4.74	0.96	8.34	0.67
3.00	2.34	1.25	0.61	0.27	3.03	2.4	2.24	1.38	1.82	0.8

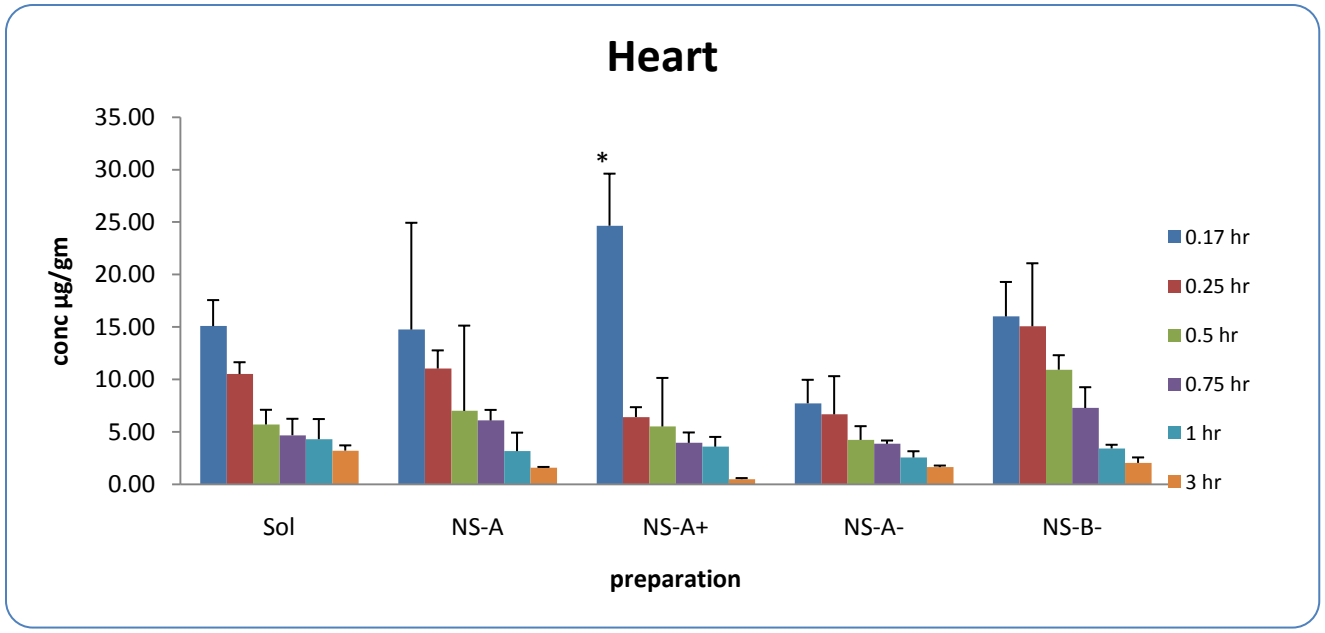

Figure 4.25 LAZ Distribution to the Heart of Nude Mice from Solution and Nanosuspension Formulations

Table 4.22 LAZ concentrations in Heart Samples from Solution and Nanosuspensions in Nude Mice

Time(hr)	Concentration of LAZ in Heart Samples µg/gm									
	Solution		NS-A		NS-A+		NS-A-		NS-B-	
	Mean	SD	Mean	SD	Mean	SD	Mean	SD	Mean	SD
0.17	15.09	2.48	14.76	10.18	24.66	4.96	7.73	2.24	16.01	3.29
0.25	10.52	1.13	11.04	1.73	6.42	0.94	6.67	3.64	15.07	6.01
0.50	5.71	1.40	7.00	8.13	5.52	4.63	4.24	1.31	10.93	1.38
0.75	4.68	1.57	6.09	1.01	3.96	0.99	3.86	0.32	7.28	1.98
1.00	4.31	1.92	3.17	1.76	3.60	0.93	2.56	0.60	3.43	0.35
3.00	3.22	1.90	1.58	0.08			1.65	0.15	2.05	0.52

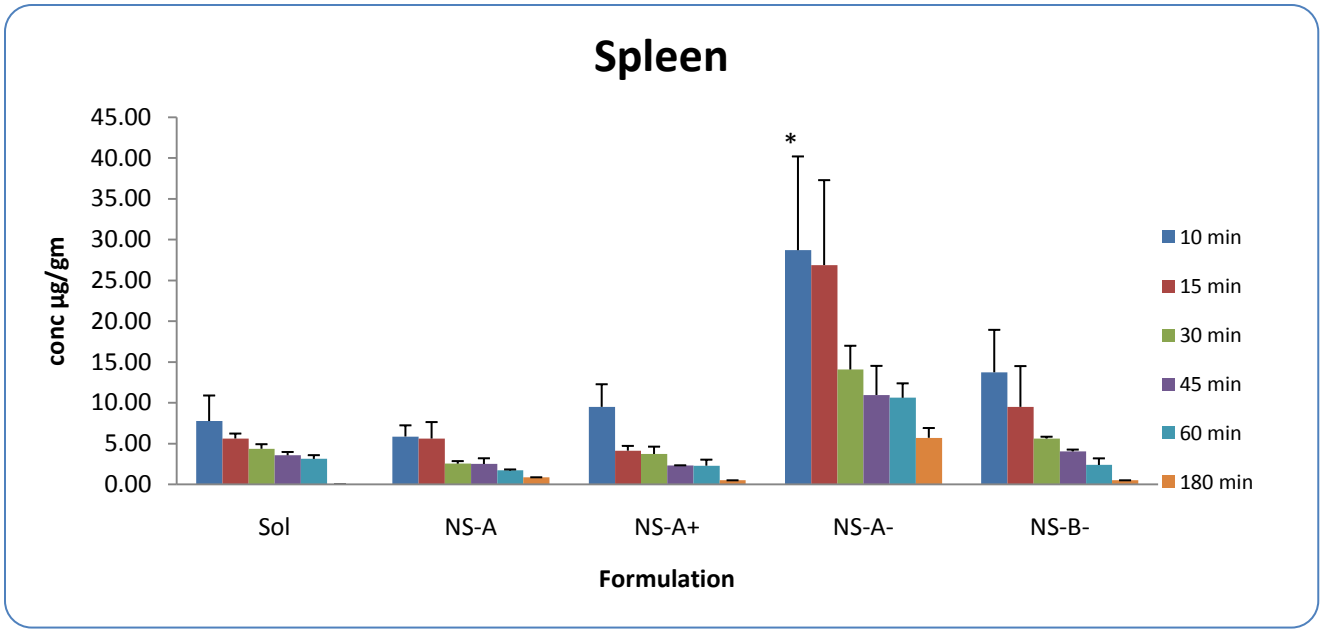

Figure 4.26 LAZ Distribution to the Spleen of Nude Mice from Solution and Nanosuspension Formulations

Table 4.23 LAZ concentrations in Spleen Samples from Solution and Nanosuspensions in Nude Mice

Time(hr)	Concentration of LAZ in Spleen Samples µg/gm									
	Solution		NS-A		NS-A+		NS-A-		NS-B-	
	Mean	SD	Mean	SD	Mean	SD	Mean	SD	Mean	SD
0.17	7.76	3.13	5.87	1.37	9.50	2.77	28.70	11.49	13.74	5.20
0.25	5.62	0.61	5.62	2.02	4.14	0.58	26.88	10.41	9.50	5.00
0.50	4.36	0.56	2.53	0.32	3.73	0.90	14.08	2.91	5.61	0.23
0.75	3.56	0.41	2.50	0.70	2.31	0.03	10.95	3.57	4.04	0.23
1.00	3.12	0.46	1.72	0.11	2.29	0.74	10.61	1.77	2.38	0.81
3.00			0.87	0.1			5.71	1.20		

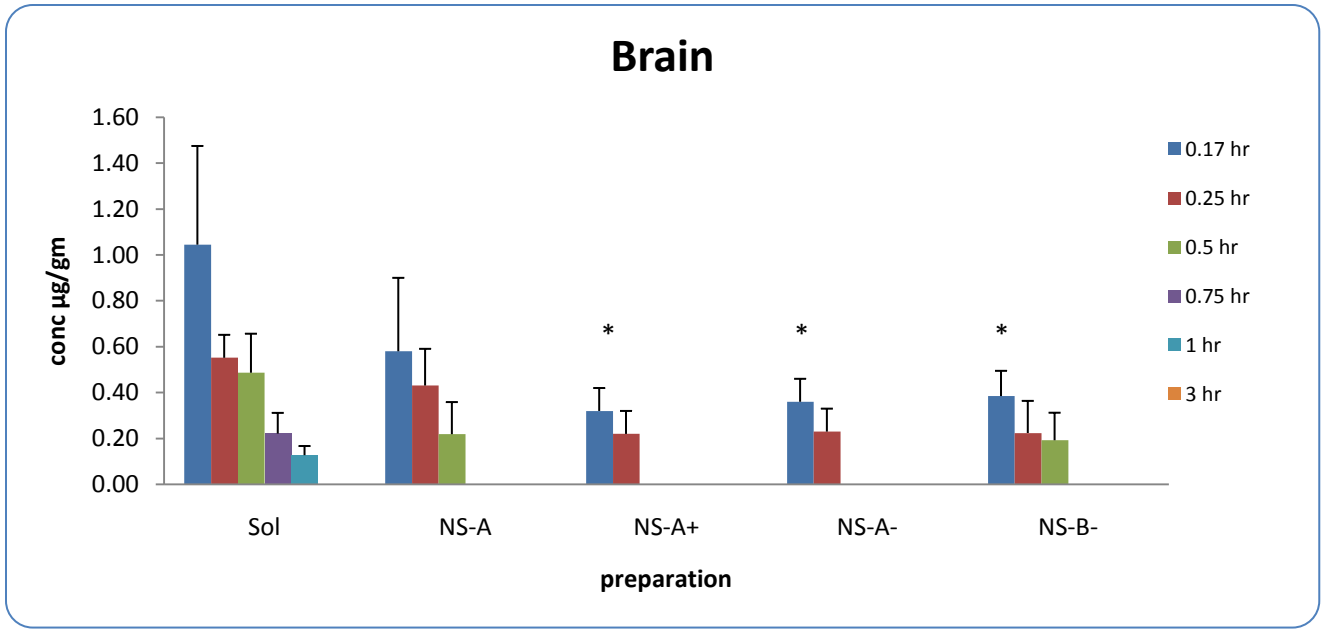

Figure 4.27 LAZ Distribution to the Brain of Nude Mice from Solution and Nanosuspension Formulations

Table 4.24 LAZ concentrations in Brain Samples from Solution and Nanosuspensions in Nude Mice

	Concentration of LAZ in Brain Samples µg/gm									
Time(hr)	Solution		NS-A		NS-A+		NS-A-		NS-B-	
	Mean	SD	Mean	SD	Mean	SD	Mean	SD	Mean	SD
0.17	1.04	0.43	0.58	0.32	0.32	0.10	0.36	0.11	0.38	0.11
0.25	0.55	0.1	0.43	0.16	0.22	0.10	0.23	0.10	0.22	0.14
0.50	0.49	0.17	0.22	0.14						
0.75	0.22	0.09								
1.00										
3.00										

4.5 Microspheres

4.5.1 Encapsulation Efficiency and Loading Capacity of LAZ Microspheres (n=3)

Different formulation compositions were presented in Tables 4.25 to examine the effects of different variables on the EE and loading capacity of the microsphere formulations. The variables tested included PLGA polymer composition, the initial loading amount of LAZ, the concentration of PVA and PLGA, and finally the modification of process conditions with centrifugation and varying temperature.

The EE and Loading capacities of various formulations were presented in Table 4.25. The effect of increasing the loading amount of LAZ was examined through the formulations 10-12 and 17-19 using 20, 40 and 80 mg of LAZ. In these 6 formulations, PLGA (50:50) with densities of 0.50 g/dL and 0.43 g/dL in a concentration of 50 mg/ml was selected with 5% PVA to examine the effect of increasing the polymer density on the formulation. The encapsulation efficiency decreased by increasing LAZ loading amount above 40 mg using 5% PVA and 50 mg/ml PLGA. There was no significant difference among the formulations containing two polymers with different densities (molecular weight) except at high LAZ loading (80 mg) that the lower density polymer (0.43 g/dL) had a significantly higher EE than that of the higher density polymer (0.50 g/dL).

In another set, the same procedure was repeated but the 5% PVA was replaced with 1%PVA to evaluate the effect of the stabilizer concentration (Formulation 7-9 compared

to Formulations 11-12). The same trend was noticed that increasing the loading amountof LAZ more than 40 mg decreased the EE of the formulations. Also, the use of 5% PVA yielded higher EE than those from 1%PVA; however it was not significantly different. Thus, 40 mg of LAZ was chosen for the rest of microsphere formulations.

The effect of PLGA polymer composition (lactic acid/glycolic acid; LA/GA) was examined using fixed 40 mg LAZ as the loading amount and 5% PVA for the stabilizer in Formulas 2 (85/15; LA/GA, 0.65 g/dL), 11(50/50; LA/GA, 0.50 g/dL) and 18 (50/50; LA/GA, 0.43g/dL). The results showed that there was no significant difference between the higher density 0.65 g/dL and 0.50 g/dL polymers (52.41±5.12% and 65.91±13.67%, respectively) but there was a significant difference between 0.65 g/dL and 0.43 g/dL (52.41±5.12% vs. 70.71±4.07%, respectively). This indicated that the higher content of lactic acid in the 85/15; LA/GA polymer did not affect the formulation compared to those from 50:50 LA:GA polymer. However, the difference in the molecular weight among the three formulations affected the EE as the use of the low density 0.43 g/dL PLGA polymer improved the EE compared to that from the higher density 0.65 g/dL PLGA.

Table 4.25 LAZ Microspheres Formulation EE and Loading Capacities

Formulation #	Drug (mg)	PLGA		PVA	EE		Loading Capacity	
		Type	Conc.		Mean	SD	Mean	SD
1	40	85/15 0.65 g/dL	250 mg/5ml DCM	1%	36.13	4.11	4.85	0.55
2	40			5%	52.41	5.12	7.77	0.75
3	40		500 mg/5ml DCM	1%	22.00	4.22	1.76	0.33
4	40			5%	26.10	2.17	1.95	0.16
5	40		1000 mg/5ml DCM	1%	13.78	2.64	0.58	0.11
6	40			5%	15.68	3.62	0.63	0.14
7	20	50/50 0.50 g/dL	250 mg/5ml DCM	1%	50.55	6.72	5.09	1.45
8	40				52.48	8.72	5.78	1.53
9	80				24.19	5.67	6.05	2.91
10	20			5%	67.09	9.01	4.95	0.88
11	40				65.91	13.67	9.13	1.95
12	80				30.17	7.45	7.29	3.97
13	40		500 mg/5ml DCM	1%	29.26	1.76	2.25	0.13
14	40			5%	22.33	9.00	1.67	0.67
15	40		1000 mg/5ml DCM	1%	14.73	0.73	0.58	0.02
16	40			5%	11.64	0.50	0.48	0.02
17	20	50/50 0.43 g/dL	250 mg/ 5ml DCM	5%	69.93	0.67	2.44	0.27
18	40				70.71	4.07	5.49	0.85
19	80				59.88	8.87	3.20	0.05
20 cold	40				74.59	12.76	8.98	0.09
20-B*	40	50/50 0.43 g/dL	250 mg/ 5ml DCM	5%	64.10	6.28	8.87	0.16
20-C*	40				84.10	6.36	12.46	0.93
20-D*	40				73.89	2.44	9.18	0.94
20-E*	40				66.59	1.16	9.53	0.31
20-F*	40				59.39	5.10	8.59	0.15
20-G*	40				60.11	3.58	7.66	0.66
20-H*	40				69.58	0.67	7.76	0.46

***Applied centrifugation and cooling**

The molecular weight of the polymer can be calculated from the corresponding density according to according to Mark–Houwink equation [72]:

$(\eta)_{inh}=(1.07\times10^{-4})\ M^{0.761}$ where $(\eta)_{inh}$ is inherent viscosity (dl/g).

Where:

$(\eta)_{inh}$ = 0.43 g/dL Mwt = 54 448 dalton (50/50)

$(\eta)_{inh}$ = 0.50 g/dL Mwt = 66 383 dalton (50/50)

$(\eta)_{inh}$ = 0.65 g/dL Mwt = 93 710 dalton (85/15)

The effect of PVA was examined on two concentration levels, 1% (Formulations 7-9) and 5% (Formulations 10-12) using 50 mg/ml of 0.50 g/dL polymer. The EE was higher using 5% PVA compared to those with 1% PVA (51%, 52% and 24% for 1% PVA vs. 67%, 66% and 30% for 5% PVA, respectively). Comparing Formulations # 10 and 11, the loading capacity is higher for formulation # 11 (9.13 %) which was loaded with 40 mg of LAZ with 5% PVA compared to formulation 10 (4.95%) which was loaded with 20 mg LAZ. This indicated that the use of 40 mg LAZ as a loading amount with 5% PVA provided the highest EE and loading capacity. In addition, the use of the low density 0.43 g/dL polymer provided higher EE compared to that of the higher density 0.65 g/dL PLGA.

There was no significant effect of the molecular weight between the 0.65 g/dL and 0.50 g/dL polymers. Therefore, they were selected to examine the effect of modifying PLGA concentration in the formulation, Formulations 3-6 (for 0.65 g/dL PLGA; 85/15) and 13-

16 (for 0.50 g/dL PLGA; 50/50) were compared to Formulations 1 & 2 and 8 & 11, respectively. The PLGA concentrations were 100 and 250 mg/ml within the Formulations 3-6 and 13-16 with PVA 1 and 5%, respectively. The EE dropped by approximately 73-83% when the concentration of PLGA 0.5 g/dL increased above 50 mg/ml compared to Formulations 8 and 11 with 50 mg/ml PLGA and PVA of 1% and 5%, respectively. For formulations with 0.65 g/dL polymer, the increase in polymer concentration more than 50 mg/ml decreased the EE by 63-71% when compared to Formulations 1 and 2.

From the previous results, the optimum concentration of PLGA was 50 mg/ml in the presence of 5% PVA and 40 mg LAZ. This formulation composition showed the highest EE among the three PLGA polymers tested for microsphere formulations. The loading capacity varied among the formulations but the highest loading capacities were achieved by using the low density PLGA 50/50 polymers (0.50 and 0.43 g/dL) compared to those of higher density PLGA 85/15 (0.65 g/dL) using the same formulation variables.

The effect of the process conditions was tested for Formulations 20-cold to 20-H, in which different procedures were used to generate the microspheres. The formulations were cooled down to various temperatures, and then the cold mixtures were centrifuged at different speeds (Table 3.2). Cooling to 15^{o}C and centrifuging the mixture at 7,000 rpm, increased the EE to 84% with 12% loading capacity for PLGA 0.43 g/dL (Formulation 20-B). The same method was used to prepare the microspheres from the other PLGA's.

4.5.2 Characterization of Microspheres Formulations

4.5.2.1 Scanning Electron Microscope

SEM photos are given in Figure 4.28. The surface of the microspheres was smooth without cracks or wrinkles. There were no open pores or channels on the surface. The size of the microspheres was evaluated using the visual microscope and size varied with the polymer used. The increase in polymer solution viscosity with high density polymers(due to higher molecular weight) led to a decrease in the particle size using homogenization to disperse the emulsion phases [73]. The size of 0.65 g/dL PLGA was 9.11±4.17 µm, comparable to those of PLGA 0.50 g/dL and PLGA 0.43 g/dL (13.89±6.51 µm and 19.44±7.50 µm, respectively).

4.5.2.2 LAZ Release from Different PLGA Microspheres in human CSF (0.43, 0.50 and 0.65 g/dL PLGA, n=3)

Three microspheres formulations of PLGA with different densities (0.43, 0.50 and 0.65 g/dL with 50/50, 50/50 and 85/15 LA/GA, respectively) were selected to study LAZ release in CSF. The *in-vitro* release profiles in CSF were characterized by multiple phases of release (Table 4.26 & Figure 4.29) where the initial release rate of the formulations varied according to the polymer used. The initial release rate up to 6 hr for low density PLGA (0.43g/dL) was faster than those from 0.50 and 0.65 g/dL (21, 18 and 14 $\%day^{-1}$, respectively) but the rates were not significantly different (Table 4.26). A

burst release after 4 days and continued till Day 8 with all the PLGA polymers. The burst effect was more obvious with the low density 0.43g/dL PLGA than the other two polymers with higher densities. The extents of release after 21 days are shown in Table 4.27. The release extent was the highest from the low density 0.43 g/dL PLGA, 91%, followed by 61% from 0.50g/dL PLGA and 44% from 0.65 g/dL PLGA.

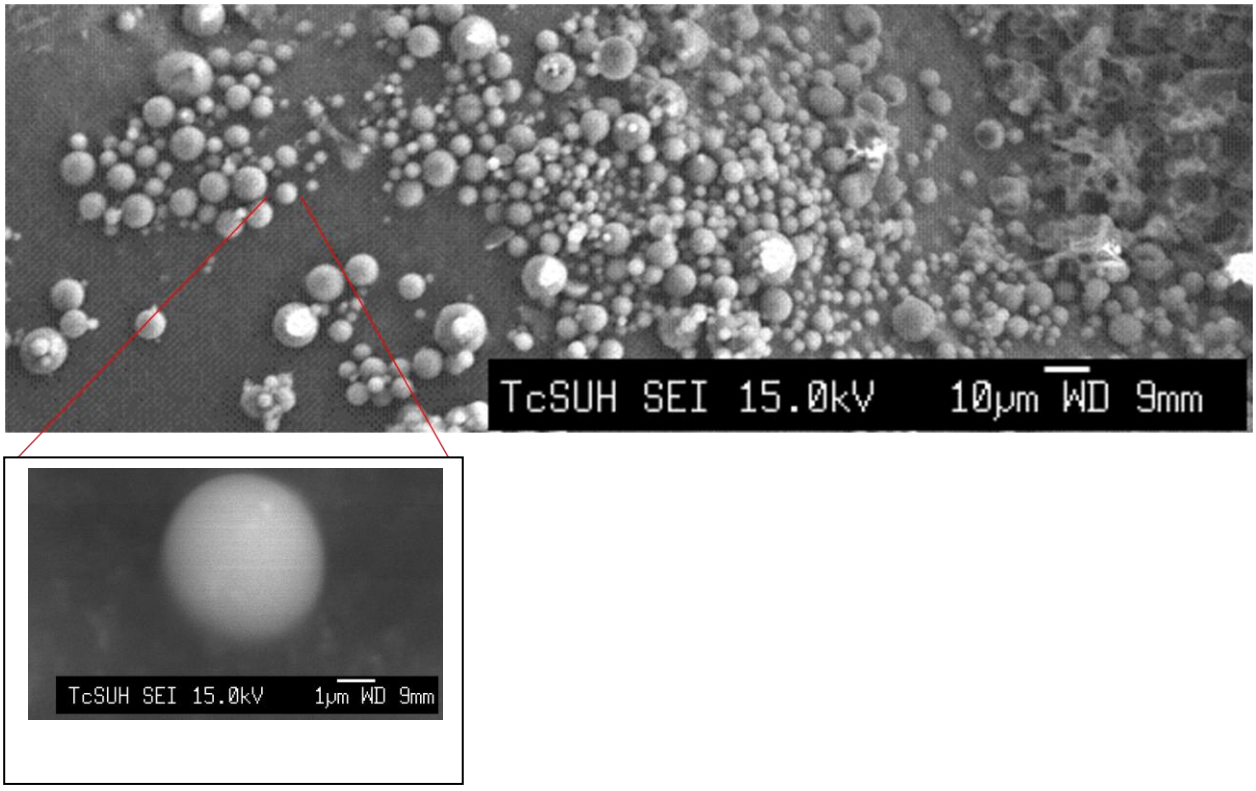

Figure 4.28 Scanning Electron Microscope Photo of Microspheres Formulation # 20-B.

Table 4.26 Cumulative LAZ Release from LAZ Microspheres of Different PLGA Polymers in CSF at 37°C (n=3).

	% Cumulative release					
Time(day)	**0.43 g/dL PLGA**	**SD**	**0.50 g/dL PLGA**	**SD**	**0.65 g/dL PLGA**	**SD**
0.01	2.78	0.31	1.91	0.24	0.99	0.19
0.02	3.34	0.66	1.96	0.20	1.28	0.16
0.04	4.19	1.14	2.86	0.94	1.91	0.54
0.08	4.19	0.54	2.90	0.41	1.84	0.27
0.17	4.97	0.39	3.88	0.07	2.86	0.52
0.25	5.65	0.50	4.73	0.69	3.82	0.50
1	7.78	0.23	6.69	0.72	5.08	0.34
2	19.36	3.36	14.96	0.78	11.81	0.46
4	25.19	3.25	18.53	1.37	14.59	0.67
6	38.80	3.57	27.86	3.33	19.56	2.06
8	65.58	5.26	41.71	2.90	27.45	3.01
12	77.37	5.88	47.42	4.65	33.71	5.49
17	86.48	4.74	58.16	4.40	35.11	5.62
21	90.67	4.09	60.91	4.09	37.27	5.88

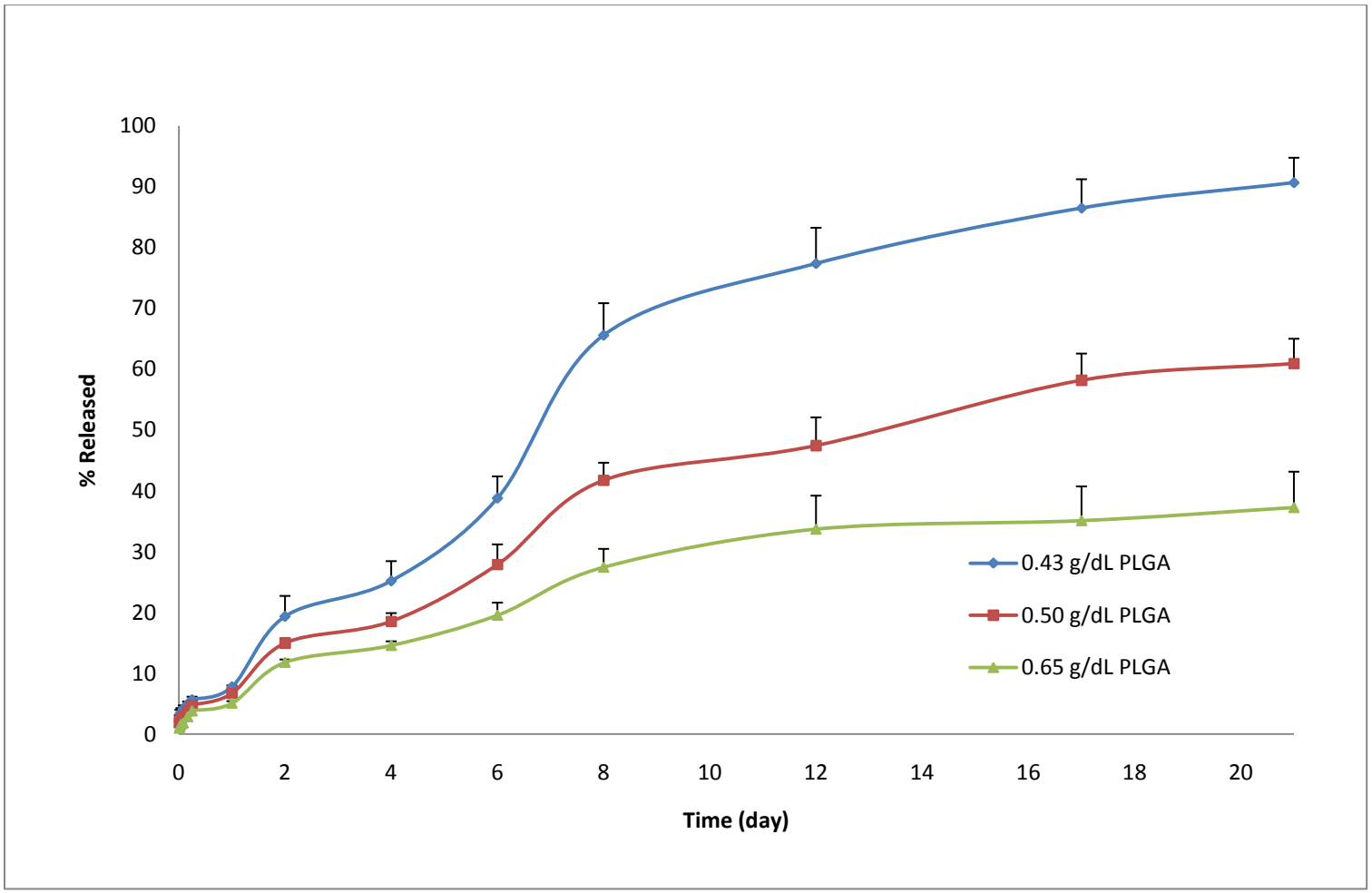

Figure 4.29 Release Profiles of LAZ Microspheres of Different PLGA polymers in CSF at 37^{o}C (n=3).

Table 4.27 Initial Release Rates (%day^{-1}) of LAZ Microspheres of Different PLGA Polymers in CSF at 37^{o}C (n=3).

Initial Release Rate after 6 hr (%hr^{-1})	1	2	3	Mean	SD
0.43 g/dL PLGA	17.03	21.41	25.22	21.22	4.10
0.50 g/dL PLGA	18.60	17.47	19.03	18.37	0.80
0.65 g/dL PLGA	17.87	11.29	13.75	14.31	3.33

Table 4.28 Extent of Release (%) of LAZ Microspheres of Different PLGA Polymers in CSF at 37^{o}C (n=3).

The extent of release of MS after 21 days in CSF (%)	1	2	3	Mean	SD
0.43 g/dL PLGA-MS	94.08	86.14	91.77	90.67	4.09
0.50 g/dL PLGA-MS	65.05	60.82	56.87	60.91*	4.09
0.65 g/dL PLGA-MS	37.12	49.73	46.31	44.39**	6.52

*** Significant difference compared to 0.43 g/dL PLGA-MS (P<0.05)**

Four kinetics equations were fitted to the data of cumulative LAZ release percentages. The goodness of fit was evaluated by comparing the correlation coefficient (R^2) of the regression lines. There was no significant difference among the kinetics equations R^2 values for fitting LAZ microsphere release profiles in human CSF (Table 4.29 & Figure 4.30).

Table 4.29 Release Kinetics Criteria for LAZ Microspheres in CSF.

PLGA Density g/dL	Zero Order		First		Higuchi		Hixson	
	K_o	r^2	K	r^2	K_H	r^2	K_{HC}	r^2
0.43	4.74 ±(0.11)	0.93 ±(0.03)	0.12 ±(0.02)	**0.97** ±(0.01)	21.22 ±(0.44)	0.95 ±(0.01)	0.13 ±(0.01)	**0.96** ±(0.02)
0.53	3.09 ±(0.26)	0.95 ±(0.01)	0.05 ±(0.01)	**0.98** ±(0.01)	13.89 ±(1.12)	**0.97** ±(0.01)	0.06 ±(0.01)	**0.97** ±(0.01)
0.65	2.33 ±(0.37)	0.90 ±(0.03)	0.03 ±(0.01)	0.92 ±(0.03)	10.62 ±(1.54)	**0.96** ±(0.01)	0.04 ±(0.01)	0.92 ±(0.03)

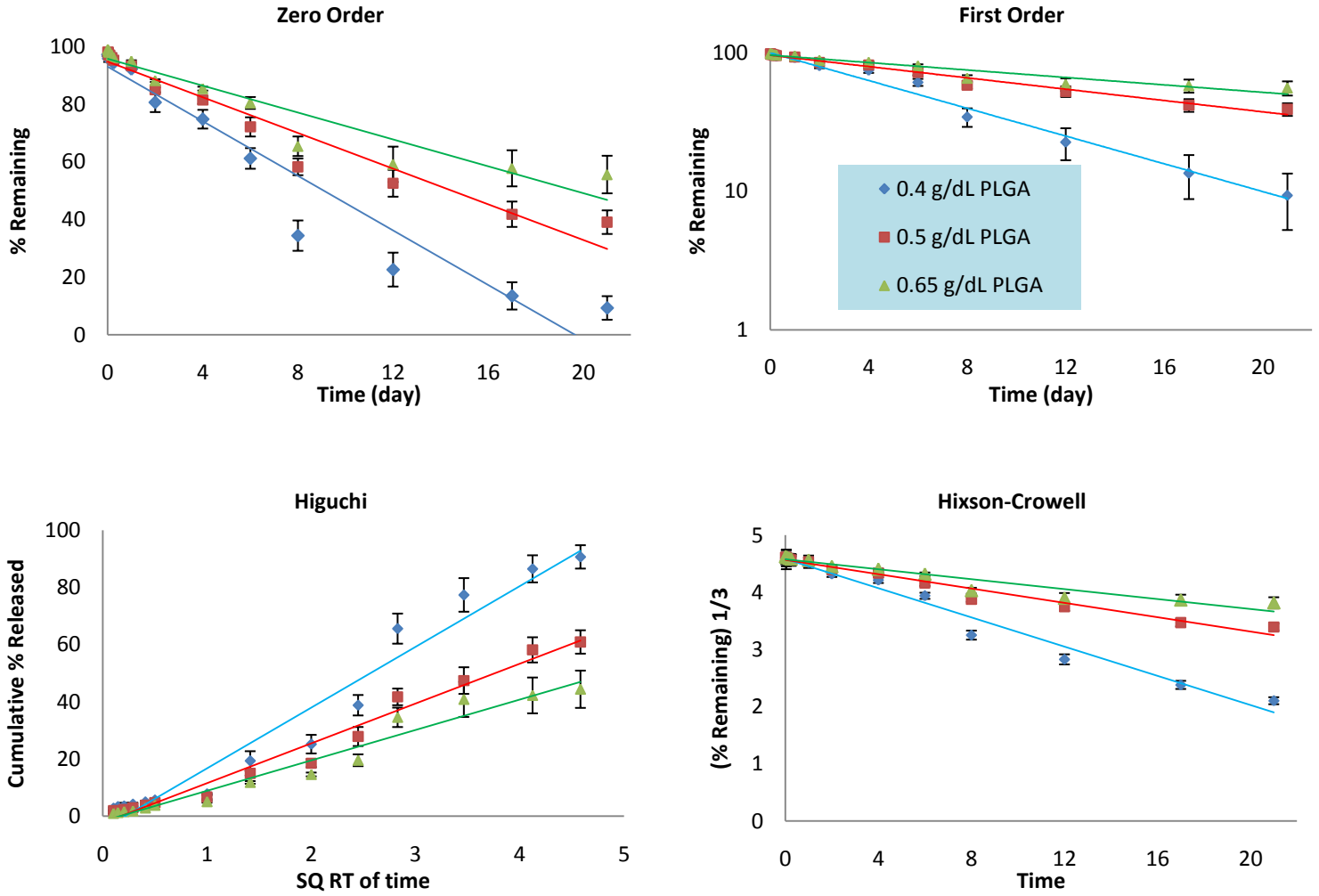

Figure 4.30 Release Kinetics of LAZ Microsphere Formulations in Human CSF

4.6. Liposomes

4.6.1 Liposomes Characterization

4.6.1.1 Vesicle Sizes and Surface Potential

LAZ liposomes were prepared using thin lipid film hydration method. After the lipid film was hydrated, liposomes were sonicated to further reduce the vesicle size and facilitate the extrusion process. The liposomal sizes, polydispersity index (PI) and Zeta potential were characterized (Table 4.30 & Figure 4.32). The EE was 25% for Lipo A, 62 % for Lipo G and 64% for Lipo B and Lipo C, respectively. The size of the liposomes was 90-122 nm with narrow polydispersity index, 0.09-0.14. The Zeta potentials of Lipo A, Lipo B and Lipo C were close to neutral with slightly positive potential of +2 *mv* on Lipo A and Lipo B and small negative potential of - 0.5 *mv* on Lipo C. The PEGylated Lipo G carried a significantly higher negative potential of -22 *mv* than those of conventional liposomes, Lipo A and Lipo B.

Table 4.30 Characterization of LAZ Liposomes with Different Lipid Ratios (n=3-5)

Liposomes	Lipids Ratio HSPC :CH:PEG	% EE	Size (nm)	PI	Zeta potential (*mv*)
A	9 : 1 : 0	24.63 ±6.11*	121.62 ±10.76*	0.12 ±0.04	2.65 ±1.16
B	8 : 2 : 0	64.06 ±7.21	90.48 ±6.22	0.14 ±0.08	2.02 ±5.63
C	7 : 3 : 0	64.51 ±16.41	92.96 ±9.05	0.14 ±0.07	-0.52 ±2.21
G	6 : 2 : 2	62.26 ±4.94	90.26 ±8.16	0.09 ±0.04	-22.31 ±9.40
*indicates significant difference among the preparations (P<0.05)					

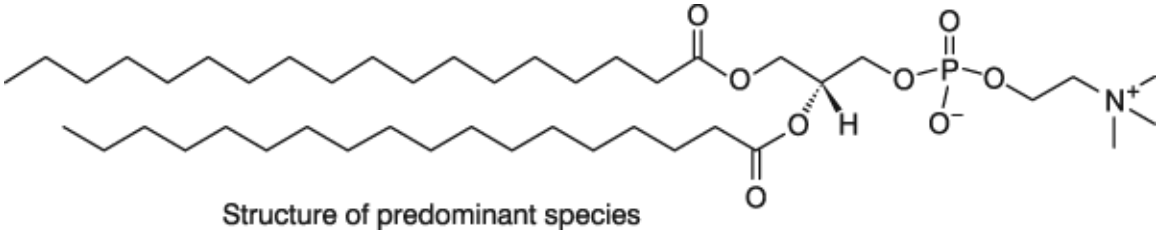

Hydrogenated Soy Phophatidylcholine – *HSPC*

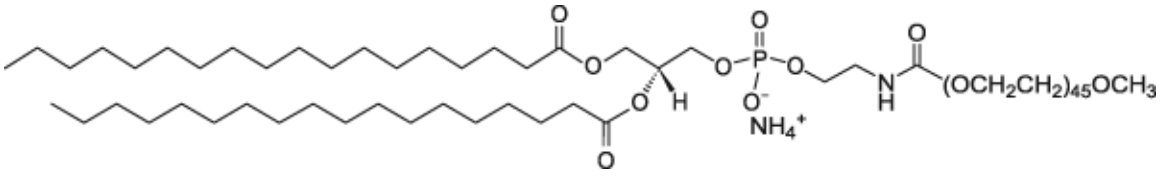

18:0 PEG2000 PE [1,2-distearoyl-*sn*-glycero-3-phosphoethanolamine-N-[methoxy(polyethylene glycol)-2000] (ammonium salt)]-*DSPE-PEG2000*

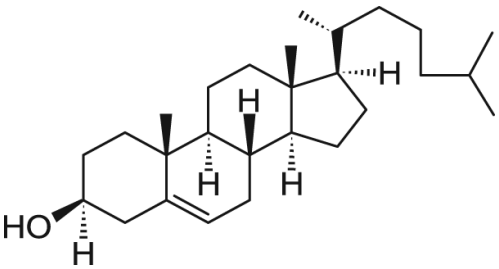

Cholesterol- *CH*

Figure 4.31 Lipid Compositions in LAZ Liposomes

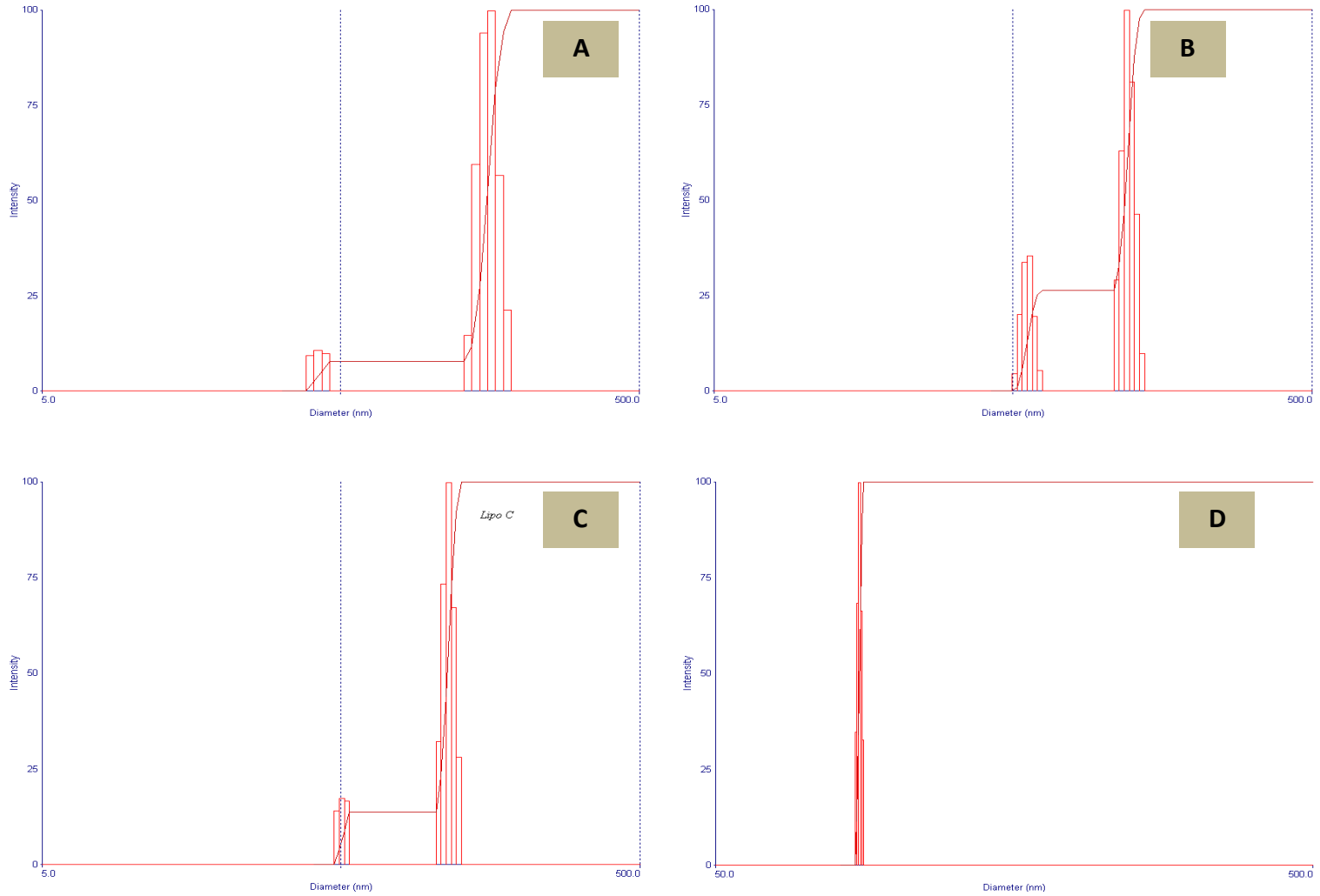

Figure 4.32 Particle Size Distribution of (A) Lipo-A, (B) Lipo-B, (C) Lipo-C and (D) Lipo G.

4.6.1.2 *In-vitro* LAZ Release from Liposomes of Four Lipid Composition (Conventional Lipo A, B, C and PEGylated Lipo G) in PBS (n=3, each)

In-vitro release of LAZ from solution and liposomes of different lipid compositions (Lipo A, B, C and G) was characterized in PBS. Tween 80 (0.2% v/v) was added in the release medium to maintain the sink condition. The release of LAZ from the solution was fast and complete by 4 hr. However, LAZ release from the liposomal formulations exhibited a biphasic profile with a slower release compared to that of the solution (Table 4.31 & Figure 4.33). The initial release rate of LAZ from the solution, 40.18 % hr^{-1} , was faster than those of the liposomes ,10.74, 21.50, 20.53 and 20.87 % hr^{-1} for Lipo A, B, C and G , respectively (Table 4.32). The release of LAZ from the solution was complete by 4 hr. The initial release rate and release extent of Lipo A were the least among the liposomal formulations. The release extents were comparable for Lipo B, C and G (90.55, 88.06 and 96.39%) after 24 hr, higher than that of Lipo A, 68.57% (Table 4.33).

4.6.1.3 *In-vitro* LAZ Release from Liposomes of Four Lipid Composition (Conventional Lipo A, B, C and PEGylated Lipo G) in Human Plasma (n=3, each)

In-vitro LAZ release from solution and liposomes of different lipid compositions (Lipo A, B, C and G) was studied in human plasma at 37^{o}C. The release of LAZ from the solution was fast and 82% of LAZ was released by 4 hr. However, LAZ release from the liposomal formulations exhibited a biphasic profile with slower release compared to that of the solution (Figure 4.34). The initial release rate of LAZ varied with the formulations

Table 4.31 Cumulative LAZ Release from LAZ Solution and Liposomes of Different Lipid Compositions in PBS at 37°C (n=3).

Time (hr)	% Released from liposomes in PBS									
	Solution		Lipo A		Lipo B		Lipo C		Lipo G	
	Mean	SD	Mean	SD	Mean	SD	Mean	SD	Mean	SD
0.25	11.92	0.78	3.66	0.48	4.40	1.92	6.88	3.51	7.71	1.23
0.5	17.89	1.43	5.93	0.58	7.12	2.34	10.95	4.97	13.21	2.26
0.75	32.01	4.28	8.19	1.64	14.23	5.50	16.03	2.19	18.60	4.85
1	40.72	2.87	-	-	-	-	-	-	-	-
1.5	52.81	3.08	-	-	-	-	-	-	-	-
2	75.23	12.77	22.00	3.91	28.31	3.39	30.21	0.65	34.92	8.54
3	96.26	3.44	-	-	-	-	-	-	-	-
4	98.22	3.69	28.38	2.14	36.40	1.62	43.31	6.33	48.49	10.63
8			42.50	2.40	64.83	1.15	73.97	4.61	71.88	6.93
10			56.94	2.18	76.22	4.07	80.30	7.00	86.88	4.96
24			68.57	1.82	90.55	4.37	88.06	8.93	96.39	2.12

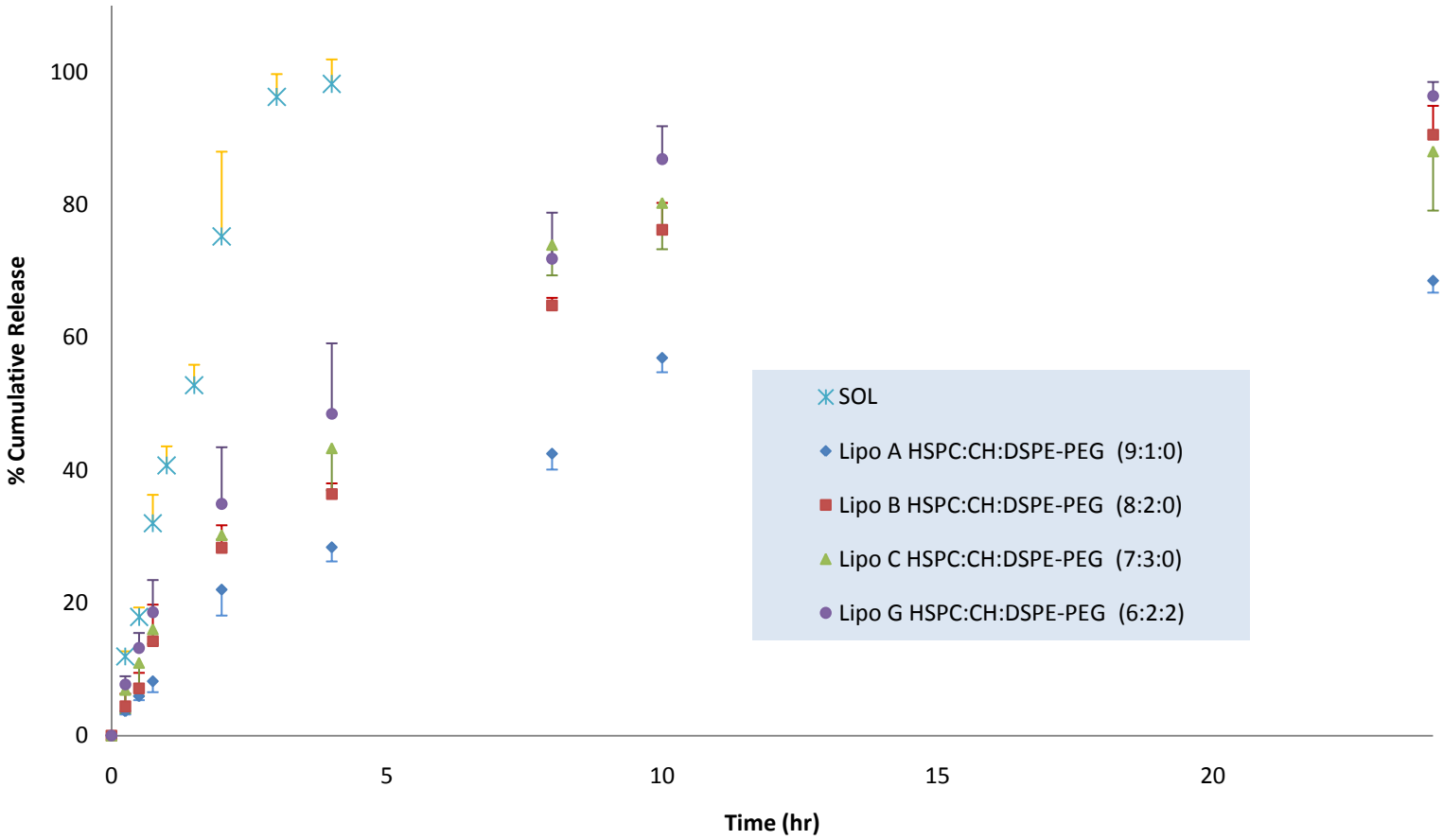

Figure 4.33 Release Profiles of LAZ from Solution and Liposomes with Different Lipid Compositions in PBS at 37°C (n=3).

Table 4.32 Initial Release Rates (%hr^{-1}) of LAZ Solution and Liposomes of Different Lipid Compositions in PBS at 37^{o}C (n=3).

The initial release rate in PBS after 0.75 hr (%hr^{-1})	1	2	3	Mean	SD
Solution	47.09	33.07	40.37	40.18	7.01
Lipo A	10.18	12.88	9.15	10.74**	1.93
Lipo B	21.48	22.7	20.32	21.50*	1.19
Lipo C	21.99	17.31	22.28	20.53*	2.79
Lipo G	21.99	17.32	23.29	20.87*	3.14

Table 4.33 Extent of Release (%hr^{-1}) of LAZ Solution and Liposomes of Different Lipid Composition in PBS at 37^{o}C (n=3).

The extent of release after 24 hr in PBS	**1**	**3**	**3**	**Mean**	**SD**
Solution	99.47	101.12	94.07	98.22	3.69
Lipo A	67.15	70.62	67.96	68.57*	1.82
Lipo B	89.65	86.70	95.29	90.55	4.37
Lipo C	93.77	92.64	77.77	88.06	8.93
Lipo G	97.25	93.98	97.94	96.39	2.12

*** Significant difference compared to the Solution (P<0.05)**

Table 4.34 Cumulative LAZ Release from LAZ Solution and Liposomes of Different Lipid Composition in Human Plasma at 37°C (n=3).

Time (hr)	% Released from liposomes in plasma									
	Solution		125 nm NS		250 nm NS		250 nm/+ NS		250 nm/- NS	
	Mean	SD	Mean	SD	Mean	SD	Mean	SD	Mean	SD
0.25	10.87	0.57	2.08	1.08	2.11	1.04	7.08	2.43	2.81	1.06
0.5	12.81	0.48	7.59	1.08	7.40	1.65	18.60	4.62	4.96	2.43
0.75	20.12	3.47	16.55	2.67	26.08	4.25	29.73	4.00	5.53	1.56
1	26.81	3.92	-	-	-	-	-	-	-	-
1.5	38.80	5.16	-	-	-	-	-	-	-	-
2	50.98	3.74	24.38	3.40	33.17	5.91	36.41	6.85	10.54	1.72
3	76.21	1.78	-	-	-	-	-	-	-	-
4	82.49	2.00	28.28	3.57	37.95	7.56	45.32	3.65	16.54	2.35
8			34.43	2.60	43.43	7.41	53.79	10.07	21.87	6.06
10			44.37	3.92	55.25	5.85	63.39	4.78	27.40	7.84
24			58.75	1.37	81.45	5.78	79.23	7.11	41.11	3.44

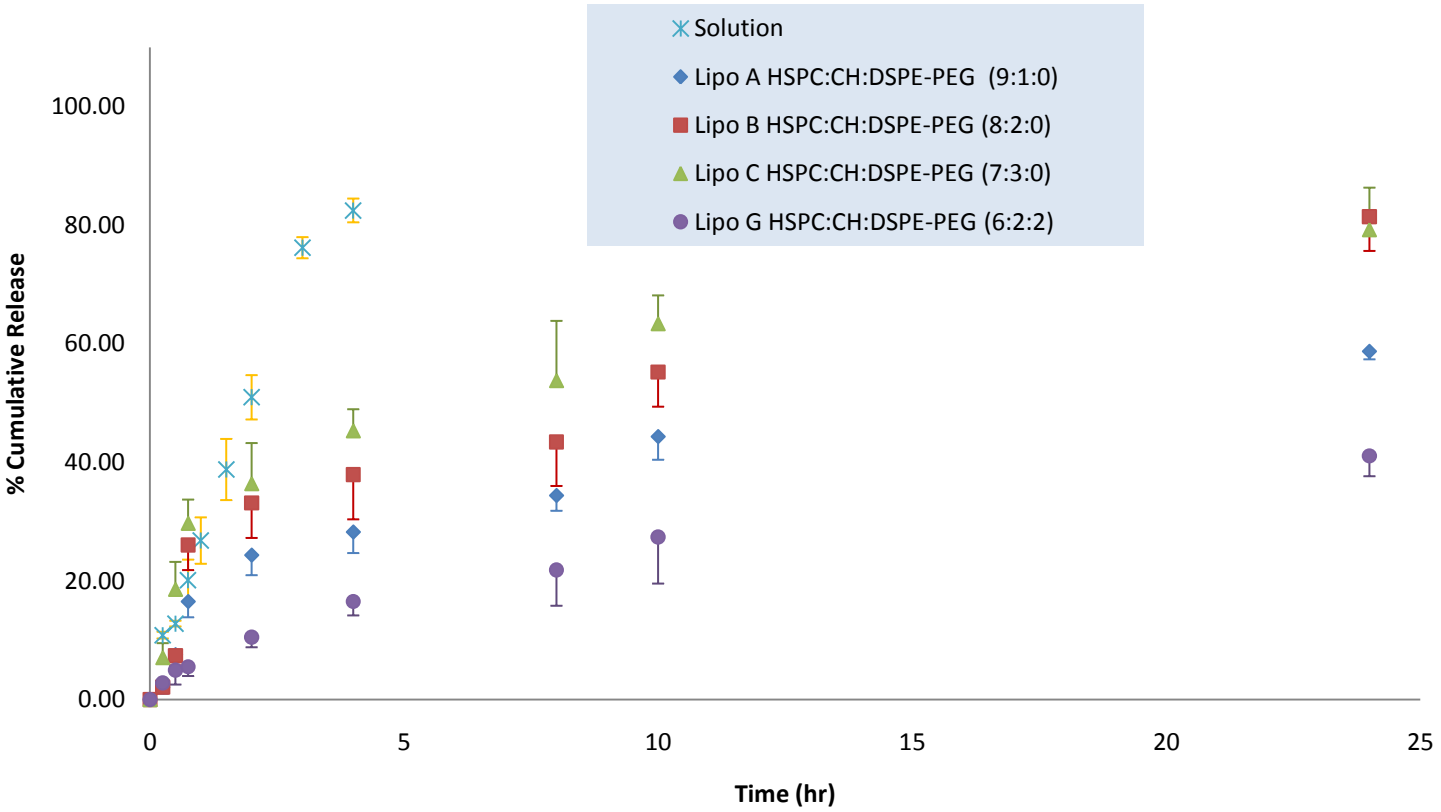

Figure 4.34 Release Profiles of LAZ from Solution and Liposomes with Different Lipid Composition in Human Plasma at 37°C (n=3).

Table 4.35 Initial Release Rates (%hr^{-1}) of LAZ Solution and Liposomes of Different Lipid Composition in Human Plasma at 37^{o}C (n=3).

The initial release rate in plasma after 0.75hr (%hr^{-1})	1	3	3	Mean	SD
Solution	22.93	22.93	9.23	18.36#	7.90
Lipo A	26.64	20.58	19.00	22.07#	4.03
Lipo B	38.23	30.52	31.51	33.42**#	4.19
Lipo C	36.72	47.64	36.48	40.28**#	6.38
Lipo G	9.54	8.99	3.94	7.49*#	3.09

Table 4.36 Extent of Release (%hr^{-1}) of LAZ Solution and Liposomes of Different Lipid Composition in Human Plasma at 37^{o}C (n=3).

The extent of release after 24 hr in Plasma	**1**	**3**	**3**	**Mean**	**SD**
Solution	80.58	82.23	84.58	82.49#	2.00
Lipo A	60.02	57.29	58.95	58.75* #	1.73
Lipo B	83.85	85.64	74.85	81.45 #	5.78
Lipo C	74.98	87.43	75.27	79.23 #	7.11
Lipo G	43.82	42.26	37.24	41.11**#	3.44

*** Significant difference compared to Solution , # Significant difference compared to PBS**

(P<0.05)

The initial release rate of LAZ from the solution (18.36 % hr^{-1}) was slower than those of Lipo B and C (33.42 and 40.28 % hr^{-1}, respectively), comparable to that of Lipo A (22.07 % hr^{-1}) and faster than that of Lipo G (7.49 % hr^{-1}). The initial release rate of Lipo G was the slowest among the liposomal formulations due to the inclusion of DSPE-PEG2000 (Table 4.35). The extent of the release was 82.4% by 4 h from the solution and those of Lipo B and C after 24 hr were 81.45 and 79.23 %, respectively. The release extent of Lipo A (58.75 %) was less than those of Lipo B and C, but higher than that of Lipo G, 41.11 % (Table 4.36).

By comparing the release extent of the same formulation in PBS and human plasma, the extent of release in plasma was less than those in PBS for the respective formulations. The release extent was less by 57% for Lipo G and by about 16 % for solution and 10-14% for Lipo A-C. This can be explained by the binding of LAZ to plasma protein which led to a smaller amount of free LAZ for release from the dialysis bags. The initial release rates from all the liposomes formulations were less in aqueous medium than those in plasma except for Lipo G whose initial release rate in plasma was less than that in PBS. This is due to the protection gained by the PEGylated layer which keeps the phospholipids from interaction with plasma lipoproteins.

4.6.1.4 Release Kinetics of LAZ from Liposomes in PBS and Human Plasma (n=3)

Four kinetics equations were fitted to LAZ cumulative release or the remaining percentages. The goodness of fit was evaluated by comparing the correlation coefficient

(R^2) of the regression lines. The solution release was described by the four equation models without best fit by one particular equation The kinetics equations of the first order and Higuchi's had a better fit and a higher R^2 to the cumulative release profiles of Lipo B and Lipo G compared to those equations of zero order and Hixson's models. The release from Lipo B and G depended on the initial liposomes concentration and diffusion distance from the liposomes. For Lipo A and C, the release was best described using Higuchi's equation. Zero order equation had poor fitting to all the profiles (Table 4.37 and Figure 4.35).

In human plasma, LAZ release from the solution was described well by all the equations. For Lipo A, the release was best described by Higuchi's equations as in the case with the release in PBS. Lipo C's profile was fitted to Hixson's, Higuchi's and First order equations. For Lipo B and G, they had the best fit with both Higuchi's and the first order's equations (Table 4.38 and Figure 4.36).

Table 4.37 Release Kinetics Criteria for LAZ Solution, Lipo A, Lipo B, Lipo C and Lipo G in PBS.

	Zero Order		First		Higuchi		Hixson	
	K_o	r^2	K	r^2	K_H	r^2	K_{HC}	r^2
Solution	24.80 ±(1.29)	0.92 ±(0.04)	1.19 ±(0.35)	0.95 ±(0.02)	64.56 ±(3.09)	**0.96** ±(0.02)	1.10 ±(0.32)	0.95 ±(0.02)
Lipo A	2.91 ±(0.10)	0.83 ±(0.01)	0.05 ±(0.00)	0.92 ±(0.01)	15.60 ±(0.52)	**0.96** ±(0.01)	0.06 ±(0.01)	0.89 ±(0.01)
Lipo B	3.89 ±(0.22)	0.81 ±(0.01)	0.11 ±(0.02)	**0.97** ±(0.02)	21.03 ±(1.13)	**0.96** ±(0.01)	0.11 ±(0.02)	0.92 ±(0.02)
Lipo C	3.76 ±(0.54)	0.74 ±(0.04)	0.10 ±(0.03)	0.88 ±(0.08)	20.94 ±(2.61)	**0.92** ±(0.02)	0.11 ±(0.02)	0.83 ±(0.07)
Lipo G	4.02 ±(0.17)	0.76 ±(0.06)	0.15 ±(0.03)	**0.96** ±(0.03)	22.23 ±(0.74)	**0.94** ±(0.02)	0.14 ±(0.02)	0.91 ±(0.05)

Table 4.38 Release Kinetics Criteria for LAZ Solution, Lipo A, Lipo B, Lipo C and Lipo G in Human Plasma.

	Zero Order		First		Higuchi		Hixson	
	K_o	r^2	K	r^2	K_H	r^2	K_{HC}	r^2
Solution	20.94 ±(0.80)	0.97 ±(0.003)	0.47 ±(0.03)	**0.97** ±(0.02)	7.68 ±(0.85)	**0.94** ±(0.02)	0.54 ±(0.03)	0.98 ±(0.02)
Lipo A	2.29 ±(0.04)	0.81 ±(0.03)	0.04 ±(0.01)	0.89 ±(0.02)	12.28 ±(0.18)	**0.94** ±(0.02)	0.05 ±(0.00)	0.87 ±(0.02)
Lipo B	3.11 ±(0.13)	0.81 ±(0.06)	0.07 ±(0.01)	**0.94** ±(0.03)	16.57 ±(0.69)	**0.93** ±(0.02)	0.08 ±(0.01)	0.91 ±(0.04)
Lipo C	2.90 ±(0.46)	0.72 ±(0.06)	0.06 ±(0.02)	0.90 ±(0.07)	16.16 ±(2.42)	**0.91** ±(0.05)	0.07 ±(0.02)	0.85 ±(0.07)
Lipo G	1.66 ±(0.15)	0.87 ±(0.06)	0.02 ±(0.00)	0.91 ±(0.06)	8.61 ±(0.65)	**0.95** ±(0.04)	0.03 ±(0.01)	0.89 ±(0.06)

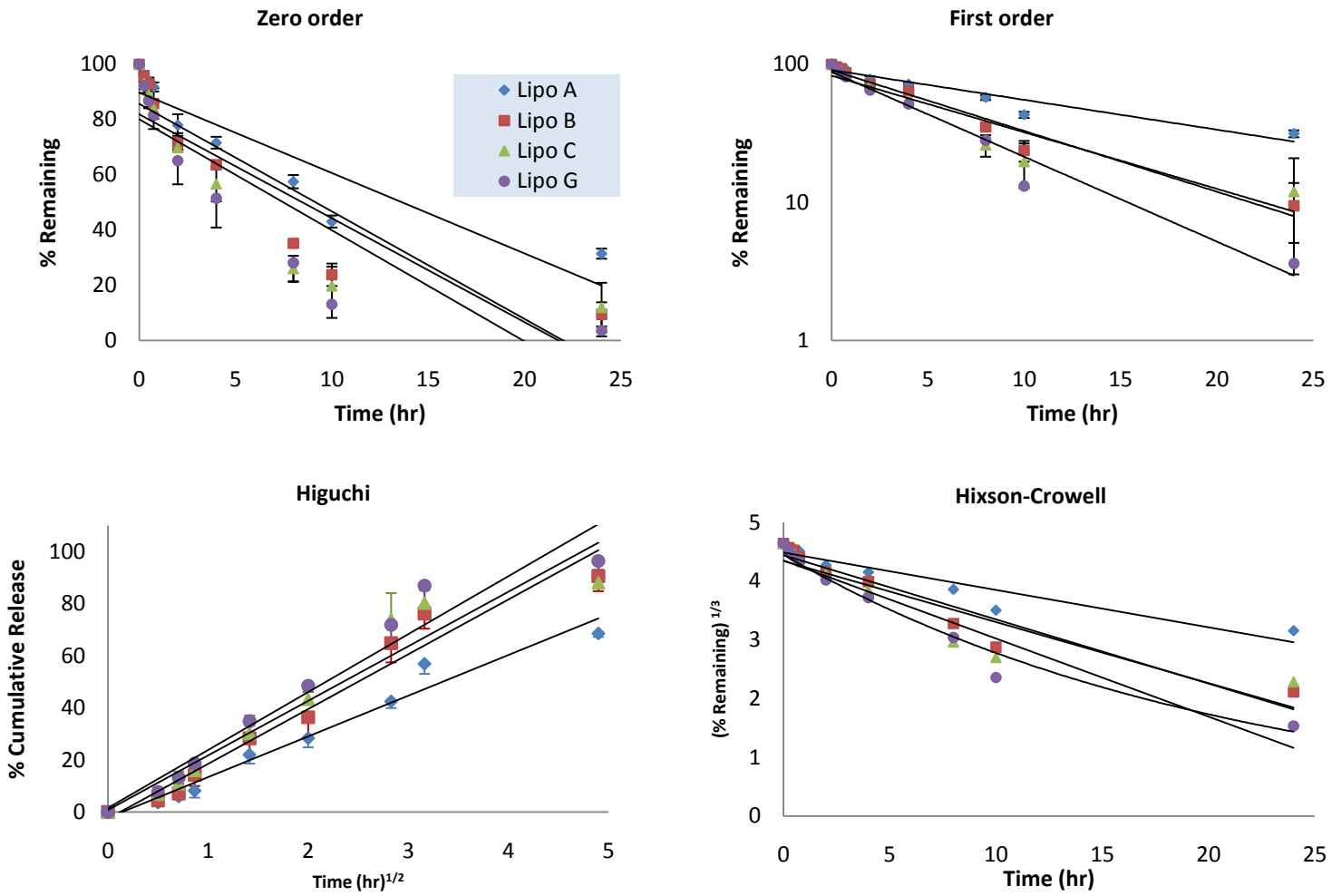

Figure 4.35 Release Kinetics of LAZ from LAZ Liposomes in PBS

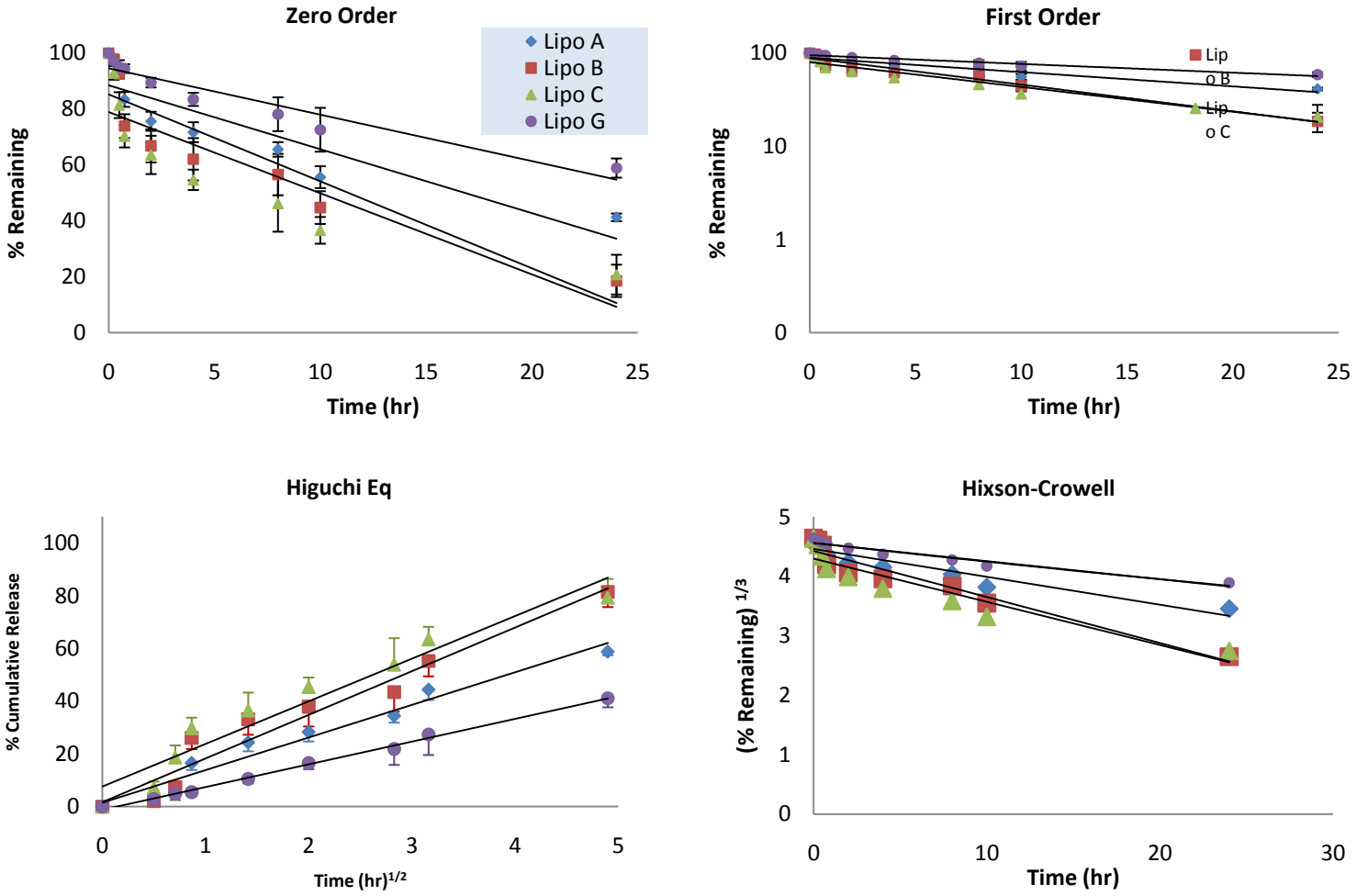

Figure 4.36 Release Kinetics of LAZ from LAZ Liposomes in Human Plasma

4.61.5 DSC of Lipo G and LAZ Powder

DSC was used to investigate the existing form of LAZ in Lipo G. As shown in Figure 4.38, the melting endothermic peak of LAZ was observed at 179.44^{o}C, while it disappeared from the thermograms of the lyophilized Lipo G (Figure 4.40). This suggests that LAZ was no longer in a crystalline state but in a molecular state distributed within the lipid bilayer. HSPC had a pre-transition temperature at 46.44 ^{o}C and a phase transition temperature at 53.61^{o}C (Figure 4.37). DSPE-PEG 2000 had a phase transition at 63.91^{o}C and melting point at 81.59^{o}C (Figure 4.38). The overlay thermograms showed that the previously observed endothermic peaks were no longer present in the formed liposomes (Figures 4.41 and 4.42).

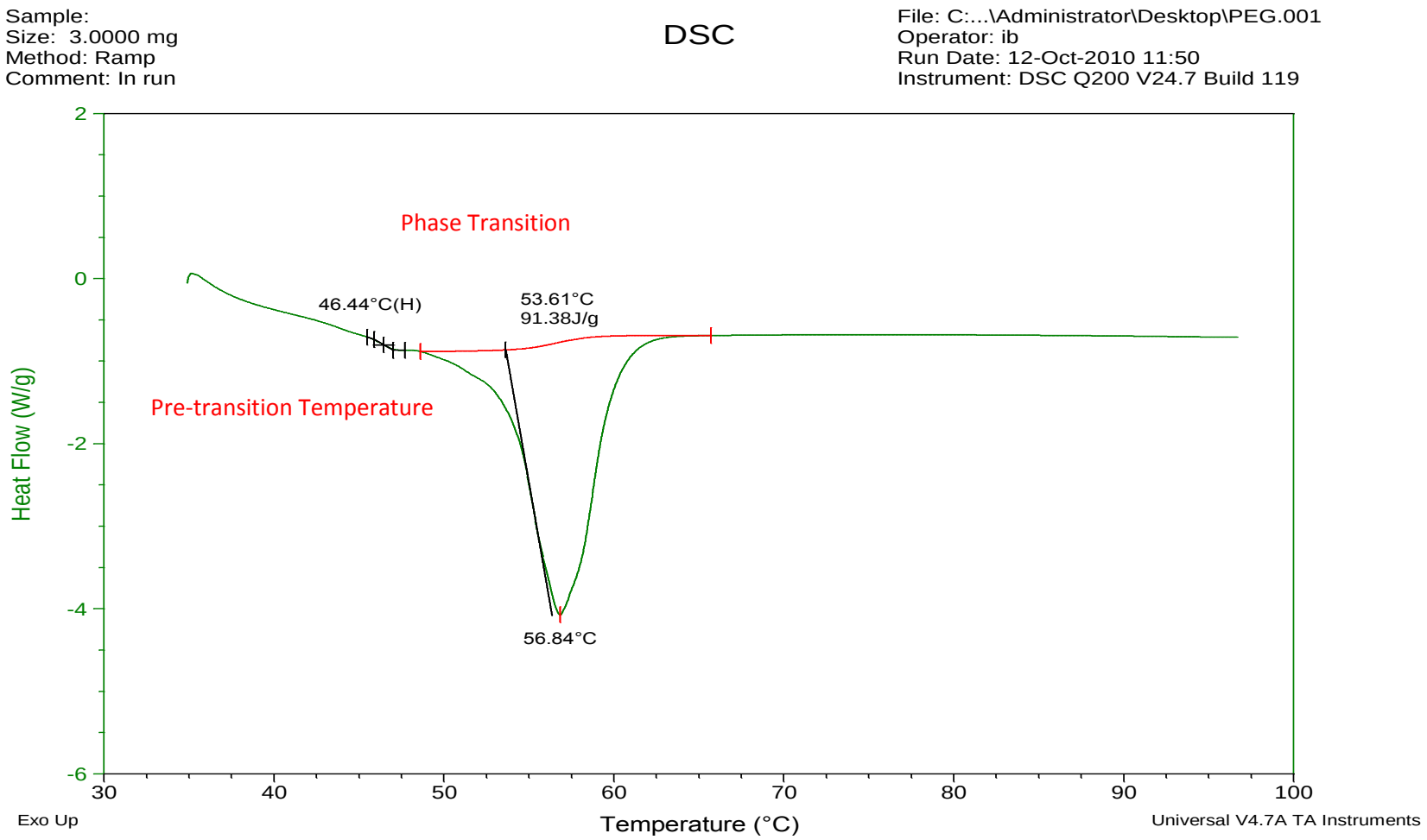

Figure 4.37 DSC Thermogram of HSPC

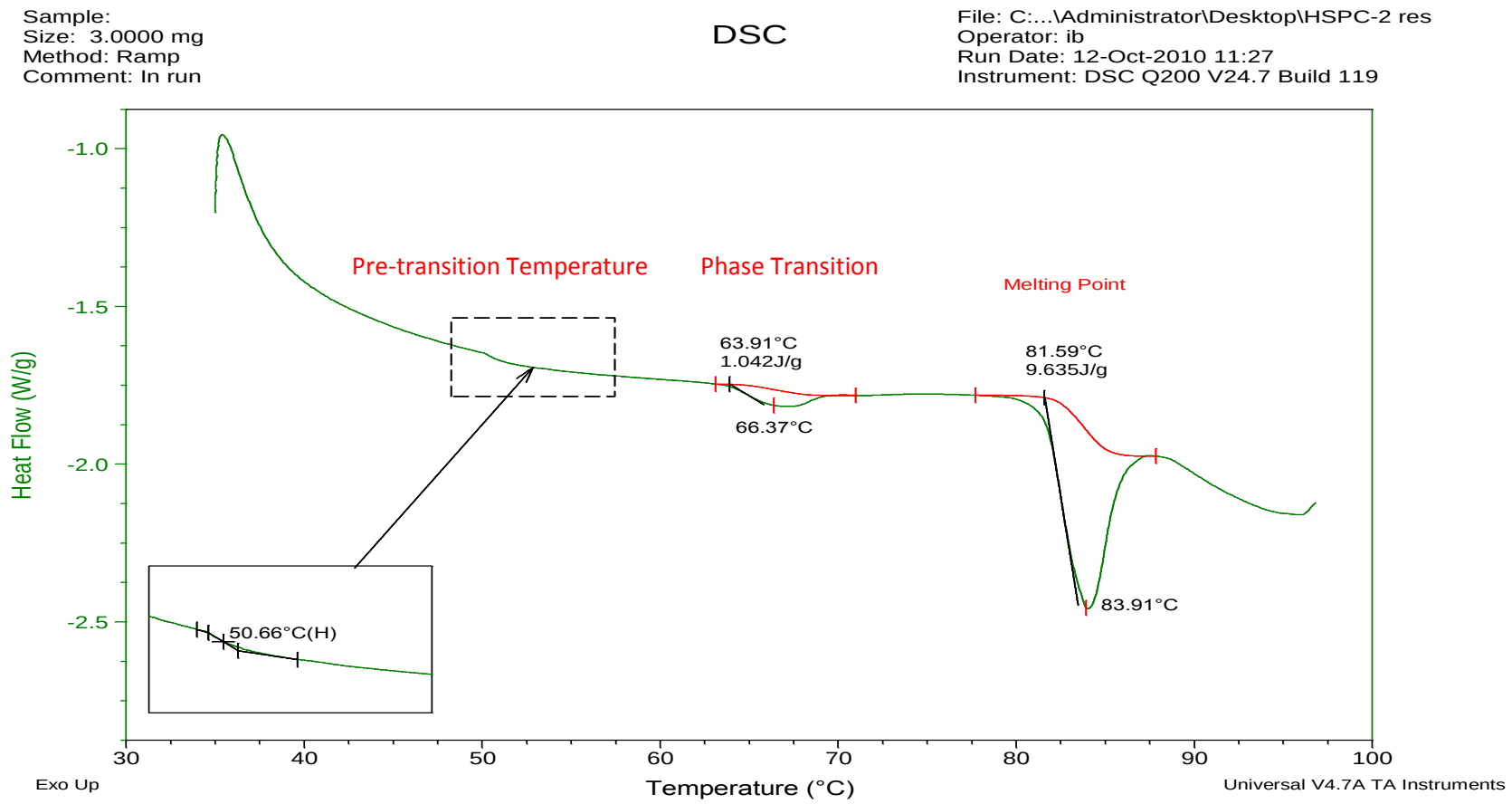

Figure 4.38 DSC Thermogram of DSPE-PEG 2000

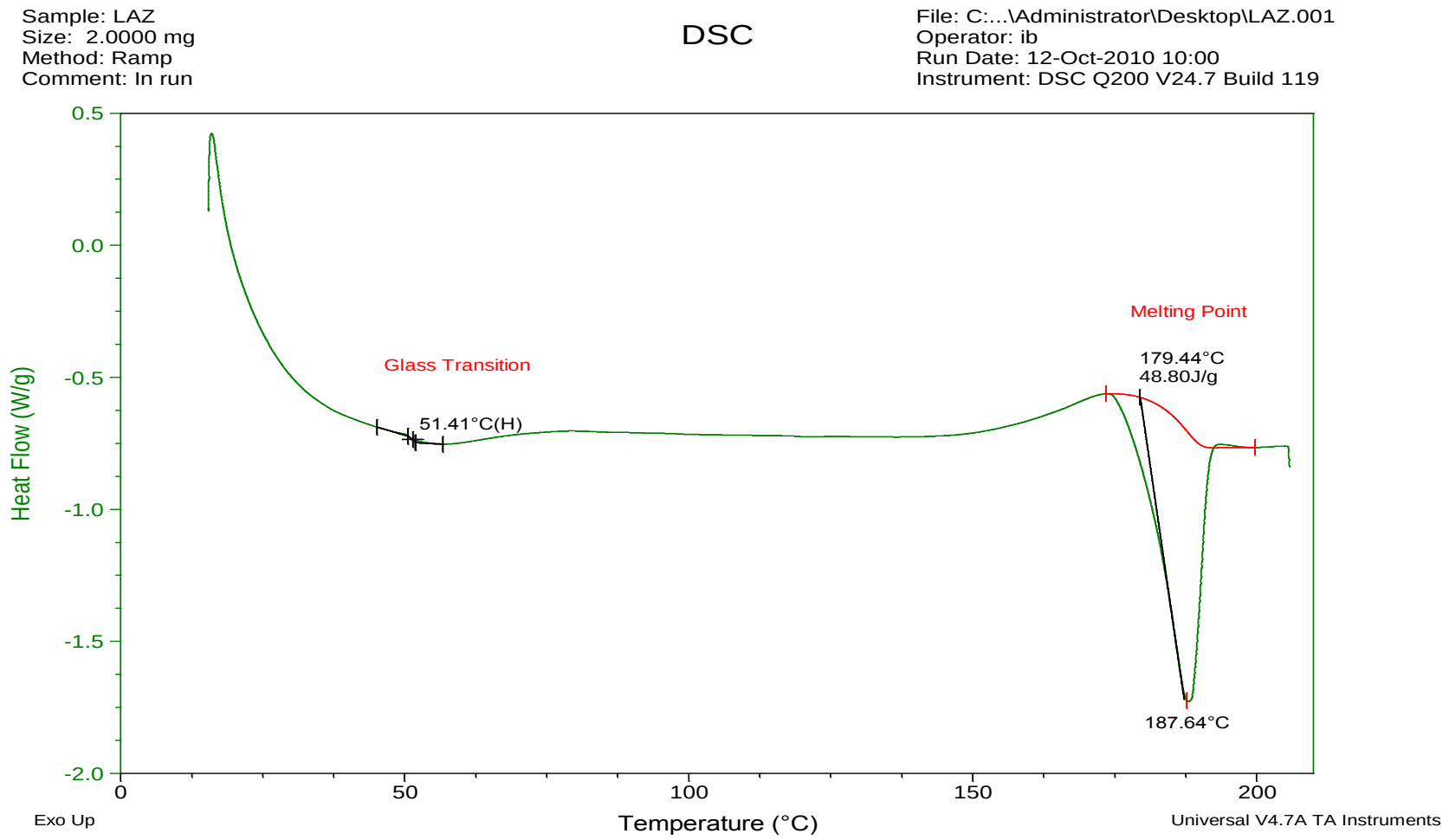

Figure 4.39 DSC Thermogram of LAZ

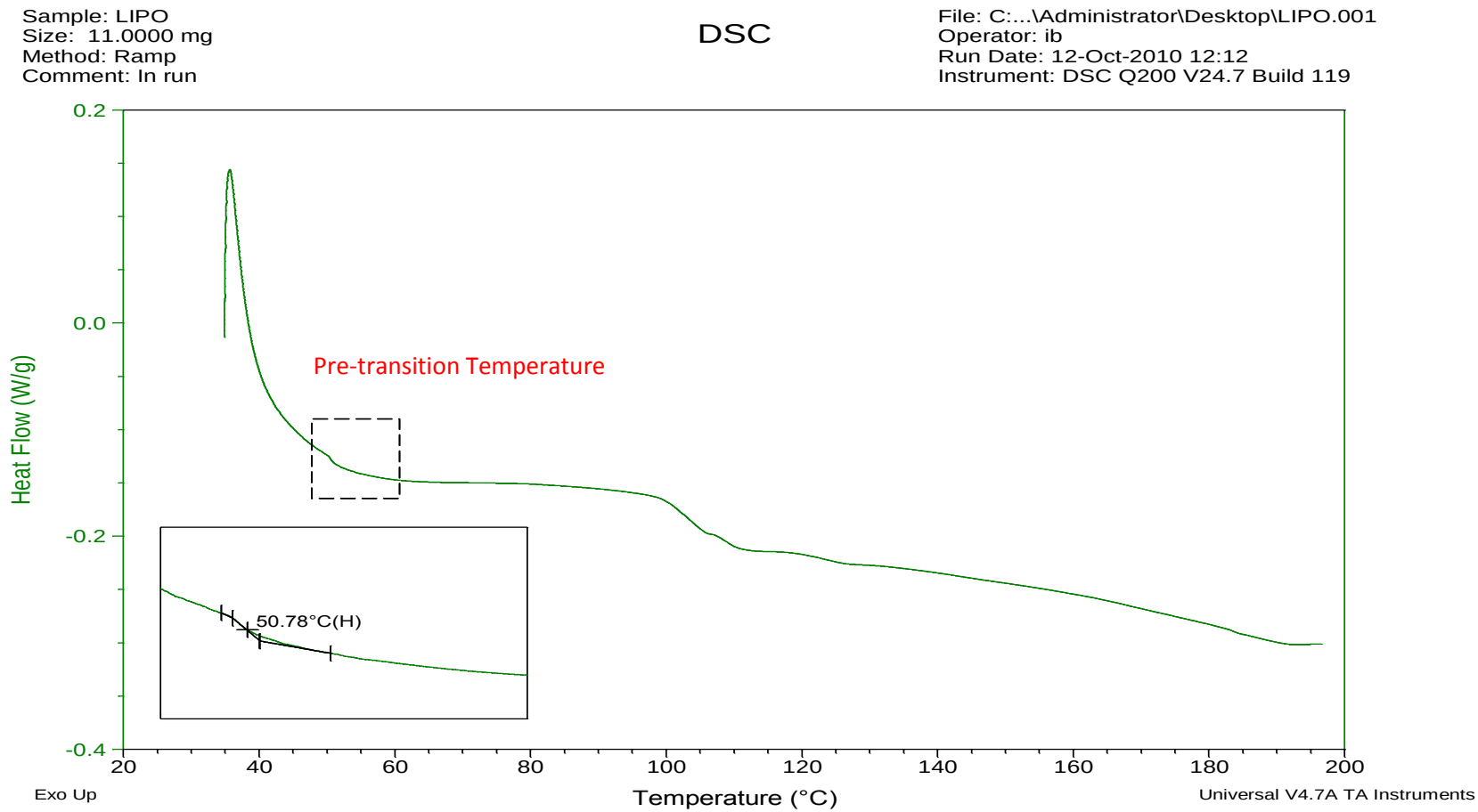

Figure 4.40 DSC Thermogram of Lipo G

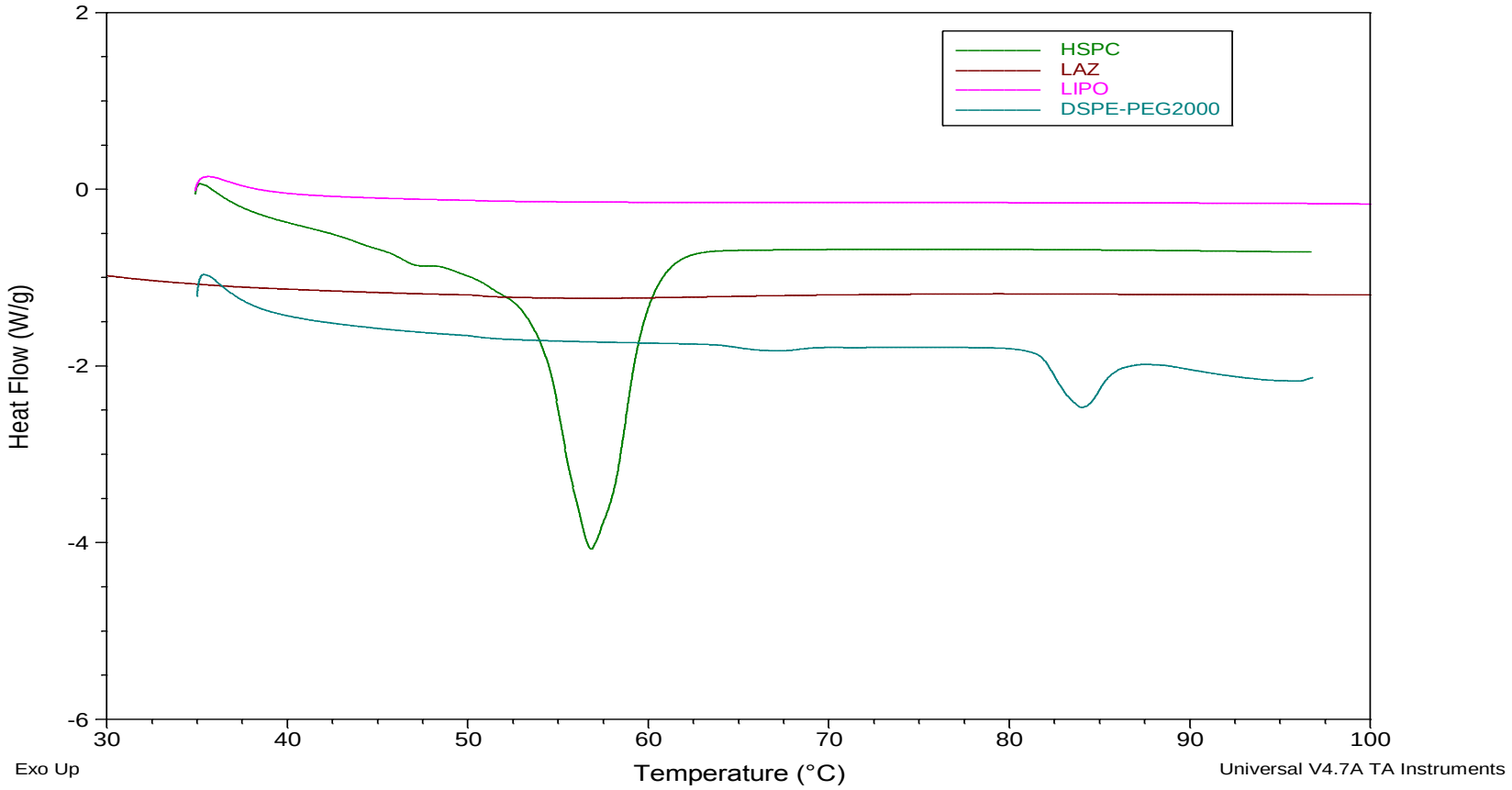

Figure 4.41 DSC Overlay Thermogram of HSPC, DSPE, LAZ and Lipo G in Temperature Range of 30-100^{o}C

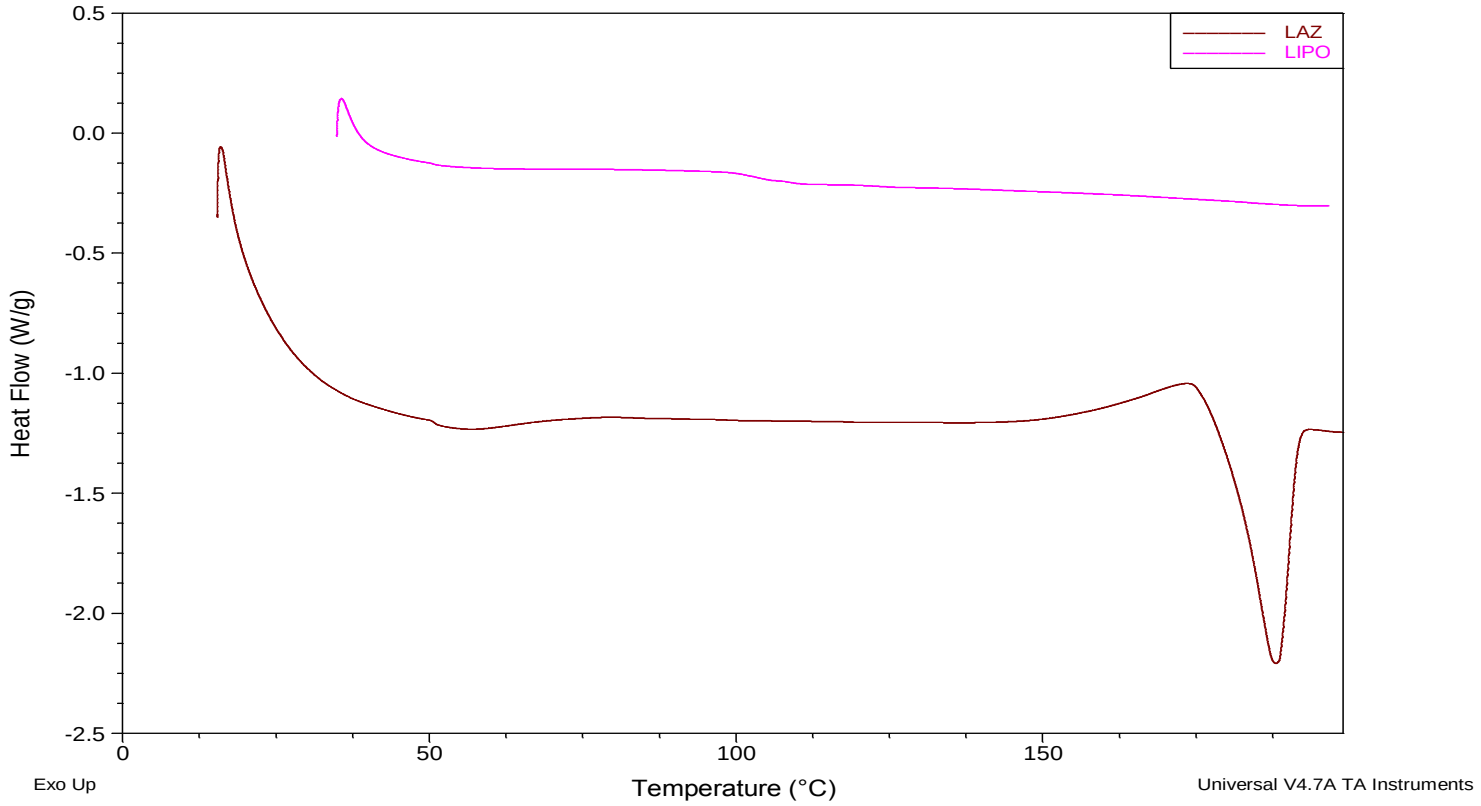

Figure 4.42 DSC Overlay Thermogram of HSPC, DSPE, LAZ and Lipo G in Temperature Range of 30-200^{o}C

4.6.1.6 Stability of Liposomes (n=3)

The stability of the liposomes was assessed over 11 months by evaluations of the size and EE of the stored formulations. The liposomes were measured for size of the fresh preparation (Day 0) and then stored at 4^{o}C. The size of the liposomes increased slightly on 1.5 months time point compared to the first measurement on Day (0), except for Lipo C which kept the same size over 11 months. Lipo B and G sizes increased by 20% over the first 1.5 months and remained unchanged over the 11 months (Table 4.39 and Figure 4.43). EE of the liposomes did not significantly differ from that of Day (0) except for Lipo A which had a significant lower EE at 11 months compared to Day (0) (Table 4.40 and Figure 4.44).

4.6.2 Plasma Pharmacokinetic of LAZ from Solution and Liposomes (Lipo B and Lipo G) in Nude Mice at 1 mg/kg Dose (n=3, each)

Plasma pharmacokinetics of LAZ solution and Liposomes (Lipo B and G) were studied in Swiss nude mice at a dose of 1 mg/kg. The formulations were given by IV injection and blood samples were collected for LAZ quantification by UPLC-MS/MS assay. LAZ plasma concentration-time profile was constructed using sparse sampling approach. The mean concentration-time profiles were generated by calculating the mean concentration at each time point for samples collected from three mice that were sacrificed at the given time point.

The profiles of the solution, Lipo B and G were similar where the initial phase had a rapid decline followed by a slower phase of elimination. Lipo G profile had higher

Table 4.39 Size of the Liposomes over 11 months Storage at 4°C (n=3).

Time	Size (nm)			
	Lipo A	Lipo B	Lipo C	Lipo G
Day (0)	120.0(±2.6)	93.8(±2.9)	91.3(±2.9)	79.2(±6.5)
1.5 Months	130.0(±3.3)*	118.0(±5.2)*	93.9(±5.2)	93.6(±3.5)*
3 Months	129.3(±5.3)*	107.0(±4.3)*	90.7(±4.3)	93.2(±1.6)*
5 Months	140.2(±2.8)*	117.2(±3.7)*	98.1(±2.8)*	98.7(±5.7)*
11 Months	141.9 (±8.2) *	119.7(±6.5)*	101.1(±5.1)*	102.7(±4.9)*

*Indicates significant difference when compared to Day (0). (P<0.05)

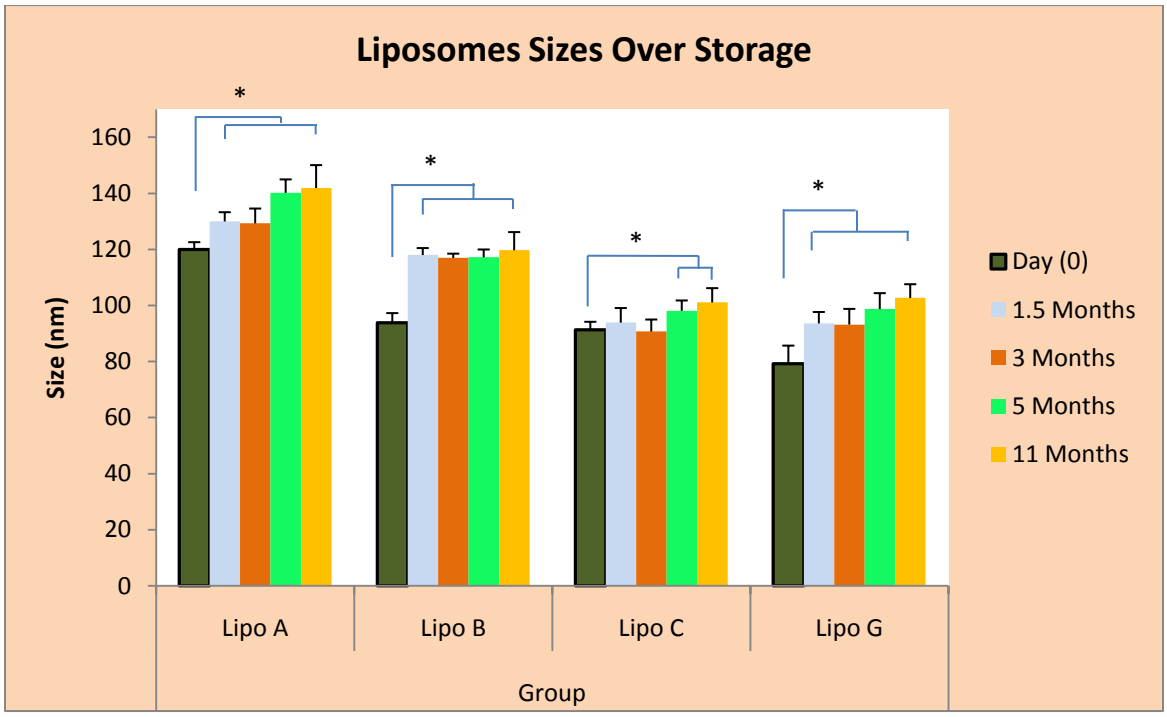

Figure 4.43 Size of the Liposomes over 11 months Storage at 4°C (n=3).

Table 4.40 EE of the Liposomes over 11 Months of Storage at 4°C (n=3).

	EE %			
	Lipo A	**Lipo B**	**Lipo C**	**Lipo BG**
Day (0)	**29.03(±4.4)**	**68.56(±7.8)**	**59.19(±4.0)**	**64.04(±5.1)**
5 Months	**22.64(±2.40)**	**66.22(±4.90)**	**61.07(±3.71)**	**62.88(±2.30)**
11 Months	**16.65 (±3.70)***	**61.94 (±6.22)**	**55.82 (±6.38)**	**61.57 (±5.36)**

*Indicates significant difference when compared to Day (0). (P<0.05)

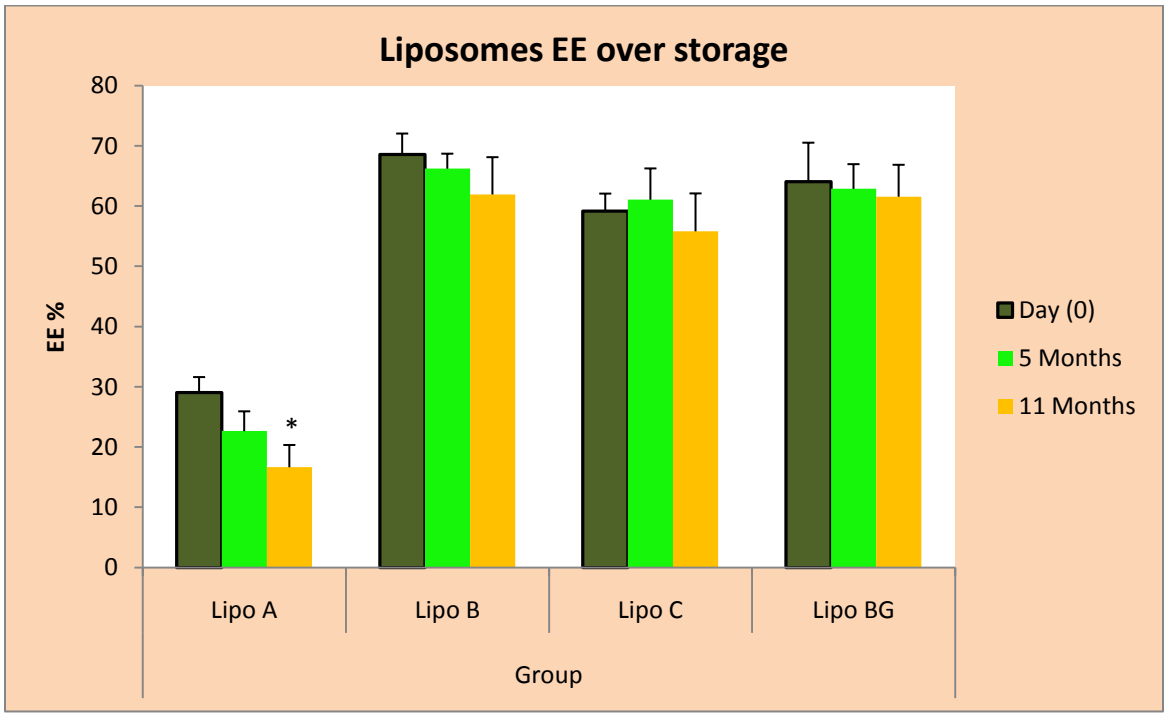

Figure 4.44 EE of the Liposomes over 11 Months of Storage at 4°C (n=3).

plasma concentrations compared to those from the solution and Lipo B at the corresponding time points (Figure 4.45 and Table 4.41). Non-compartmental models by WinNonlin were fitted to the mean plasma concentration profiles to derive the pharmacokinetics parameters.

The pharmacokinetics parameters were presented as the mean without the standard deviation (Table 4.41 and Figure 4.45). Due to the application of sparse sampling design in data collection, the variance of AUC_{0-t} was estimated using the method described by Bailer,1988 [71]. This method allows the determination of the variability in the AUC estimate from the variability about the mean concentration at each time point, assuming that the mean at each time point is independent and the terminal rate constant is the same for each animal.

Lipo G has a higher C_o than those from the solution and Lipo B (8.81 µg/ml vs. 0.58 and 0.80 µg/ml). LAZ AUC_{0-t} from Lipo G (7.28 hr. µg/ml) was 4 and 10 folds of those of Lipo B and solution (1.67 and 0.75 hr. µg/ml, respectively). The PEGylated Lipo G had a slower clearance compared to those of the solution and Lipo B (3.66 ml/hr vs. 33.31 and 16.81 ml/hr, respectively). The elimination rate constant of the solution was comparable to that of Lipo G but less than that of Lipo B (0.26 and 0.27 ml/hr vs. 0.35 ml/hr). At the same time, the volume of distribution (V_d) of Lipo G was smaller than those of solution and Lipo B (11.76 ml vs. 109.65 and 48.11 ml, respectively) (Table 4.41).

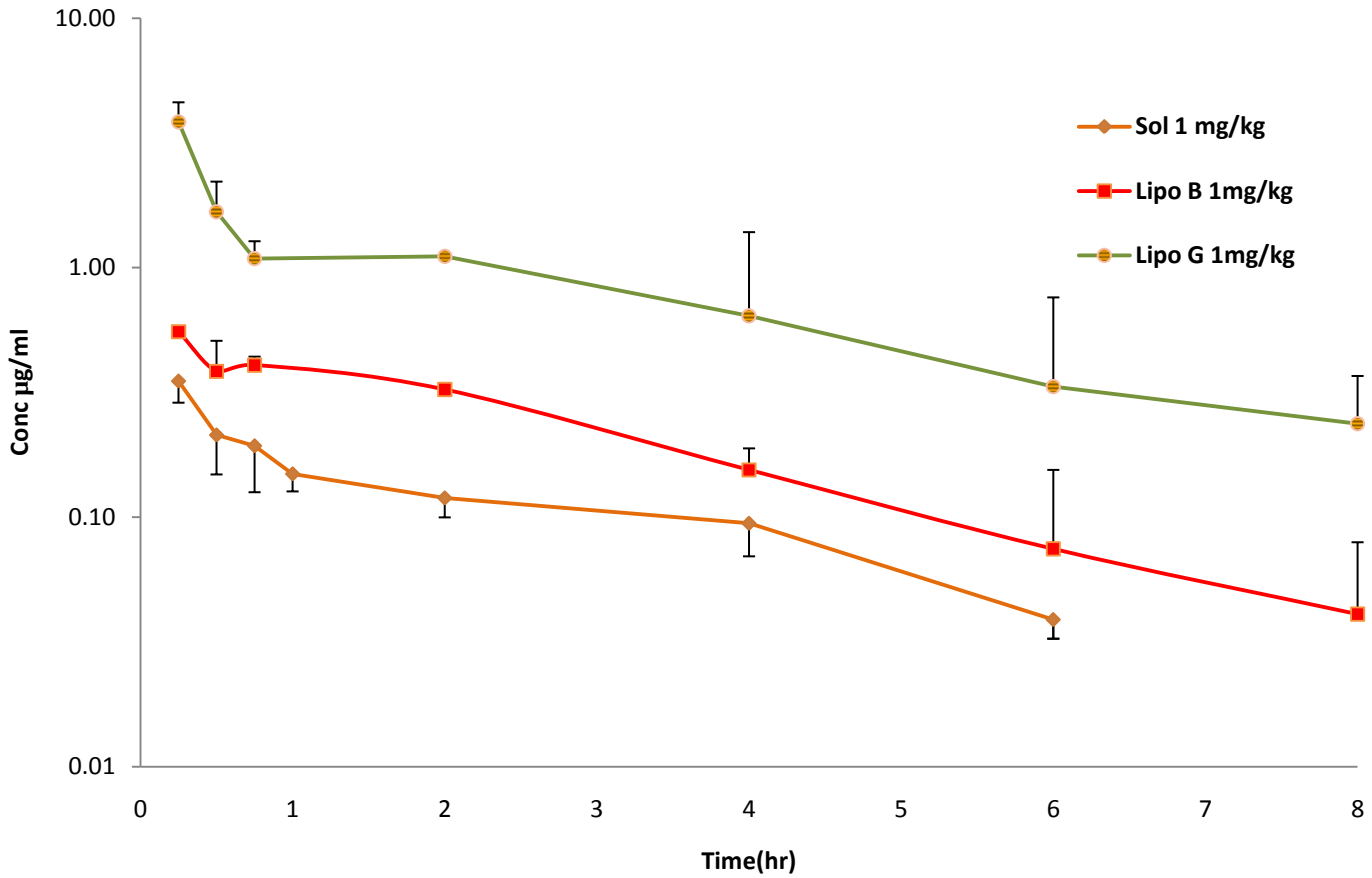

Figure 4.45 Plasma Concentration-Time Profiles of LAZ Solution, Lipo B and Lipo G in Mice (n=3, each)

Table 4.41 Pharmacokinetcs Parameters of LAZ Solution and Liposomes in Mice Plasma Derived by Non-Compartmental Analysis (from Naïve Pool Data, 3 Mice per each Datum Point)

	Sol	Lipo B	Lipo G
C_o (g/mL)	0.58	0.80	8.81
AUC_{0-t} (hr.µg/ml)	0.75 (±0.04)	1.67* (±0.11)	7.28** (±0.77)
Cl (ml/hr)	33.31	16.81	3.66
Vss (ml)	109.65	48.11	11.76
Kel (1/hr)	0.27	0.35	0.26
$t_{1/2}$ (hr)	2.53	1.99	2.62
Systemic Exposure	1	2.21	9.66

Table 4.42 Plasma Concentrations of LAZ Solution and Liposomes at Different Time Points in Nude Mice.

	Solution 1mg/kg		Lipo B 1mg/kg		Lipo G 1mg/kg	
Time (hr)	**mean conc. µg/ml**	**S.D**	**mean conc. µg/ml**	**S.D**	**mean conc. µg/ml**	**S.D**
0.25	0.35	0.06	0.55	0.01	3.84	0.76
0.5	0.21	0.07	0.38	0.13	1.67	0.54
0.75	0.19	0.07	0.41	0.03	1.09	0.19
1	0.15	0.02	-	-	-	-
2	0.12	0.02	0.32	0.03	1.11	0.75
4	0.09	0.02	0.15	0.08	0.64	0.43
6	0.04	0.01	0.07	0.04	0.33	0.13
8	0.00	0.00	0.04	0.02	0.24	0.02

4.6.3 Organ Distribution of LAZ from Solution and Liposomes (Lipo B and Lipo G) in Nude Mice at 1 mg/kg Dose (n=3)

The biodistribution study in mice was comparatively evaluated for the solution, Lipo B and Lipo G. The organ peak concentrations were reached before the collection at the first time point. LAZ uptake from the solution was comparable among the liver, lungs , kidneys and heart (1.42-1.56 µg/gm), but lower by the brain and the spleen was less than those of the other organs (0.29 and 0.09 µg/gm, respectively) (Figure 4.46 & Table 4.43). The exposure (AUC) of the liver from LAZ solution was 2.4 hr.µg/gm and was the highest among the organs. The exposures of the lungs, kidneys and the heart were comparable (1.13, 1.9 and 1.11 hr.µg/gm) and higher than those of the spleen and the brain (0.38 and 0.06 hr.ug/gm, respectively). The half lives were comparable among all the organs (0.94 - 1.0 hr) except those of the spleen and the brain that was shorter than other organs (0.75 and 0.25 hr, respectively) (Figure 4.46 & Table 4.43).

The distribution pattern from Lipo B was different from that of the solution. The highest uptake was in the liver with the highest C_{max} (4.16 µg/gm) followed by the kidneys, spleen / lungs, heart and the brain (1.56, 0.36 / 0.32, 0.17 and 0.10 µg/gm, respectively). The LAZ exposures among the organs from Lipo B followed the same pattern of C_{max} except that the lung exposure was larger than that of the spleen. The highest LAZ exposure from Lipo B was seen in the liver followed by the kidneys (15.33 and 3.36 hr.µg/gm, respectively). The smallest exposure from Lipo B was in the brain (0.2 hr.µg/gm). The exposure from Lipo B was higher than that from the solution in the

organs if liver, kidneys and brain (Table 4.42). The $t_{1/2}$ of LAZ in the liver was 4.83 hr which was the longest among the organs. The $t_{1/2}$ in the brain (3.55 hr) was comparable to that in the spleen (3.47 hr) and longer than those from the lungs, kidneys and heart (1.05, 1.67 and 2.90 hr, respectively). The half lives of LAZ from Lipo B were longer than those from solution in all the organs except that in the lungs (Figure 4.48 & Table 4.45).

The distribution pattern from Lipo G was different from those of the solution and Lipo B. The highest uptake was observed in the lungs, 2.26 µg/gm, while the other organs were in the following rank liver> heart / spleen > kidneys > brain (1.32, 1.05, 1.11, 0.89 and 0.29 µg/gm, respectively). The lung exposure was the highest among the organs 3.61 µg.hr/gm. The exposure was comparable between the liver and heart (1.98 and 1.76 µg.hr/gm) and between kidneys, spleen and brain (0.94, 0.91 and 0.80 µg.hr/gm). The half life was surprisingly the longest in the brain and the shortest in the heart (5.73 vs. 1.16 hr, respectively). The exposure in the brain was higher from Lipo G compared to those from solution and Lipo B (0.8 µg.hr/gm vs 0.06 and 0.2 µg.hr/gm, respectively).

By comparing the biodistribution patterns among the three formulations, Lipo B formulation had exposure in the liver (6-8 times) and kidneys (2-3.5 times) as compared to those of the solution and Lipo G. However, Lipo-G had 3.5 fold of lung exposure of those from the solution and Lipo-B. The brain exposure from Lipo G was 13 and 4 folds of those from the solution and Lipo B, respectively. Lipo G was selected to perform proof-of-concept efficacy study in brain tumor bearing mice (Figure 4.52 & Table 4.49).

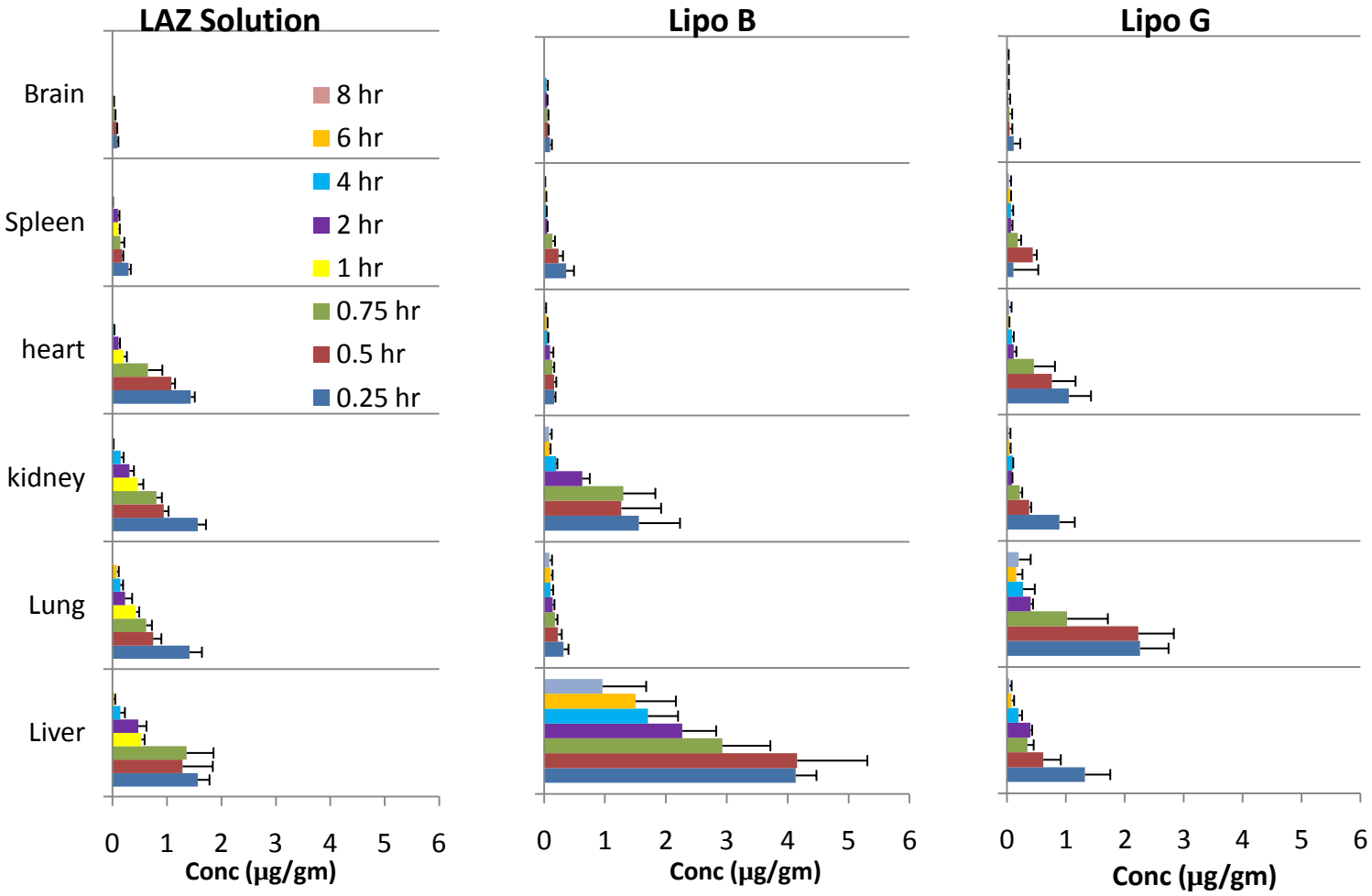

Figure 4.46 Organ Distribution of LAZ in Swiss Nude Mice from LAZ Solution, Lipo B and Lipo G at a dose of 1 mg/kg

Table 4.43 Non-Compartmental Parameters of LAZ Biodistribution from Formulations in Mouse Organs at 1 mg/kg Dose

			Solution			
	Liver	**Lungs**	**Kidneys**	**Heart**	**Spleen**	**Brain**
C_{max} (µg/gm)	1.56	1.42	1.56	1.43	0.29	0.09
AUC_{0-t} (hr.µg/gm)	2.40 (± 0.17)	1.13 (± 0.11)	1.9 (± 0.08)	1.11 (± 0.05)	0.38 (± 0.02)	0.06 (± 0.01)
$t_{1/2}$(hr)	0.94	1.09	0.98	0.96	0.76	0.25
			Lipo B			
	Liver	**Lungs**	**Kidneys**	**Heart**	**Spleen**	**Brain**
C_{max} (µg/gm)	4.16	0.32	1.56	0.17	0.36	0.10
AUC_{0-t} (hr.µg/gm)	15.33 (±1.17)	1.04 (± 0.07)	3.36 (± 0.21)	0.60 (± 0.07)	0.49 (± 0.03)	0.20 (± 0.03)
$t_{1/2}$(hr)	4.83	1.05	1.67	2.90	3.47	3.55
			Lipo G			
	Liver	**Lungs**	**Kidneys**	**Heart**	**Spleen**	**Brain**
C_{max} (µg/gm)	1.32	2.26	0.89	1.05	1.11	0.29
AUC_{0-t} (hr.µg/gm)	1.98 (±0.12)	3.61 (± 0.30)	0.94 (± 0.04)	1.26 (± 0.22)	0.91 (± 0.08)	0.80 (± 0.04)
$t_{1/2}$(hr)	1.71	2.14	2.19	1.61	3.91	5.73

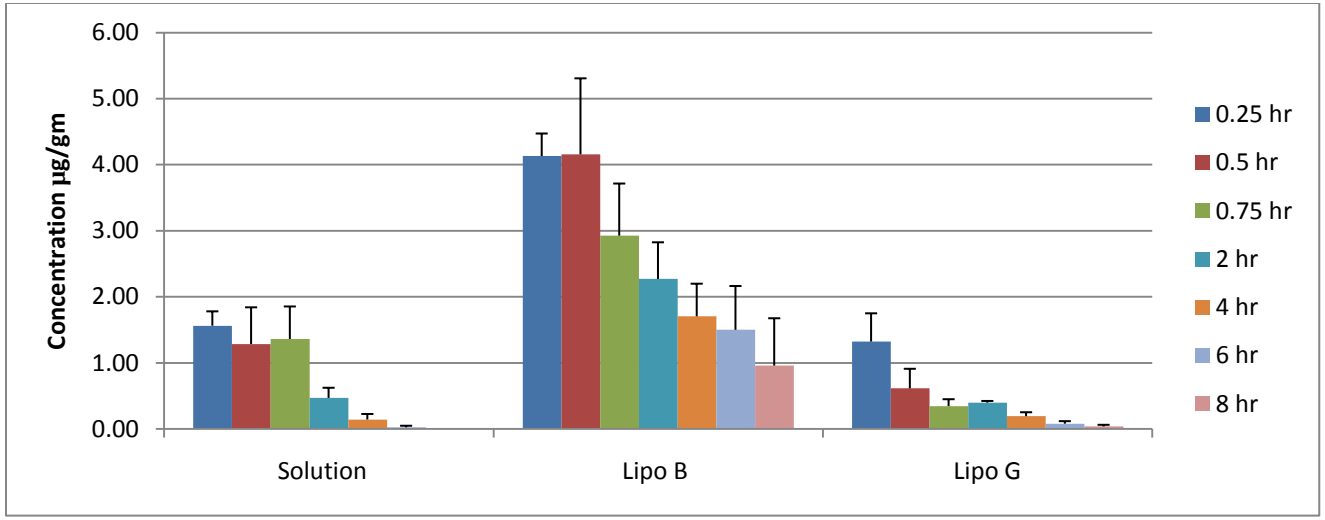

Figure 4.47 LAZ Distributions to the Liver of Nude Mice from Solution and Liposomes Formulations

Table 4.44 LAZ concentrations in Liver Samples from Solution and Liposomes in Nude Mice

	Solution 1mg/kg		Lipo B 1mg/kg		Lipo G 1mg/kg	
Time (hr)	mean conc. µg/gm	S.D	mean conc. µg/gm	S.D	mean conc. µg/gm	S.D
0.25	1.563	0.218	4.132	0.340	1.324	0.427
0.5	1.287	0.555	4.157	1.151	0.614	0.297
0.75	1.362	0.492	2.927	0.789	0.346	0.105
1	0.530	0.059	-	-	-	-
2	0.471	0.153	2.271	0.555	0.398	0.026
4	0.143	0.084	1.705	0.494	0.194	0.059
6	0.025	0.024	1.501	0.663	0.080	0.038
8	ND	ND	0.960	0.716	0.038	0.025

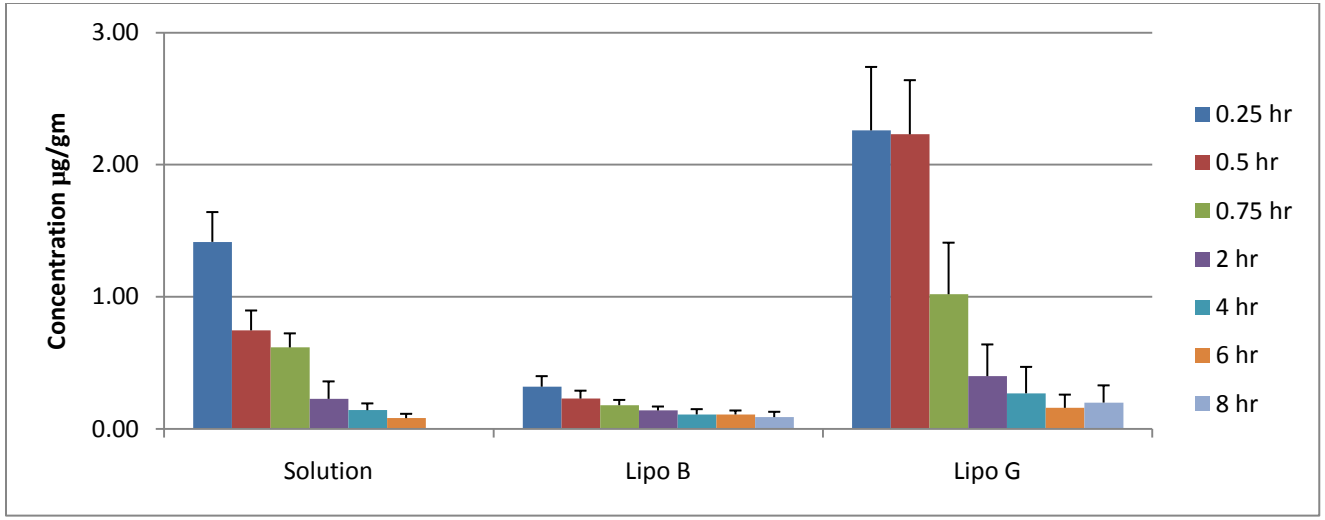

Figure 4.48 LAZ Distributions to the Lungs of Nude Mice from Solution and Liposomes Formulations

Table 4.45 LAZ concentrations in Lung Samples from Solution and Liposomes in Nude Mice

	Solution 1mg/kg		Lipo B 1mg/kg		Lipo G 1mg/kg	
Time (hr)	mean conc. µg/gm	S.D	mean conc. µg/gm	S.D	mean conc. µg/gm	S.D
0.25	1.416	0.226	0.321	0.085	2.260	0.481
0.5	0.747	0.150	0.233	0.056	2.231	0.599
0.75	0.617	0.106	0.176	0.041	1.016	0.691
1	0.431	0.058	-	-	-	-
2	0.228	0.132	0.141	0.026	0.399	0.040
4	0.142	0.051	0.114	0.038	0.274	0.197
6	0.082	0.033	0.114	0.035	0.163	0.097
8	ND	ND	0.094	0.036	0.205	0.128

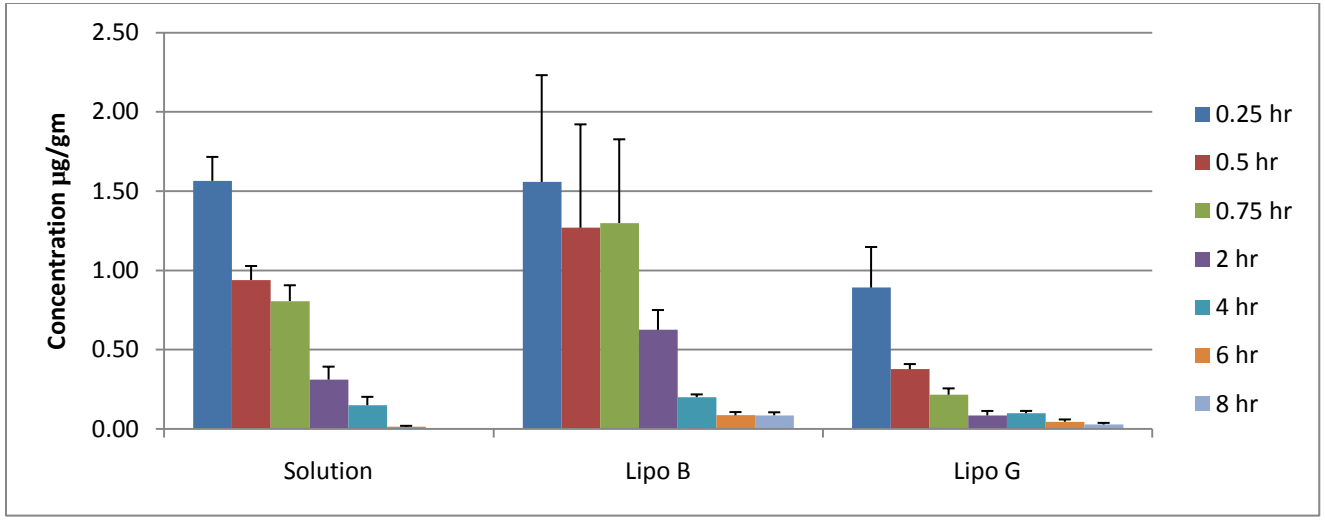

Figure 4.49 LAZ Distributions to the Kidneys of Nude Mice from Solution and Liposomes Formulations

Table 4.46 LAZ concentrations in Kidney Samples from Solution and Liposomes in Nude Mice

	Solution 1mg/kg		Lipo B 1mg/kg		Lipo G 1mg/kg	
Time (hr)	mean conc. µg/gm	S.D	mean conc. µg/gm	S.D	mean conc. µg/gm	S.D
0.25	1.565	0.151	1.558	0.673	0.892	0.256
0.5	0.940	0.088	1.269	0.652	0.377	0.033
0.75	0.807	0.100	1.299	0.528	0.216	0.040
1	0.466	0.100	-	-	-	-
2	0.311	0.082	0.625	0.125	0.086	0.005
4	0.150	0.052	0.201	0.017	0.099	0.004
6	0.015	0.004	0.086	0.020	0.046	0.014
8	ND	ND	0.086	0.039	0.028	0.010

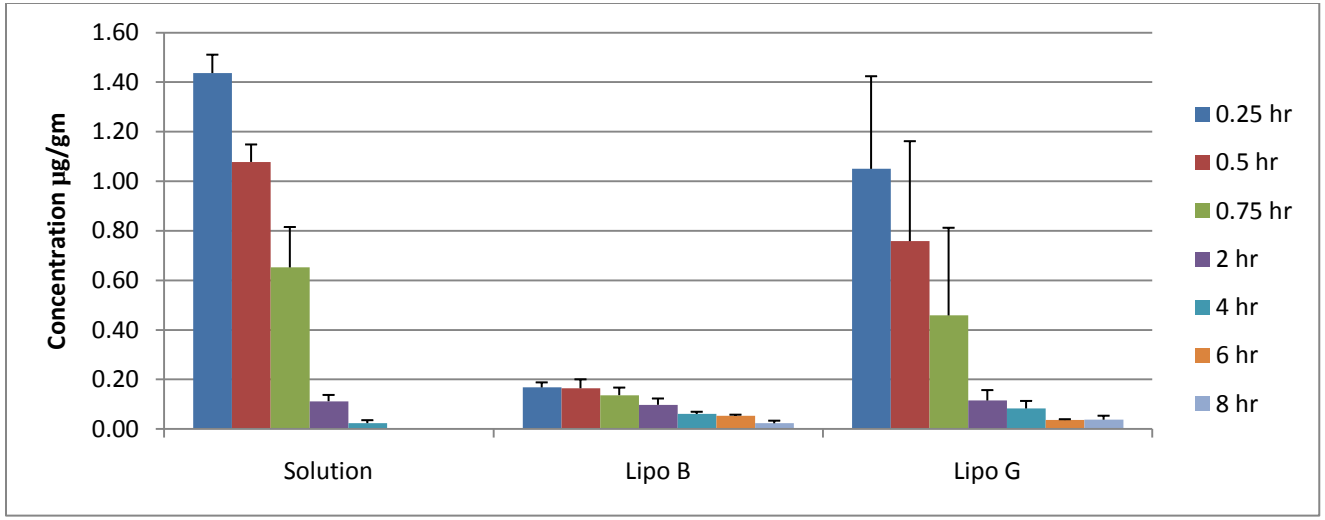

Figure 4.50 LAZ Distributions to the Heart of Nude Mice from Solution and Liposomes Formulations

Table 4.47 LAZ concentrations in Heart Samples from Solution and Liposomes in Nude Mice

	Solution 1mg/kg		Lipo B 1mg/kg		Lipo G 1mg/kg	
Time (hr)	mean conc. µg/gm	S.D	mean conc. µg/gm	S.D	mean conc. µg/gm	S.D
0.25	1.437	0.074	0.168	0.020	1.050	0.374
0.5	1.078	0.070	0.164	0.036	0.758	0.404
0.75	0.652	0.263	0.136	0.031	0.458	0.354
1	0.206	0.058	-	-	-	-
2	0.112	0.025	0.098	0.055	0.115	0.042
4	0.024	0.012	0.060	0.009	0.083	0.030
6	ND	ND	0.054	0.004	0.036	0.003
8	ND	ND	0.023	0.011	0.037	0.016

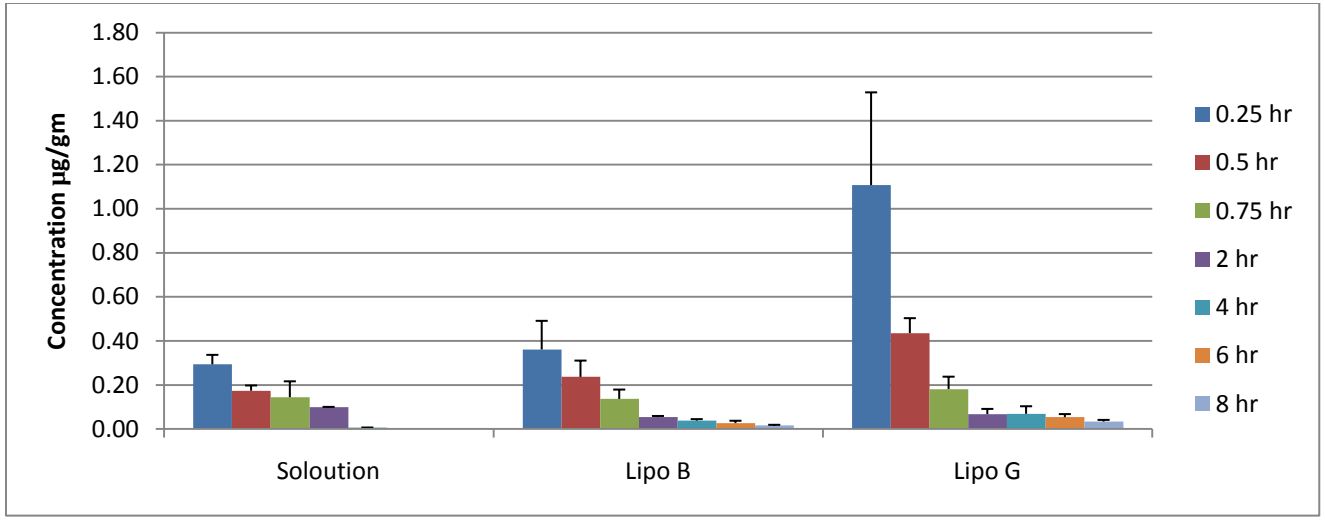

Figure 4.51 LAZ Distributions to the Spleen of Nude Mice from Solution and Liposomes Formulations

Table 4.48 LAZ concentrations in Spleen Samples from Solution and Liposomes in Nude Mice

	Solution 1mg/kg		Lipo B 1mg/kg		Lipo G 1mg/kg	
Time (hr)	mean conc. µg/gm	S.D	mean conc. µg/gm	S.D	mean conc. µg/gm	S.D
0.25	0.294	0.043	0.361	0.130	1.107	0.421
0.5	0.174	0.024	0.237	0.074	0.435	0.068
0.75	0.144	0.072	0.137	0.043	0.181	0.056
1	0.111	0.022	-	-	-	-
2	0.099	0.029	0.054	0.005	0.067	0.024
4	0.007	0.002	0.038	0.007	0.069	0.034
6	ND	ND	0.027	0.011	0.053	0.014
8	ND	ND	0.016	0.003	0.034	0.008

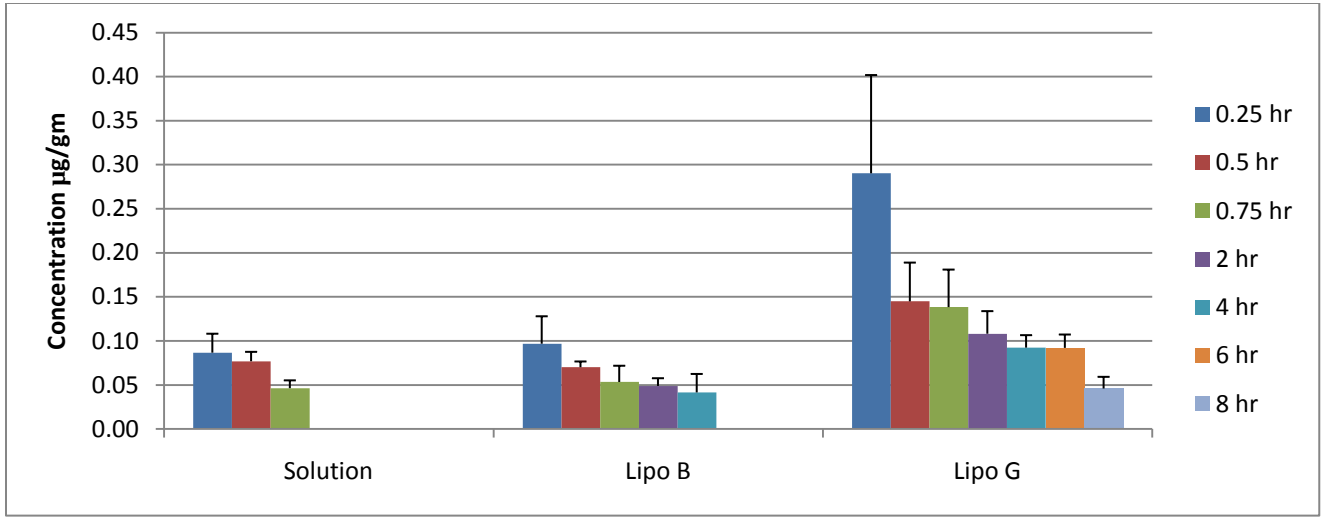

Figure 4.52 LAZ Distributions to the Brain of Nude Mice from Solution and Liposomes Formulations

Table 4.49 LAZ concentrations in Brain Samples from Solution and Liposomes in Nude Mice

	Solution 1mg/kg		Lipo B 1mg/kg		Lipo G 1mg/kg	
Time (hr)	mean conc. µg/gm		mean conc. µg/gm	SD	mean conc. µg/gm	SD
0.25	0.09	0.02	0.10	0.03	0.290	0.11
0.5	0.08	0.01	0.07	0.01	0.145	0.04
0.75	0.05	0.01	0.05	0.02	0.138	0.04
1	0.02	0.01	-	-	-	-
2	ND	ND	0.05	0.01	0.108	0.03
4	ND	ND	0.04	0.02	0.092	0.01
6	ND	ND	ND	ND	0.092	0.02
8	ND	ND	ND	ND	0.046	0.01

4.6.4 Co-Modeling of LAZ Concentration in Plasma and Brain from Solution and PEGylated Liposomes using ADAPT II Modeling

The co-modeling of plasma and brain concentrations of LAZ in Swiss nude mice from the solution and Lipo G was done by fitting three-compartment models with first order elimination using ADAPT II program. Two models were self-constructed to co-model the concentrations. Both models had common features of having one peripheral compartment (X_2) with distribution parameters of K_{pc} and K_{cp}, a central compartment (X_1 and V_c) and the brain compartment (X_3 and V_B) (Figures 4.53 and 4.54). Both models described forth and back distribution from the central compartment to the peripheral compartments. The first model treated the brain as a closed peripheral compartment with both directional distribution, but the second model described only the distribution from the central compartment to the brain which was considered as an open compartment. Two differential equations were written to derive AUC of the central and brain compartments during the simulation process. In the modeling step, a weighing factor (plasma: brain of 1:5) has been applied to the data to account for the concentration differences between the plasma and the brain. For LAZ concentrations in the brain from the solution, additional points were added beyond the detection limit of the assay to enable the software to have a balance between the numbers of plasma and brain concentration points. Selection of the best model was based on (a) AIC values, (b) R^2 values and (c) the visual inspection of the fit between the predicted and observed data.

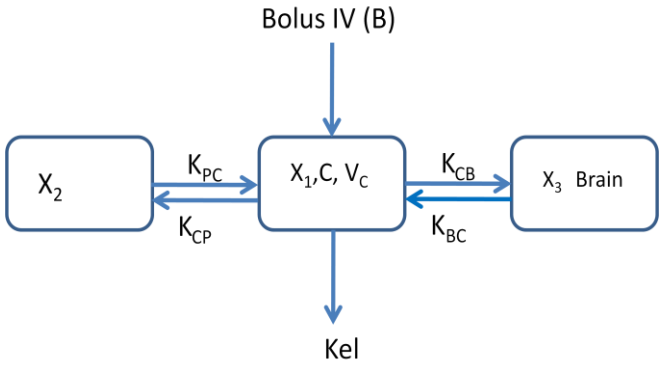

Differential Equations

$$\frac{dx_1}{dt} = B(1) + x_2 K_{PC} + x_3 K_{BC} - x_1 (K_{el} + K_{CP} + K_{CB})$$

$$\frac{dx_2}{dt} = x_1 K_{CP} - x_2 K_{PC}$$

$$\frac{dx_3}{dt} = x_1 K_{CB} - x_3 K_{BC}$$

$$\frac{dx_4}{dt} = \frac{x_1}{V_C}$$

$$\frac{dx_5}{dt} = \frac{x_3}{(V_c \times K_{CB}) / K_{BC}}$$

Output Equations

$$y_1(t) = \frac{x_1}{V_c}$$

$$y_2(t) = \frac{x_3}{(V_c \times K_{CB}) / K_{BC}}$$

$$y_3(t) = x_4$$

$$y_4(t) = x_5$$

Secondary Parameters

$$Cl_t = K_{el} \times V_C$$

$$Cl_B = K_{BC} \times (V_c \times K_{CB}) / K_{BC}$$

Figure 4.53 Structure of the First Model for Co-Modeling of LAZ Concentrations in Plasma and Brain

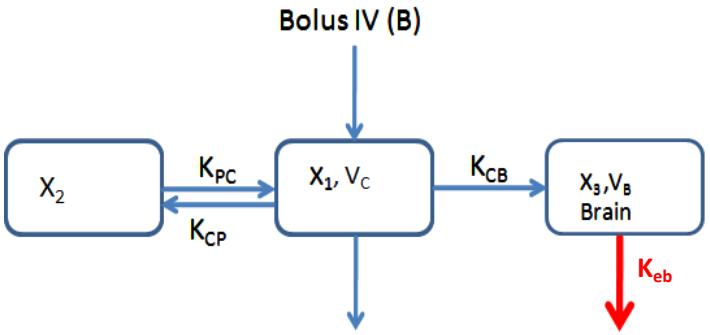

Differential Equations

$$\frac{dx_1}{dt} = x_2 K_{PC} - x_1(K_{el} + K_{CP} + K_{CB})$$

$$\frac{dx_2}{dt} = x_1 K_{CP} - x_2 K_{PC}$$

$$\frac{dx_3}{dt} = x_1 K_{CB} - x_3 K_{eb}$$

$$\frac{dx_4}{dt} = \frac{x_1}{V_C}$$

$$\frac{dx_5}{dt} = \frac{x_3}{V_B}$$

Output Equations

$$y_1(t) = \frac{x_1}{V_c}$$

$$y_2(t) = \frac{x_3}{V_B}$$

$$y_3(t) = x_4$$

$$y_4(t) = x_5$$

Secondary Parameters

$$Cl_t = K_{el} \times V_C$$

$$Cl_B = K_{BC} \times V_B$$

Figure 4.54 Structure of the Second Model for Co-Modeling of LAZ Concentrations in Plasma and Brain

For LAZ solution, by comparing the goodness of fit between the two models, the second model had higher R^2 and lower AIC values for both plasma and brain concentrations (R^2 =0.991, 0.825 and AIC= -72.456 for the second model vs. R^2 = 0.946, 0.718 and AIC= -27.811 for the first model) (Figures 4.55 and 4.56). For Lipo G, the second model had a better prediction than the first model. The second model had comparable R^2 values for plasma and brain to the first model, but with a lower AIC than that from the first model (R^2 =0.993, 0.981 and AIC= 42.204 vs. R^2 =0.993, 0.982 and AIC=-17.960, respectively) (Figures 4.57and 4.58). The correlation between the predicted and the observed data for the second model had a high correlation and a good prediction as demonstrated by the R^2 values of the plots with the predicted vs. the observed values for the plasma and the brain samples (Figure 4.59).

By comparing the results from the second model to those obtained from the non-compartmental analysis using WinNonlin, the AUC's from the solution and Lipo G were similar. The AUC in the brain was comparable between the second model and that of WinNonlin except that for the solution. Additional concentration-time points were added to the solution profile in the brain to balance those in the plasma during the modeling step. The same trend was observed among the parameters derived from WinNonlin and ADAPT. For example, equal elimination rate constants for the solution and Lipo G were derived using both modeling softwares (Table 4.49).

Solution

Output	R-squared	Weighted Sum of Squares	Sum of Squares
Y(1)	0.946	0.355960E-01	0.355960E-01
Y(2)	0.718	0.418684E-01	0.418684E-01

Model Selection Criteria
AIC: -27.811
SCHWARZ: -25.255

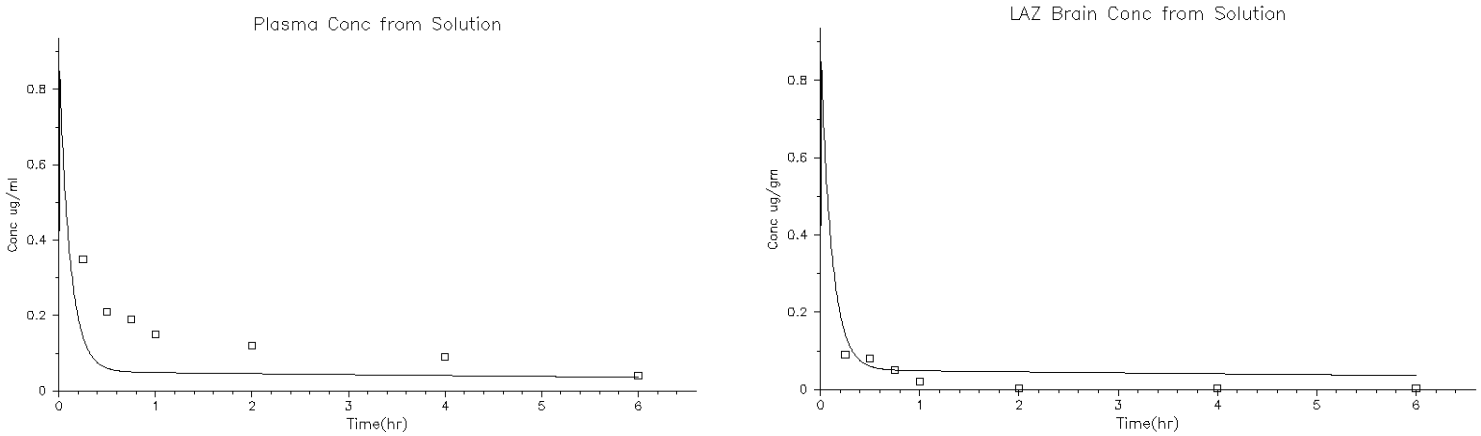

Figure 4.55 Results of the First Model for the Solution

Solution

Output	R-squared	Weighted Sum of Squares	Sum of Squares
Y(1)	0.991	0.620816E-03	0.620816E-03
Y(2)	0.825	0.214693E-02	0.214693E-02

Model Selection Criteria
AIC: -72.456
SCHWARZ: -69.261

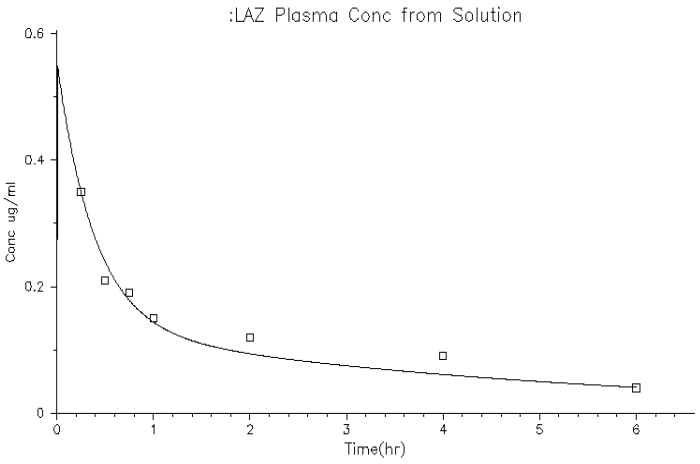

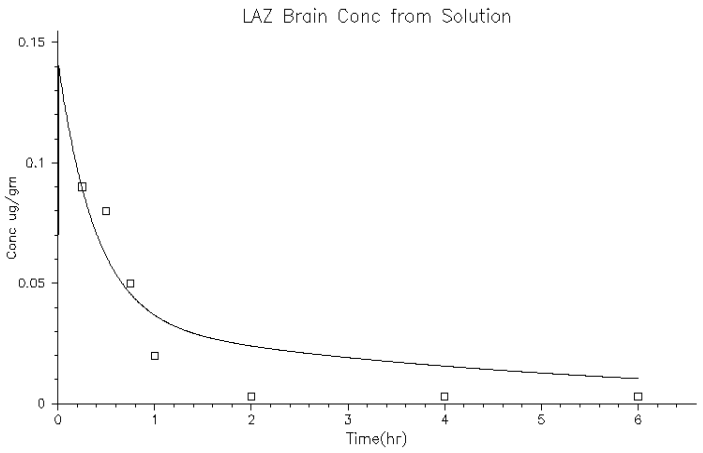

Figure 4.56 Results of the Second Model for the Solution

Liposomes

Output	R-squared	Weighted Sum of Squares	Sum of Squares
Y(1)	0.993	4.35484	4.35484
Y(2)	0.982	4.29414	4.29414

Model Selection Criteria
AIC: 42.204
SCHWARZ: 46.039

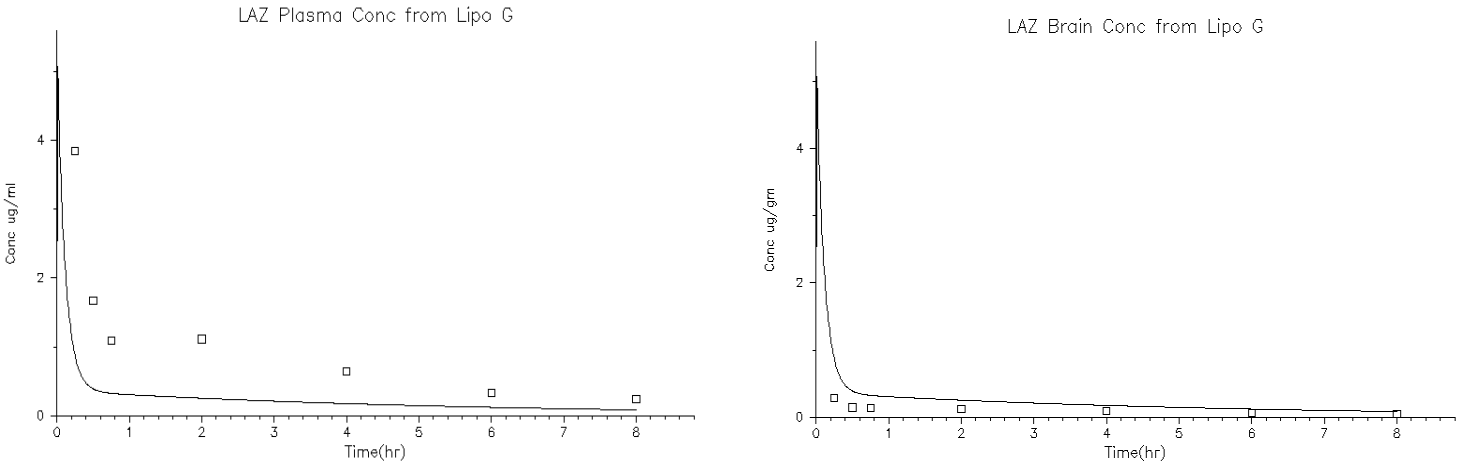

Figure 4.57 Results of the First Model for the Liposomes (Lipo G)

Liposomes

Output	R-squared	Weighted Sum of Squares	Sum of Squares
Y(1)	0.993	0.700534E-01	0.700534E-01
Y(2)	0.981	0.319390E-01	0.638779E-02

Model Selection Criteria

AIC:	-17.960
SCHWARZ:	-13.487

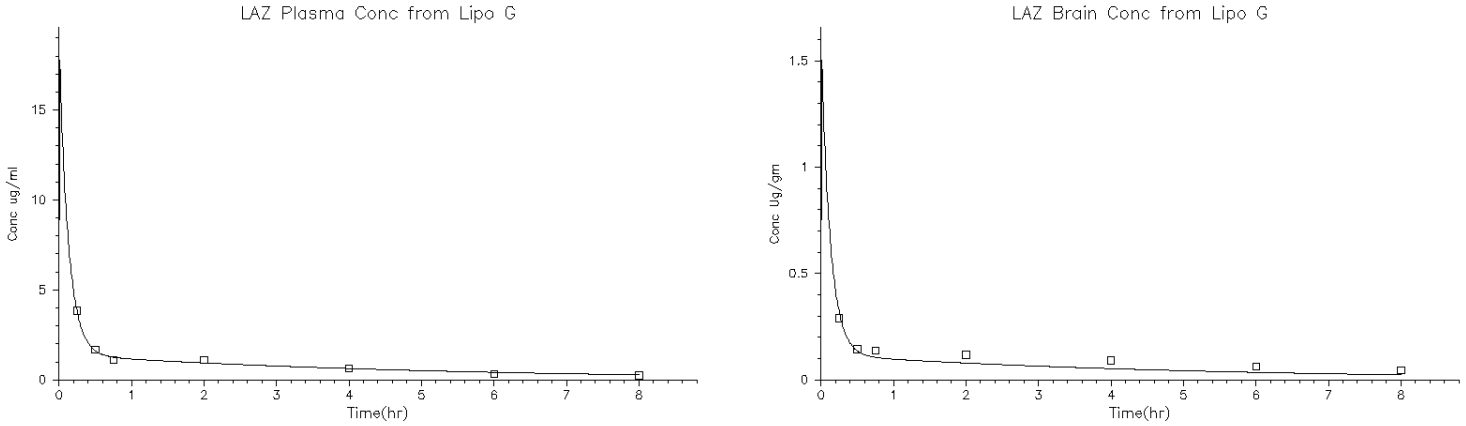

Figure 4.58 Results of the Second Model for the Liposomes (Lipo G)

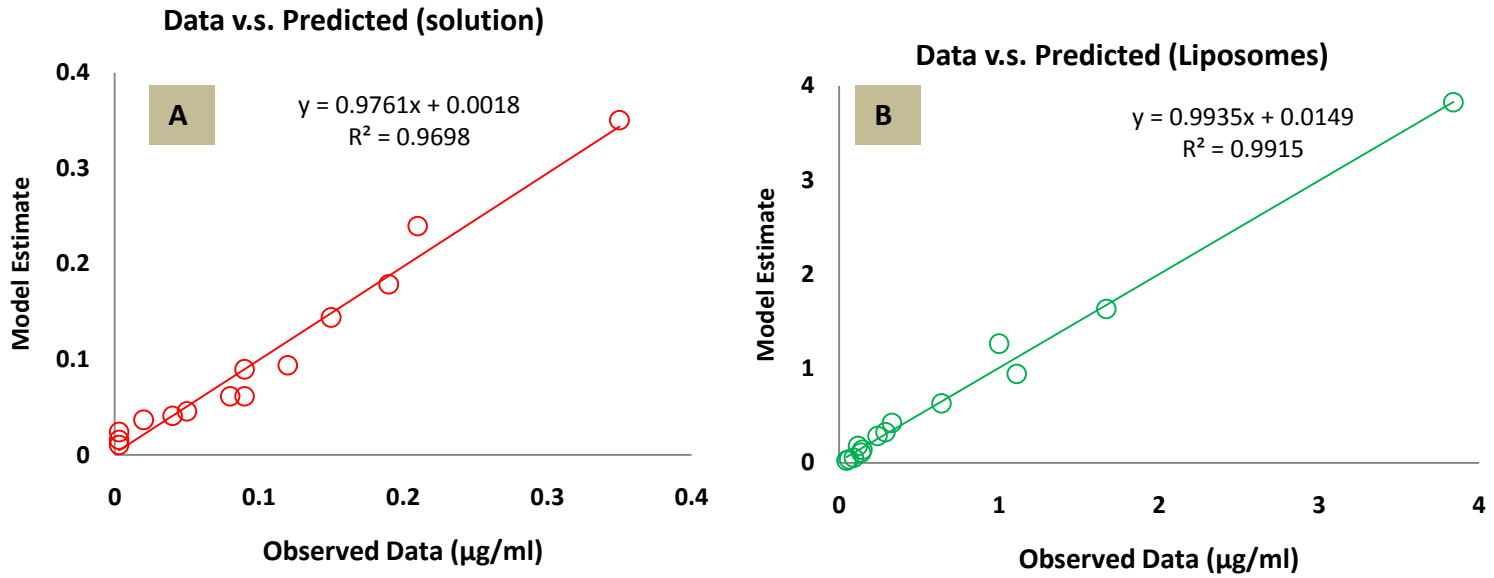

Figure 4.59 Goodness of Fit Plots of the Second Model from (A) Solution and (B) Liposome (Lipo G)

Table 4.50 Final Parameter Estimates from the Second ADAPT II Model

Parameter	Solution		Liposomes	
	3-Compartment ADAPT II	Non-Compartment WinNonlin	3-Compartment ADAPT II	Non-Compartment WinNonlin
K_{el} (hr^{-1})	0.43	0.27	0.45	0.26
V_d (ml)	115.95 *	109.65	12.39 *	11.76
K_{pc} (hr^{-1})	1.49		0.77	
K_{CB} (hr^{-1})	0.54		1.57	
V_B (ml)	0.0004		0.03	
K_{cp} (hr^{-1})	3.55		5.17	
K_{eb} (hr^{-1})	1.8×10^{5}		922.10	
Cl_T ($ml\ hr^{-1}$)	14.54	33.31	0.72	3.66
Cl_B ($ml\ hr^{-1}$)	73.29		29.89	
AUC_{plasma} ($\mu g.hr.ml^{-1}$)	0.71	0.75	7.84	7.28
AUC_{Brain} ($\mu g.hr.ml^{-1}$)	0.18	0.06	0.66	0.8

Note: The parameters were derived from the mean profile which was constructed from sparse sampling design. Therefore, there is no statistical analysis was done

*Vd= $V_c+V_p+V_B$

4.6.5 Pharmacokinetics and Proof of Concept Efficacy of LAZ PEGylated Liposomal Formulation of Suppressing Glioblastoma Tumor Growth in Mice

4.6.5.1 Tumor Growth

Bioluminescence imaging (BLI) is an optical molecular imaging technology based on the sensitive detection of visible light generated during the enzyme-mediated oxidation of a molecular substrate. The enzyme is expressed as a reporter for the tumor mass and the extent of substrate oxidation, and hence the light intensity is proportional to the amount of the expressed enzyme [74]. Because BLI does not require an excitation light source, it has very low background noise and can be used to detect very weak BL signals with a high level of sensitivity. In addition, the quantification of emitted light within a region of interest can be defined noninvasively as a measure of cell number in vitro or tumor size in vivo [75, 76].

The size of the tumor was estimated by measuring the amount of the emitted light from substrate oxidation by the expressed enzyme. The cell line U87-L glioblastoma multiform with luciferase reporter grew intracranially and the developed tumor size was traced by BLI (Figure 4.60-A). The BLI started after a week from cell line inoculation. The relative BL intensity was calculated by comparing the BLI intensity in the second and third week to that of the first week for the animal ‘s own control (Figure 4.60). The tumor size was expressed as the relative photon intensity measured by BLI (Table 4.51 and Figure 4.61).

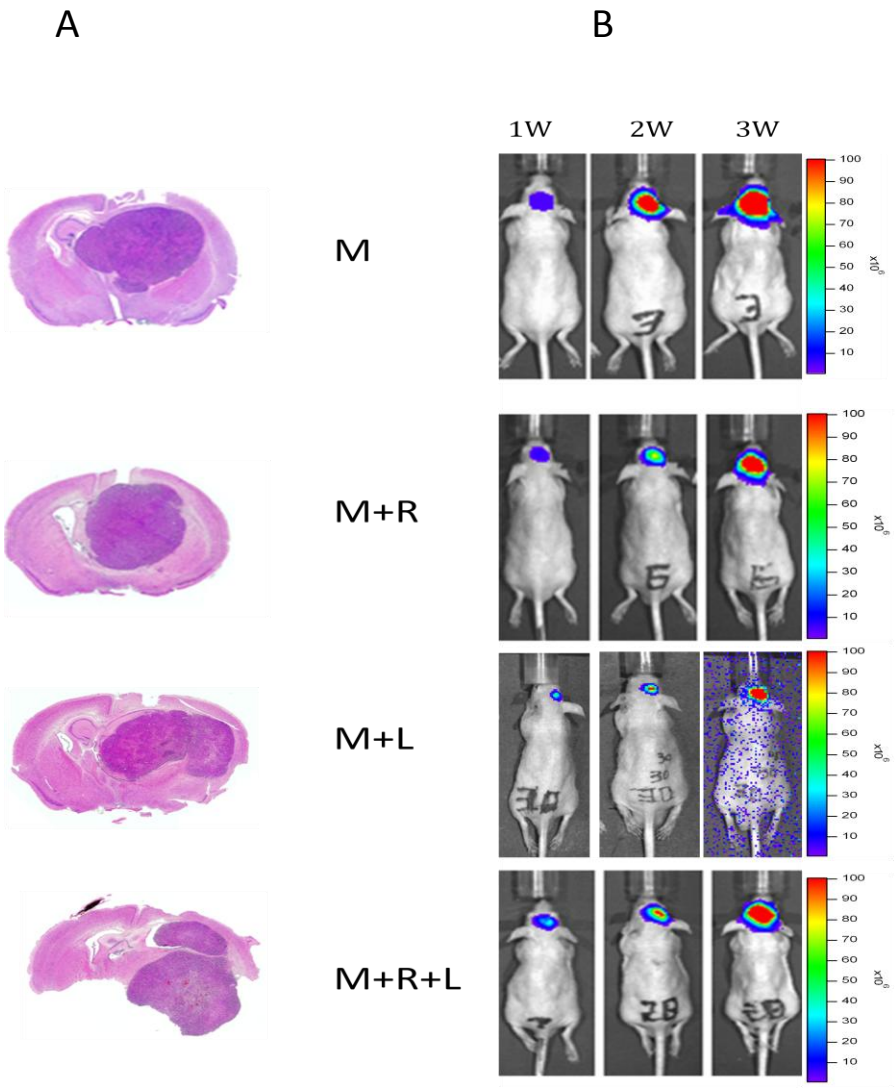

Figure 4.60 A) Histological Images Taken a Week Post U87-L Tumor Cell Implantation B) Continuous Bioluminescent Imaging were Taken Weekly of Each Group

The mice in the control group did not receive any treatment and showed exponential growth of the tumor size. The tumor growth in the control group was faster compared to the other three treatment groups. However, for the radiation treated groups (M+R) and (M+R+L), there was no significant difference in the tumor size compared to the model (M) group on the third week of treatment. On the other hand, the (M+L) group, which was treated using the liposomal LAZ formulation alone, had a significant smaller tumor size compared to that of the control model group (M) on the third week (65 % reduction in tumor size). There was no significant difference among the M+L group and the radiation treated groups, M+R and M+R+L (Figure 4.62).

Malondialdehyde (MDA) is widely used as an indicator for lipid peroxidation [77]. The amount of MDA expressed as µM/ gm tissue wt is indicative of the necrosis that happened due to the radiotherapy. The MDA concentrations in the brain tissues of M+L and M+R+L groups was significantly less than that detected in the M+R group (8.27±0.78 and 10.37±3.30 µM/gm vs. 23.09± 3.79 µM/gm, respectively) (Figure 4.63 & Table 4.52).

The survival of the mice in control (M), M+R, M+R+L and M+L were shown in Figure 4.64. The survival was expressed as percent of mice surviving from original number at time 0. The Kaplan-Meier estimator was used for survival analysis with P value set at 0.05. The LAZ treated groups (M+L and M+R+L) had significantly longer survival duration than that of the control group (M). There was no significant difference in survival duration between (M+R) group and the control group (M). The mean survival

durations were 22.67, 25.33, 25.22 and 27.13 days for the M, M+R, M+R+L and M+L groups, respectively.

CD34 is used as a marker for angiogenesis in the tissues. The signal intensity of angiogenesis marker CD34 was reduced in the groups that received Lipo G LAZ (M+L and M+R+L) and radiation (M+R) treatments compared to the control (M) group. The group that received Lipo G and radiation (M+R+L) had a significant CD34 signal reduction compared to that received radiation alone (M+R) (Figure 4.66-A). Ki67 is a nuclear protein that is associated with cellular proliferation. The staining of Ki67 showed that the group which received radiation alone (M+R) had a significant increase in cell proliferation compared to that of the control group (M). The administration of Lipo G to the radiation-treated group (M+R+L) reduced the proliferation of the (M+R) group. The treatment of Lipo G alone (M+L) significantly decreased the proliferation compared to the control group (M) (Figure 4.66-B).

There was no significant difference in LAZ concentration samples, 1 and 2 hr post dose, between the M+R+L and M+L groups (Figure 4.65). However, it appeared that LAZ concentrations in M+R+L group which received whole body radiation were less than those from M+L group.

Table 4.51 Relative Quantitative BLI Indicating the Relative Tumor Sizes for (M) Control, (M+R) Control Received Radiation, (M+L) Group Received Lipo G and (M+R+L) Group Received Radiation and Lipo G (n=8-9, each).

Group		Relative BLI Intensity (%)		
		1st week	2nd week	3rdweek
M	Mean	100.00	973.12	4002.03
	SD	0.00	223.49	1737.67
	SE	0.00	74.50	579.22
M+R	Mean	100	471.85	2034.95
	SD	0	162.93	737.72
	SE	0	54.31	245.91
M+R+L	Mean	100.00	826.76	2498.89
	SD	0.00	911.72	2521.32
	SE	0.00	303.91	840.44
M+L	Mean	100.00	1005.63	1387.36
	SD	0.00	1081.76	684.53
	SE	0.00	382.46	242.02

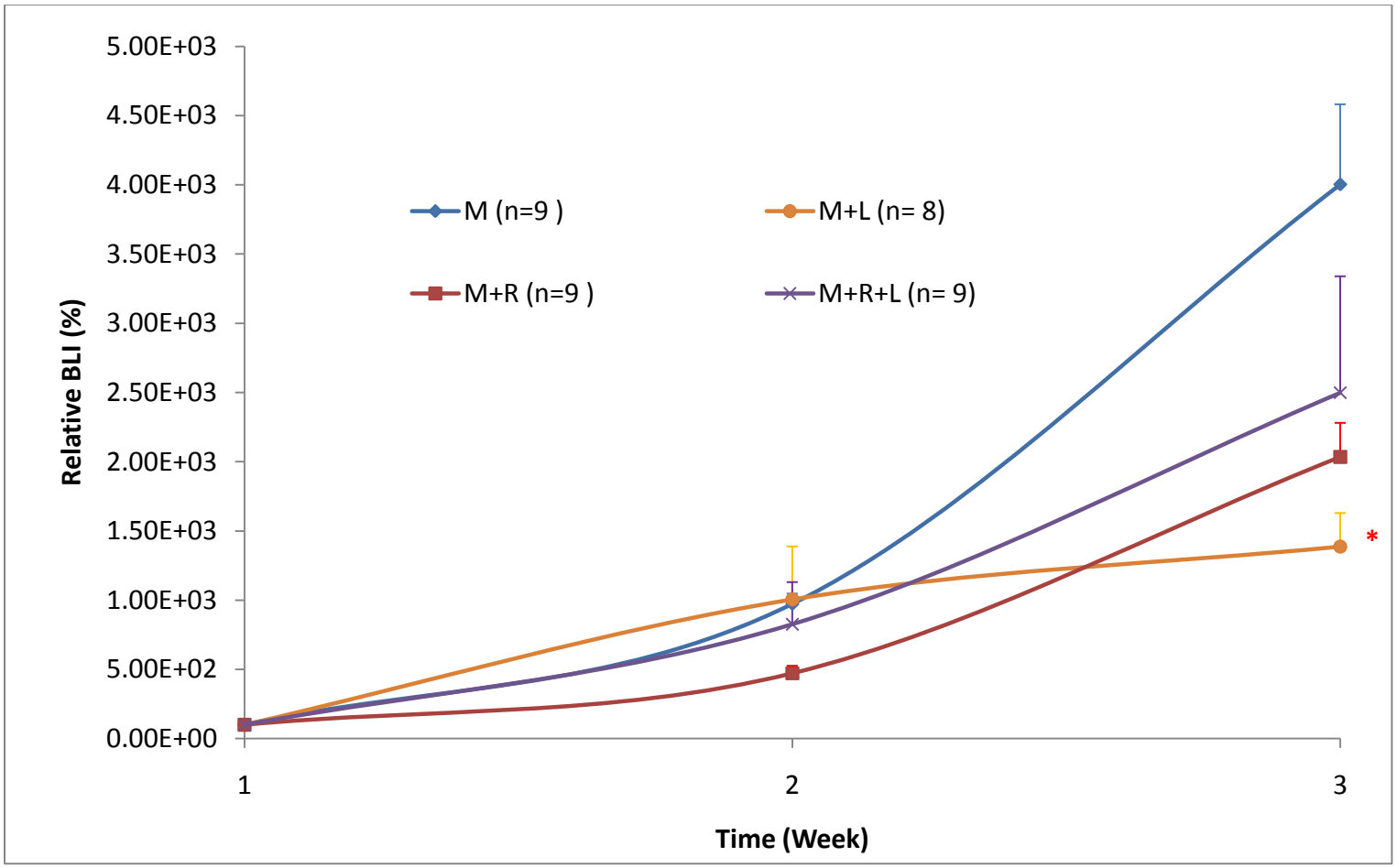

Figure 4.61 Relative BLI Indicating the Relative Tumor Sizes for (M) Control, (M+R) Control Received Radiation, (M+L) Group Received Liposomal LAZ alone and (M+R+L) Group Received Radiation and Liposomal LAZ. Data presented as Mean and SE.

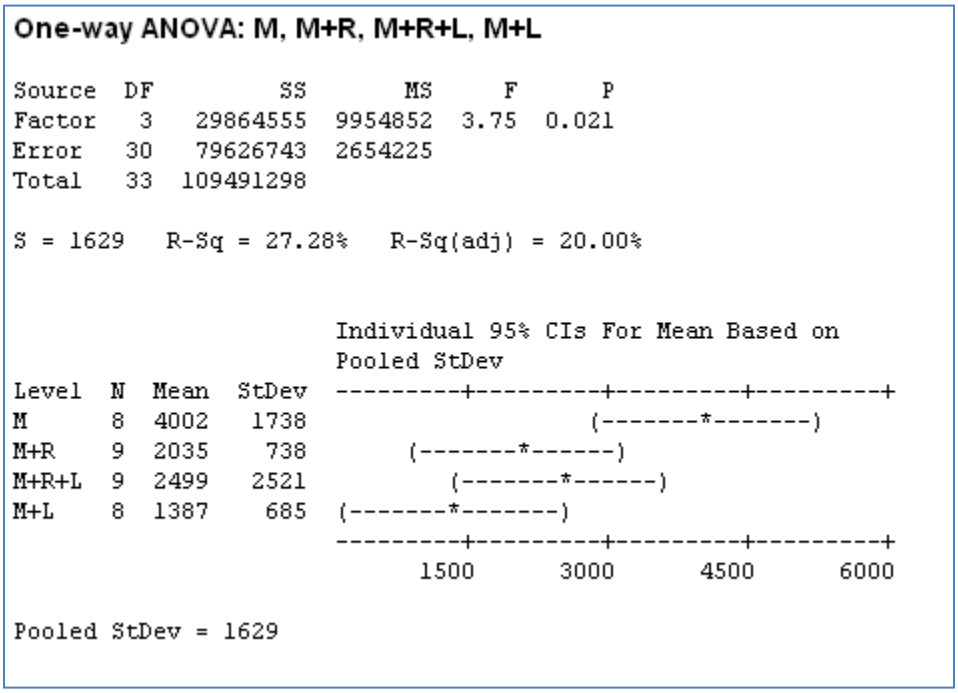

Figure 4.62 One –Way ANOVA Test for the Relative Tumor Size on the Third Week for the Control and Treatment Groups

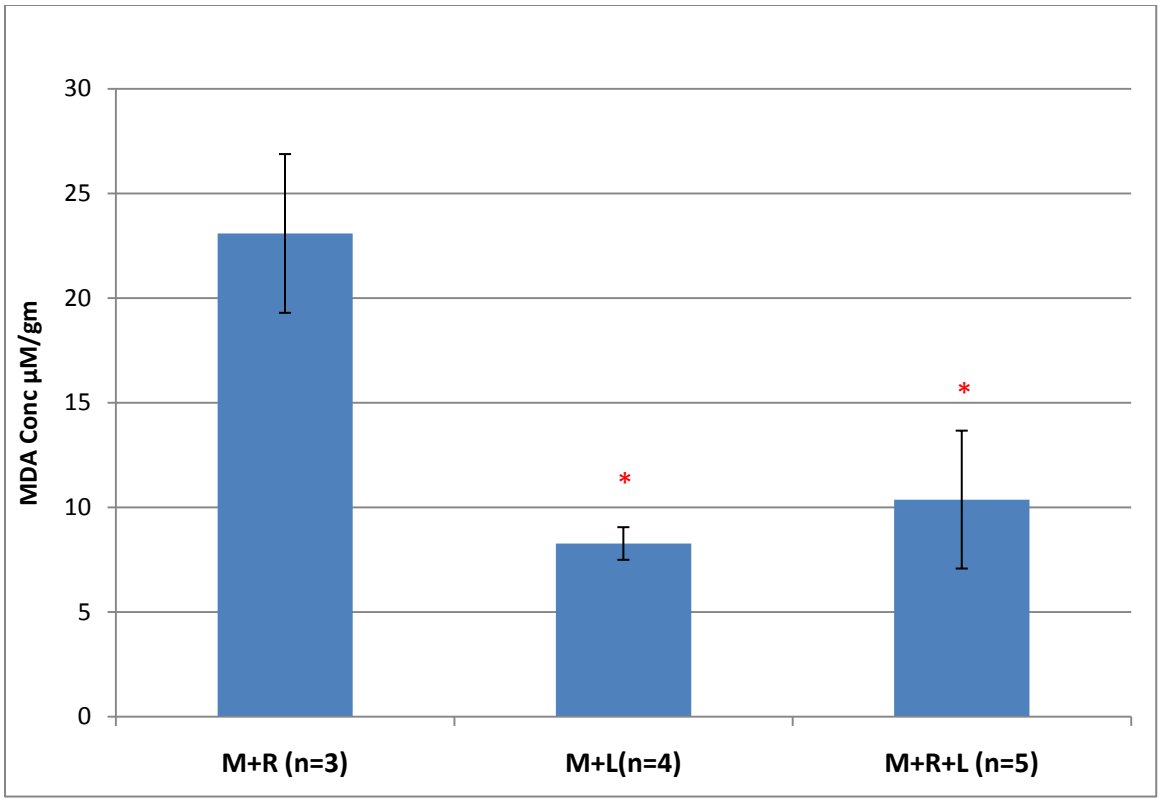

Figure 4.63 MDA Concentrations in the Brain Tissues at the End of the Three-Week Treatment

Table 4.52 MDA Concentration in the Brain Tissue at the End of the Three-Week Treatment

	MDA Concentration µM/gm		
	M+R (n=3)	M+L (n=4)	M+R+L (n=5)
Mean	23.09	8.27	10.37
SD	3.79	0.78	3.30

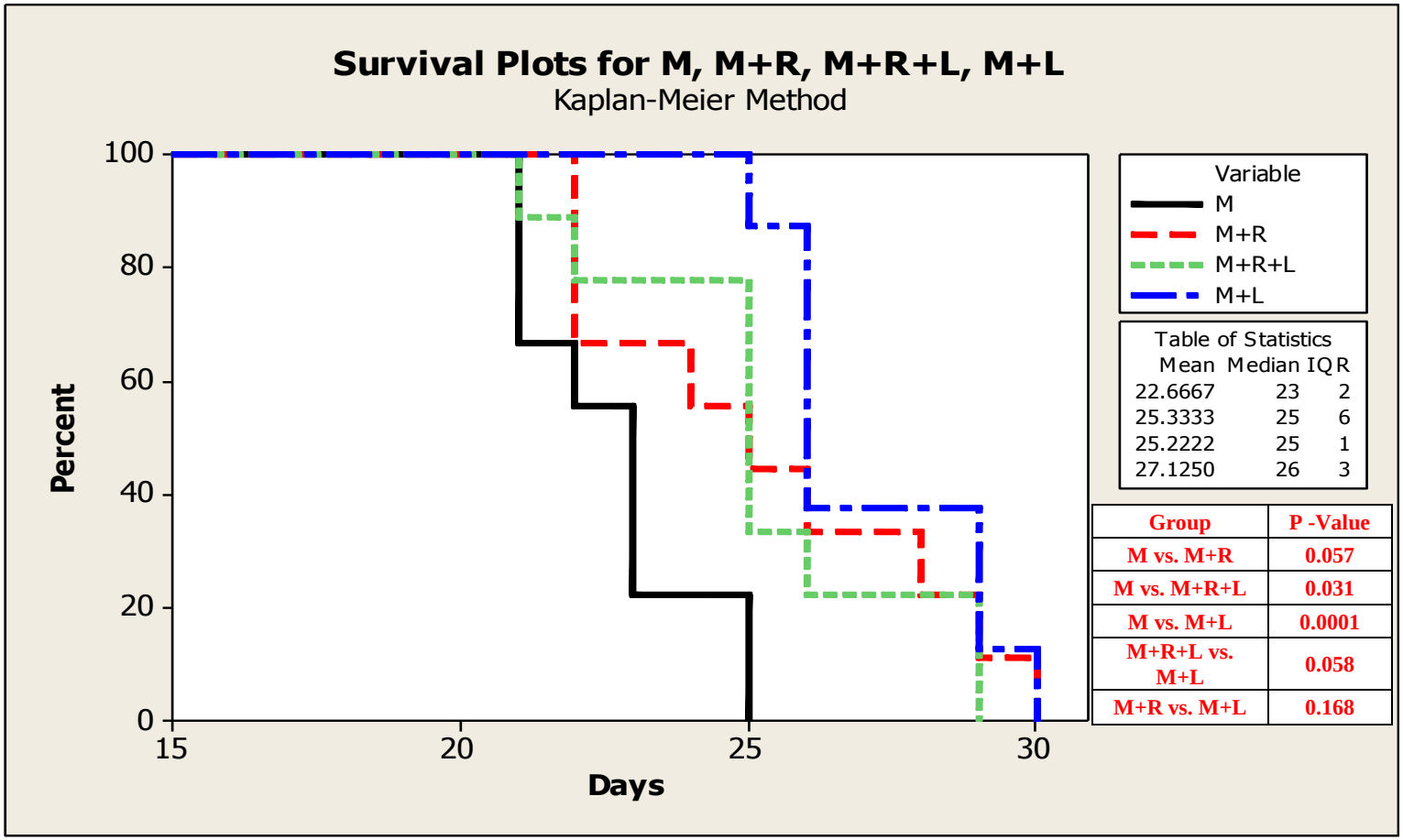

Figure 4.64 Survival of Brain Tumor Bearing mice in groups of (M) Control, (M+R) Received Radiation, (M+L) Received Liposomal LAZ and (M+R+L) Received Radiation and Liposomal LAZ.

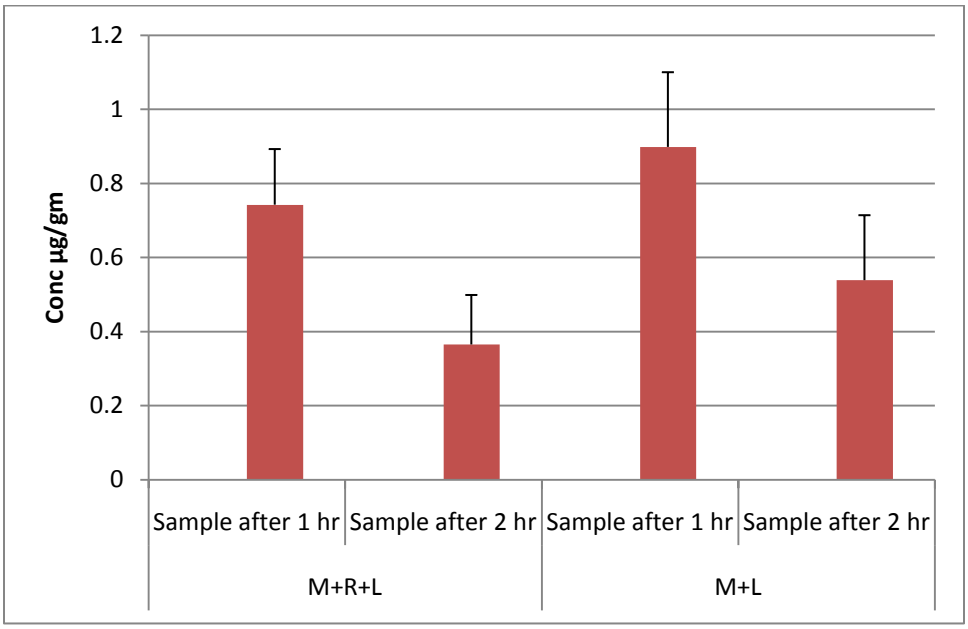

Figure 4.65 LAZ Concentrations in Plasma Samples from Various Treatment Groups

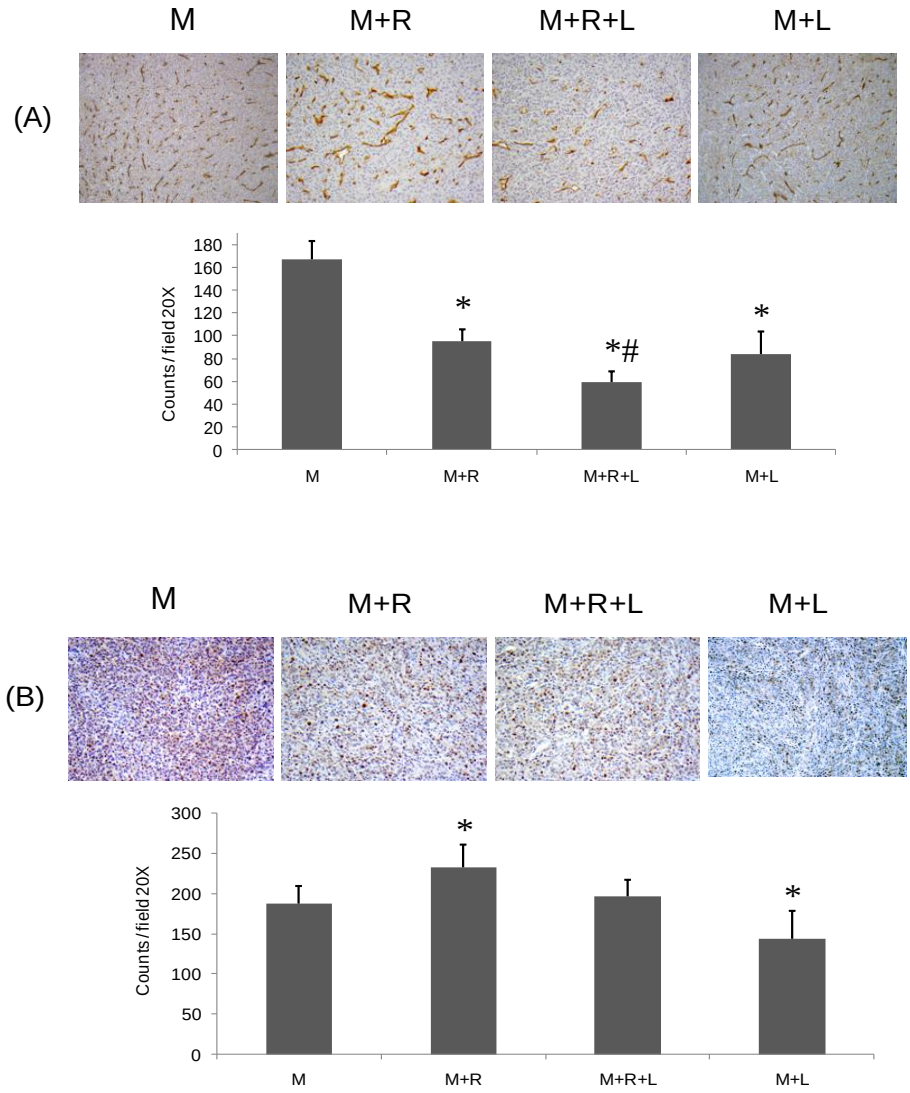

Figure 4.66 Immunohistochemical Analysis of (A) CD34 and (B) Ki67 Xenograft U87 Tumor Masses Derived from Control and Treated Groups.

The samples were taken at the end of experiments (* $P < 0.05$ vs. M, # $P < 0.05$ vs. M+R, n = 7). [performed by Dr. Kemi Cui at Methodist Research Institute, Houston, TX]

4.6.5.2 Population Pharmacokinetics of LAZ in Brain Tumor Bearing Mice after Lipo G Treatment at a Dose of 5 mg/kg (n=30)

Plasma concentration data were available from 30 mice from two batches with 105 collected plasma samples. The samples were drawn 1 or 2 hr post dose for 3 weeks period from randomly selected mice (Figure 4.67). The mice were treated with either Lipo G (M+L) at a dose of 5mg/kg IP twice weekly alone or with the previous Lipo G protocol followed by radiation (M+R+L) of 2 Gy once a week. A third LAZ treated group was treated with Sunitinib solution 40 mg/kg five times a week. The population pharmacokinetics model building process is shown in Table 4.53. A one-compartment model with zero-order input and first-order elimination (Modeel#1) described the data better than two- or three- compartment model (Model # 2&3) as showed with constant OFV among the three tested compartmental models and reduction of AIC values moving from 3- to 1- compartmental models. As the liposomal LAZ formulation was given intra-peritoneally, the modeling was developed using extra-vascular input but it did not improve the fit (there was no reduction in OFV and AIC values).

Different methods were used to include the covariates in the base model (additive, proportional, both additive and proportional and exponential), no improvement was achieved in the fit using the aforementioned methods for error inclusion. The additive method was chosen as it is the simplest method. Different covariates [weight (WT), tumor size (TUM), Sunitinib administration (SUN) and radiation treatment (RAD)] were tested for their abilities to improve the model and to reduce inter-individual variability in

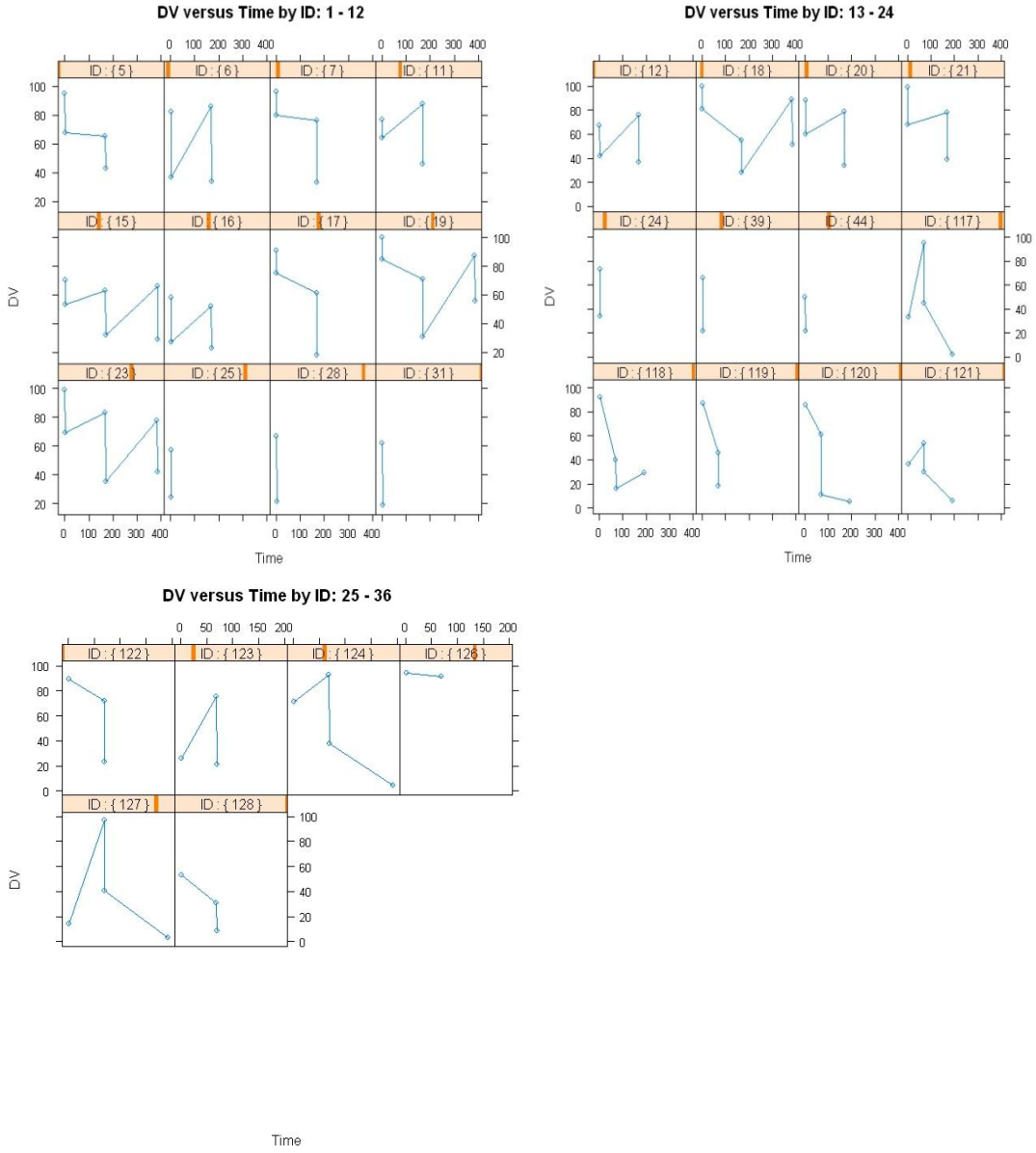

Figure 4.67 Animal ID and Sampling Points from the First and Second Batch
(First batch ID>100)

Table 4.53 Development of Population Pharmacokinetic Model

Model	COMP	Covariate	IOV	OFV	AIC	K (hr^{-1})	$(CV)_{\Omega K}$	V (ml)	$(CV)_{\Omega V}$	$(CV)_{\sigma}$
1	1			-227.48	-217.48	0.44	1.96%	89.70	7.91%	21.38%
2	2			-227.48	-209.48	0.44	0.32%	89.30	7.95%	21.40%
3	3			-228.00	-202.00	2.25	9.09%	10.70	0.32%	21.50%
4	1 Oral			-227.62	-213.62	0.03	0.32%	0.39	7.92%	21.40%
5	2 Oral			-227.90	-205.90	0.05	4.24%	0.37	1.21%	21.10%
6	3 Oral			-189.39	-159.39	0.05	0.32%	11.40	0.32%	14.80%
7	1	WT x K		-227.46	-213.46	0.44	0.20%	89.70	7.96%	21.40%
8	1	WT x K & V		-227.45	-209.45	0.44	0.20%	89.50	7.97%	21.40%
9	1	TUM x K & V		-180.90	162.90	0.35	60.60%	80.50	0.20%	22.40%
10	1	SUN x K & V		-227.48	-209.48	0.44	0.20%	89.80	8.20%	21.40%
11	1	RAD x K & V		-231.19	-213.19	0.34	0.20%	89.70	6.58%	21.20%
12	1	RAD x K		-231.19	-217.18	0.34	0.83%	89.80	6.58%	21.20%
13	1	RAD x V		-228.58	-214.58	0.43	1.63%	84.80	7.78%	21.30%
14	1		TUM on K & V	-229.08	-215.08	0.43	0.20%	89.00	3.47%	20.90%
15	1		ID on K & V	-229.08	-215.08	0.43	0.20%	89.00	3.47%	20.90%
16	1	RAD x K & V	TUM on K & V	-229.81	-207.81	0.42	0.20%	90.20	0.20%	20.50%
17	1	RAD x K & V	TUM on K	-232.58	-214.58	0.36	0.20%	89.30	5.02%	20.20%
18	1	RAD x K & V	TUM on V	-231.19	-213.19	0.34	0.20%	89.30	6.57%	21.20%
19	1	RAD x K & V	ID on K & V	-229.81	-207.81	0.42	0.20%	90.20	0.20%	20.50%

the pharmacokinetic parameters of K and V. The inclusion of the WT, TUM or SUN as covariates in both K and V did not improve the fit or decrease the variability in the pharmacokinetics parameters. Only the inclusion of the radiation covariate in K and V improved the fit (OFV= -231.185). The reduction of the OFV more than 3.84 at a significance level of 0.05 is considered a significant difference (Model #11). In addition, the incorporation of RAD as a covariate reduced the between-subject variability (BSV) in the pharmacokinetics parameters (Ω_K reduced from 1.96% to 0.2% and Ω_V from 7.91% to 6.58%, respectively). However, the inclusion of radiation as a covariate in V alone did not improve the fit (Model #13). Only radiation as a covariate in K improved the model fit (Model #12).

Parameters for inter-occasion variability (IOV) in K and V were tested for variation between the two batches regarding the overall experimental conditions or for the variation in the measured tumor size due to the technical variability in the image-capturing camera. Inclusion of IOV between the two batches to the additive error model did not improve the fit of the base model (Model#15) or radiation–covariate model (Model #19) (OFV reduction < 3.84 for both models compared to Models # 1 and 11, respectively). The inclusion of tumor size as an IOV between the two batches did not improve the base model (Model #14) or radiation-covariate model (Model#16) (OFV reduction < 3.84 for both models compare to Models # 1 and # 11, respectively).

The residual error or the unexplained variability was 21.38% of the base Model #1 and just reduced to 21.20% with radiation covariate Models # 11 and # 12. The residual error

decreased using the extravascular three-compartment Model #6 but without a good fit of the data.

The goodness of fit plots of the base Model and radiation covariate Model #11 are shown in Figures 4.68 & 4.69. The deviation of the prediction from the data was evenly distributed. The distribution of the prediction in relation to the data was closer to the identity line in Model #11 compared to that of Model #1, as shown by the slope and the correlation coefficient R^2 (0.944 and 0.536 vs. 0.931 and 0.521, respectively). In addition, the relative deviations of the population model from the data are evenly distributed over the whole range for Model #11(Figure 4.70).

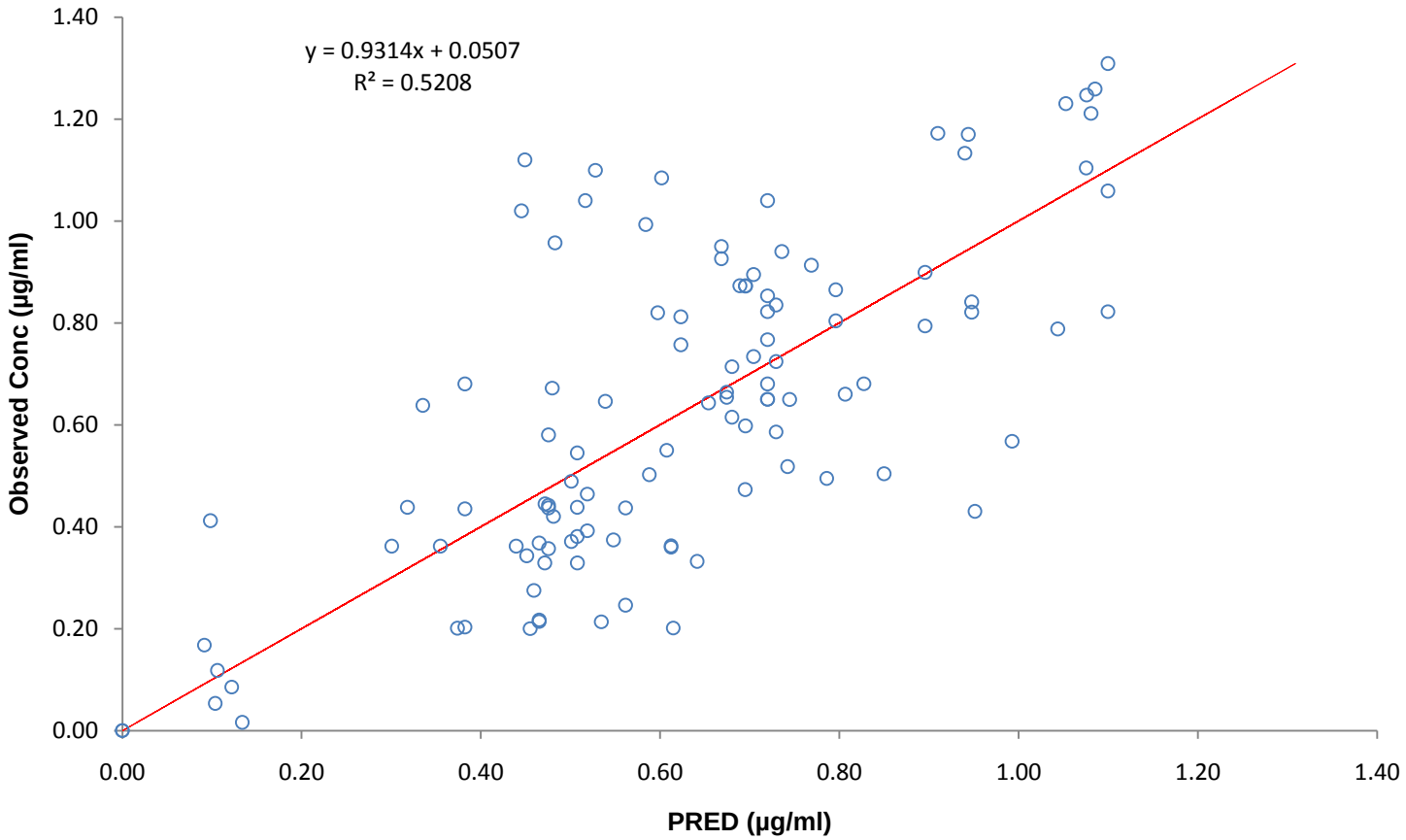

Figure 4.68 Goodness of Fit Plot for Base Model #1

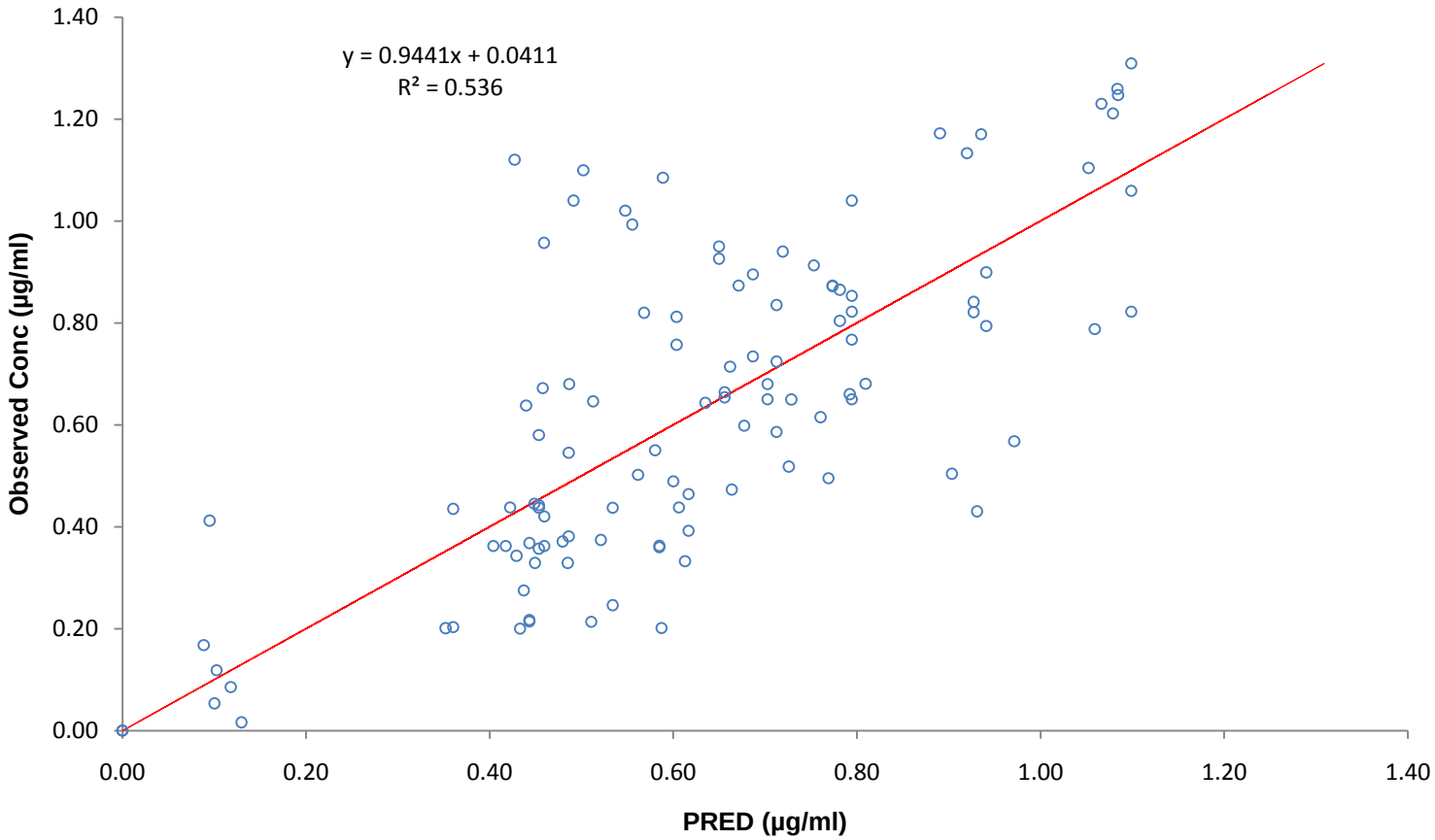

Figure 4.69 Goodness of Fit Plot for Covariate Model # 11

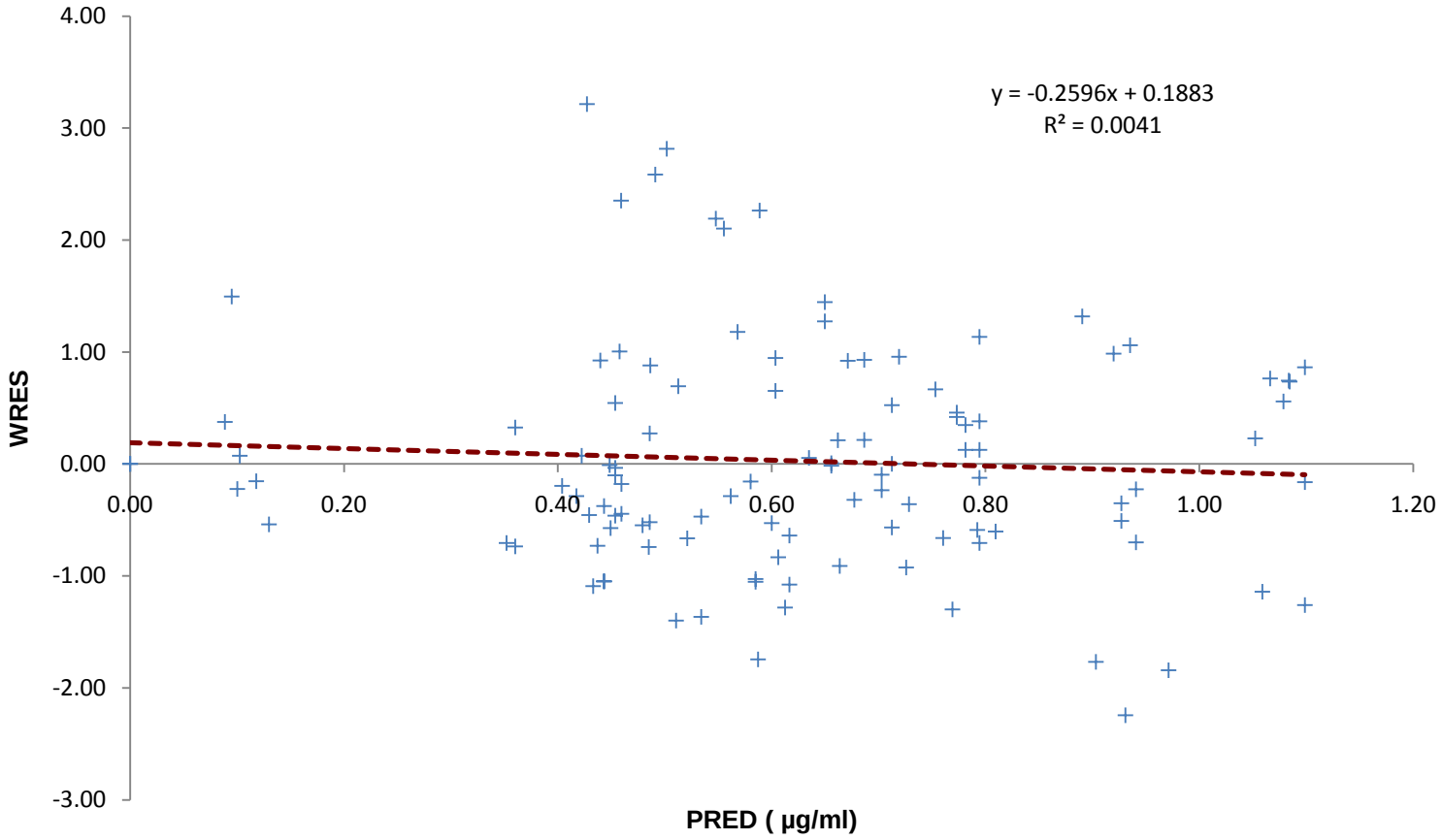

Figure 4.70 Population Model Prediction vs. Weighted Residual of the Population Model.

CHAPTER 5 DISCUSSION

Lazaroid U-74389G (LAZ) belongs to the 21-aminosteroid family. Lazaroid family inhibits lipid peroxidation which is the first step in brain tissue necrosis post radiotherapy. LAZ has antioxidant capacity especially in neural tissue of animals exposed to trauma, subarachnoid hemorrhage and ischemia [8]. LAZ has antiproliferative effects in a dose-dependent manner on Glioblastoma especially the primary cultures. Moreover, LAZ prevents free radical-mediated blood-brain barrier damage [19].

An efficient antioxidant activity requires sustained tissue exposure to LAZ. Cuifi et al., (1994), reported that U-74500A, which is another member of Lazaroid family, had no effect on lipid peroxidation when was dissolved in an acidic buffer but the antioxidant activity was retained after using a retard formulation (dissolved in PEG 4000, S.C. administration)[78].

Another member of this family, Tirilazad Mesylate (TMZ), underwent two phase III clinical trials in acute head stroke patients where they received 6 mg/kg solution in the first trial [79, 80] and 12.5-15 mg/kg solution in the second trial [81] as a rapid intravenous infusion over 10 to 30 minutes. TMZ was dropped from further research because there was no significant differences in patient survival duration between the control and the treated groups [82]. This inconsistency in the outcome could be due to a low exposure of the brain to TMZ resulting from its inability to cross the BBB. Another possibility is that TMZ has a rapid clearance from the circulation by high hepatic

extraction. These two factors may lead to the reduction in the therapeutic concentration in the brain.

In the view of the facts that (a) LAZ is subject to high hepatic extraction, (b) higher efficacy resulting from a retard formulation and (c) its inability to cross the BBB, we aimed to formulate LAZ in the following formulations:

1- Nanosuspension formulations with different sizes and charges to modify the PK and organ distribution.
2- Microsphere formulations using biodegradable polymer PLGA to be implanted in the brain for a sustained release into the brain tissues.
3- Liposomal formulation to enhance LAZ transport across the BBB and decrease the extent of hepatic extraction.

The purpose of developing these formulations is to enhance LAZ exposure in the body by sustaining its release from the formulations. The nanosuspensions with various sizes and charges can modify the organ distribution pattern. This modification may by-pass the liver uptake and improves drug accumulation in other organs. The formulation of LAZ in biodegradable microspheres allows the implantation of the microspheres in the brain tissues during surgery. The implantation can take place in various sites to cover a wide area of the brain and at the same time will overcome the difficulty of acrossing the BBB. The third formulation is LAZ liposomes. The liposomal formulations are characterized by their unique methods of preparation and *in-vivo* fate inside the body. There are several commercial formulations on the market recruiting liposomes as the carrier system such as

Doxil® for doxorubicin. The incorporation of LAZ in liposomes enhances the exposure in the body and will offer the potential merit of targeting the brain depending on the lipid compositions and the size of the liposomes.

5.1 HPLC assay

The reported HPLC assay is a rapid and convenient method for the quantification of LAZ in mouse plasma and organs including liver, lungs, kidneys, spleen, lungs, heart and brain. This is the first assay reported to monitor LAZ *in-vivo*. The recovery from plasma and other organs is 93-105 %, significantly higher than those reported by Laizure et al, 66-77% for TMZ [17]. However, the extraction recovery of LAZ from liver samples is 68%. The assay is validated with the linearity of 0.4-100 µg/ml and LLOQ of 0.4 µg/ml. The sensitivity of the assay enables the pharmacokinetics and biodistribution evaluations to an extended period post dose. The accuracy and precision of the assay are $< 11\%$ and 96-107%, within the requirement set by FDA [83, 84]. The stability studies show that LAZ in the biomatrices is stable during short- and long-term periods for sample preparation and analysis. Therefore, this method is suitable for routine analysis of LAZ in evaluations of innovative formulations of LAZ for organ targeting.

5.2 UPLC-MS/MS Assay

This is the first UPLC-MS/MS method reported to quantify LAZ in biological tissues. The developed method is simple using solvent extraction with acetonitrile. Daidzein is chosen as internal standard for being detected at the same positive mode as LAZ with high sensitivity. The Calibration curves for LAZ in all the matrices are linear in the

concentration range of 15.6–4,000 ng/ml with correlation coefficient values >0.99. The LLOQ is 15.6 ng/ml. The intra-day precision is less than 7% and accuracy range from 95 to 108%. The inter-day precision is less than 9% and accuracy range from 96 to 114%.

The mean extraction recovery varies according the matrix. The lowest recovery is from the heart samples (59-65%) and the highest recoveries are from the spleen, lung and kidney samples (86-99%). The recoveries from other tissues are 73-84% from brain samples and 79-87% from liver samples. For matrix effect, the ionization of LAZ is suppressed by the biological matrices by about 70 % and 50% from liver and heart, respectively. The suppression is less in case of kidney (35%), plasma and brain (15%), and lung (5%) samples.

5.3 Nanosuspension

5.3.1 Formulation of Nanosuspension

The milling technique is used in nanosuspension preparation where the solid drug particles are sheared between the sliding surfaces of the moving glass beads. This shear movement imparts energy into the system leading to the reduction in the particle size. Due to the energy introduced into the system to reduce the particle size, the system becomes unstable due to the formation of fresh surfaces. It tends to reduce the high energy by re-agglomeration in larger particles to minimize the newly created surfaces. To overcome the agglomeration tendency, Tween 80 and Pluronic F108 are added as steric stabilizers to overcome the attractive interactions between the sheared particles. The presence of the stabilizers keeps the particles apart and prevents the re-agglomeration

step [85]. To further reduce the particle size, the shear forces are increased by minimizing the distances that separate the sliding beads, using a mixture of glass beads with various sizes to incorporate the smaller beads in-between the larger ones. The single-sized glass beads produces particles with larger polydispersity index (bi-modal size distributions), but the mixture of multi-sized glass beads produces a narrow polydispersity index (mono-modal particle size distribution). Similar results were reported by Yang et al. 2008 [86].

5.3.2 Pharmacokinetics and Organ Distribution

5.3.2.1 Pharmacokinetics of LAZ Nanosuspensions in Mouse Plasma

The surface properties and the size of the nanosuspension particles can be manipulated to modify the PK and biodistribution of LAZ [87, 88]. A pooled averaged data approach was used to construct plasma-time profiles for LAZ solution and nanosuspensions. The plasma profiles show not only differences between the solution and the nanosuspension preparations but also among the nanosuspensions with different sizes and charges. The solution has a higher C_o than those of the nanosuspensions except that of the cationic NS-$A^{(+)}$. The uptake of the nanosuspension particles by RES and other organs affects the clearance of the nanosuspensions. In addition, the slow dissolution and consequently the slow release of LAZ particles which are engulfed by RES and the macrophages circulating in the blood can affect the plasma levels of the nanosuspensions. The C_o of NS-$B^{(-)}$ is comparable to that of the solution due to the rapid dissolution of the small particles and the escape from the macrophages.

The positively charged surface of the NS-$A^{(+)}$ is responsible for the high plasma concentration that is observed in the early time points of detection. The positively charged particles undergo an electrostatic attraction with the negatively charged circulating RBCs and other blood components. This attraction can delay the uptake of these particles by RES at the early detection points[89].

By comparing the AUC's of the formulations, the AUC of the solution is higher than those of NS-A and NS-$A^{(-)}$. This could be due to the uptake of the particulate drug by the liver and other RES organs leading to distinctly lower concentration of NS-A and NS-$A^{(-)}$ in plasma. The AUC of the cationic NS-$A^{(+)}$ is higher than the other nanosuspensions because at the early points it undergoes a temporary attraction to the RBC's. These particles are then captured by the circulating macrophages due to adsorption of other plasma proteins and components. The AUC of NS-$B^{(-)}$ is higher than that of NS-$A^{(-)}$ due to a faster dissolution and escape from the macrophages back to the blood stream. Similar results were reported by Hiromitsu, *et al*. 1997, and Manjunath *et al*. 2006 [89, 90].

The half life of the cationic NS-$A^{(+)}$ is the shortest among the nanosuspension formulations. This could be due to the extensive uptake of the cationic NS by the liver. The large positive charge (+40 *mv*) on the cationic NS-$A^{(+)}$,which is the reason at the beginning to slow down the clearance by the attraction to RBCs, could be the same reason for a rapid recognition and elimination by the circulating macrophages. Polystyrene microparticles with a primary amine at the surface, is known to impart a

positive charge after the protonation of the amine, and undergo a significantly more phagocytosis as compared to microparticles that contain sulfate, hydroxyl, and carboxyl groups. The protonated particles are also expected to have a short blood circulation half-life [91].

The total clearance of LAZ from plasma varies among the formulations. The clearance of the drug solution is comparable to those of NS-$A^{(+)}$ and NS-$B^{(-)}$ but slower than those of NS-A and NS-$A^{(-)}$. The clearance of NS-$B^{(-)}$ is slower than that of NS-$A^{(-)}$ due to the smaller size of NS-$B^{(-)}$ that results in a faster dissolution and faster escape from the macrophage after capture. The cationic NS-$A^{(+)}$ has K_{el} which is two folds of that of the solution; however, the clearance of the cationic nanosuspension is comparable to that of the solution. This is due to the use of the AUC value to calculate the clearance where Cl=Dose/AUC. The cationic nanosuspension has high plasma concentrations at the beginning of the profile which led to a high AUC estimate and slower clearance as compared to that of the solution.

5.3.2.2 Tissue Distribution

Lazaroids family members have high hepatic clearance which is dependent on the liver blood flow [17, 92, 93]. Also, Lazaroids are metabolized mainly in the liver [94]. In our study, the results match what has been reported. The drug concentrations in the liver show high levels in the early detection points followed by a rapid decline. This could be explained by the accumulation of plasma opsonins on the drug particle which is the pre-

requisite for mononuclear phagocytic system (MPS) recognition. LAZ is mainly metabolized in the liver and this could be the reason for the rapid concentration decline in the hepatic tissues. As a result, the charged particles of NS-$A^{(+)}$ have higher liver exposure than the solution and the neutral nanosuspensions do.

The anionic nanosuspensions NS-$A^{(-)}$ and NS-$B^{(-)}$ have 3-8 folds higher exposure in the lungs as compared to those of the solution, as well as the cationic and the neutral nanosuspensions. The exposure is more prolonged in case of NS-$A^{(-)}$ as compared to NS-$B^{(-)}$ probably due to the slower dissolution of NS-$A^{(-)}$ particles. This behavior is also observed with Campothecin formulated in solid lipid nanoparticles (CA-SLN) [95]. The AUC of CA-SLN in the lungs was the highest among the tested organs. The CA-SLN was 196.8 nm in size and a zeta potential of -45.2 *mv*. Similar results were reported by Lo¨benberg *et al.,* 1998 for azidothymidine nanoparticles [96] and by Kurihara *et al.*, 1996 for palmitoyl rhizoxin lipid emulsions [97].

The particle size of the nanosuspension has an effect on the systemic exposure and distribution of LAZ among body organs. This could be due to the difference in the dissolution rate and the contact surface area with blood proteins which in turn affects the capture of the nanoparticles by MPS. According to Noyes Whitney equation, as the particle size decreases, the surface area and hence the dissolution rate increase for the same particle mass (Equation 5.1).

$$\frac{dC}{dt} = \frac{DA}{h}(Cs - C) \qquad \text{Equation 5.1}$$

$\frac{dc}{dt}$ *= rate of drug dissolution at time t, D = diffusion rate constant, A= surface area of the particle, Cs = concentration of drug (equal to solubility of drug) in the stagnant layer, C = concentration of drug in the bulk solvent, h = thickness of the stagnant layer*

For anionic 250 nm NS-$A^{(-)}$, a slower dissolution rate is responsible for the prolonged $t_{1/2}$ as compared to that of 125nm NS-$B^{(-)}$. Moreover, due to the larger particles of NS-$A^{(-)}$, the lung and spleen uptakes are higher than that of NS-$B^{(-)}$ but the liver uptake is comparable for both nanosuspensions. LAZ distribution to the brain is not improved by formulating LAZ in nanosuspensions. The use of Tween 80 as a stabilizer in nanosuspension does not improve the transport across the BBB although it is known to inhibit the efflux transporters across the BBB and recruit apolipoprotein E which facilitates the transfer of LDL across the BBB [28].

5.3.2.3 Comparison of Charge Effect on Distribution among Mouse Organs

The charges carried on the particulated system affect the fate of the particles. The charged NS results in a higher RES uptake as compared to the neutral NS. The charge on the particles may activate a complementary system which is required for the adsorption of plasma proteins (opsonins), a pre-requisite for MPS recognition [98]. The negatively charged NS-$A^{(-)}$ showed the highest uptake as compared to the positively charged NS in the liver, lungs and spleen. Similar results have been reported by Levchenko *et al.*, 2002. [99]. Levchenko *et al.* prepared liposomes with different charges approximately 200 nm

in size and studied their tissue distribution in mice over a period of time. He demonstrated that the rate of clearance from the blood was significantly higher for the negatively charged liposomes (ζ potential ~ -40 mV) than for neutral liposomes (ζ potential~ -10 mV). The negatively charged liposomes also showed an increased rate of MPS uptake in the liver compared to the neutral liposomes, indicating that phagocytic cells favored the uptake of negatively charged particles [99].

5.4 LAZ Microspheres

The idea of controlled release implants was enforced in the 1960s [31] but the problem of non-degradation restricted the use of these systems at that time. The microspheres have overcome the problem of biocompatibility since the biodegradable polymers were used. In 1970s the idea of using the biodegradable polymers surfaced to circumvent the removal procedures of the implanted devices [100].

PLGA microspheres were chosen to incorporate LAZ due to the ease of formulation and the safety of biodegradable PLGA to be implanted in the living tissues. LAZ is incorporated successfully in PLGA microspheres using solvent/evaporation method. Various drug loading amounts, polymer type, polymer concentration and stabilizer concentration were tested to optimize the formulation conditions to get the highest loading capacity and EE. In this method, the polymer and LAZ constitute the discontinuous phase of the O/W emulsion which is then dispersed in a larger volume of the aqueous stabilizer solution to allow the organic solvent to evaporate. The

hydrophobic components' solubility in the discontinuous phase drops after the evaporation of the organic solvent leading to the precipitation in a spherical shape, the same as that of the emulsion micelles.

Due to the stirring of the emulsion and the slow extraction and evaporation of the organic solvent, there is a chance for the polymer not to completely enclose LAZ inside the microspheres. In addition, some of the precipitated LAZ or PLGA can be shed away from the micelle core during the microsphere formation due to the slow process of solvent evaporation and the continous stirring motion in the system.

Another procedure was developed in our laboratory to facilitate the formation of microsphere formulations by cooling the system and centrifugation. Cooling of the primary emulsion to 15^{o}C increases the viscosity and keeps the micelles intact when pouring the mixture in the large volume stabilizer solution. The cooling step enhances the separation of the hydrophobic components of the micelle. The separation of the formed micelles is also augmented by a centrifugation step at the cold temperature. Thus, the separated microspheres are of high EE and yield, as compared to the procedures without the cooling and/or centrifugation.

Morphology examination shows that the microspheres have a spherical shape with a smooth surface without wrinkles or cracks. The absence of the surface fractures decreases the possibility of rapid water penetration to the bulk of the microspheres and decreases the possibilities of rapid burst during the first period of release. The release profile shows

a multiphasic pattern in accordance with the degradation pattern of PLGA which varies with the PLGA type used. The highest density polymer (PLGA 85/15 0.65 g/dL) has the highest molecular weight and the slowest release pattern among the formulations as it has the largest proportion of lactic acid which imparts the hydrophobic properties to the polymer. The fastest release is from the polymer with the lowest density and molecular weight (PLGA 50/50 0.43 g/dL).

PLGA's are known to undergo bulk erosion in an aqueous medium, which means that the penetration rate of the medium is faster than polymer solubilization. The biodegradation of PLGA is believed to start with a hydration step when aqueous medium penetrates the polymer matrix, which results in polymer relaxation. An initial degradation starts in the hydrated region of the polymer through ester bond hydrolysis which cleaves the polymer backbone and leads to molecular weight decreases. As the polymer molecular weight declines, the polymer loses its mechanical strength but maintains its integrity. At a further degradation stage, the polymer chain continues to be cleaved and the molecular weight of the polymer decreases to a point that the polymer can no longer hold its integrity. Therefore, mass loss of the polymer begins. In the final stage, the fragments of the polymer are further cleaved to molecules that are soluble in the aqueous media [39]. The process of degradation can explain the presence of a second burst release especially with the low molecular weight PLGA 0.43 g/dL. Water can rapidly penetrate into the bulk of the microspheres and increase the rate of polymer degradation and loss of integrity, upon

which the microspheres dump its content into the medium at a faster rate as compared to the high density polymers.

5.5 LAZ Liposomes

Liposomes demonstrated the ability to target the brain for the purposes of therapy and diagnosis [101, 102]. Being lipophilic in nature, liposomes are expected to cross the BBB by passive diffusion through the lipophilic endothelial cells, by endocytosis or by fusion with brain capillary endothelial cells [103]. The endocytosis is the most important pathway especially for liposomes with 80-100 nm vesicle size [56, 104].

The pharmacological effects of LAZ in the brain are limited by the low exposure of the brain tissue to LAZ. The low exposure in the brain could be explained by the difficulty of crossing the BBB. Incorporating LAZ in long circulating PEGylated liposomes will increase the chances for LAZ to cross the BBB by passive diffusion of the released LAZ and/or by endocytosis of the intact liposomes.

5.5.1 Formulation and Characterization of LAZ Liposomes

A preliminary experiment was performed to select the optimal lipid composition of the liposomes. The fundamental properties of size, surface potential and stability of the liposomes are dependent on the lipid quantity and the structure in the bilayer membrane. Cholesterol is a common component of liposomes providing the rigidity to the membrane, controlling the permeability and improving plasma stability [105]. The

inclusion of cholesterol in the formulation in a percentage >10%, increases the EE of LAZ in the formulated liposomes more than two folds. The enhanced EE of the liposomes may be attributed to the increased hydrophobicity of the membrane by incorporating cholesterol [106]. The size of liposomes is affected by the amount of the included cholesterol in the membrane where inclusion of more than 10% cholesterol reduces the size from 120 nm to 90 nm. This size reduction may be due to the increased fluidity of the membrane with higher cholesterol content [107]. There is no improvement in EE or size by increasing the percentage of cholesterol from 20% (Lipo B) to 30% (Lipo C). Thus, Lipo B was selected as the conventional formulation that will be modified by adding PEGylated lipid to the membrane (Lipo G).

There are controversial opinions about the effect of cholesterol on liposomal formulations. Cholesterol stabilizes the liposomes *in-vivo* and elongates the plasma half life due to the prevention of phospholipids exchange with the HDL and other plasma proteins [108]. On the other hand, the presence of cholesterol may prevent the phospholipids from forming a highly ordered structure [109, 110]. Therefore, the effects of the increasing cholesterol concentration were evaluated based on the release profiles in PBS and plasma.

The inclusion of cholesterol affects LAZ release profiles from liposomes in PBS and plasma. In both media, the inclusion of cholesterol in a ratio less than 20% slowed down the release of LAZ from the liposomes at 37^{o}C compared to the formulations with higher cholesterol contents. High levels of cholesterol have been reported to interfere with the

close packing of lipids in the membrane and increase the membrane fluidity. The increase in membrane fluidity improves the EE but reduces the retention of LAZ molecules upon contact with the release medium and leads to an increased distribution of aqueous phase within the liposomal vesicle thereby reduces the entrapment of the hydrophobic LAZ upon contact with the release medium [111].

The exposure of liposomes to plasma components induces faster release profiles compared to those from PBS except for that of the Lipo G. Plasma protein components such as albumin, apolipoproteins and high density lipoproteins (HDL) displace the phospholipids in the liposomes resulting in an enhanced fluidity thereby causing a fast release of the drug [106, 112]. The slower release from PEGylated liposomes could be explained by the fast hydration process at the PEG layer on the surface of the vesicles leading to a reduction in the amount of the adsorbed plasma components on the liposome surface [69]. Liposomes with 0.8 mol% of PEGylated lipids has a faster release in plasma as compared to liposomes containing 8 mol% of PEGylated lipids. The larger PEG content provides a higher protection of liposome surface from contact with plasma protein components. At a higher PEG concentration, the PEG tends to be arranged in the form of a brush-like structure which provides a better coverage than the mushroom-like structure with the lower concentration of PEG [113].

The physical stability of liposomes was assessed by measuring the liposome size and EE over the period of storage. The liposomes are stable for at least 11 months except for Lipo A. The changes in size and EE are insignificant for liposomes containing 20-30%

cholesterol in the liposomal membrane, but a significant leakage of LAZ is achieved when encapsulated in Lipo A with 10% cholesterol content. The inclusion of cholesterol affected the integrity of liposomal membrane which had an effect on how much of the drug leaks overtime. The storage of LAZ liposomes at 4^{o}C is optimal for keeping the integrity of the liposomal membranes. HSPC phospholipids have a phase transition temperature (T_m) of 53^{o}C, as shown by the DSC thermogram, which imparts a good stability *in-vivo* and on storage for a long period *in-vitro* at temperatures lower than the T_m.

5.5.2 Pharmacokinetics and Organ Distribution of LAZ Liposomes in Healthy Mice

5.5.2.1 Plasma Pharmacokinetics of LAZ Liposomes in Healthy Mice

PK parameters of plasma concentration-time profiles in healthy mice were derived using non-compartmental analysis by WinNonlin program. The conventional and PEGylated liposomes have slower clearance from plasma compared to that of the solution. In general, the slow clearance of the liposomes is attributed to the blockage of the macrophage uptake by the lipids forming the liposomal membranes [114]. After administration of the liposomes, plasma lipoprotein is adsorbed on the vesicle surface in a manner dependent on the hydrophilic and steric properties of the surface. The hydrophobic surfaces of Lipo B are coated with opsonins, e.g., immunoglobulins (Ig), and complement (C), and rapidly removed from the circulation, owing to liver and spleen macrophages which possess specific receptors for these opsonins [114]. The presence of

PEG on the surface of the liposomes imparts a hydrophilic nature on the surface and provides a steric hindrance that prevents the adsorption of opsonins on the vesicle surface [115]. The hydrophilicity and steric hindrance imparted by the presence of PEG leads to a slower recognition by macrophages and thereby a slower clearance from plasma.

5.5.2.2 Mouse Organ Distribution of LAZ Liposomes

There are differences in organ distribution among the three formulations (solution, Lipo B and Lipo G) in healthy mice. LAZ distribution to the organs from the solution was even among the examined organs except high in the liver and low in the brain. It is a common feature of Lazaroid family that they have high accumulation in the liver [17, 92, 93].

The formulation of LAZ in conventional liposomes slows the total clearance as compared to the unformulated solution. The accumulation in liver is 6 and 8 folds higher than those from the solution and Lipo G, respectively. The high accumulation of the conventional liposomes in the liver is due to the fast opsonization of the hydrophobic surface of Lipo B. The accumulations of LAZ in lungs and brain are higher from Lipo G as compared to those of the solution and the conventional Lipo B. The PEGylated liposomes carried a negative potential of -22*mv* which may be the cause of lung accumulation. The higher accumulation in the lungs is noticed in the anionic nanosuspension formulations of LAZ and in other reports from other negatively charged formulations [95-97].

The accumulation in the brain from Lipo G is 4 and 14 folds of those from Lipo B and solution, respectively. This high exposure is due to the large amount of LAZ that gets access to the brain tissue when encapsulated in Lipo G. Lipo G yields a high LAZ concentration in plasma which enhances the passage of LAZ across the BBB either by passive diffusion of the released LAZ or by the endocytosis or membrane fusion of LAZ-encapsulated liposomes.

5.5.2.3 Inter-Compartmental Modeling of LAZ from Solution and Lipo G

Two 3-compartment models were tried to co-model the plasma and brain concentration profiles in healthy mice. The first model described LAZ inter-compartmental distribution to a peripheral compartment and the brain which was considered as a close model. The second model resembled the first one except that the brain was an open compartment without the back distribution to plasma. The second model fits the data better than the first model. The open brain compartment in the second model can be described by two processes; the first is a physiological process describing LAZ elimination from the brain by its distribution to the cerebrospinal fluid (CSF) and the second is an assay underestimation due to the complexation between LAZ and iron in the brain tissues. The formation of iron complex decreases the signal intensity during mass detection using UPLC-MS/MS assay [116]. This process cannot be eliminated by using calibration curves as the iron complex is formed only *in-vivo* not in organic solvent solutions [116, 117].

The same data set was modeled using non-compartmental analysis by WinNonlin software. There is no significant difference between the compartmental and non-compartmental estimations for V_d and AUC, but there is a difference in the K_{el} and Cl estimations. The use of non-compartmental analysis simplifies the parameterization but does not derive the most correct parameters (Table 4.50).

The PK study was performed for the reference LAZ solution in two dose levels, 1 and 10 mg/kg in nude mice. The non-compartmental analysis of the plasma profiles showed that LAZ solution follows a linear PK profile. By normalizing both C_o and $AUC_{0-\infty}$ by the given doses, the PK parameters were comparable between the two dose levels (Table 5.1)

Table 5.1 Comparison of PK Parameters of Reference LAZ Solution Using 1 and 10 mg/kg Doses in Nude Mice

PK parameters	LAZ Solution	
	1 mg/kg	10 mg/kg
C_o (µg/ml)/ µg Dose	0.05	0.02
$AUC_{0-\infty}$ (hr.µg/ml)/ µg Dose	0.03	0.03
Cl (ml/hr)	38.28	33.31
V_{ss} (ml)	119.86	109.65
K_{el} (hr^{-1})	0.25	0.27
$t_{1/2}$(hr)	2.85	2.57

5.5.3 Proof of Concept Efficacy of Lipo G in Brain Tumor Bearing Mice

5.5.3.1 BLI and Tumor Size

In order to evaluate the antineoplastic efficacy of LAZ, BLI was used to measure the photon emission intensity that resulted from an enzyme oxidation process. The amount of emitted light is proportional to the enzyme amount that has been produced by the tumor cells. As the tumor grows, more enzyme quantity is expressed. This technique is non-invasive and sensitive with a lower limit of detection of 8 cells [76].

From the tumor progression data, there is a significant reduction, 65% reduction, in the tumor size on the third week in the group that received LAZ liposomes alone as compared to the control that did not receive any treatment. This result supported the dose-dependent anti-proliferative effect of LAZ on cultured cancer cells [18, 19]. Due to the similarity of LAZ with glucocorticoid structure, LAZ may interact with the glucocorticoid receptors and exert an antiproliferative action as glucocorticoids inhibiting the growth of glioma cells [118]. Glucocorticoids can exert antineoplastic effects by reducing the expression of at least one angiogenic factor, Angpt2, leading to a partial normalization of the tumor vasculature but only when it is used at a relatively high concentration [20]. The effect of LAZ liposomes on suppressing angiogenesis in the tumor tissue is demonstrated in this study by suppressing the signal intensity of CD34 marker in the tumor.

The treatment groups that received radiation with or without LAZ liposomes had a larger tumor size than that of the group that was treated with LAZ liposomes alone. At the same time, the radiation-treated groups had a smaller tumor size than that of the control group. There was no significant differences in the tumor size of the radiation treated groups and those of the control and Lipo G- treated group.

The differences in the tumor size among the groups that received both liposomes and radiation and that received only liposomes may be due to the low LAZ concentration in the radiation–treated group (Figure 4.65). Even though both groups received the same dose of liposomes, the LAZ concentration in the brain samples of radiation-liposomes-treated group (M+R+L) was less than that in liposomes-treated group (M+L) but without significant difference. The radiation produces free radicals which may consume a great deal of LAZ, an antioxidant, in the brain tissues. Thereby, the antiproliferative effect of LAZ is diminished if accompanied by radiation. Another explanation of the larger tumor sizes in the radiation-treated groups (M+R and M+R+L) could be due to the proliferation of the radiation-resistant tumor cells after exposure to a sublethal dose of radiation. This happens especially for cells deep in the tumor mass away from the tumor surface. The exposure to a sublethal dose of radiation activates the growth factor receptors and prosurvival signaling pathways leading to an augmentation of the cell proliferation [119]. This is demonstrated by the larger signal of Ki67 marker of proliferation after exposure to 2Gy radiation in radiation treated group (M+R). In this group, the tumor proliferation was even higher than that of the control group.

5.5.3.2 Lipo G Decreased Lipid Peroxidation after Radiation Exposure

MDA is the most abundant carbonyl by-product of lipid peroxidation in biological tissues. The exposure to radiation increases MDA formation due to the lipid peroxidation especially in the brain. The use of Lipo G prior to the exposure to radiation reduced the level of MDA significantly as compared to that of the group that received radiation without Lipo G treatment. The MDA was also detected in the animals that did not receive radiation due to the formation of lipid peroxides during the process of tissue homogenization by the heat generated during the process [120].

5.5.4 Population Pharmacokinetics of LAZ in Brain Tumor Model

NONMEM is a software package designed to examine the central tendency of population data using parametric methods. The use of NONMEM software provides the advantage of analyzing profiles constructed from dense and sparse sampling protocols. Also, it provides an advantage of analyzing samples of unbalanced design (different number of samples from each subject). LAZ plasma profile in the brain tumor bearing animals is constructed by sparse sampling from 30 mice using 1 and 2 hr post dose samples. The first step in deriving the PK parameters is to select which base model will be used. Various subroutines were tried for 1-, 2- and 3- compartment models with IV or EXIV routes of administration. By comparing the OFV results from those base models, there are no improvements in OFV values using the 2- and 3- compartment models as compared to that of the 1-compartment model. AIC values are used to discriminate the base models after having equal OFV values. AIC value of 1-compartment model is less

than those of 2-and 3- compartment models. Therefore, 1-compartment model is selected as the base model

NONMEM implements the maximum likelihood estimation method. In order to apply the maximum likelihood estimation approach, different approximation methods are applied for the marginal likelihood. NONMEM uses 3 different expansion methods for likelihood estimation: the first-order (FO) method, the first-order expansion about the conditional estimates of the inter-individual random effects (FOCE method) and a second-order expansion about the conditional estimates of the random effects (Laplacian method). The aforementioned methods were tried to get a better fit of the model to the data but there was no improvement in model fit using the second and third method when compared to the model fit using the first estimation method. The first order (FO) method was selected to be used in all the models for the fast calculation process time.

The inter-individual variability was implemented to the fixed effect model either by addition or exponential terms. Both methods gave the same OFV values and the additive model was selected with the base model for simplicity.

The various covariates of animal weight, radiation treatment, tumor size and Sunitinib treatment were tested for a significant drop in OFV to be included in the base model. Only the inclusion of radiation as a covariate in the model showed a significant drop in OFV by > 3.84 units. Also, by visual examination of the PRED vs. Observed data plots from the base model and the radiation covariate model, there was a slight improvement in data distribution around the line of identity in the upper left side of the curve. By

examining the effect of radiation on K and V parameters, the effect of radiation was significant on K but not on V. This indicates that the radiation had an effect on the elimination process of LAZ rather than on its distribution pattern. Another possible variability which is inter-occasional variability was tested for better model representation of the data. Inter-occasional variability was tested for the variability between the two animal batches and the variability in the tumor size measurement. There was no further improvement in the OFV in either the base or the covariate model by implementing the inter-occasional variabilities.

The inter-individual variability was represented by the CV% of the distribution variance Ω^2 of the vector θ (K and V). The CV% of the base model was higher than that of the radiation covariate model in K alone and both K and V (Models#11 and #12). The radiation covariate model in K and V explained some of the variability in the model by reducing the value of CV% in Ω_K (0.2%) than that of the radiation covariate model in K alone (0.8%). But the former model contains radiation as a covariate in V which was proven to be ineffective in improving the model fit (Model#13). Thus, we selected the radiation covariate in K alone to represent the covariate model instead of both K and V. The inter-individual variability in V (CV% Ω_v) showed an improvement from 7.91% to 6.58% from the base to the radiation covariate model which is not a major improvement. The residual unexplained error of the model remained constant during the model building. This indicated that the covariates that were implemented in the model building were not enough to explain all the variabilities in the population.

CHAPTER 6 SUMMARY

6.1 Formulation of LAZ Nanosuspensions

The milling technique was used in nanosuspension preparation where the solid drug particles were sheared between the sliding surfaces of the moving glass beads. Tween 80 and Pluronic F108 were added as steric stabilizers to overcome the attractive interactions between the sheared particles and yielded a nanosuspension of 250 nm particle size. To further reduce the particle size, the shear forces was increased by minimizing the distance that separates the sliding beads by using a mixture of glass beads with various sizes. The glass beads mixture yielded a smaller particle size nanosuspension of 125 nm as compared to the single sized glass beads media with a unimodal distribution pattern.

6.2 Dissolution Profiles of LAZ Nanosuspensions with Two Sizes and Various Charges in PBS and Human Plasma

The release profiles of the nanosuspensions in PBS and human plasma had the same pattern except for the magnitude of the release rate and extent. The small particle NS-B (125 nm) had a faster release rate and higher release extent than those of NS-A (250 nm) group in PBS and plasma. By comparing the release in PBS to plasma, there was a reduction in the rate and extent of release in plasma due to the binding of LAZ to plasma proteins. The release profiles were best described by first order kinetic equation in both release media. Moreover, the 250 nm NS-A had a better fit to Hixson's equation owing to the effect of particle size on the dissolution and release from the nanosuspension.

6.3 Plasma Pharmacokinetics of LAZ Solution and Nanosuspension Formulations of 250nm (Neutral, cationic and Anionic) and 125 nm (Anionic) in Nude Mice

The mouse plasma profile of LAZ solution was used as a reference for the profiles from other nanosuspensions. The initial plasma concentration from the solution is higher than those of nanosuspensions due to the rapid removal by RES from the circulation except for that of the cationic NS-$A^{(+)}$. The AUC of the cationic NS-$A^{(+)}$ is higher than those of other nanosuspensions because at the early time points NS-$A^{(+)}$ was retained in the circulation by a temporary attraction to the RBC's. These particles are then rapidly captured by the circulating macrophages due to the adsorption of other plasma proteins and opsonins. The total clearance of the drug from plasma varies depending on the formulations. The clearance of the drug solution is comparable to those of NS-$A^{(+)}$ and NS-$B^{(-)}$ but slower than those of NS-A and NS-$A^{(-)}$.

6.4 Organ Distribution of LAZ Solution and Nanosuspension Formulations of 250nm (Neutral, cationic and Anionic) and 125 nm (Anionic) in Nude Mice

Being a particulate system, the nanosuspensions have a higher hepatic uptake as compared to that of the reference solution due to the opsonization. The charged particles have higher liver accumulations than those of the solution and the neutral nanosuspensions. The anionic nanosuspensions NS-$A^{(-)}$ and NS-$B^{(-)}$ show 3-8 folds of exposure in the lungs as compared to those of the solution, the cationic and the neutral nanosuspensions. LAZ distribution to the brain is not improved using the various nanosuspensions as compared to that of the reference solution.

6.5 Formulation and Characterization of LAZ Microspheres

LAZ is a hydrophobic drug that can be easily incorporated in the microspheres by solvent evaporation method. The usual method has a fair EE of 70% and loading capacity of 9%. By adapting a new method in which cooling the mixture to 15^{o}C and using centrifugation speed of 7,000 rpm, we increase the EE to 84% with 12% loading capacity for PLGA 0.43 g/dL. The other PLGA polymer produced microspheres with EE of 63.84%±5.23 and 76.41± 7.82, and loading capacity of 9.54±1.8% and 11.48±3.76% for PLGA 0.65 g/dL and PLGA 0.50 g/dL, respectively.

SEM pictures showed the microspheres with a smooth surface and a spherical shape. The release of the microspheres in CSF lasted for 21 days for the low density PLGA polymer and 40% released from the high density PLGA polymer after the same period. The overall release pattern and duration can be tailored by using a mixture of various compositions of PLGA polymers.

6.6 *In-vitro* LAZ Release from Liposomes of Four Lipid Compositions (Conventional Lipo A, B, C and PEGylated Lipo G) in PBS and Plasma

The release of LAZ from liposomal formulations depends on the lipid content and the release media. In PBS and plasma, the inclusion of cholesterol more than 10% of the lipid content increases LAZ leakage from all the liposome formulations at 37^{o}C. For Lipo G, the release rate in plasma is less than that in PBS. The presence of the PEGylated lipids stabilizes the bilayer membrane by forming a steric shield of the PEG layer keeping the

phospholipids away from the plasma proteins. The release rates in plasma was faster than those in PBS due to the exchange between the phospholipids and plasma proteins which destabilize the bilayer in plasma. The release extent in plasma was less than that in PBS due to plasma protein binding.

6.7 Plasma Pharmacokinetics of LAZ from Solution and Liposomes (Lipo B and Lipo G) in Healthy Nude Mice at 1mg/kg Dose

The profiles of the solution, Lipo B and G are similar where the initial phase has a rapid decline followed by a slower phase of elimination. Lipo G has a higher LAZ plasma concentrations compared to those from the solution and Lipo B at the corresponding sampling points. The relative systemic exposure of the PEGylated Lipo G was 9.7 times higher than that of the solution and 4.3 times higher than that of Lipo B. This can be explained by the slow clearance of the Lipo G which was 5 and10 times slower than those of Lipo B and the solution, respectively.

6.8 Organ Distribution of LAZ from Solution and Liposomes (Lipo B and Lipo G) in Healthy Nude Mice at 1mg/kg Dose

The organ distribution of LAZ from the liposomes differed depending on the formulations. Lipo B formulation has high exposures in the liver (6-8 times) and kidneys (3-4 times) as compared to those of the solution and Lipo G. However, Lipo G has higher exposure in the lungs (3 folds) as compared to those of the solution and Lipo B. The brain exposure from Lipo G is 13 times of that of the solution and 4 times of that of Lipo B.

6.9 Proof of Concept Efficacy of LAZ PEGylated Liposomal formulation in Brain Tumor Bearing Mice

Male SCID mice were used in this study to eliminate the possibility of tumor growth suppression. The tumor growth was quantified using BL imaging where the emitted light intensity was used as a measure of the tumor size. The treatment group that received 5 mg/kg Lipo G has a significantly smaller tumor size as compared to that of the control group. On the other hand, the group that received both 2Gy radiation and Lipo G does not show a further reduction in the tumor size as compared to the control group. The radiation dose has a crucial role in suppressing or stimulating the tumor growth. The exposure of tumor resistant cells to sublethal doses of radiation activates the pro-survival pathways and triggers the tumor growth at late stages of the treatment. The survival duration in Lipo G treated groups (27 days) is significantly longer than that of the control group (22 days).

The level of lipid peroxidation in brain samples is significantly reduced after administration of Lipo G to the treatment groups with and without radiation.

The use of PEGylated LAZ liposomes proves to serve as a cargo to carry LAZ into the brain to exert both antineoplastic and radioprotective effects. The PEGylated liposomes showed a higher preferential distribution to the brain and lungs. The use of Lipo G to target the brain is effective in shrinking the GBM tumor size and minimizing lipid peroxidation. The role of LAZ as an antiproliferative is significant in the absence of radiotherapy which may consume some of the available LAZ as a result of the free

radicals production. Another protocol should be followed either by using a higher dose of LAZ or by alternating the radiotherapy and LAZ treatment in cycles. The reduction of lipid peroxidation in brain after radiotherapy is a milestone towards minimizing the radiation-induced necrosis especially in the late stages of the therapy.

6.10 Population Pharmacokinetics of LAZ from PEGylated Liposomal Formulation in Brain Tumor Bearing Mice Model

NONMEM software was used to derive the PK parameters of Lipo G that was given to the tumor model mice because of the sparse nature of sampling design. The K_{el} and V_d were derived using the base model to be 0.44 $hr^{-1}$and 89.70 ml. Only, the inclusion of radiation as a covariate in the model showed an improvement in the model fit indicating that radiation had an effect on the elimination PK of the formulation.

REFERENCES:

1. Bondy, M.L., et al., *Brain tumor epidemiology: consensus from the Brain Tumor Epidemiology Consortium.* Cancer, 2008. **113**(7 Suppl): p. 1953-68.
2. Koo, Y.E., et al., *Brain cancer diagnosis and therapy with nanoplatforms.* Adv Drug Deliv Rev, 2006. **58**(14): p. 1556-77.
3. Pardridge, W.M., *Drug targeting to the brain.* Pharm Res, 2007. **24**(9): p. 1733-44.
4. Loscher, W. and H. Potschka, *Blood-brain barrier active efflux transporters: ATP-binding cassette gene family.* NeuroRx, 2005. **2**(1): p. 86-98.
5. Erol, F.S., et al., *Protective effects of melatonin and vitamin E in brain damage due to gamma radiation: an experimental study.* Neurosurg Rev, 2004. **27**(1): p. 65-9.
6. Halliwell, B., *Oxidants and human disease: some new concepts.* FASEB J, 1987. **1**(5): p. 358-64.
7. Yehuda, S., S. Rabinovitz, and D.I. Mostofsky, *Essential fatty acids and the brain: from infancy to aging.* Neurobiol Aging, 2005. **26 Suppl 1**: p. 98-102.
8. Villa, R.F. and A. Gorini, *Pharmacology of lazaroids and brain energy metabolism: a review.* Pharmacol Rev, 1997. **49**(1): p. 99-136.
9. Hall, E.D., R.A. Vaishnav, and A.G. Mustafa, *Antioxidant therapies for traumatic brain injury.* Neurotherapeutics, 2010. **7**(1): p. 51-61.
10. Alhan, E., et al., *Effects of lazaroid U-74389G on acute necrotizing pancreatitis in rats.* Eur Surg Res, 2006. **38**(2): p. 70-5.
11. Tsaroucha, A.K., et al., *The effect of U-74389G on liver recovery after acute liver ischemia-reperfusion injury in a swine model.* J Surg Res, 2009. **151**(1): p. 10-4.
12. Vignes, J.R. and J. Hugon, *In vitro efficacy of three lazaroids in a model of acute chemical neuronal hypoxia.* Neurosci Lett, 2006. **407**(2): p. 171-5.
13. Wang, J., et al., *A lazaroid mitigates postresuscitation myocardial dysfunction.* Crit Care Med, 2004. **32**(2): p. 553-8.
14. Durmaz, R., et al., *Lazaroid U-74389G attenuates edema in rat brain subjected to post-ischemic reperfusion injury.* J Neurol Sci, 2003. **215**(1-2): p. 87-93.
15. Buatti, J.M., et al., *The lazaroid U74389G protects normal brain from stereotactic radiosurgery-induced radiation injury.* Int J Radiat Oncol Biol Phys, 1996. **34**(3): p. 591-7.
16. Kondziolka, D., et al., *Radioprotective effects of the 21-aminosteroid U-74389G for stereotactic radiosurgery.* Neurosurgery, 1997. **41**(1): p. 203-8.
17. Laizure, S.C., et al., *Disposition of tirilazad (U74006F), a 21-aminosteroid, in the plasma, heart, brain, and liver of the rat.* Drug Metab Dispos, 1993. **21**(5): p. 951-4.
18. Kim, R.S., et al., *Antiproliferative properties of aminosteroid antioxidants on cultured cancer cells.* Cancer Lett, 1992. **64**(1): p. 61-6.
19. Durmaz, R., et al., *Antiproliferative properties of the lazaroids U-83836E and U-74389G on glioma cells in vitro.* Pathol Oncol Res, 1999. **5**(3): p. 223-8.
20. Maciunas, R.J., et al., *Determination of the lethal dose of dexamethasone for early passage in vitro human glioblastoma cell cultures.* Neurosurgery, 1993. **33**(3): p. 485-8; discussion 488.

21. Xiong, R., et al., *Distribution of an intravenous injectable nimodipine nanosuspension in mice.* J Pharm Pharmacol, 2008. **60**(9): p. 1155-9.
22. Afergan, E., et al., *Delivery of serotonin to the brain by monocytes following phagocytosis of liposomes.* J Control Release, 2008. **132**(2): p. 84-90.
23. Garbayo, E., et al., *Effective GDNF brain delivery using microspheres--a promising strategy for Parkinson's disease.* J Control Release, 2009. **135**(2): p. 119-26.
24. Gao, L., et al., *Preparation and characterization of an oridonin nanosuspension for solubility and dissolution velocity enhancement.* Drug Dev Ind Pharm, 2007. **33**(12): p. 1332-9.
25. Keck, C.M. and R.H. Muller, *Drug nanocrystals of poorly soluble drugs produced by high pressure homogenisation.* Eur J Pharm Biopharm, 2006. **62**(1): p. 3-16.
26. Gao, L., et al., *Studies on pharmacokinetics and tissue distribution of oridonin nanosuspensions.* Int J Pharm, 2008. **355**(1-2): p. 321-7.
27. Wong, J., et al., *Suspensions for intravenous (IV) injection: a review of development, preclinical and clinical aspects.* Adv Drug Deliv Rev, 2008. **60**(8): p. 939-54.
28. Sun, W., et al., *Specific role of polysorbate 80 coating on the targeting of nanoparticles to the brain.* Biomaterials, 2004. **25**(15): p. 3065-71.
29. Patravale, V.B., A.A. Date, and R.M. Kulkarni, *Nanosuspensions: a promising drug delivery strategy.* J Pharm Pharmacol, 2004. **56**(7): p. 827-40.
30. Rabinow, B.E., *Nanosuspensions in drug delivery.* Nat Rev Drug Discov, 2004. **3**(9): p. 785-96.
31. Folkman, J. and D.M. Long, *The Use of Silicone Rubber as a Carrier for Prolonged Drug Therapy.* J Surg Res, 1964. **4**: p. 139-42.
32. Brem, H., et al., *Placebo-controlled trial of safety and efficacy of intraoperative controlled delivery by biodegradable polymers of chemotherapy for recurrent gliomas. The Polymer-brain Tumor Treatment Group.* Lancet, 1995. **345**(8956): p. 1008-12.
33. Ranganath, S.H., et al., *The use of submicron/nanoscale PLGA implants to deliver paclitaxel with enhanced pharmacokinetics and therapeutic efficacy in intracranial glioblastoma in mice.* Biomaterials, 2010. **31**(19): p. 5199-207.
34. Turkoglu, O.F., et al., *Local administration of chitosan microspheres after traumatic brain injury in rats: a new challenge for cyclosporine--a delivery.* Br J Neurosurg, 2010. **24**(5): p. 578-83.
35. Baumann, M.D., et al., *Intrathecal delivery of a polymeric nanocomposite hydrogel after spinal cord injury.* Biomaterials, 2010. **31**(30): p. 7631-9.
36. Ozeki, T., et al., *Treatment of rat brain tumors using sustained-release of camptothecin from poly(lactic-co-glycolic acid) microspheres in a thermoreversible hydrogel.* Chem Pharm Bull (Tokyo), 2010. **58**(9): p. 1142-7.
37. Nie, H., Y. Fu, and C.H. Wang, *Paclitaxel and suramin-loaded core/shell microspheres in the treatment of brain tumors.* Biomaterials, 2010. **31**(33): p. 8732-40.
38. Kohane, D.S., et al., *Biodegradable polymeric microspheres and nanospheres for drug delivery in the peritoneum.* J Biomed Mater Res A, 2006. **77**(2): p. 351-61.

39. Spenlehauer, G., et al., *In vitro and in vivo degradation of poly(D,L lactide/glycolide) type microspheres made by solvent evaporation method.* Biomaterials, 1989. **10**(8): p. 557-63.
40. Freiberg, S. and X.X. Zhu, *Polymer microspheres for controlled drug release.* Int J Pharm, 2004. **282**(1-2): p. 1-18.
41. Allen, T.M. and P.R. Cullis, *Drug delivery systems: entering the mainstream.* Science, 2004. **303**(5665): p. 1818-22.
42. Cukierman, E. and D.R. Khan, *The benefits and challenges associated with the use of drug delivery systems in cancer therapy.* Biochem Pharmacol, 2010. **80**(5): p. 762-70.
43. Drulis-Kawa, Z. and A. Dorotkiewicz-Jach, *Liposomes as delivery systems for antibiotics.* Int J Pharm, 2010. **387**(1-2): p. 187-98.
44. Korting, H.C. and M. Schafer-Korting, *Carriers in the topical treatment of skin disease.* Handb Exp Pharmacol, 2010(197): p. 435-68.
45. Samad, A., Y. Sultana, and M. Aqil, *Liposomal drug delivery systems: an update review.* Curr Drug Deliv, 2007. **4**(4): p. 297-305.
46. Hamidi, M., A. Azadi, and P. Rafiei, *Pharmacokinetic consequences of pegylation.* Drug Deliv, 2006. **13**(6): p. 399-409.
47. Dadashzadeh, S., et al., *Peritoneal retention of liposomes: Effects of lipid composition, PEG coating and liposome charge.* J Control Release, 2010.
48. Gaitanis, A. and S. Staal, *Liposomal doxorubicin and nab-paclitaxel: nanoparticle cancer chemotherapy in current clinical use.* Methods Mol Biol, 2010. **624**: p. 385-92.
49. Loukas, Y.L., *A computer-based expert system designs and analyzes a 2(k - p) fractional factorial design for the formulation optimization of novel multicomponent liposomes.* J Pharm Biomed Anal, 1998. **17**(1): p. 133-40.
50. Cryan, S.A., et al., *Increased intracellular targeting to airway cells using octaarginine-coated liposomes: in vitro assessment of their suitability for inhalation.* Mol Pharm, 2006. **3**(2): p. 104-12.
51. Cheng, W.W. and T.M. Allen, *The use of single chain Fv as targeting agents for immunoliposomes: an update on immunoliposomal drugs for cancer treatment.* Expert Opin Drug Deliv, 2010. **7**(4): p. 461-78.
52. Sarko, D., et al., *The Pharmacokinetics of Cell-Penetrating Peptides.* Mol Pharm, 2010.
53. Ying, X., et al., *Dual-targeting daunorubicin liposomes improve the therapeutic efficacy of brain glioma in animals.* J Control Release, 2009. **141**(2): p. 183-92.
54. Gulati, M., et al., *Lipophilic drug derivatives in liposomes.* International Journal of Pharmaceutics 1998. **165**: p. 129–168.
55. Danhier, F., O. Feron, and V. Preat, *To exploit the tumor microenvironment: Passive and active tumor targeting of nanocarriers for anti-cancer drug delivery.* J Control Release.
56. Torchilin, V.P., *Drug targeting.* Eur J Pharm Sci, 2000. **11 Suppl 2**: p. S81-91.
57. Matsumura, Y. and H. Maeda, *A new concept for macromolecular therapeutics in cancer chemotherapy: mechanism of tumoritropic accumulation of proteins and the antitumor agent smancs.* Cancer Res, 1986. **46**(12 Pt 1): p. 6387-92.

58. Heldin, C.H., et al., *High interstitial fluid pressure - an obstacle in cancer therapy.* Nat Rev Cancer, 2004. **4**(10): p. 806-13.
59. Yang, X., et al., *A novel liposomal formulation of flavopiridol.* Int J Pharm, 2009. **365**(1-2): p. 170-4.
60. Teshima, M., et al., *Prednisolone retention in integrated liposomes by chemical approach and pharmaceutical approach.* J Control Release, 2004. **97**(2): p. 211-8.
61. Moribe, K., K. Maruyama, and M. Iwatsuru, *Encapsulation characteristics of nystatin in liposomes: effects of cholesterol and polyethylene glycol derivatives.* Int J Pharm, 1999. **188**(2): p. 193-202.
62. Zhang, J.A., et al., *Development and characterization of a novel Cremophor EL free liposome-based paclitaxel (LEP-ETU) formulation.* Eur J Pharm Biopharm, 2005. **59**(1): p. 177-87.
63. Liu, J., et al., *Liposome formulation of a novel hydrophobic aryl-imidazole compound for anti-cancer therapy.* Cancer Chemother Pharmacol, 2006. **58**(3): p. 306-18.
64. Lopez-Pinto, J.M., M.L. Gonzalez-Rodriguez, and A.M. Rabasco, *Effect of cholesterol and ethanol on dermal delivery from DPPC liposomes.* Int J Pharm, 2005. **298**(1): p. 1-12.
65. Sun, W., et al., *Preparation and evaluation of N(3)-O-toluyl-fluorouracil-loaded liposomes.* Int J Pharm, 2008. **353**(1-2): p. 243-50.
66. Garg, M., et al., *Ethinylestradiol-loaded ultraflexible liposomes: pharmacokinetics and pharmacodynamics.* J Pharm Pharmacol, 2006. **58**(4): p. 459-68.
67. Mura, P., et al., *Development, characterization and in vivo evaluation of benzocaine-loaded liposomes.* Eur J Pharm Biopharm, 2007. **67**(1): p. 86-95.
68. Chen, Y., et al., *Enhanced bioavailability of the poorly water-soluble drug fenofibrate by using liposomes containing a bile salt.* Int J Pharm, 2009.
69. Panwar, P., et al., *Preparation, characterization, and in vitro release study of albendazole-encapsulated nanosize liposomes.* Int J Nanomedicine, 2010. **5**: p. 101-8.
70. Koda, Y., et al., *In vitro stability and permeability studies of liposomal delivery systems for a novel lipophilic endomorphin 1 analogue.* Int J Pharm, 2008. **356**(1-2): p. 37-43.
71. Bailer, A.J., *Testing for the equality of area under the curves when using destructive measurement techniques.* J Pharmacokinet Biopharm, 1988. **16**(3): p. 303-9.
72. Charlier, A., B. Leclerc, and G. Couarraze, *Release of mifepristone from biodegradable matrices: experimental and theoretical evaluations.* Int J Pharm, 2000. **200**(1): p. 115-20.
73. Jeyanthi, R., et al., *Effect of processing parameters on the properties of peptide-containing PLGA microspheres.* J Microencapsul, 1997. **14**(2): p. 163-74.
74. Contag, C.H., et al., *Visualizing gene expression in living mammals using a bioluminescent reporter.* Photochem Photobiol, 1997. **66**(4): p. 523-31.
75. Szentirmai, O., et al., *Noninvasive bioluminescence imaging of luciferase expressing intracranial U87 xenografts: correlation with magnetic resonance imaging determined tumor volume and longitudinal use in assessing tumor growth and antiangiogenic treatment effect.* Neurosurgery, 2006. **58**(2): p. 365-72; discussion 365-72.

76. Zhao, H., et al., *A screening platform for glioma growth and invasion using bioluminescence imaging. Laboratory investigation.* J Neurosurg, 2009. **111**(2): p. 238-46.
77. Smith, A.M., et al., *Neonatal alcohol exposure increases malondialdehyde (MDA) and glutathione (GSH) levels in the developing cerebellum.* Brain Res Dev Brain Res, 2005. **160**(2): p. 231-8.
78. Ciuffi, M., et al., *Effect of 21-aminosteroid U74500A (pregna-1,4,9(11)-triene-3,20-dione, 21-(4-(5,6-bis(diethylamino)-2-pyridinyl)-1-piperazinyl)-16-methyl-, HCl (16 alpha)) on rat brain cortex lipid peroxidation induced "in vivo" by iron-carbohydrate.* Biochem Pharmacol, 1994. **47**(12): p. 2181-6.
79. Kassell, N.F., et al., *Randomized, double-blind, vehicle-controlled trial of tirilazad mesylate in patients with aneurysmal subarachnoid hemorrhage: a cooperative study in Europe, Australia, and New Zealand.* J Neurosurg, 1996. **84**(2): p. 221-8.
80. Investigators, T.R., *A randomized trial of tirilazad mesylate in patients with acute stroke (RANTTAS). The RANTTAS Investigators.* Stroke, 1996. **27**(9): p. 1453-8.
81. Haley, E.C., Jr., *High-dose tirilazad for acute stroke (RANTTAS II). RANTTAS II Investigators.* Stroke, 1998. **29**(6): p. 1256-7.
82. Maiese, K., *Neurovascular Medicine Pursuing Cellular Longevity for Healthy Aging* 2009, New York: Oxford University Press, Inc.
83. FDA, *Guidance for Industry: Analytical Procedures and Methods Validation (Draft guidance), Food and Drug Administration*, CDER, Editor. 2000: Rockville, MD.
84. FDA, *Reviewer Guidance: Validation of Chromatographic Methods, Food and Drug Administration*, CDER, Editor. 1994: Rockville, MD.
85. Kesisoglou, F., S. Panmai, and Y. Wu, *Nanosizing--oral formulation development and biopharmaceutical evaluation.* Adv Drug Deliv Rev, 2007. **59**(7): p. 631-44.
86. Yang, J.Z., et al., *Fluticasone and budesonide nanosuspensions for pulmonary delivery: preparation, characterization, and pharmacokinetic studies.* J Pharm Sci, 2008. **97**(11): p. 4869-78.
87. Goldberg, M., R. Langer, and X. Jia, *Nanostructured materials for applications in drug delivery and tissue engineering.* J Biomater Sci Polym Ed, 2007. **18**(3): p. 241-68.
88. Allen, T.M., et al., *Pharmacokinetics and pharmacodynamics of lipidic nano-particles in cancer.* Anticancer Agents Med Chem, 2006. **6**(6): p. 513-23.
89. Hiromitsu Aoki , T.T., Fuminori Sakurai , Kaoru Fuji and Koichiro Miyajima *Effects of positive charge density on the liposomal surface on disposition kinetics of liposomes in rats* International Journal of Pharmaceutics, 1997. **156**(2): p. 163-174.
90. Manjunath, K. and V. Venkateswarlu, *Pharmacokinetics, tissue distribution and bioavailability of nitrendipine solid lipid nanoparticles after intravenous and intraduodenal administration.* J Drug Target, 2006. **14**(9): p. 632-45.
91. Alexis, F., et al., *Factors affecting the clearance and biodistribution of polymeric nanoparticles.* Mol Pharm, 2008. **5**(4): p. 505-15.
92. Cox, J.W., et al., *Pharmacokinetics and excretion of the 21-aminosteroid antioxidant U-74006F in rat and perfused rat liver.* Drug Metab Dispos, 1989. **17**(4): p. 373-9.

93. Wienkers, L.C., et al., *Biotransformation of tirilazad in human: 3. tirilazad A-ring reduction by human liver microsomal 5alpha-reductase type 1 and type 2.* J Pharmacol Exp Ther, 1998. **287**(2): p. 583-90.
94. Wienkers, L.C., et al., *Biotransformation of tirilazad in human: 1. Cytochrome P450 3A-mediated hydroxylation of tirilazad mesylate in human liver microsomes.* J Pharmacol Exp Ther, 1996. **277**(2): p. 982-90.
95. Yang, S.C., et al., *Body distribution in mice of intravenously injected camptothecin solid lipid nanoparticles and targeting effect on brain.* J Control Release, 1999. **59**(3): p. 299-307.
96. Lobenberg, R., et al., *Body distribution of azidothymidine bound to hexyl-cyanoacrylate nanoparticles after i.v. injection to rats.* J Control Release, 1998. **50**(1-3): p. 21-30.
97. Kurihara, A., et al., *Enhanced tumor delivery and antitumor activity of palmitoyl rhizoxin using stable lipid emulsions in mice.* Pharm Res, 1996. **13**(2): p. 305-10.
98. Ishida, T., H. Harashima, and H. Kiwada, *Interactions of liposomes with cells in vitro and in vivo: opsonins and receptors.* Curr Drug Metab, 2001. **2**(4): p. 397-409.
99. Levchenko, T.S., et al., *Liposome clearance in mice: the effect of a separate and combined presence of surface charge and polymer coating.* Int J Pharm, 2002. **240**(1-2): p. 95-102.
100. Mason, N., C. Thies, and T.J. Cicero, *In vivo and in vitro evaluation of a microencapsulated narcotic antagonist.* J Pharm Sci, 1976. **65**(6): p. 847-50.
101. Garcia-Marco, J.A., et al., *Efficacy and safety of liposomal cytarabine in lymphoma patients with central nervous system involvement from lymphoma.* Cancer, 2009. **115**(9): p. 1892-8.
102. Oku, N., et al., *PET imaging of brain cancer with positron emitter-labeled liposomes.* Int J Pharm, 2010.
103. Tiwari, S.B. and M.M. Amiji, *A review of nanocarrier-based CNS delivery systems.* Curr Drug Deliv, 2006. **3**(2): p. 219-32.
104. Fenske, D.B. and P.R. Cullis, *Liposomal nanomedicines.* Expert Opin Drug Deliv, 2008. **5**(1): p. 25-44.
105. Deniz, A., et al., *Celecoxib-loaded liposomes: effect of cholesterol on encapsulation and in vitro release characteristics.* Biosci Rep, 2010. **30**(5): p. 365-73.
106. Ramana, L.N., et al., *Development of a liposomal nanodelivery system for nevirapine.* J Biomed Sci, 2010. **17**: p. 57.
107. Atyabi, F., et al., *Preparation of pegylated nano-liposomal formulation containing SN-38: In vitro characterization and in vivo biodistribution in mice.* Acta Pharm, 2009. **59**(2): p. 133-44.
108. Kirby, C., J. Clarke, and G. Gregoriadis, *Effect of the cholesterol content of small unilamellar liposomes on their stability in vivo and in vitro.* Biochem J, 1980. **186**(2): p. 591-8.
109. Bedu-Addo, F.K. and L. Huang, *Effect of matrix lipid chain length on liposomes containing cholesterol and ganglioside GM1: implications in drug delivery.* J Pharm Sci, 1996. **85**(7): p. 714-9.

110. Chong, P.L. and D. Choate, *Calorimetric studies of the effects of cholesterol on the phase transition of C(18):C(10) phosphatidylcholine.* Biophys J, 1989. **55**(3): p. 551-6.
111. Coderch, L., et al., *Influence of cholesterol on liposome fluidity by EPR. Relationship with percutaneous absorption.* J Control Release, 2000. **68**(1): p. 85-95.
112. Guo, L.S., et al., *Interaction of unilamellar liposomes with serum lipoproteins and apolipoproteins.* J Lipid Res, 1980. **21**(8): p. 993-1003.
113. Li, C., et al., *Lipid composition and grafted PEG affect in vivo activity of liposomal mitoxantrone.* Int J Pharm, 2008. **362**(1-2): p. 60-6.
114. Luck, M., et al., *Complement activation by model drug carriers for intravenous application: determination by two-dimensional electrophoresis.* Biomaterials, 1999. **20**(21): p. 2063-8.
115. Dadashzadeh, S., A.M. Vali, and M. Rezaie, *The effect of PEG coating on in vitro cytotoxicity and in vivo disposition of topotecan loaded liposomes in rats.* Int J Pharm, 2008. **353**(1-2): p. 251-9.
116. Hayen, H. and D.A. Volmer, *Different iron-chelating properties of pyochelin diastereoisomers revealed by LC/MS.* Anal Bioanal Chem, 2006. **385**(3): p. 606-11.
117. Braughler, J.M., et al., *Novel 21-amino steroids as potent inhibitors of iron-dependent lipid peroxidation.* J Biol Chem, 1987. **262**(22): p. 10438-40.
118. Villeneuve, J., et al., *Reduced glioma growth following dexamethasone or anti-angiopoietin 2 treatment.* Brain Pathol, 2008. **18**(3): p. 401-14.
119. Park, C.M., et al., *Ionizing radiation enhances matrix metalloproteinase-2 secretion and invasion of glioma cells through Src/epidermal growth factor receptor-mediated p38/Akt and phosphatidylinositol 3-kinase/Akt signaling pathways.* Cancer Res, 2006. **66**(17): p. 8511-9.
120. Esterbauer, H., R.J. Schaur, and H. Zollner, *Chemistry and biochemistry of 4-hydroxynonenal, malonaldehyde and related aldehydes.* Free Radic Biol Med, 1991. **11**(1): p. 81-128.